January 2010

UNIVERSITY OF CANTERBURY
Te Whare Wānanga o Waitaha
CHRISTCHURCH NEW ZEALAND

Cobalt(III) Complexes For Surface Engineering

A thesis submitted in partial fulfilment of the requirements

for the Degree of

Doctor of Philosophy in Chemistry

in the University of Canterbury

by

Reuben Thomas Jane

Acknowledgements

I would like to thank a number of people who have contributed to the preparation of this thesis. Firstly, I must extend my sincere thanks to my supervisor, Dr Richard Hartshorn, for providing excellent and patient guidance both in the science of this thesis and in my development as a researcher. Also thank you my secondary supervisor, Professor Peter Tasker of the University of Edinburgh, for his expertise and hospitality.

The experimental work in this thesis would not have been possible without the assistance of several people who ran or assisted with various aspects of the research. I would like to thank Dr Chris Fitchett and Dr Jeni Burgess for collecting and solving the X-ray crystal structures, and Dr Matt Polson for running the cif checks. Thanks also to Dr Marie Squire for running the mass spectra experiments, Josh Lehr for the cyclic voltammetry and Deborah Clearwater for the SEM and EDS. For running some of the isotherm experiments, thanks must also go to Dr David Henderson and Tom Jeffs, both of the University of Edinburgh. Additionally, thank you to Norzita Ngadi for assistance with the QCM and to Dr Ken Morison for assistance with the contact angle measurements.

A large thank you must go to the departmental technical staff. In particular Danny Leonard, Nick Oliver, Wayne Mackay and Rob McGregor who have all contributed many hours towards assisting with this work.

Thank you to the University of Canterbury for the award of a doctoral scholarship.

To the past and present members of the Hartshorn group, thank you for providing an enjoyable work environment and many stimulating discussions.

A big thank you to Mum and Dad and the rest of my family for their ongoing love and support, and to Dad for venturing into an unfamiliar topic to proofread this thesis.

Finally, many, many thanks to my partner, Frances, for taking time out of her own busy research project to read several drafts at different stages, but more importantly, for her unconditional love and encouragement.

Table of contents

Abbreviations

A	absorbance
AAS	atomic absorption spectrometry
AES	Auger electron spectroscopy
AFM	atomic force microscopy
ast	*N*-(3-amino-2,2-bis(aminomethyl)propyl)-*N*-benzyl-anthraquinone-2-sulfonamide
BCE	before common era
BET	Brunauer, Emmett and Teller
CCC	chromate conversion coating
COSY	2D ^{1}H NMR correlation spectroscopy
CSD	Cambridge Structural Database
CVD	chemical vapour deposition
cst	*N*-(3-amino-2,2-bis(aminomethyl)propyl)-*N*-benzyl-d-camphor-10-sulfonamide
CV	cyclic voltammetry
dien	*N*-(2-aminoethyl)ethane-1,2-diamine
DMF	*N*,*N*-dimethylformamide
DMSO	dimethylsulfoxide
DNA	deoxyribonucleic acid
DSSC	dye sensitised solar cell
E_{corr}	corrosion potential
EDS	energy-dispersive X-ray spectroscopy
ESI-MS	electrospray ionisation mass spectrometry
en	ethane-1,2-diamine
EXAFS	extended X-ray absorption fine structure
fac	facial
FTIR	Fourier transform infrared spectroscopy
GDP	gross domestic product
HMBC	heteronuclear multiple bond coherence

HSQCAD	heteronuclear single quantum coherence adiabatic
IBX	2-iodoxybenzoic acid
i_{corr}	corrosion current density
ICP-OES	inductively coupled plasma optical emission spectrometry
IR	infrared
mer	meridional
NMR	nuclear magnetic resonance
nst	*N*-(3-amino-2,2-bis(aminomethyl)propyl)-*N*-benzyl-naphthalene-2-sulfonamide
PFG	pulsed field gradient
QCM	quartz crystal microbalance
SAM	self assembled monolayer
SCE	saturated calomel electrode
SEM	scanning electron microscopy
tacn	1,4,7-triazacyclononane
tame	1,1,1-tris(aminomethyl)ethane
tamm	tetrakis(aminomethyl)methane
tamt	α,α,α-tris(aminomethyl)toluene
Tf	trifluoromethylsulfonyl
TGA	thermogravimetric analysis
TMPS	sodium 3-(trimethylsilyl)-1-propane sulfonate
TMS	tetramethylsilane
tpa	tris(2-pyridylmethyl)amine
tren	tris(2-aminoethyl)amine
Ts	*p*-toluenesulfonyl
tst	*N*-(3-amino-2,2-bis(aminomethyl)propyl)-*N*-benzyl-toluene-4-sulfonamide
UV	ultraviolet
XANES	X-ray absorption near edge structure
XAS	X-ray absorption spectroscopy
XPS	X-ray photoelectron spectroscopy

List of Figures

List of Tables

Abstract

This thesis addresses the potential for use of cobalt(III) complexes for functionalisation of lightly oxidised iron surfaces.

In Chapter 2 the preparation of cobalt(III) complexes of a series of ligands based on 1,1,1-tris(aminomethyl)ethane is described. The synthesis was approached in two ways. Firstly, preparation of functionalised triol molecules as precursors to functionalised triamine ligands was investigated. This approach utilised the Tollens condensation of aldehydes with formaldehyde. In a second approach, the functionalisation of tetrakis(aminomethyl)methane in which one amine arm has been differentiated was used. The tetraamine was reacted with benzaldehyde and reduced with borohydride ion to give a secondary amine molecule that was then functionalised using alkyl or aryl sulfonyl chloride molecules.

Chapter 3 describes the measurement of the binding of some cobalt(III) complexes to the surface of high surface area goethite. It was observed that complexes that have three exchangeable ligands bind more strongly than those with two exchangeable ligands. This is rationalised as being due to there being more bonds to the surface formed by complexes with three exchangeable ligands. It was also observed that complexes with three exchangeable ligands give greater surface coverage than those with two. This is likely due to the larger cross sectional area of the complexes with two exchangeable ligands in comparison to that of those with three, which blocks potential adjacent sites.

Preliminary experiments on the use of the contact angle, SEM, EDS and QCM to characterise complex binding are explored in Chapter 4 . The results from the EDS and QCM experiments show that these may be valuable tools for measuring this binding and the subsequent surface properties, but have not yielded detailed results at this point.

In Chapter 5 the use of cobalt(III) complexes as inhibitors of corrosion of iron in hydrochloric acid is investigated. All the complexes tested, even those that showed no binding to goethite surfaces, inhibit the corrosion to some degree. The level of inhibition is dependent on the complex, with $[Co(tren)Cl_2]Cl$ showing maximum inhibition of 81% and $[Co(tame)Cl_3]$ showing maximum inhibition of 53%. For some of the complexes, their concentration in solution over the course of the experiment was monitored by UV-vis. It was found that the

complex disappears in a zero order reaction, the rate of which is dependent on the complex. However, the exact nature of this reaction is unknown. Furthermore, it was observed that inhibition of corrosion continues after the complex is no longer observed in solution. There is a difficulty in rationalising the inhibition being dependent on the complex identity, but not its continued presence in solution. Consequently, the mechanism of corrosion inhibition that explains all of these observations is still not known.

Chapter One

Introduction

1.1. General introduction

Materials that have been modified at their surface are of widespread use. Many ceramics must be modified at their surface by use of a glaze in order to be watertight, and the decorative plating of precious metals, such as gold, onto less expensive substrates is well-known. The earliest surface improvements came about by shaping of an object, which simultaneously reduced its roughness. Artificially smoothened stone implements have been found in Asia from as early as 7,000 BCE. The first surface engineering technology was heat treatment, which was used in India and Egypt as early as 2,000 BCE. Homer describes the hardening of projectiles in *The Odyssey* from around 700 BCE, and carbonitriding of steel using soy beans was carried out in China in approximately 100 BCE.[1]

The *ASM Handbook*[*] defines surface engineering as "treatment of the surface and near-surface regions of a material to allow the surface to perform functions that are distinct from those functions demanded from the bulk of the material."[2] In a modern context, the function imparted by the engineered surface may be an increase in resistance to corrosion or wear, an increase in strength, improved electronic properties, improved insulation or a better aesthetic appearance.

1.1.1. Engineering techniques for improving surface properties

The surface properties of a material can be improved using several technologies, which will be described in the following paragraphs. These include heat treatment, anodisation and the use of coatings. Types of coating techniques include painting, hot dip coating, electroplating and vapour deposition methods.

Surface hardening is used to improve the wear resistance of the exterior of a metal, particularly steel, while retaining the tough, fracture resistant properties of the interior.[3, 4] Surface hardening can be achieved using an oxyacetylene flame, by induction heating, or through the use of an electron or laser beam. The steel is heated to a sufficiently high temperature to cause a transition from the body-centred cubic allotrope ferrite (α-iron) to the

[*] Published by ASM International, formerly known as the American Society for Metals.

face-centred cubic austenite (γ-iron).[5] Rapid quenching in water results in the formation of a hard body-centred tetragonal martensite phase at the surface, while the bulk remains unchanged.[1, 3, 4]

A requirement of heat based hardening is sufficient carbon content to form the martensite phase. The steel must be at least 0.3% carbon for the process to be successful.[4] If the steel does not have sufficient carbon, the surface chemistry may be altered by diffusion of carbon or nitrogen into the surface to allow the surface to undergo quench hardening as described above. Introduction of carbon is known as carburizing, while the introduction of nitrogen is called nitriding. Carbonitriding involves the diffusion of both carbon and nitrogen into the surface. Carburizing can be achieved by heating the part in a closed container with a carbon containing solid, such as charcoal. For both carbon and nitrogen diffusion, the elements may be introduced by the use of gas, liquid or plasma (ion).[3, 4]

Anodisation is a method of increasing the natural oxide layer on the surface of a metal, most commonly aluminium. The protection of aluminium substrates against corrosion is of high interest, particularly to the aerospace industry.[6-8] Anodisation involves the assembly of an electrolytic cell in which the part to be treated is made the anode, and the electrolyte utilised is an acid, usually sulfuric or chromic acid.[4] This results in the growth of a thin non-porous oxide layer, with a much thicker porous layer on top (Figure 1.1).[7, 8]

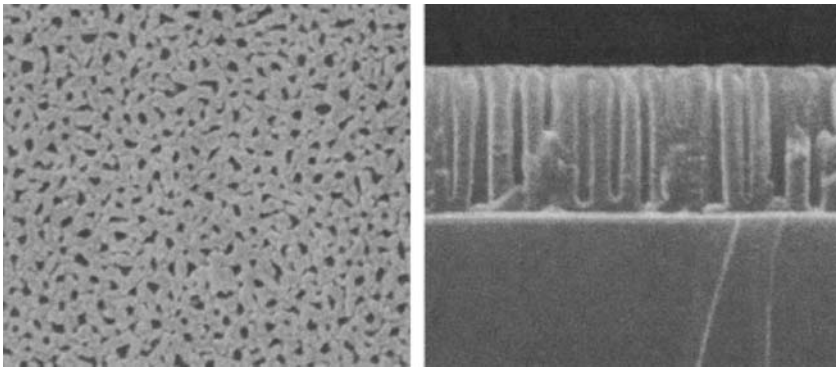

Figure 1.1: SEM images of anodised aluminium surface. Left: Looking down on the porous surface. Right: Profile of the surface layers. The grey area at the lowermost region of the picture is the bulk aluminium. The thin non-porous layer is visible as a solid white line, with the thicker porous layer on top.[9]

The film is composed of aluminium oxide (either amorphous or γ-Al_2O_3) and the total thickness varies from 5 to 1,500 nm, depending on the anodisation process used.[8, 10] The use of chromates in anodisation processes is covered in more detail in Section 1.4.3.

Although painting is known from as early as 35,000 BCE, it was not until the late nineteenth century that paint coatings came to be used for protective purposes.[1] Modern paints comprise three main parts: The solvent (either water or an organic solvent), a resin (also known as the binder) and the pigments. Commonly used pigments include titanium dioxide, zinc chromate and indigo. These often have additional functions within the formulation, such as corrosion inhibition.[1, 3]

Metallic coatings may be applied through either the use of a hot dip or by electroplating. Hot dip coating involves immersion of a component in a bath of molten metal. A common example is the hot dipping of steel in a bath of zinc to produce galvanised steel. Many other metals and alloys can be used to coat components, with aluminium being a common ingredient in alloy coatings.[3, 4]

Electroplating allows the deposition of metallic coatings with much greater control over layer thickness than those formed by hot dip methods. The use of chromium in electroplating is described in Section 1.4.2. The component to be plated is made the cathode in an electrolytic cell; the metal to be deposited forms the anode and/or is part of the electrolyte. The application of a DC voltage causes deposition of the plating metal on the cathodic component. Electroplating has drawbacks, including the inability to plate non-conductors, the large amount of energy required and the difficulty in obtaining a uniform film. For this reason, electroless plating has been developed.[4] In this process, the coating is deposited by an autocatalytic chemical reduction of metal ions in solution by reducing agents such as hypophosphite, aminoborane or borohydride compounds. Nickel is the most commonly plated metal, with copper and gold also prevalent.[2]

Vapour deposition processes can be divided into physical vapour deposition and chemical vapour deposition. Physical vapour deposition can further be divided into sub-types including thermal evaporation and sputtering. Thermal evaporation involves heating the coating material inside a vacuum that also contains the substrate to be coated. The coating material evaporates and then condenses on the cold substrate. Sputtering takes place in a low pressure chamber containing a gas such as argon. A high voltage is then applied between the coating material acting as a cathode and the substrate acting as an anode. The high applied potential ionises the argon, which accelerates toward the negatively charged cathode,

dislodging atoms of the coating material upon impact. These then travel across the electrode gap to coat the substrate (Figure 1.2).[4]

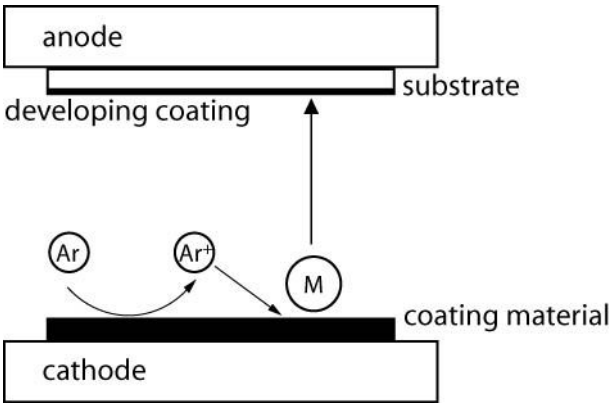

Figure 1.2: Schematic representation of sputtering. Argon cations generated at the cathode dislodge atoms of coating material by impact, which then coat the substrate at the anode.

Chemical vapour deposition (CVD) occurs by the reaction or decomposition of a coating substance at the substrate. The coating precursor is vaporised, travels to the substrate within a chamber and then reacts to form the required coating. CVD allows deposition of metals that cannot be deposited by electroplating such as tungsten, molybdenum and niobium.[3]

Ion implantation was originally conceived for the doping of semiconductors. It involves ionisation of the element to be implanted, which is then accelerated by a particle accelerator toward the target substrate. The ion loses its kinetic energy upon impact, and eventually rests in subsurface locations, usually within the outermost micrometre. Ion implantation has the advantage that any ionisable species can be introduced, and the process operates at relatively low temperatures.

1.1.2. Chemical techniques for altering surface properties

The surface properties of a material can be modified by the introduction of a thin layer of organic molecules on its surface. This can alter the material's wettability, or its mechanical, optical or electronic properties, amongst others.[11] The most common methods of growing an organic film are shown schematically in Figure 1.3.

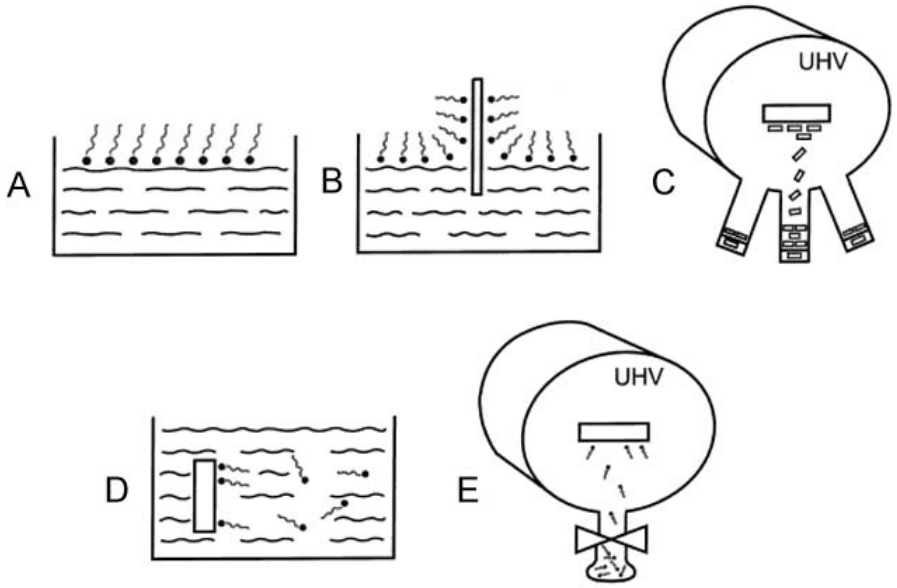

Figure 1.3: Methods of manufacturing chemical layers on a surface. A: Langmuir film, B: Langmuir-Blodgett film, C: Molecular beam epitaxy, D: Self assembled monolayer from solution, E: Self assembled monolayer from vapour.[11]

Langmuir films consist of amphiphilic molecules spread over the surface of water. The hydrophilic head groups have a greater affinity for the water than air, whereas the hydrophobic tail has a greater affinity for the air, resulting in an anisotropic interaction of the surfactant with the water surface. Langmuir-Blodgett films are formed by dipping a substrate into water with a homogenous Langmuir film on top, and transferring this film onto the solid by sliding it through the film.[11, 12] Molecular beam epitaxy, a type of CVD in which layers of single crystals are deposited,[2] can be applied to organic molecules. Self assembled monolayers (SAMs) are grown by the spontaneous chemisorption of molecules from solution or vapour phase. The molecule used to form the monolayer contains a functional end group, a spacer, and a head group that has affinity for the substrate to which it is to bind.[13] Many head groups have been utilised for binding to bulk material, thin films and nanoparticles of various metals, metal oxides and semiconductors. Among the more widely used head groups are thiols, silicon derivatives, phosphonates and carboxylates.[13-15]

A common method for the formation of SAMs is through the use of alkanethiols, which have been investigated for modification of gold surfaces since 1983.[16] The molecule binds to the surface through a sulfur-gold bond which has a high energy of ~18 kcal. The thiol binds in the three-fold hollow of the metal lattice which spaces the molecules around 5 Å apart.

Because this is higher than the van der Waals diameter of the alkane chain, the chains tilt to maximise the beneficial interactions between neighbouring chains (Figure 1.4).[17] Alkanethiols have also been shown to form layers on other metals and alloys, including silver,[18] copper,[18] platinum,[19] palladium[20] and stainless steel.[21] The angle of tilt is dependent on the substrate used, with lower angles seen for adsorbed thiols on copper and silver than on gold.[18] Using organothiols, a wide range of surface functionalities can be made, as these surfaces reproducibly form layers with the tail group exposed at the interface.[17]

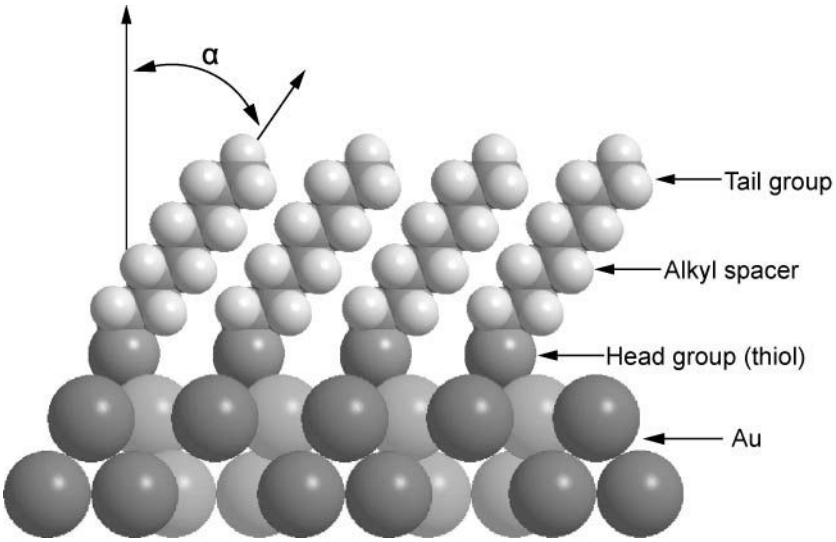

Figure 1.4: Binding of an alkanethiol to a gold substrate. The alkane chains tilt at an angle α in order to form a regular array.

Hydroxylated surfaces can be modified by the use of various alkylsilanes, commonly trichloroalkylsilanes. The mechanism of formation of these layers is thought to be extraction of surface moisture, followed by silane hydrolysis and subsequent formation of a polysiloxane at the substrate surface (Figure 1.5). Consequently, the successful deposition of a layer is dependent on moisture and temperature. The presence of too little water results in an incomplete monolayer; too much causes facile polymerisation in solution. Similarly, temperatures above the optimum cause excessive polymerisation in solution, while low temperatures result in slow deposition. Surfaces of this type have been prepared on aluminium oxide, germanium oxide and silicon dioxide.[15]

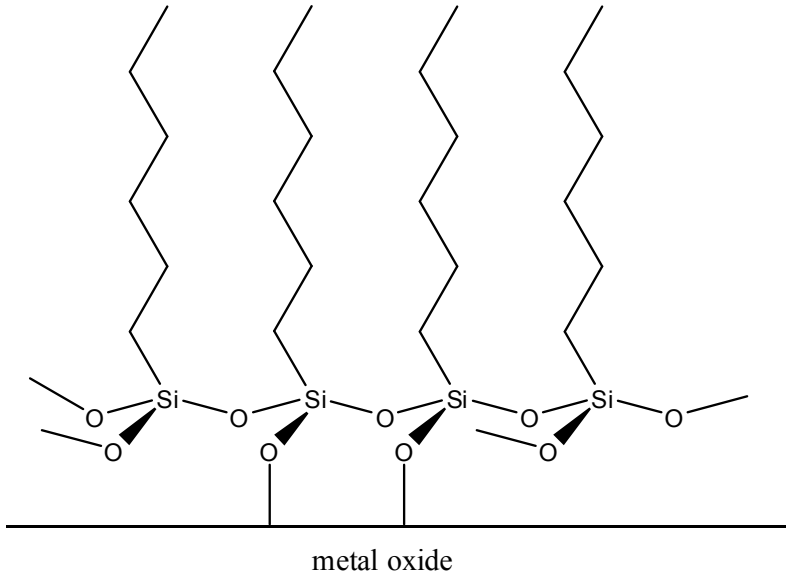

Figure 1.5: Schematic representation of a polysiloxane at a metal oxide surface.

The binding of carboxylic acid molecules to metal surfaces has been widely studied.[15] The binding of retinoic acid to titanium dioxide was examined by Weng *et al*, who identified six possible modes of binding (Figure 1.6): Type A (ionic bonding), and types E and F (hydrogen bonding) were found to only contribute 3% of the total bound species, while the bridging (type D) and chelating (type C) made up 34% and the ester-type linkage (type B) 63%.[22]

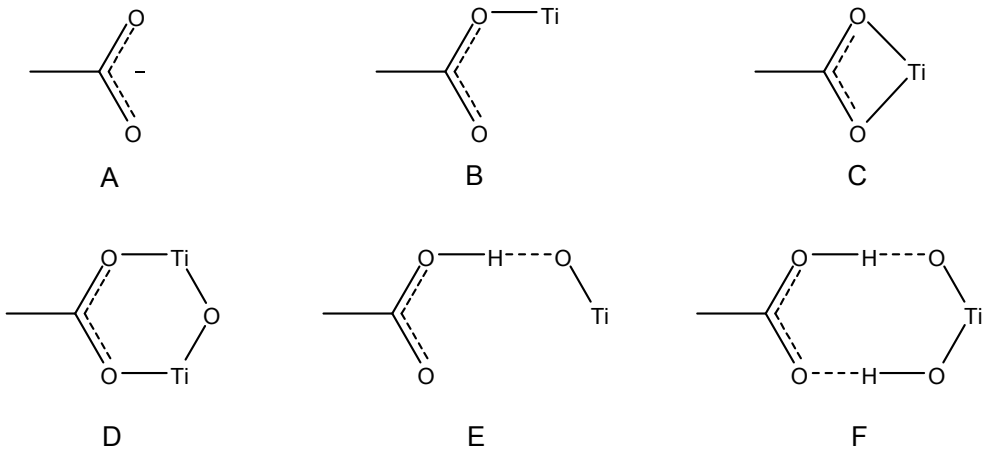

Figure 1.6: Six possible modes of binding a carboxylate to a titanium dioxide surface.

One disadvantage of the use of carboxylic acids is that fatty acid groups always bind to form a hydrocarbon terminated surface. That is, any terminal functionality is not exposed at the interface.[17] However, one application that does utilise the binding of carboxylate groups to titanium dioxide surfaces is the manufacture of dye sensitised solar cells (DSSCs). A

conventional solar cell comprises a semiconductor with a band gap of an appropriate size that photons of visible light are able to excite electrons from the valence band into the conduction band in order to generate a current. DSSCs utilise cheaper and more widely available large band gap semiconductors, such as titanium dioxide. Population of the conduction band is achieved through the use of a dye sensitiser bound to the titanium dioxide surface (Figure 1.7). The dye must have an excited state that is accessible through excitation by visible light, and of sufficient energy to inject electrons into the TiO_2 conduction band.[23, 24] The most successful dyes are based on ruthenium(II) complexes bearing thiocyanate and carboxypolypyridyl ligands, the latter of which provides the means for the complex to bind to the TiO_2 surface (Figure 1.7).[25]

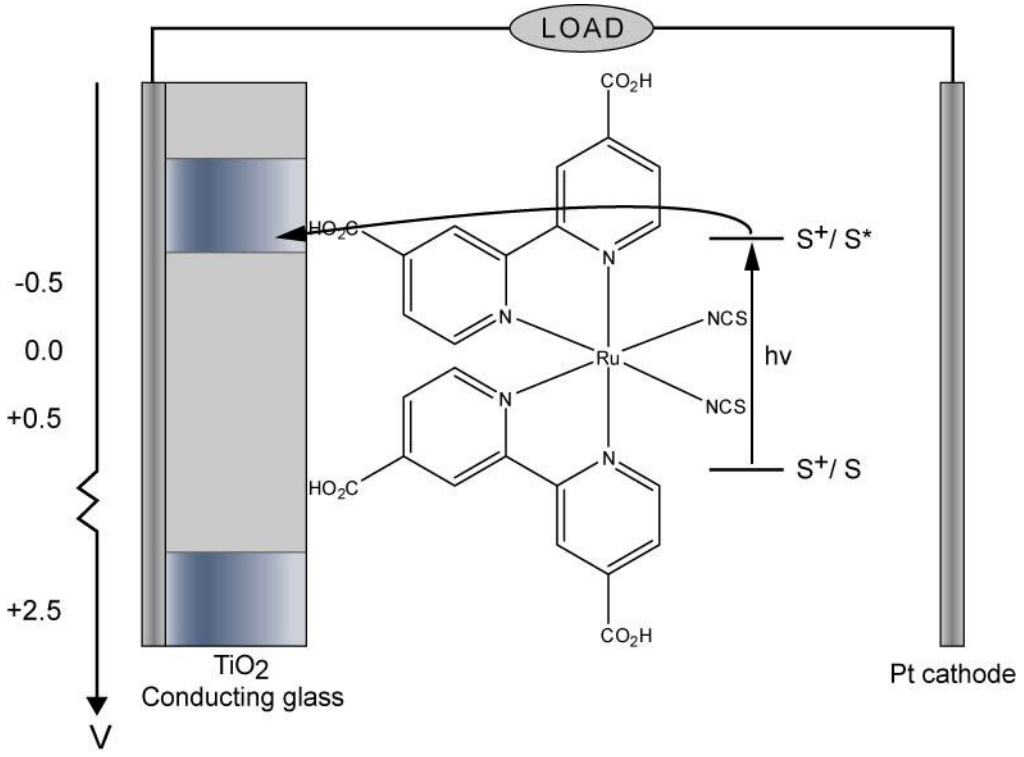

Figure 1.7: Schematic representation of a DSSC with ruthenium based dye (N-3) superimposed.

Phosphonic acids have been shown to bind more strongly to some metals than do carboxylic acids, which has been attributed to the formation of more chemical bonds to the substrate surface.[26, 27] Furthermore, phosphonic acids bearing polar functional groups, such as carboxylate groups, have been demonstrated to present the polar functionality to the solid-vapour interface.[28] The binding of phosphonic acids has been studied on metals such as aluminium,[26, 27] iron[29] and brass,[30] and metal oxides of aluminium,[26, 27] iron[26, 27] and

titanium.[31] An alkylphosphonic acid may bind in a mono-, bi-, or tridentate fashion (Figure 1.8). The measured FTIR spectrum of an alkylphosphonic acid bound to aluminium substrate did not show a band for the P=O bond, suggesting tridentate binding is most favourable in this case.[32]

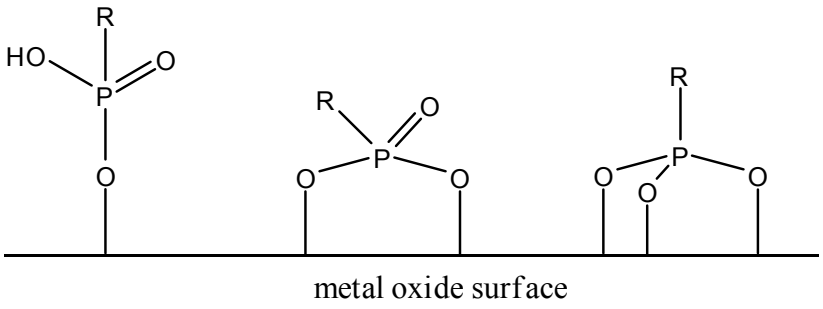

Figure 1.8: Possible modes of binding of an alkylphosphonic acid to a metal oxide surface.

1.2. Corrosion

An important application of surface engineering is the prevention of corrosion.[3] Corrosion of metallic surfaces is very costly and has a large impact on the economy of developed nations. It was estimated in 2001 that the annual cost of corrosion to the economy in the USA was $276 billion in 1998, which equated to 3.1% of its GDP.[33]

Corrosion is a reaction between a material and its environment that results in a deterioration of that material and its properties. The word corrode is derived from the Latin *corrodere*, which means 'to gnaw to pieces'.[34] Most metals are found in nature in combination with other elements as minerals. Corrosion is one process by which the metal returns to a form that is more thermodynamically stable under the conditions to which it is exposed. The energy released is roughly equivalent to that required to extract the metal from its ore.[34, 35] All metals corrode, but the rate is so slow in bronze, brass, zinc, pure aluminium and some stainless steels that protection is not needed for long service lifetimes. However, without protection, corrosion proceeds very rapidly on structural cast iron and steel, and some aluminium alloys.[3]

Most corrosion involves electrochemical reactions in aqueous solution. The corroding metal is oxidised from its zero valence state to a positively charged cation. This is accompanied by the reduction of some other species at an electrically connected location.

Consider the corrosion of iron by hydrochloric acid (1.1):

$$Fe + 2HCl \rightarrow FeCl_2 + H_2 \quad \textbf{(1.1)}$$

This can be separated into the component oxidation and reduction half equations.

$$Fe \rightarrow Fe^{2+} + 2e^- \text{ (anodic reaction)} \quad \textbf{(1.2)}$$

$$2H^+ + 2e^- \rightarrow H_2 \text{ (cathodic reaction)} \quad \textbf{(1.3)}$$

The iron metal is oxidised to the more stable iron(II) ion. The electrons generated by this reaction are consumed by the reduction of hydrogen ions to gaseous hydrogen. The general form of the anodic reaction is shown in Equation (1.4):

$$M \rightarrow M^{n+} + ne^- \quad \textbf{(1.4)}$$

The reduction of hydrogen ions to give gaseous hydrogen (1.3) is by far the most common cathodic reaction. Others include the reduction of Fe^{3+} or Sn^{4+} ions, and the reduction of water in neutral and acidic conditions (Equations (1.5) and (1.6), respectively).

$$O_2 + 2H_2O + 4e^- \rightarrow 4OH^- \quad \textbf{(1.5)}$$

$$O_2 + 4H^+ + 4e^- \rightarrow 2H_2O \quad \textbf{(1.6)}$$

If Equation (1.3) is supplied with electrons at a greater rate than it can consume them, the surface will accumulate a negative potential, known as cathodic polarisation. Similarly, if Equation (1.2) is deficient in electrons, a positive potential will accumulate, known as anodic polarisation. For any pair of cathodic and anodic reactions, there will be a potential at which the two reactions proceed at equal rate. This is known as the corrosion potential and is given the symbol E_{corr}.

If the surface potential is raised above the corrosion potential, that is, the surface is anodically polarised, the rate of corrosion increases, as shown in Figure 1.9. Conversely, cathodic polarisation of the surface results in a decrease in the rate of corrosion, and is sometimes used as a method of corrosion protection.[34]

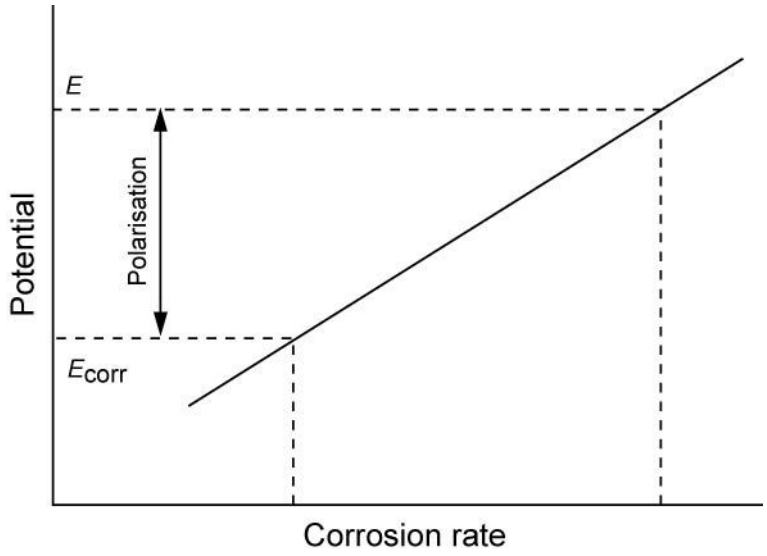

Figure 1.9: Variation of corrosion rate as a function of surface potential. Anodic polarisation (shown with dotted lines) results in an increase in corrosion rate, whereas cathodic polarisation slows corrosion.

1.2.1. Types of corrosion

Corrosion can be divided into different groups based on the mechanism or appearance of the corrosion. These are uniform or general corrosion, galvanic corrosion, pitting corrosion, crevice corrosion, erosion-corrosion, dealloying, intergranular corrosion and environmentally induced cracking.[34, 35]

Uniform corrosion accounts for the greatest loss of material by mass of all forms of corrosion. It is caused by many local corrosion cells acting over the surface at one time. Because the anodic and cathodic regions move about the surface, the net effect is uniform corrosion across the surface. The surface must have equal exposure to the environment and be unvarying in order for this type of corrosion to occur. Common examples are atmospheric corrosion, especially in polluted environments, and exposure to soil or chemicals.

Galvanic corrosion occurs when two dissimilar metals or alloys are electrically coupled in the same corrosive electrolyte. The two different materials will have a characteristic E_{corr} in this electrolyte, and the difference in potential creates a local corrosion cell, in which the metal or alloy with the less positive corrosion potential (termed active) acts as the anode, and is therefore corroded (Figure 1.10).

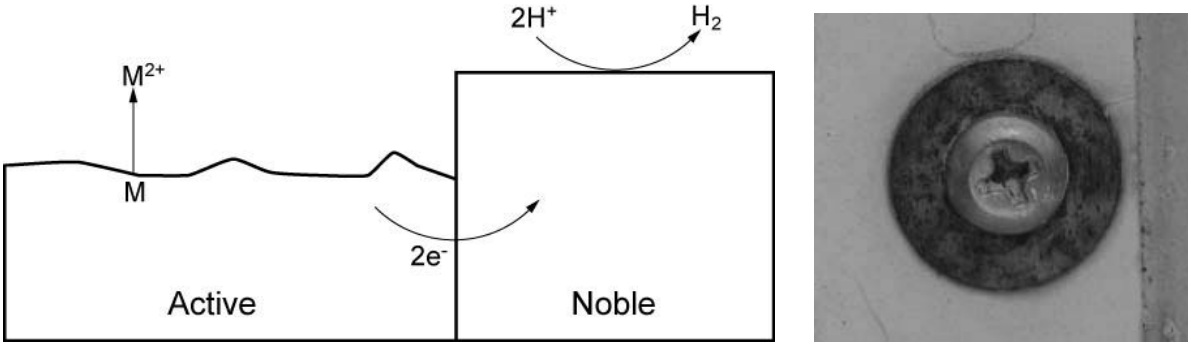

Figure 1.10: Left: Schematic showing galvanic corrosion. The more noble metal acts as a cathode, the less noble (active) metal corrodes. Right: Galvanic corrosion of a cadmium coated washer in contact with a stainless steel screw.[36]

The extent of the corrosion is dependent on, amongst other things, the potential difference between the substrates. Galvanic corrosion can be utilised as a method of corrosion control, as can be seen in the use of zinc coated (galvanized) steel. The zinc coating corrodes preferentially to the more noble steel substrate, which protects the bulk steel, even in the event of the steel being exposed by mechanical processes.

Pitting is a type of localised cell corrosion that is predominantly responsible for the failure of iron and steel water related structures, such as boilers and radiators. It occurs when the cathodic region is large in comparison to the corroding anode (Figure 1.11). An example of this situation is at a nick or other failure in the passive layer on stainless steels, where the bulk metal oxide passive layer acts as a cathode to the small area of exposed metal. Stainless steels are particularly susceptible to pitting corrosion due to their reliance on passive layers for their corrosion resistance (see Section 1.4.1).

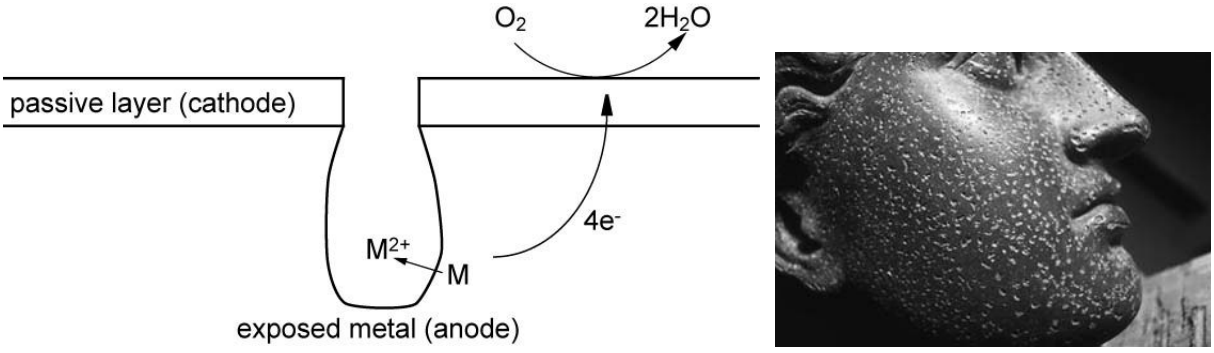

Figure 1.11: Left: Schematic showing pitting corrosion. The large surface area cathode (the passive layer) causes extensive corrosion in the smaller exposed metal anode. Right: Pitting corrosion on the surface of a zinc sculpture.[37]

Crevice corrosion is related to pitting, occurring in the small gaps between a metal, or

alloy, and another material with which it is in contact. The electrolyte within the crevice becomes oxygen starved while oxygen remains more plentiful in the bulk solution. This results in a concentration cell in which the material within the crevice acts as the anode and the exterior the cathode (Figure 1.12). Crevice corrosion may also be compounded by galvanic coupling between the two components in contact.

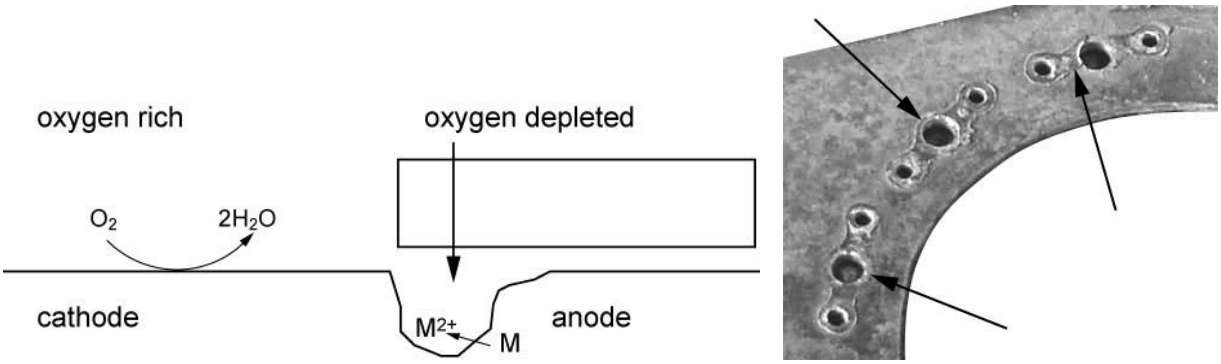

Figure 1.12: Left: Schematic showing crevice corrosion. The concentration cell formed between the oxygen depleted solution in the crevice and the oxygen rich solution outside causes corrosion under the object. Right: Crevice corrosion visible on an aircraft panel (shown with arrows).[38]

Erosion-corrosion is an increase in the rate of corrosion due to the effects of abrasion or wear. A corrosive solution moving over a substrate at high velocity will cause it to corrode more quickly than the same solution moving at a slower rate. The fast moving solution both physically erodes the surface, and also causes the removal of corrosion products, increasing the exposure of the substrate to the corrosive solution (Figure 1.13).

Figure 1.13: Erosion-corrosion on an oil-field check valve. The high velocity flow of corrosive solution leaves distinctive grooves.[39]

The microstructure of metals and alloys consists of crystalline grains separated by amorphous intergranular boundaries. Intergranular corrosion is the selective dissolution of the boundary between grains while leaving the grains themselves intact (Figure 1.14). This is caused by a potential difference between the grain and the boundaries which may be rich in alloying elements, precipitates or impurities in the alloy.

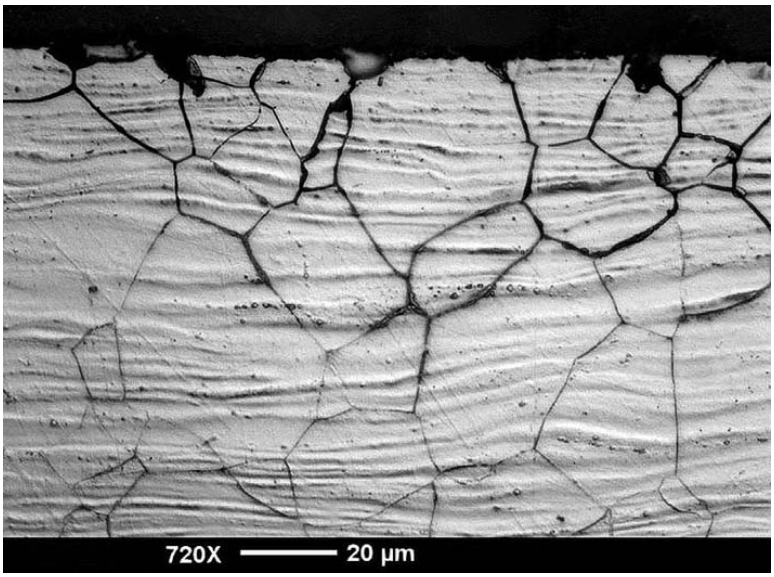

Figure 1.14: Intergranular corrosion attack in austenitic cold rolled stainless steel sheet.

Dealloying is the selective dissolution of the more active metal from an alloy, leaving behind a weak and porous structure of the more noble metal. This is also often referred to as selective leaching or parting corrosion. It may also be referred to by the element that is dissolving, such as dezincification for the removal of zinc from brass (Figure 1.15), or destannification for the removal of tin from bronze.

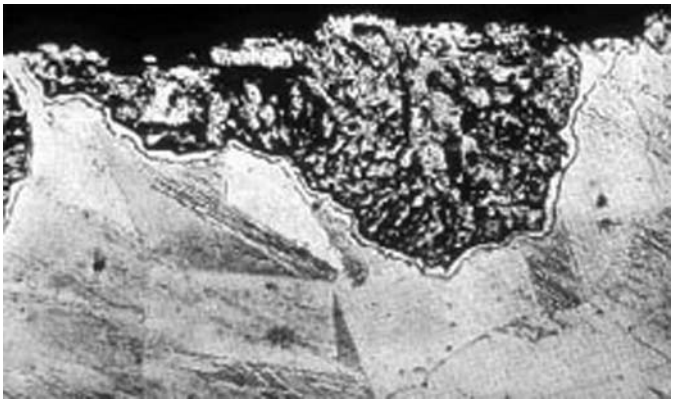

Figure 1.15: Dealloying of brass leaving a porous copper deposit on the surface.[40]

Environmentally induced cracking refers to corrosion that is enhanced by environmental factors such as tensile stress or the diffusion of hydrogen gas from cathodic reactions into the metal lattice.[34, 35]

1.3. Chromium

Chromium is extensively used for protection against corrosion. This includes its use as an ingredient in corrosion resistant alloys, as a metallic plating, and in chemical conversion coatings.

Chromium was discovered in the late eighteenth century. In 1797, French chemist Nicholas-Louis Vauquelin isolated an oxide of chromium from a Siberian mineral that is now known as crocoite, $PbCrO_4$ (Figure 1.16). He subsequently isolated metallic chromium by heating this oxide with charcoal. The name is derived from the Greek *chroma*, meaning colour, for the many coloured compounds of chromium.[41, 42]

Figure 1.16: Crocoite ($PbCrO_4$) from Red Lead Mine, Tasmania, Australia (photo: Eric Hunt).

The earth's crust comprises 122 ppm chromium, but it rarely occurs as free metal in nature due to a strong reaction with oxygen. It is an important ingredient in many mineral colours, being responsible for the colour of crocoite (Figure 1.16) and also for that of emerald, ruby, and some sapphires, amongst others. The primary commercial source of chromium is chromite ($FeCr_2O_4$), with crocoite ($PbCrO_4$) and chrome ochre (Cr_2O_3) being less plentiful resources.[41, 42]

Chromium metal can be obtained by oxidation of chromite by air in the presence of

sodium carbonate to give Na_2CrO_4, which is precipitated and reduced to Cr_2O_3 with carbon. Reduction of Cr_2O_3 with aluminium or silicon produces metallic chromium (1.7):[41-43]

$$Cr_2O_3 + 2Al \rightarrow 2Cr + Al_2O_3$$
$$2Cr_2O_3 + 3Si \rightarrow 4Cr + 3SiO_2 \quad \textbf{(1.7)}$$

Alternatively, reduction of chromite with coke in an electric arc furnace produces ferrochrome, an alloy used directly as an additive to make stainless steels.[41, 42]

Chromium belongs to Group 6 of the periodic table, has a ground state electron configuration of $[Ar]3d^5 4s^1$ and can exist in oxidation states -2 to +6.[44] However, only the 0, 3+ and 6+ oxidation states occur naturally.[45] Some aspects of the chemistry of the 6+ and 3+ oxidation states of chromium will be outlined in the following sections.

1.3.1. Chromium(VI)

The compounds of chromium(VI) include CrO_3, $CrOX_4$ (X = F, Cl), CrO_2X_2, CrO_3X^- (X = F, Cl, Br, I) and the chromium oxyions $Cr_nO_{3n+1}^{2-}$ (n = 1 – 4) including the common anions chromate (CrO_4^{2-}) and dichromate ($Cr_2O_7^{2-}$).[43] Chromium(VI) is strongly oxidizing:

$$\tfrac{1}{2}Cr_2O_7^{2-} + 7H^+ + 3e^- \rightleftharpoons Cr^{3+} + 3\tfrac{1}{2}H_2O; \quad E^\circ = 1.33 \text{ V} \quad \textbf{(1.8)}$$

Chromium in the 6+ oxidation state is a suspected carcinogen. Although the precise mechanism of chromium(VI) carcinogenicity is not known, it is thought that chromium(V) and/or chromium(IV) species play an important role. This is supported by the observation that chromium(VI) compounds are unreactive towards DNA in the absence of reducing agents, while some chromium(V) and chromium(IV) species are able to cause DNA damage under a range of conditions.[46] Possible exposure pathways include drinking contaminated water, entrance through breaks in the skin, inhalation through industrial processes such as welding, cutting and heating of chromium-containing alloys. Ingestion is not considered a major exposure route as chromium(VI) is rapidly reduced by gastric juices and blood.[47]

Common environmental reductants, such as ferrous iron and organic material, can transform chromium(VI) to chromium(III), but manganese oxides are the only inorganic oxidants found in the environment that cause the rapid oxidation of chromium(III) to chromium(VI).[48] Measurement of the kinetics of chromium transformations under typical

environmental conditions found that reaction rates for the oxidation of chromium(III) to chromium(VI) tend to be relatively slow, with $t_{½}$ in the order of years, but rates for the conversion of chromium(VI) to chromium(III) tend to be very rapid, with $t_{½}$ ranging from instantaneous to the order of days.[49]

1.3.2. Chromium(III)

Chromium(III) forms complexes with almost any species capable of donating an electron pair.[41] Complexes of chromium(III) are mostly six coordinate and octahedral, although complexes with higher coordination numbers are known.[50] These complexes are noted for their kinetic inertness, with half times for ligand substitution or rearrangement in the order of hours. This is due to the half filled t_{2g} level arising from an octahedral d^3 formation, which is resistant to distortions leading to either five or seven coordinate intermediates required for substitution reactions.[51] Measurements of the water exchange between hydrated cations and solvent showed the half reaction time for $[Cr(H_2O)_6]^{3+}$ was around 40 hours.[52] Furthermore, related work on the rate of exchange of $[Cr(NH_3)_6]^{3+}$ in ammonia solvent led to similar conclusions.[53]

Chromium(III) aqua complexes characteristically polymerise to form polynuclear complexes containing OH^- bridges in a process known as olation.[54-57] The hydrolysis of the hexaaquachromium(III) ion was first reported by Bjerrum in 1908.[58] It is thought to proceed by deprotonation of a water ligand to OH^-, followed by coordination of this OH^- ligand to a second cationic centre (Figure 1.17).[41]

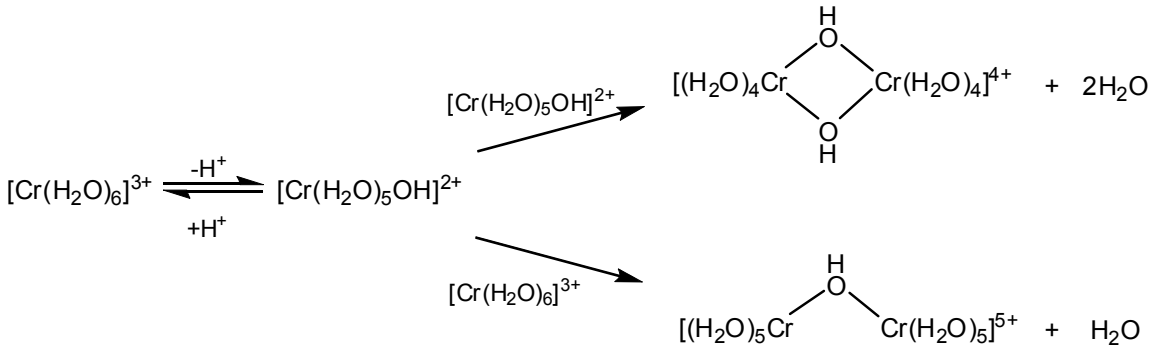

Figure 1.17: Deprotonation and polymerisation of $[Cr(H_2O)_6]^{3+}$ to form multinuclear OH^- bridged complexes.

Polynuclear chromium complexes are commercially important to the dying and tanning

industry. In dying it is used as a mordant to fix the dye, and in tanning it has replaced tannin as the product to crosslink the neighbouring protein chains.[41, 59] The distance between fibres varies from 10 Å to 17 Å, which makes bridging by polynuclear chromium complexes more likely than by single chromium atoms. Coordination to chromium is via aspartic acid or glutamic acid residues. Cross linking of fibres can occur by coordination of a carboxylate group to a chromium complex that is already bound to another fibre (Figure 1.18 – A) or by olation between chromium complexes on two different fibres (Figure 1.18 – B).[60]

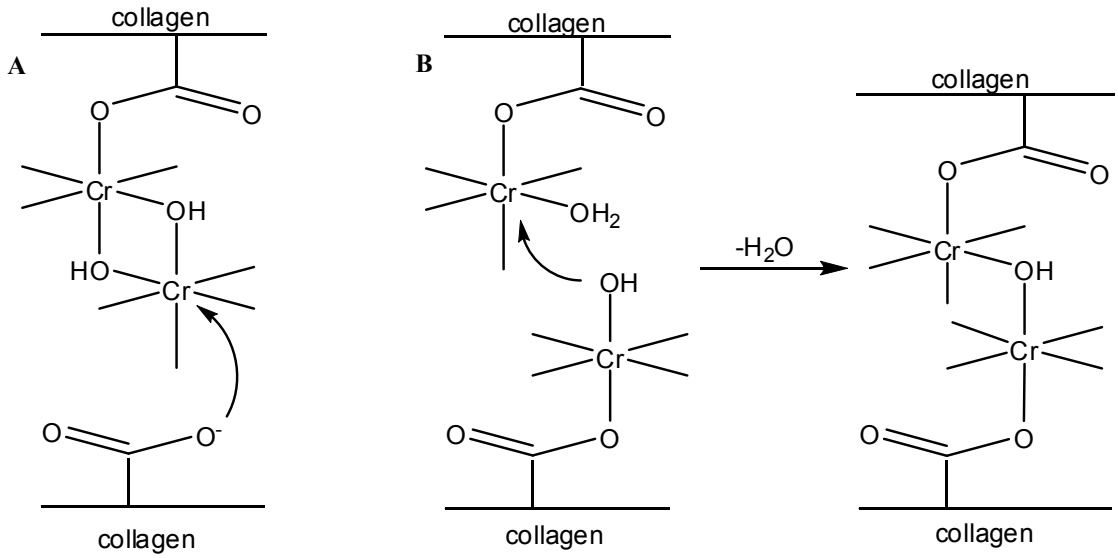

Figure 1.18: Two possible routes to crosslink collagen fibres by polynuclear chromium complexes in leather tanning. A: Coordination of a carboxylate to a bound chromium complex, B: Olation between two chromium complexes on different fibres. The simplified diagrams employed are not meant to imply any specific reaction mechanism.

1.4. Use of chromium in corrosion prevention

1.4.1. Iron – chromium alloys

The superior corrosion resistance of stainless steels is due to the incorporation of chromium into the thin surface film, the nature of which is dependent on the method of passivation and the chromium content of the alloy.[61] Prior to anodic passivation, there is usually cathodic removal of the natural air-formed oxide, which is a mixture of iron and chromium oxides in a ratio similar to the alloy.[61-63] The anodically formed film has been estimated, by XPS and AES, to be 1 – 3 nm thick, and is enriched in chromium relative to the alloy substrate.[61-64] It has been suggested that the film forms a double layer after a certain

period of anodic passivation, consisting of an inner layer comprising a mixture of iron(III) and chromium(III) species, and an outer layer that is almost exclusively chromium(III) species.[63, 64] The preferential dissolution of iron(II) species over the more stable chromium(III) species leads to the formation of a chromium-enriched protective outer coating.[62-64] The nature of the chromium in the protective layer was previously thought to be Cr_2O_3, based on interpretation of XPS and AES results.[61, 63, 64] However, XAS experiments suggest the chromium is in an environment more like that of $Cr(OH)_3$ – that is, CrO_6 octahedra linked by hydrogen bonds.[62, 65] The corrosion protection gained by this coating is through a synergistic relationship between the iron and chromium species. The chromium protects against dissolution of iron at cathodic polarisation. Iron is reduced to iron(II) and dissolves, but chromium(III) remains, forming a protective barrier against further iron dissolution. Similarly, under anodic polarisation iron may protect against dissolution of chromium(VI) species.[62] However, the oxidation of chromium(III) to chromium(VI) is slow compared to the oxidation of chromium(0) to chromium(III) so there is most likely always chromium(III) species at the surface.[66]

1.4.2. Chrome plating

The electroplating of chromium onto the surface of other metals can be divided into decorative chrome plating and industrial hard chrome plating. Chrome plating for decorative purposes involves deposition of a thin layer of chromium which rarely exceeds 1.3 μm, while industrial hard chrome, used to reduce friction and impart corrosion and wear resistance, requires a much thicker layer of 2.5 – 500 μm.[2] In both cases the plating usually utilises a bath of chromium(VI) anions with a sulfuric acid catalyst. Decorative chromium is sometimes deposited from baths containing chromium(III). The process of chrome electroplating poses several health and environmental hazards due to the use of chromium(VI). Of particular concern is exposure to chromium(VI) mist formed due to the bursting of hydrogen and oxygen bubbles formed during the plating process.[67]

1.4.3. Chromate anodisation

1.4.3.1. Iron

Passivation of iron in chromate containing solutions also imparts improved corrosion resistance. The surface film incorporates chromium from the solution, with the amount incorporated increasing with longer exposure time.[68] As with iron-chromium alloys, there is a double layer, with an inner layer comprising both iron and chromium, and an outer layer made up predominantly of insoluble chromium.[68, 69] XAS and ellipsometric measurements suggest this chromium over-layer has a $Cr(OH)_3$ like structure,[65, 70] and its thickness, estimated by XPS, is 1 – 1.5 nm.[68] The formation of the layer proceeds with a direct relationship between the oxidation of iron and the reduction of chromate.[70] Iron dissolves as $Fe(OH)_2$ and then is oxidized to $Fe(OH)_3$ as chromium(VI) is reduced to $Cr(OH)_3$. A study of the corrosion resistance of chromate passivated iron electrodes in chromate free solution showed that films formed at open-circuit potential were much more susceptible to oxidative and reductive dissolution than those formed by potentiostatic cycling.[71] A possible explanation for this is that the constant dissolution and re-uptake of the iron and chromium hydroxide species leads to the formation of a coating of optimum composition for protection of each metal by the other. Using artificial mixed chromium/iron oxides, it has been shown that at an appropriate Fe/Cr ratio, neither cathodic nor anodic dissolution occurs, although both iron and chromium are electroactive within the solid. This ratio is dependent on the nature of the solution to which the oxide is exposed.[72]

1.4.3.2. Aluminium

When aluminium is anodised in chromate solution, the formed oxide layer contains chromium taken up from the chromate solution.[10, 73] Chromium exists in the layer as both chromium(VI) and chromium(III), the former being located in the outermost part of the coating, possibly as a monolayer of adsorbed chromate, and the latter within the outer 3 nm. XANES analysis suggests the chromium(III) is of a $Cr(OH)_3$ like nature, and may be incorporated by adsorption of chromium(VI) species at the growing oxide-electrolyte interface.[10]

1.4.4. Chromate conversion coatings

Many metals and metal alloys, notably aluminium and its alloys, can be treated through the use of a chromate conversion coating (CCC).[74] Despite the superior corrosion resistance of anodisation, chromate conversion coatings, formed by the chemical growth of a barrier layer, are more commonly used due to them being much cheaper to produce.[7] A chromate conversion coating is formed by immersing the metal in a bath containing chromic acid or a soluble chromate or dichromate salt, along with either hydroxide or fluoride.[75] The fluoride removes the 6 – 8 nm thick layer of alumina from the aluminium surface until it is sufficiently thin that electrons may tunnel across and reduce the chromate species.[75, 76] The overall reaction is shown in Equation (1.9).[77, 78]

$$2Al + Cr_2O_7^{2-} + 8H^+ \rightleftharpoons 2Cr(OH)_3 + 2Al^{3+} + H_2O \quad \textbf{(1.9)}$$

However, the chromate species is not directly reduced by the aluminium. The bath also includes a reaction accelerator, normally $Fe(CN)_6^{3-}$, which acts as an intermediate, being reduced by Al to $Fe(CN)_6^{4-}$, which then is oxidised back to $Fe(CN)_6^{3-}$ by the reduction of the chromate species to chromium(III).[79, 80] The high concentration of chromium(III) species at the surface leads to the formation of polymeric chromium species and the deposition of an insoluble layer at the surface.[6, 54, 57]

Using XPS data, the conversion coating was shown to comprise mainly chromium and oxygen, with a small amount of residual reaction accelerator.[81] AES data shows the thickness of the layer varies from 70 – 750 nm, depending on the alloy and the treatment time.[75, 81] The chromium is present as both chromium(VI) and chromium(III), with the amount of chromium(VI) being 20 – 30% of the total chromium present,[75, 81, 82] and XANES has been used to show that the chromium(III) is in a similar environment to $[Cr(H_2O)_6]^{3+}$.[81]

The effectiveness of chromate conversion coatings as protection against corrosion stems not only from the formation of a barrier coating, but also from its ability to store and release chromium(VI) compounds, themselves potent corrosion inhibitors.[6] Upon exposure to water, chromate conversion coatings release chromium(VI) species, the exact nature of which is dependent on pH.[78] Monitoring of a conversion coating in water by UV-visible spectroscopy showed that the concentration of chromium(VI) in solution increased with time and eventually

reached an equilibrium value.[83] The equilibrium concentration was higher if a larger area to volume ratio was used, the coating was not aged or a NaCl solution was used in place of ultra pure water. Similar behaviour was seen by an artificial chromium(III)/chromium(VI) mixed oxide. Furthermore, when $Cr(OH)_3$ was immersed in a chromate solution, the chromium(VI) concentration decreased to an equilibrium value.[83] The relative amount of chromate in solution compared with that in the solid matrix has been shown to have a dependence on pH,[83] and the release of chromate from a conversion coating has been observed to be accompanied by the release of an approximately equivalent amount of H^+.[82] A possible mechanism for the storage and release of chromate from conversion coatings is shown in Figure 1.19. The existence of the Cr(III)-O-Cr(VI) bond is consistent with spectroscopic data.[82]

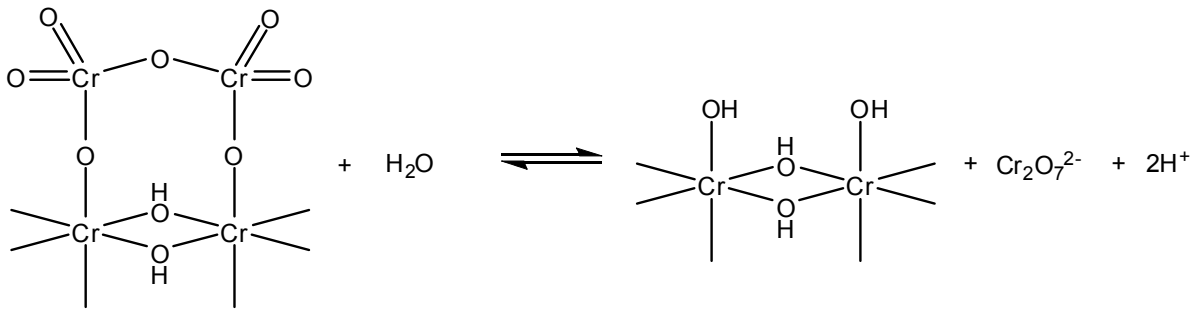

Figure 1.19: Proposed mechanism for storage and release of chromium(VI) in a CCC.

Chromates are thought to act as active corrosion inhibitors by preventing both open-circuit corrosion and the cathodic reduction of oxygen.[84, 85] Separate measurement of the cathodic and anodic curves showed a significant decrease in the reduction of oxygen on addition of as little as 1 mM $Cr_2O_7^{2-}$.[86] This inhibition is accompanied by a current equal to that of formation of a monolayer of chromium(III).[87] While evidence suggests the observed inhibition is not due to the formation of a large three-dimensional network such as seen in the bulk treatment,[88] this monolayer of chromium(III) species may provide a barrier against oxidation of the metal surface by oxygen.

1.5. Cobalt

The ores of cobalt have been used for thousands of years as a blue colouration for pottery and glass. However, the source of the colour was not known until Georg Brandt

isolated a crude sample of cobalt metal in 1735. The new element was named for the German *kobold*, meaning goblin. This is because cobalt is obtained from arsenite and sulfide ores as a by-product of the mining of other metals, particularly nickel. Early European miners found that smelting of these ores would not only fail to give the expected metal, but also produce highly toxic fumes. This was blamed on the behaviour of spiteful goblins. Today, the pure metal is isolated from its ores using solvent extraction-electrowinning techniques. The terrestrial abundance of cobalt is 29 ppm, making it the second rarest first row transition metal, after scandium.[41, 89]

Cobalt belongs to Group 9 of the periodic table and has a ground state electron configuration of [Ar]$3d^7 4s^2$. The most important oxidation states are 2+ and 3+.

1.5.1. Cobalt(III)

Simple salts of cobalt(III) are rare, as the ion $[Co(H_2O)_6]^{3+}$ is strongly oxidising, and rapidly reacts with water to evolve oxygen.

$$[Co(H_2O)_6]^{3+} + e^- \rightleftharpoons [Co(H_2O)_6]^{2+};\ E^\circ = 1.83\ V \quad \textbf{(1.10)}$$

In contrast, there are many coordination complexes of cobalt(III), particularly of nitrogen donor ligands. Like those of chromium(III), complexes of cobalt(III) are mostly six coordinate, octahedral and kinetically inert. In the case of cobalt(III) complexes, this is due to their being low spin which results in a high crystal field stabilisation energy associated with the filled t_{2g} level. Furthermore, the rates of aquation of pentaammine complexes for both cobalt(III) and chromium(III) are very slow (Table 1.1).[90]

Table 1.1: Rate constants for aquation of complexes $[M(NH_3)_5(OH_2)]^{3+}$.[90]

	Rate constant (s^{-1})
$[Co(NH_3)_5(OH_2)]^{3+}$	5.7×10^{-6}
$[Cr(NH_3)_5(OH_2)]^{3+}$	6.1×10^{-5}

In a further similarity to chromium(III), cobalt(III) is also known for the formation of hydroxo bridged polynuclear complexes by the hydrolysis of aqua complexes.[58]

Cobalt(III) complexes played an important role in the genesis of coordination chemistry.

By application of the theory of fixed valence, chemists such as Jørgenson proposed a structure for $CoCl_3.6NH_3$ (Figure 1.20 – A). Alfred Werner proposed the alternate structure of a single cobalt atom surrounded by six ammonia molecules (Figure 1.20 – B), which is known today to be the correct structure.

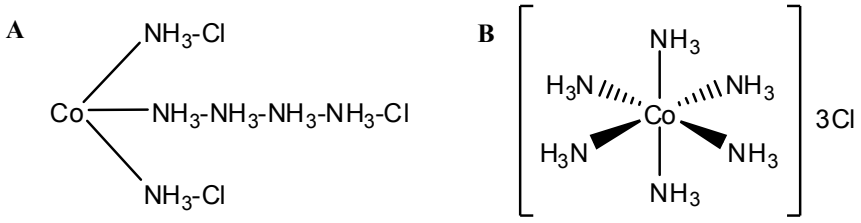

Figure 1.20: Jørgenson's (A) and Werner's (B) proposals for the structure of $CoCl_3.6NH_3$.

Werner also demonstrated the first example of optical isomerism at a centre other than carbon. This was done by synthesis and resolution of a tetranuclear hydroxo-bridged cobalt complex he called hexol (Figure 1.21).[91]

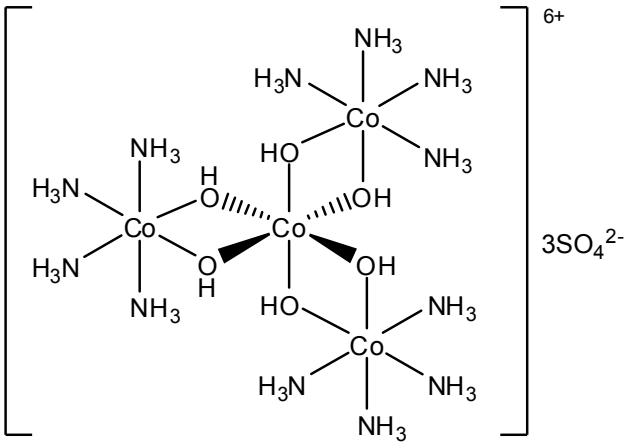

Figure 1.21: One enantiomer of the hexol compound.

1.6. Hypothesis

Metal surfaces treated with chromium based species show improved resistance to corrosion. This appears to be due to the formation of a three-dimensional network of chromium(III) species at the surface. This provides a barrier layer against the permeation of corrosive species which, due to the slow dissolution rate of chromium(III) species, is not easily removed. Given that cobalt(III) is also able to form hydroxo-bridged species, it seems likely that cobalt(III) complexes could bind to metal oxide surfaces using similar linkages. The kinetic inertness of cobalt(III) species may lead to similar behaviour of the bound species as

seen in chromium(III) based layers. It is proposed that the oxide and/or hydroxide functionalities at the surface of a metal oxide/hydroxide could act as ligands for cobalt(III) complexes. Some possible modes of coordination of a cobalt complex to a metal oxide surface are shown in Figure 1.22. The CoL_6 octahedron could share a face, edge or corner with the surface.

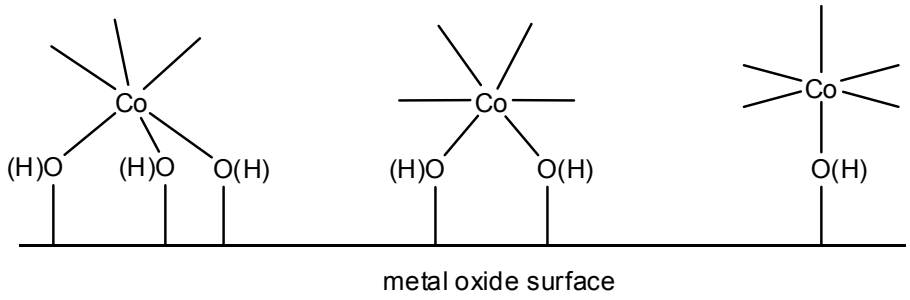

Figure 1.22: Possible modes of a cobalt octahedron binding to a metal oxide surface. Face (left), edge (middle) and corner (right).

A cobalt(III) complex bearing exchangeable ligands may bind at a metal oxide surface via exchange of these ligands for the oxide or hydroxide surface functionalities. If the other ligand of the complex was to contain some functionality, this could provide a novel method for chemical modification of a surface.

The use of cobalt as a replacement for chromium in conversion coatings has been explored by several researchers. These generally involve immersion of the substrate in a bath containing cobalt salts and subsequent oxidation to form a thick polymeric layer of cobalt oxide on the surface, similar to those seen in chromate conversion coatings.[92-94]

In order to test whether polyamine cobalt(III) complexes bearing exchangeable ligands are able to bind to metal oxide surfaces, an initial pilot study was carried out by Rachel Cooper at the University of Edinburgh, UK.[27] In this study, the surface binding to goethite of three cobalt(III) complexes bearing zero ($[Co(en)_3]Cl_3$), two (*trans*-$[Co(en)_2Cl_2]Cl$) or three (*mer*-$[Co(dien)Cl_3]$) exchangeable ligands was measured (Figure 1.23).

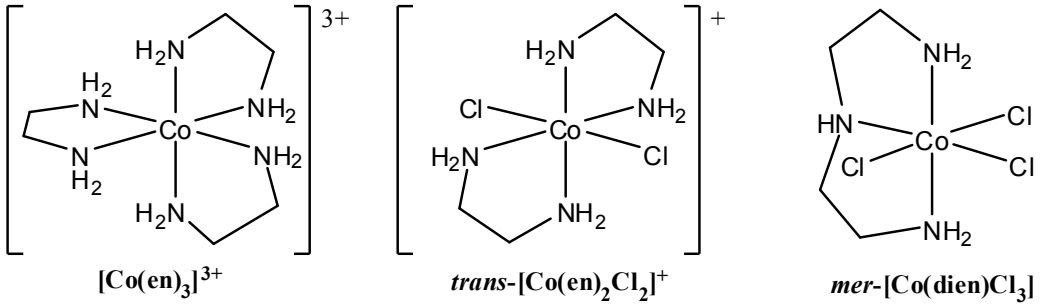

Figure 1.23: Cobalt(III) complexes studied by Cooper.

It would be expected that the complex $[Co(en)_3]Cl_3$, with no exchangeable ligands, would show no binding to the surface. It may be expected that *mer*-$[Co(dien)Cl_3]$, with three exchangeable ligands, would show stronger binding than *trans*-$[Co(en)_2Cl_2]Cl$, with two. The measured adsorption isotherms showed that the complexes *trans*-$[Co(en)_2Cl_2]Cl$ and *mer*-$[Co(dien)Cl_3]$ were adsorbed onto goethite from solution, and that the complex $[Co(en)_3]Cl_3$ was not adsorbed (Figure 1.24).

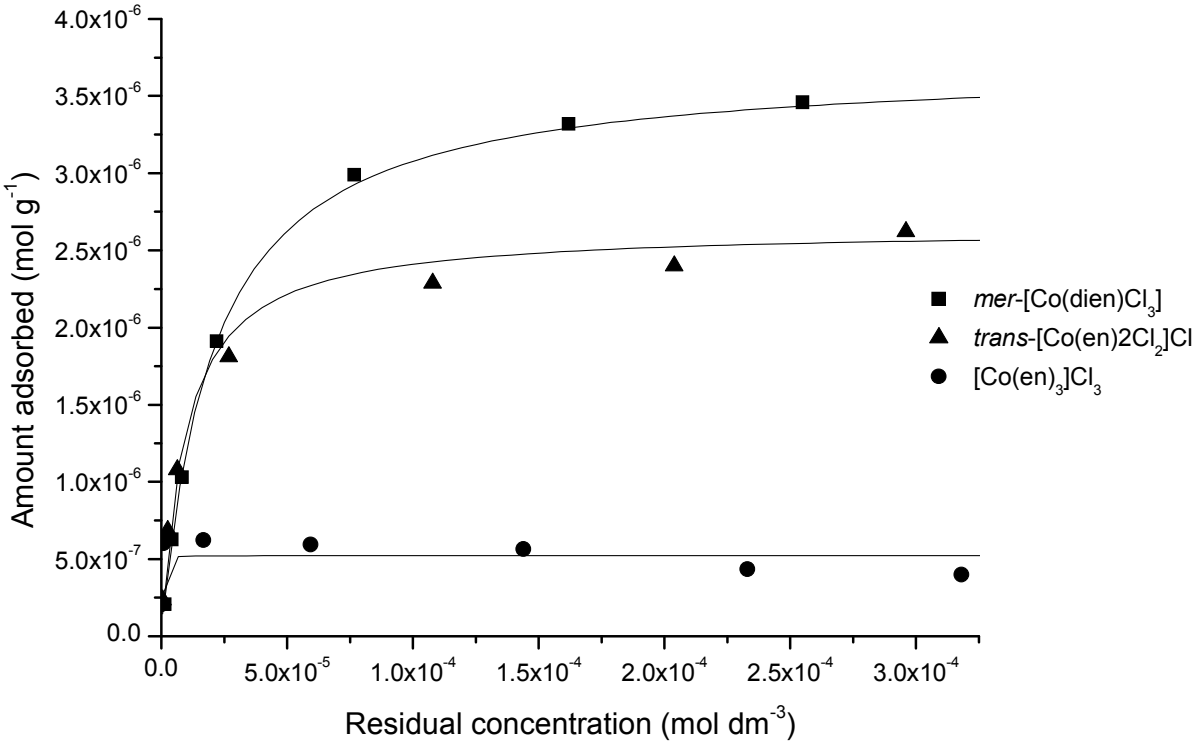

Figure 1.24: Adsorption isotherm of $[Co(en)_3]Cl_3$, *trans*-$[Co(en)_2Cl_2]Cl$, *mer*-$[Co(dien)Cl_3]$.

The adsorption isotherm parameters are tabulated in Table 1.2. The data has been fitted to a Langmuir isotherm model, which yields parameters that can be interpreted as representing the maximum surface coverage of the adsorbate ($[S_{max}]$) and the adsorption equilibrium

constant (K_{ad}). See Section 3.1.3 for a more detailed discussion.

Table 1.2: Adsorption isotherm parameters for Figure 1.24.

Complex	*a* ([S_{max}]) (mol g^{-1})	*b* (K_{ad})
mer-[Co(dien)Cl_3]	3.78 (± 0.08) x 10^{-6}	5.2 (± 0.4) x 10^4
trans-[Co(en)$_2Cl_2$]Cl	2.64 (± 0.09) x 10^{-6}	10.3 (± 2.0) x 10^4
[Co(en)$_3$]Cl_3	0.52 (± 0.04) x 10^{-6}	-

This supports the idea that cobalt(III) complexes bearing exchangeable ligands can bind to the surface of goethite through coordination of the surface oxides and/or hydroxides. The complex [Co(en)$_3$]Cl_3, without any exchangeable ligands, only shows insignificant adsorption to the surface whereas *trans*-[Co(en)$_2Cl_2$]Cl and *mer*-[Co(dien)Cl_3], with two and three, respectively, show Langmuir type binding to the surface. It is not clear whether *mer*-[Co(dien)Cl_3], with three exchangeable ligands, does bind to the surface more strongly than *trans*-[Co(en)$_2Cl_2$]Cl, with two exchangeable ligands, as might be expected. The calculated K_{ad} for *trans*-[Co(en)$_2Cl_2$]Cl is higher (10.3 (± 2.0) x 10^4 c.f. 5.2 (± 0.4) x 10^4), but this may not be representative of the binding process alone. When exposed to the substrate, the complexes may isomerise to the *cis* and *fac* orientations in order to bind in the more favourable orientation.[95, 96] The calculated equilibrium constant may represent the overall equilibrium of both isomerisation and binding processes.

1.6.1. Thesis outline

This thesis describes further studies into the use of cobalt(III) complexes for the surface engineering of ferrous metals. Chapter 2 describes the preparation of complexes of functional ligands designed to modify the surface properties of the substrate. Chapter 3 outlines the binding of some cobalt(III) complexes to the surface of goethite, used as a model for an oxidised iron surface, utilising linkages similar to those seen with chromium treatments. Chapter 4 describes investigations into the binding of some complexes to iron and steel surfaces to investigate potential industrial applications. Chapter 5 explores the use of cobalt(III) complexes as inhibitors of corrosion on iron.

Chapter Two

Cobalt complexes of ligands based on tame (1,1,1-tris(aminomethyl)ethane)

2.1. Introduction

The preliminary research by Cooper into the ability of cobalt(III) complexes with exchangeable ligands to bind to goethite surfaces suggests that the greatest surface coverage is achieved with complexes bearing three exchangeable ligands.[27] It is expected that binding to the surface in a face sharing manner (Figure 2.1 – left) would be more favourable than edge sharing binding (Figure 2.1 – right).

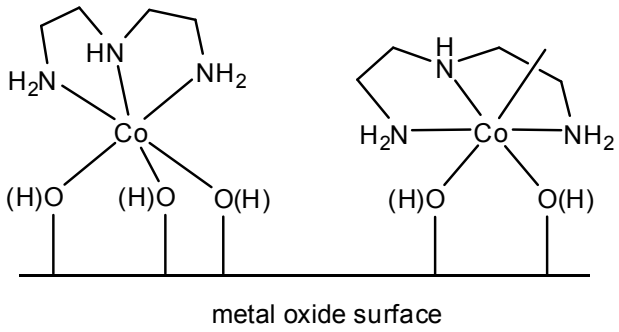

Figure 2.1: Possible modes of $[Co(dien)]^{3+}$ binding to a metal oxide surface.

In order to bind in a face sharing manner, $[Co(dien)Cl_3]$ must first isomerise from the meridional isomer to the facial isomer. This is supported by the observation that the hydrolysis of the complex *mer*-$[Co(dien)Cl_3]$ to $[Co(dien)(OH_2)_3]Cl_3$ is accompanied by an isomerisation to the facial configuration.[96] It was suggested that this isomerisation may affect the overall adsorption equilibrium constant of this complex binding to goethite.

In order to simplify the binding equilibrium, it was proposed that a series of cobalt(III) complexes bearing three exchangeable ligands and a tridentate facially constrained polyamine ligand would be most suitable for binding to metal oxide surfaces. Additionally, the use of C_3 symmetrical ligands would be advantageous, because the metal complexes would be more easily characterised, and should pack on the oxide surface more efficiently.

The widely known ligands 1,4,7-triazacyclononane (tacn) and 1,1,1-tris(aminomethyl)ethane (tame) (Figure 2.2) fulfil these criteria, and are therefore potential parent molecules for a series of functionalised cobalt complexes.

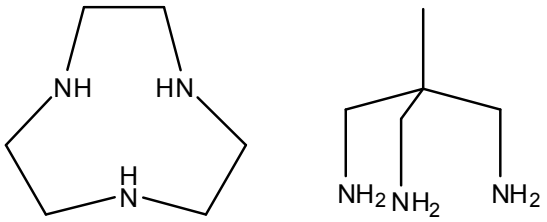

Figure 2.2: The ligands tacn (left) and tame (right).

2.1.1. 1,4,7-Triazacyclononane (tacn)

Many cobalt complexes of the ligand tacn have been reported, including $[Co(tacn)_2]Cl_3$,[97] $[Co(tacn)(NO_2)_3]$,[98] $[Co(tacn)Cl_3]$,[98] $[Co(tacn)(OTf)_3]$,[99] $[Co(tacn)(NH_3)_3]Cl_3$[100] and $[Co(tacn)(OH_2)_3]OTf_3$.[12] In addition, chiral mixed monodentate complexes of the type $[Co(tacn)(NH_3)(a)(b)]^{n+}$, where a and b are different but chosen from CN^-, NO_2^-, SO_3^-, NCS^-, N_3^-, CH_3COO^-, H_2O, OH^-, Cl^- or Br^- have been prepared.[101, 102]

The synthesis of many tacn based ligands and their cobalt complexes has also been reported. Most of the prepared ligands bear functionality at one or more of the amine nitrogen atoms. These include the trisubstituted methyl,[103, 104] ethyl,[104] propyl[104] and benzyl[105] derivatives. There have also been reported ligands bearing only one or two such amine substituents, and ligands of mixed substitution.[19, 104, 106] Ligands bearing groups that are themselves able to coordinate to a metal centre, leading to ligands with denticity greater than three, have also been synthesised.[19, 106, 107] Figure 2.3 shows an example of a cage structure (A)[108] and a binuclear complex of a bridging ligand (B)[109] based on tacn.

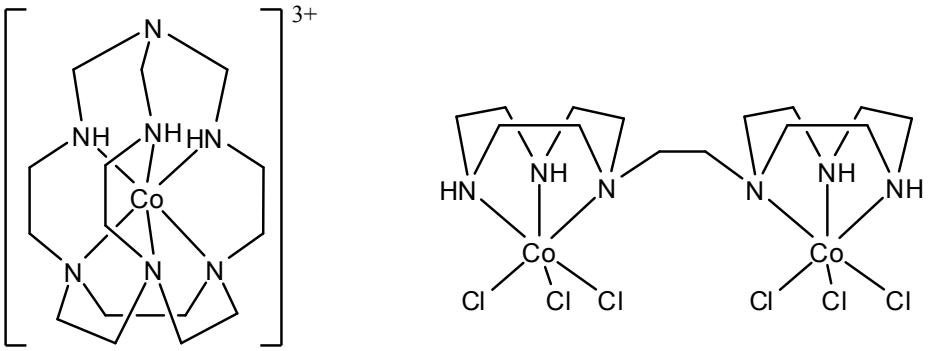

A **B**

Figure 2.3: Examples of cobalt complexes of ligands based on tacn.

In addition, molecules based on tacn featuring substitution at one or more of the methylene carbon atoms have also been synthesised. Derivatives bearing substitution at a

single carbon centre that have been prepared include methyl[110, 111] and benzyl[112, 113] derivatives, and cobalt complexes of the monsubstituted methyl derivative have been reported.[100, 110] Disubstituted molecules featuring methyl and isopropyl functionalisation have also been prepared (Figure 2.4).[114, 115]

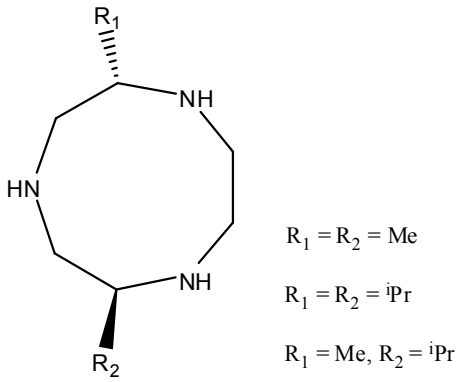

Figure 2.4: Disubstituted tacn derivatives bearing methyl and isopropyl functionalities.

2.1.2. 1,1,1-Tris(aminomethyl)ethane (tame)

Several cobalt complexes of tame have been prepared, including $[Co(tame)_2]Cl_3$[116] and $[Co(tame)Cl_3]$.[117] A series of complexes of the type $[Co(tame)(NH_3)(am)]^{2+}$ where am = glycinate, L-alaninate, L-serinate, L-valinate and L-isoleucinate has been prepared and the different diastereoisomers separated by crystallisation or column chromatography.[118]

Syntheses of several tame based molecules and the metal complexes of some of these ligands have been reported. A series of ligands based on tame has been synthesised in which all three nitrogen atoms have been singly substituted with identical groups. The methyl, ethyl, isopropyl, dimethylsilyl and trimethylsilyl derivatives have been synthesised and their interaction with lithium studied.[119] Like tacn, tame has also been used as the basis for larger, more complex ligands with higher denticity than the parent molecule.[120-122] Figure 2.5 shows a cage structure (A)[122] and a chiral iron complex used in spin crossover studies (B)[120] derived from the tame molecule.

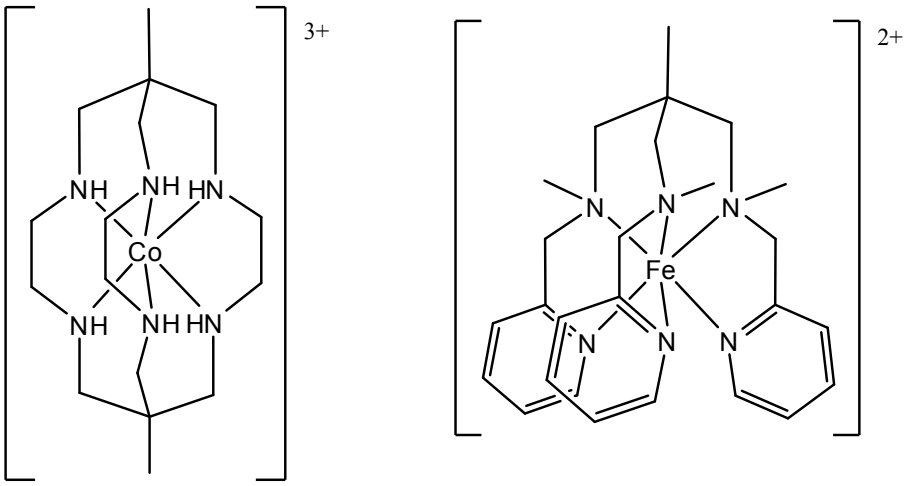

A B

Figure 2.5: Examples of complexes based on the ligand tame.

2.1.3. Choice of parent molecule for a functional ligand series

Figure 2.6 shows the proposed mode of binding of the complex fragments $[Co(tacn)]^{3+}$ and $[Co(tame)]^{3+}$ to a metal oxide surface. In order to effectively functionalise the metal oxide surface, the complex should bear that functionality in a way that projects it away from the surface.

In the case of tame, this would suggest that functionalisation at the methyl group would be most suitable for this purpose; for tacn, functionalisation at the methylene carbon atoms would be better than amine functionalisation.

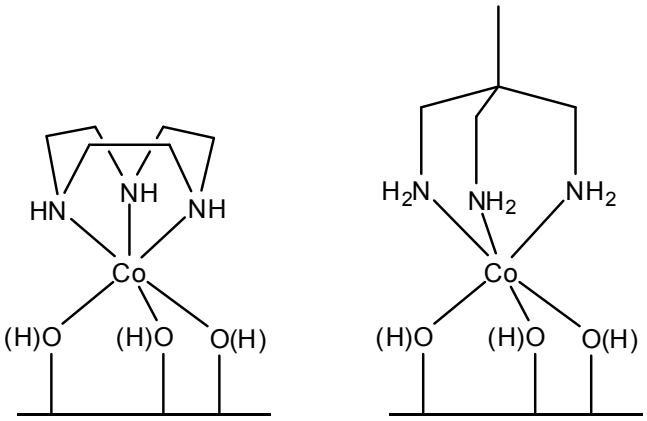

Figure 2.6: Proposed mode of binding of cobalt complexes of tacn and tame to a metal oxide surface.

The most commonly used method to synthesise tacn involves the reaction of a tritosyl

dien derivative with a ditosyl derivative of ethylene glycol (Figure 2.7).[123, 124]

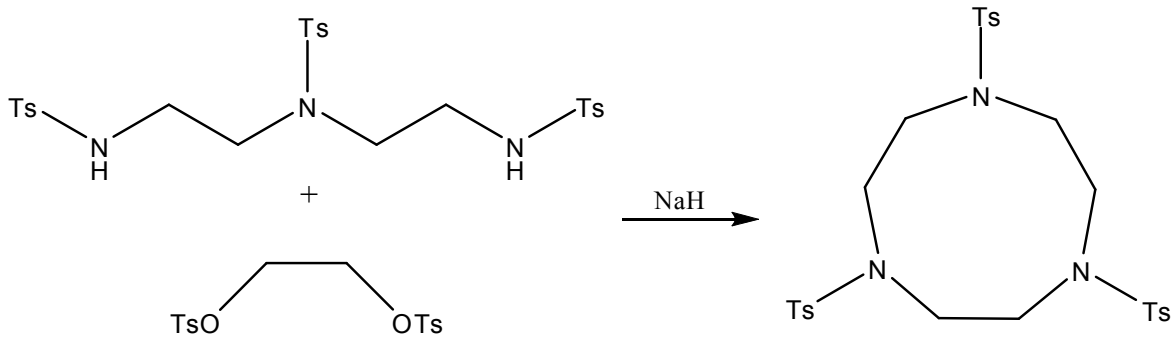

Figure 2.7: Standard synthesis of tacn by Richman-Atkins methodology.

The synthesis of a C_3 symmetrical tacn derivative bearing functionalisation at the methylene carbon atoms would involve the reaction of an unsymmetrical disubstituted dien with an unsymmetrical substituted tosylated ethylene glycol (Figure 2.8). This reaction would also produce the unsymmetrical derivative through the reaction of the two unsymmetrical starting materials in the opposite manner.

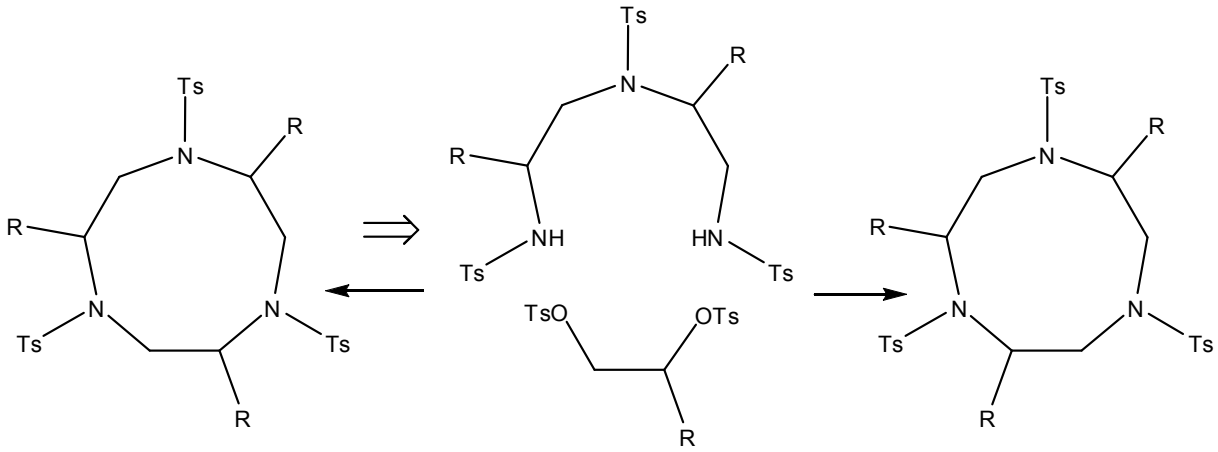

Figure 2.8: Retrosynthetic analysis for an symmetrical trisubstituted tacn derivative.

It would be possible to avoid the problems of regioselectivity outlined above through the use of a hexasubstituted derivative in which the configuration at each methylene carbon atom alternates (Figure 2.9).

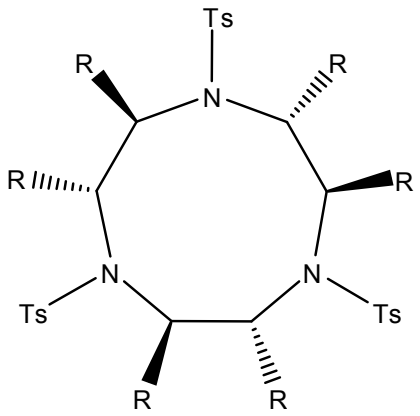

Figure 2.9: Possible substitution pattern for regioselective synthesis of a tacn derivative with C_3 symmetry.

In this case, either of the possible reaction modes produces the same molecule. The requisite substituted dien should also be synthetically accessible for similar reasons. However, the prospect of being able to functionalise tame with a single substitution at the pendant methyl group makes it a much more attractive candidate for this work, and tame was therefore chosen over tacn as the parent structure for a series of functionalised ligands for cobalt.

2.2. Results and Discussion

The following sections outline the synthesis of 1,1,1-tris(aminomethyl)ethane (tame) and its cobalt complexes, followed by the synthesis of functional analogues of tame and their cobalt complexes.

2.2.1. Synthesis of 1,1,1-tris(aminomethyl)ethane (tame)

The ligand 1,1,1-tris(aminomethyl)ethane (tame) can be synthesised from the readily available triol precursor 1,1,1-tris(hydroxymethyl)ethane (Figure 2.10).

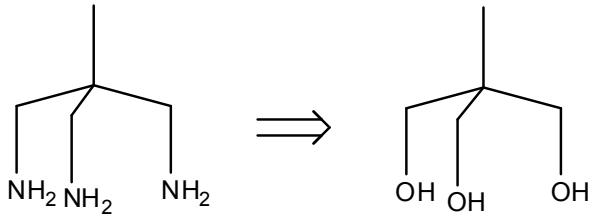

Figure 2.10: The ligand tame can be prepared from its triol equivalent.

This can be approached in two ways. Using a Gabriel Synthesis,[125, 126] the hydroxyl groups can be replaced by phthalimide groups which are then removed to yield the primary

amine, tame (Figure 2.11).[121, 127]

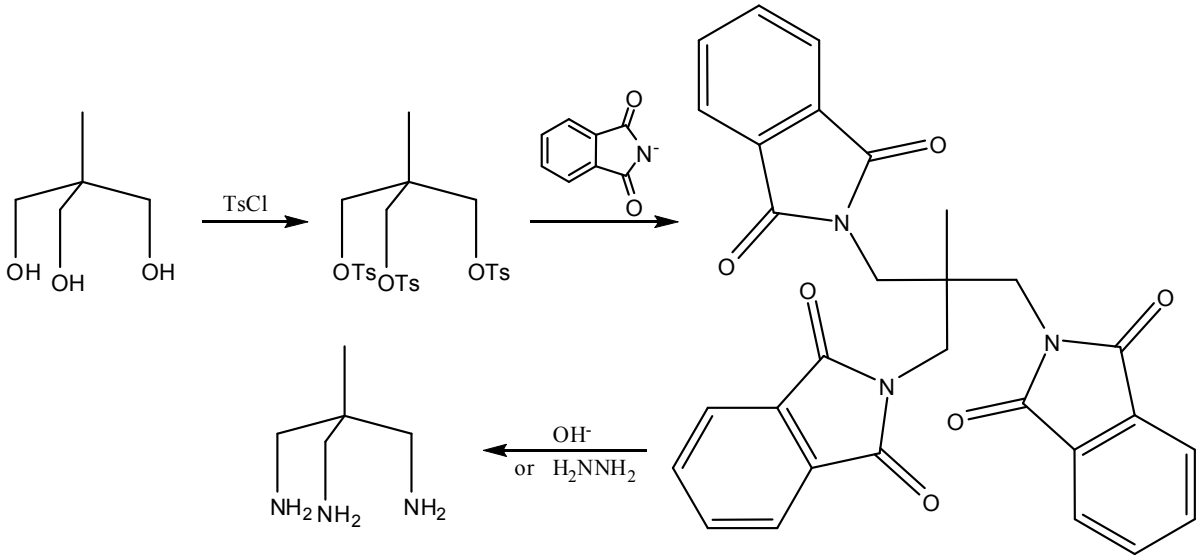

Figure 2.11: Synthesis of tame using a Gabriel Synthesis.

This synthesis is particularly suited to large scale production where utilisation of the alternative azide route may not be feasible. In the azide route, the hydroxyl groups can be replaced by azide groups, which are then reduced to the primary amine using either lithium aluminium hydride[128] or catalytic hydrogenation (Figure 2.12).[129]

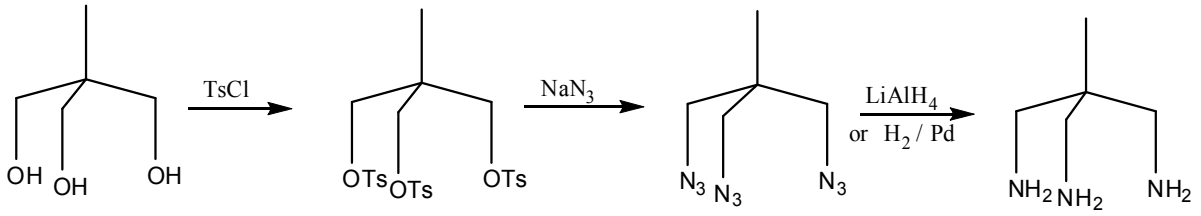

Figure 2.12: Synthesis of tame by the reduction of 1,1,1-tris(azidomethyl)ethane.

Due to the potential hazards associated with organic azides, the phthalimide method was attempted first. However, synthesis of the tris(phthalimido) species proved to be extremely low yielding. This can be rationalised as a manifestation of the so called neo-pentyl effect. Neo-pentyl halides have been observed to be unreactive to S_N2 substitution,[130, 131] with significantly slower rates of reaction than methyl, ethyl, n-propyl or isobutyl halides.[132-136] This has been attributed to the steric bulk around the tertiary carbon centre, which results in there being no conformation that provides a clear path for the incoming nucleophile.[137, 138] The phthalimide anion is a very bulky nucleophile, and the neo-pentyl centre in this case becomes increasingly bulky as successive phthalimide groups attach, making subsequent

substitution all the more difficult.

The removal of phthalimide was attempted using Ing-Manske methodology.[139] This was chosen due to the relative ease of performing an ethanolic reflux in the presence of hydrazine compared with the much harsher conditions reportedly required for alkaline hydrolysis.[121] The Ing-Manske hydrazinolysis proceeds by nucleophilic attack of the hydrazine molecule at one of the amido carbonyl groups, followed by an intramolecular attack at the other resulting in the loss of the primary amine (Figure 2.13).[140]

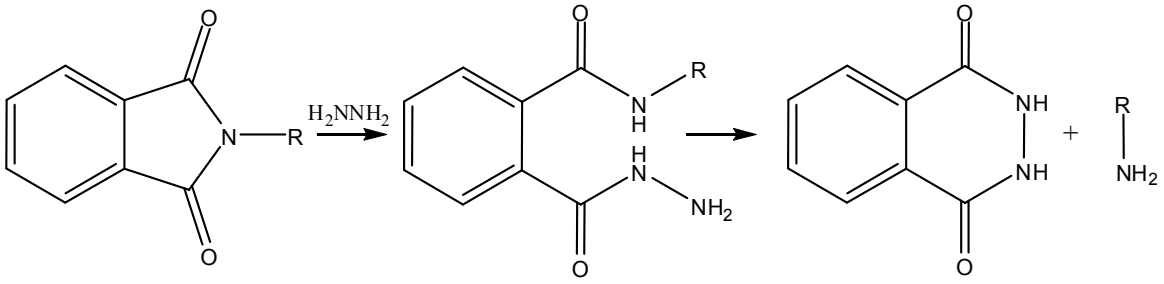

Figure 2.13: Hydrazinolysis of a substituted phthalimide to give a primary amine - the Ing-Manske procedure.

In this instance, treatment of the phthalimide with hydrazine did not result in liberation of the primary amine. This is likely again due to steric crowding at the neopentyl centre, causing the carbonyl groups to be less exposed to nucleophilic attack by hydrazine.

The low yields in generating the phthalimide species, and subsequent the failure to generate any amine from the mild Ing-Manske procedure led to the azide reduction route being utilised for the synthesis of tame. There were initial reservations about the use of this route, due to the potentially hazardous nature of organic polyazides. A guideline to the safety of organic azides is the 'rule of six', by which a molecule with six or more carbon and oxygen atoms per azide group is deemed to be relatively safe.[141] The azide intermediate in this case, 1,1,1-tris(azidomethyl)ethane, has only 1.6 carbon atoms per azide group, and so considerable caution was taken when handling this material. No attempt was ever made to purify the azide, and only very small amounts were sampled for analysis by ^{1}H NMR. In order to avoid crystallisation, which may increase the likelihood of an explosion, the time spent with the material out of solvent was kept to a minimum.

Using this technique, tame was successfully synthesised by reduction of the azide

intermediate with $LiAlH_4$.[128] Due to the additional hazard associated with the use of this reducing agent, and the relatively poor overall yield, catalytic hydrogenation of the azide using the method of Zompa[129] was attempted. This was initially unsuccessful, but the later discovery of a preparation of a similar triamine[142] that used a much greater amount of palladium catalyst allowed successful hydrogenation to give tame. This was the method of choice for all subsequent synthesis of tame.

2.2.2. Cobalt(III) complexes of tame

The synthesis of cobalt(III) complexes of amine ligands can be approached in several ways. Two of the more versatile starting materials are the sodium or potassium salts of $[Co(NO_2)_6]^{3-}$ and $[Co(CO_3)_3]^{3-}$.[143] For this work, the use of the $[Co(CO_3)_3]^{3-}$ material may not be as appropriate due to the bidentate nature of the carbonate ligand. Substitution of three coordination sites by a tridentate amine ligand is not possible as it would require one and a half carbonate ligands to leave. For this reason, cobalt(III) complexes were prepared using the $[Co(NO_2]_6]^{3-}$ complex. The complex $[Co(tame)Cl_3]$ has previously been prepared[117] in this manner via the method used by Okamoto *et al* for the analogous reaction with tacn.[98]

2.2.2.1. $[Co(tame)Cl_3]$

Cobalt(II) nitrate and sodium nitrite are aerated in an $AcOH/AcO^-$ buffer solution, leading to in situ formation of sodium cobaltinitrite, $Na_3[Co(NO_2)_6]$. The triamine ligand displaces three nitrite ligands,[144] resulting in the complex $[Co(tame)(NO_2)_3]$. This complex has been characterised by ^{13}C NMR and observation of the IR absorbance bands at approximately 1420, 1330 and 830 cm^{-1} characteristic of an M-NO_2 group.[145] Unfortunately, ^1H NMR was not able to be used as the peaks were too broad to interpret the spectrum.

The trichlorido complex was also prepared by the method of Okamoto *et al*[98] by heating $[Co(tame)(NO_2)_3]$ in 3 M HCl to dryness. During the reaction, the brown yellow solid dissolved to give a purple solution, and after concentration of the solution to saturation a blue green solid began to precipitate. At this point a sample of the mixture was removed and filtered to give a concentrated solution of cobalt-tame complexes. Purple block crystals suitable for analysis by X-ray crystallography were obtained by diffusion of methanol into this concentrated solution. The data collection, solution and structural refinement were performed

by Dr Chris Fitchett. The complex crystallises from solution as $[Co(tame)(OH_2)_2Cl]Cl_2$ (Figure 2.14). It is expected that in solution the complex would include at least one water ligand in order to adopt a water soluble cationic form. The elemental analysis is consistent with the blue-green solid containing one associated water molecule. However, as the product is a blue-green colour, and not the red-purple colour that would be expected if this water was coordinated to the cobalt centre, we conclude that all three chloride ions are coordinated to the cobalt centre. The product is, therefore, the trichlorido complex with an associated water molecule, $[Co(tame)Cl_3].H_2O$.

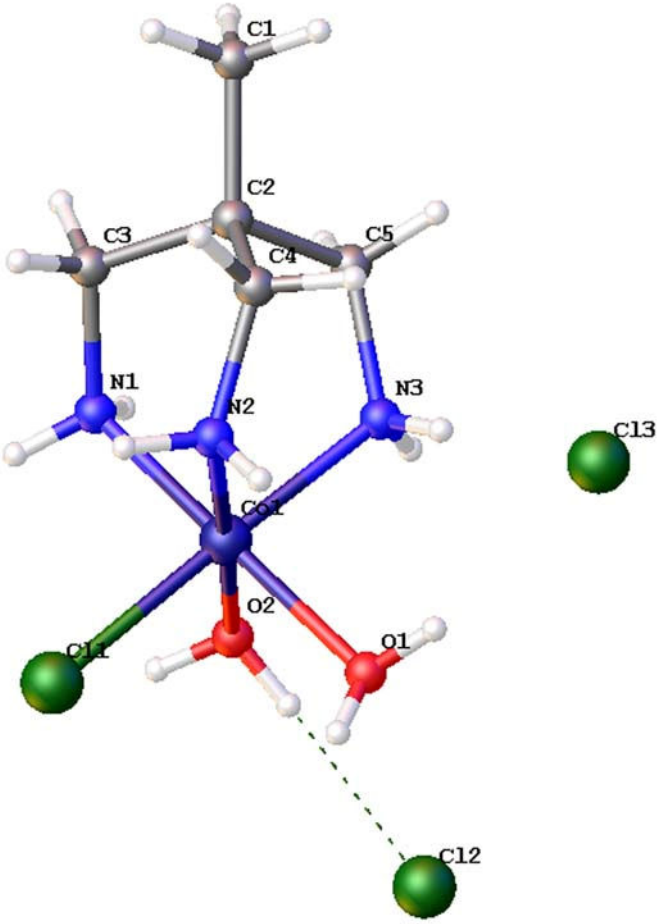

Figure 2.14: Crystal structure of $[Co(tame)(OH_2)_2Cl]Cl_2$.

2.2.2.1.1. Description of the structure of $[Co(tame)(OH_2)_2Cl]Cl_2$

The crystal system is monoclinic and the space group is $P2_1/n$. 32,302 reflections were collected and the structure has been refined to 2.24%. Further crystallographic data is available in Appendix 1.The cobalt(III) atom adopts octahedral geometry with the tame

nitrogen atoms, N1, N2 and N3 adopting a facial orientation. The other three coordination sites are occupied by two water ligands and a chloride ligand, and there are two chloride counter ions, one of which is hydrogen bonded to one of the water ligands. The tame ligand is twisted, with the average Co-NX-CX-C2 torsion angle being 28.4° and the average NX-CX-C2-C1 torsion angle being 162.9°. This compares well to the equivalent angles in cobalt complexes of tame found in the Cambridge Structural Database (CSD), with similar angles within the range of 20.0° – 29.2° and 162.6° – 169.0°.[116, 146, 147] In an untwisted tame these would be expected to be 0° and 180° respectively.

2.2.2.2. A triply hydroxo-bridged binuclear cobalt complex of tame

The synthesis of several triply hydroxo-bridged binuclear cobalt complexes of triamino ligands have been previously reported in the literature.[103, 148-150] The link between the two cobalt atoms in these structures is similar to the proposed bridging mode of the cobalt complexes to the iron atoms in goethite. Although the binuclear complex with tame ligands has previously been synthesised,[150] no crystal structure has been reported. Using similar methodology to that reported,[150] the complex $[(tame)Co(\mu\text{-}OH)_3Co(tame)](NO_3)_3$ has been prepared. Recrystallisation from 0.5 M $NaNO_3$ yielded red hexagonal crystals suitable for analysis by X-ray crystallography. Data collection, structural solution and refinement were performed by Dr Chris Fitchett, and the structure is shown in Figure 2.15.

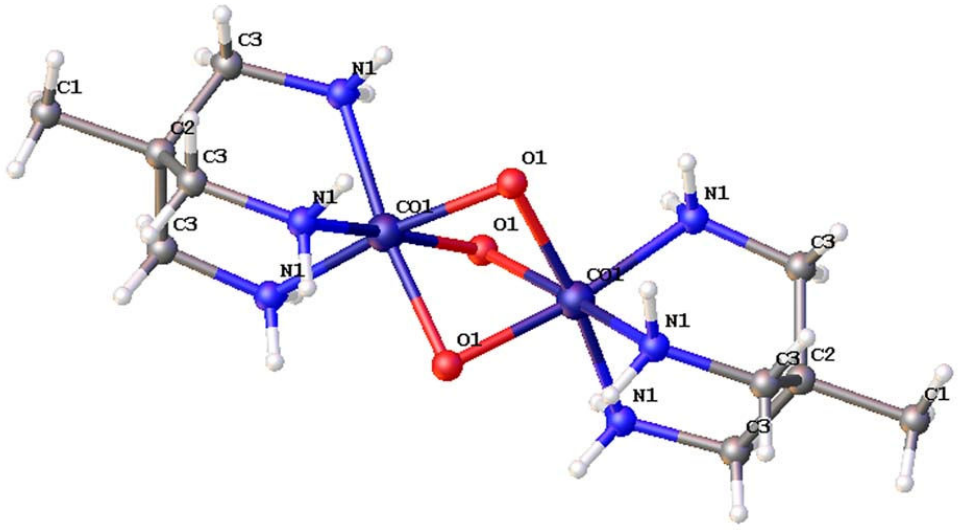

Figure 2.15: Crystal structure of $[(tame)Co(\mu\text{-}OH)_3Co(tame)](NO_3)_3.H_2O$. Counter ions and solvent molecules omitted for clarity.

2.2.2.2.1. Description of the structure of $[(tame)Co(\mu\text{-}OH)_3Co(tame)](NO_3)_3$

The crystal system is hexagonal and the space group is $P6_3/mmc$. 21,046 reflections were collected and the structure refined to 5.64%. The cobalt atoms adopt an octahedral geometry, with the three nitrogen atoms of a tame ligand occupying three coordination sites in a facial orientation. The other three sites are occupied by oxygen atoms, which also bridge to the other cobalt atom. Although no hydrogen atoms are detected in the structure, the presence of three nitrate counter ions shows an overall charge for the complex of +3, suggesting all three oxygen atoms are hydroxide groups. The tame is highly symmetrical with a Co1-N1-C3-C2 torsion angle of 0° and a N1-C3-C2-C1 torsion angle of 180°. This symmetry in a cobalt complex of tame is not found in the CSD, with the closest being angles of 0.772° and 179.825°.[146] The distance between the cobalt atoms is 2.573 Å which is consistent with the literature value for the equivalent tacn based complex of 2.549 Å[89]. Figure 2.16 shows the unit cell of the structure in which the hydrogen bonding between the amine nitrogen atoms of the tame ligand and the oxygen atoms of the nitrate counter ions can be seen. The nitrate anion that is hydrogen bonded to the amine groups is split across unit cells.

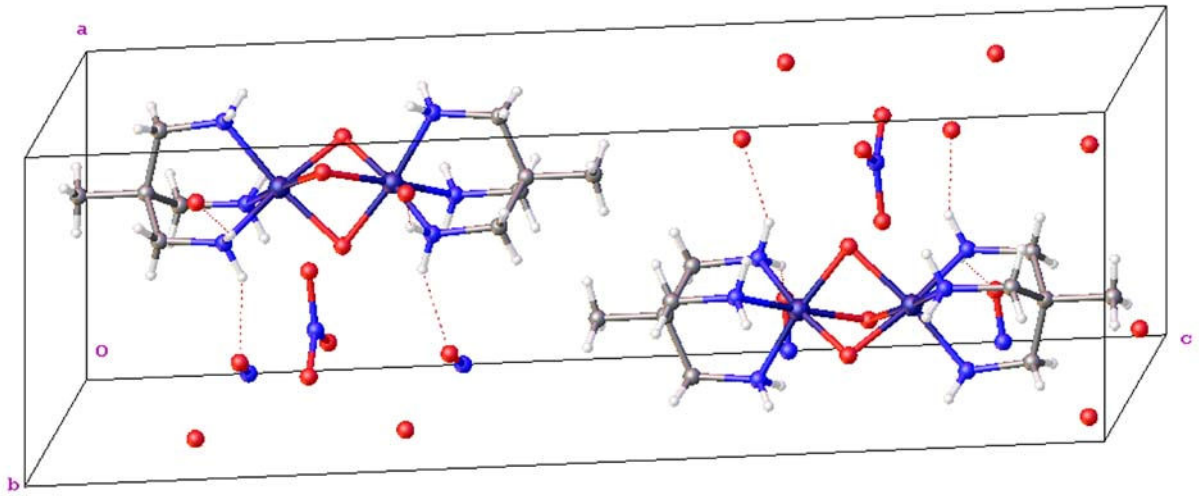

Figure 2.16: Unit cell of $[(tame)Co(\mu\text{-}OH)_3Co(tame)](NO_3)_3.H_2O$. Solvent molecules omitted for clarity.

This hydrogen bonding gives rise to an extended network of hydrogen bonding between the complex and its nitrate counter ions which leads to the highly symmetrical crystal system and molecular structure. Figure 2.17 shows the structure as viewed along the length of the complex. This allows the extended H-bonding interactions between the complex and its counter ions, shown with dotted lines, and the resultant high symmetry to be appreciated.

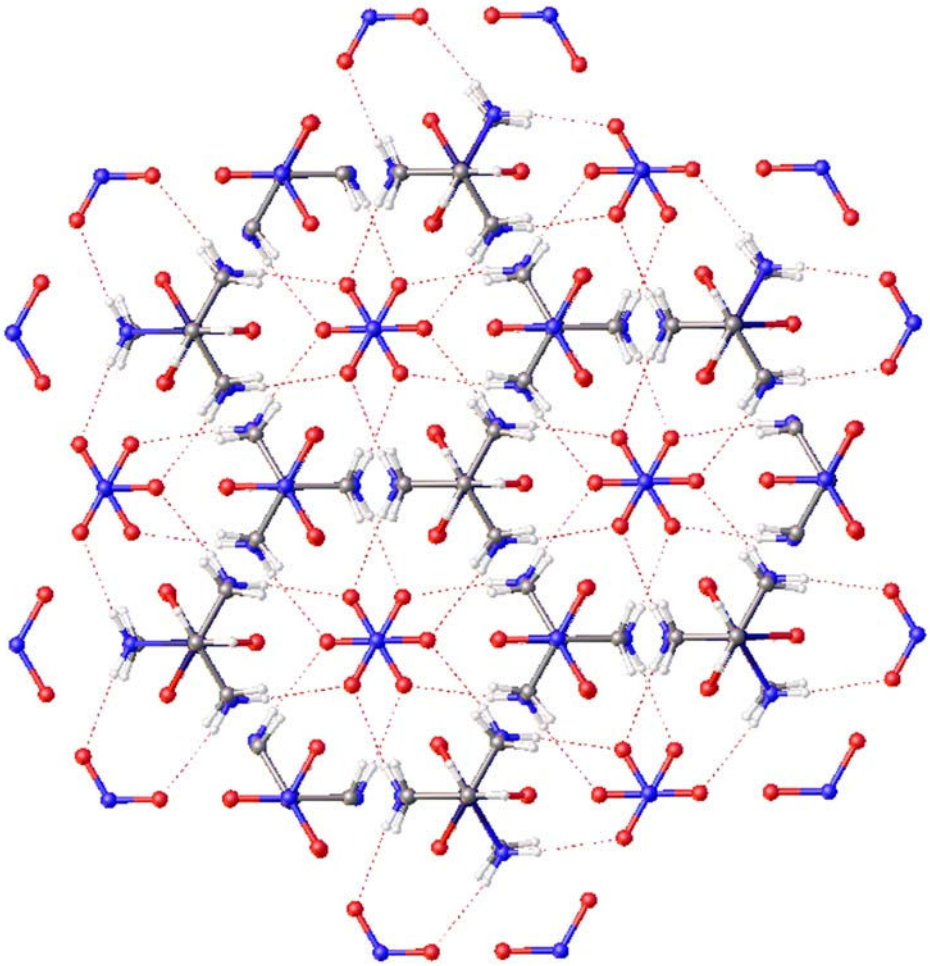

Figure 2.17: Extended structure of [(tame)Co(μ-OH)$_3$Co(tame)](NO$_3$)$_3$.H$_2$O as viewed along the 3-fold axis of the complex. Solvent molecules omitted for clarity.

2.2.3. Difficulties associated with the use of tame based systems

Despite the advantages of working with complexes of the type [Co(triamine)X$_3$] (where X is an exchangeable ligand) as outlined in Section 2.1, there have been problems related to their solubility. The work outlined in Chapters 3 4 and 5 in which these complexes are bound to metals and metal oxide surfaces, is carried out in aqueous solution. However, due in part to these complexes being neutral, they are not very soluble in water. Upon dissolution in water, the complex exchanges one or more of its chloride ligands for a water molecule. The complex [Co(tame)Cl$_3$] takes up to eight hours to fully dissolve in water, and the complexes of more complicated ligands are even less soluble (see Section 2.2.4.3).

Another issue with these complexes, related in part to their insolubility, is that of adequate characterisation by NMR methods. Although the complexes can be at least sparingly

dissolved into water, their ^{13}C NMR spectrum in D_2O shows many more peaks than would be expected. This is possibly due to the exchange of an inconsistent number of chloride ligands throughout the sample. The measured spectrum may be that of up to four different complexes: $[Co(tame)Cl_3]$, $[Co(tame)(OH_2)Cl_2]Cl$, $[Co(tame)(OH_2)_2Cl]Cl_2$ and $[Co(tame)(OH_2)_3]Cl_3$. Furthermore, two of these complexes do not have C_3 symmetry, causing the aminomethyl groups in the tame to be inequivalent and giving rise to further complications in the spectrum. A similar effect is seen if the complex is dissolved in DMSO.

2.2.3.1. Synthesis of iminodiacetate complexes to infer product formation

A proposed solution to the problem of being unable to obtain a suitable NMR spectrum of the complexes of the type $[Co(triamine)Cl_3]$ was to replace the chloride ligands with less labile donors to make a new complex, which would then be able to be analysed by NMR. The successful synthesis of $[Co(triamine)Cl_3]$ would be able to be inferred by characterisation of this new complex. This would be achieved by dissolution of the chlorido complex in water, and introduction of the new ligand or ligands. Success in replacing the exchangeable ligands with new donors in this manner would additionally serve as further evidence for the suitability of these complexes for attachment to metal oxide surfaces using similar linkages. For this purpose, the new donor ligand or ligands should meet several criteria. The first and most important is to be readily available and as structurally simple as possible. A tridentate ligand would be useful in order to take advantage of the chelate effect and to better model a metal oxide surface. An overall charge that is not equal to minus three would be best to avoid making a neutral complex. Separation of the free ligand from the cobalt(III) complex by ion exchange chromatography would be possible provided the overall charge of the complex and that of the ligand are different. This excludes other triamine ligands, as this would produce a complex of charge 3+, with the charge of the triply protonated amine in acidic solution also being 3+. A readily available ligand that does fulfil all these requirements is iminodiacetate (ida) (Figure 2.18).

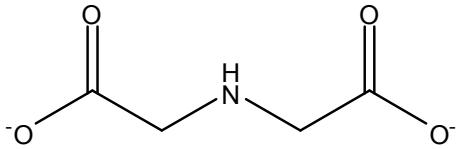

Figure 2.18: Iminodiacetate (ida).

Its overall charge is minus two, and the charge of a cobalt(III) complex of tridentate ida and a tridentate neutral triamine, such as tame, is plus one. This means the complexes should be able to be separated from the free ligand by ion exchange chromatography. Furthermore, these complexes should be soluble in D_2O and thus more easily characterised than the chlorido complexes.

The complexes [Co(tame)(ida)]Cl and [Co(tamt)(ida)]Cl (see Section 2.2.4.1) have been synthesised (Figure 2.19) and characterised by ^{13}C NMR.

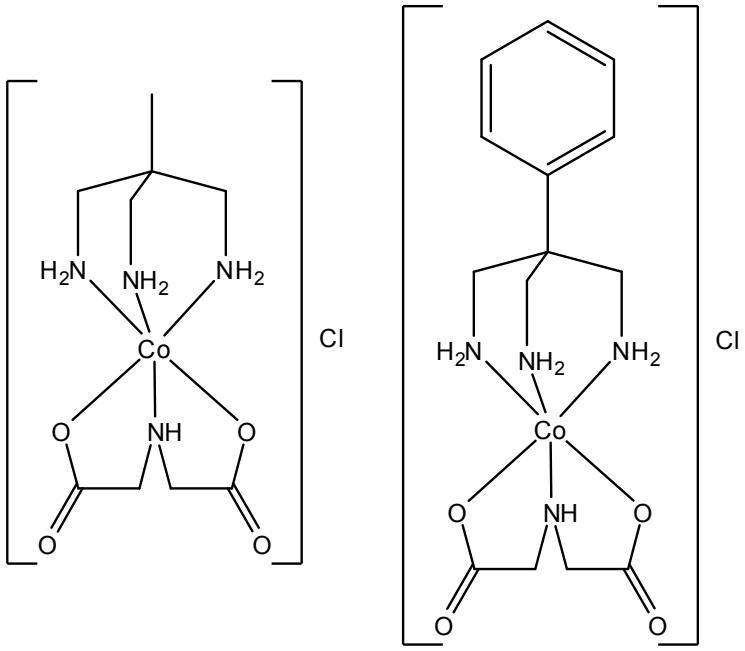

Figure 2.19: The complexes [Co(tame)(ida)]Cl (left) and [Co(tamt)(ida)]Cl (right).

Red block crystals of the complex [Co(tame)(ida)]Cl suitable for X-ray analysis have been obtained by diffusion of methanol into an aqueous solution of the complex. Data collection and solution were performed by Dr Jeni Burgess with additional refinement performed by Dr Chris Fitchett. The structure is shown in Figure 2.20.

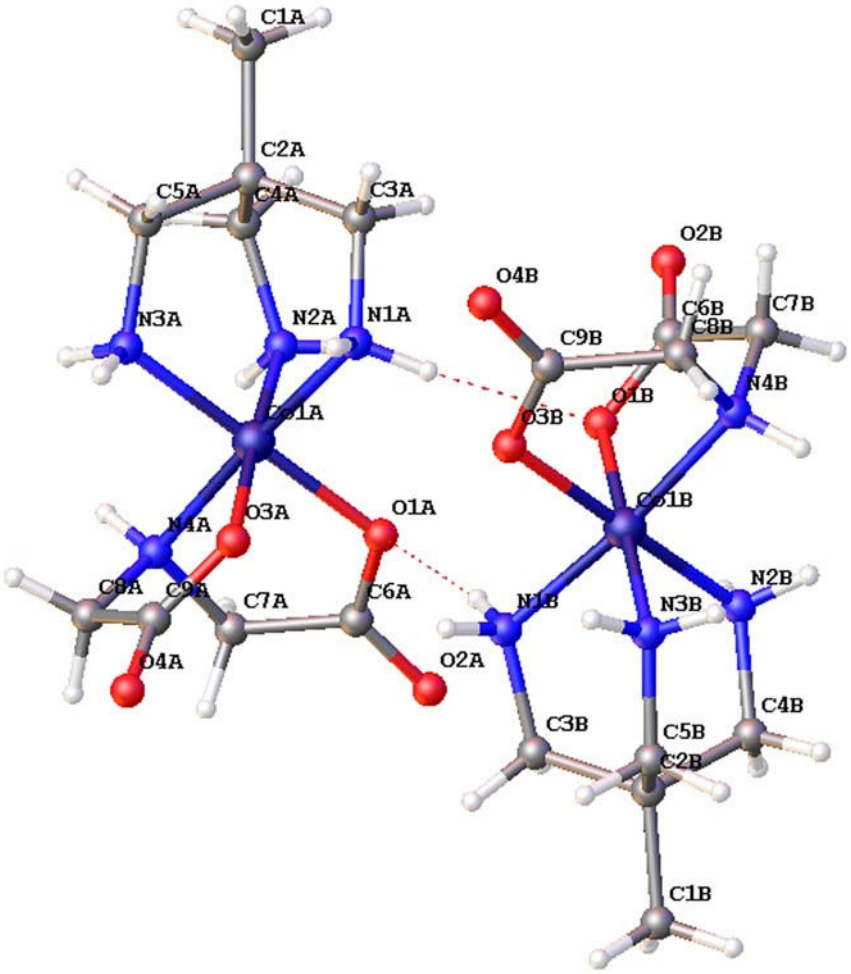

Figure 2.20: Crystal structure of $[Co(tame)(ida)]_2Cl_2.2CH_3OH.2H_2O$. Counter ions and solvent molecules omitted for clarity.

2.2.3.1.1. Description of the structure of [Co(tame)(ida)]Cl.

The crystal system is monoclinic and the unit cell is $P2_1/n$. 62,589 reflections were collected and the structure refined to 6.83%. There are two molecules within the asymmetric unit, herein referred to as molecule A and B. In both molecule A and molecule B the cobalt(III) adopts an octahedral geometry. The tame molecule binds in a facial orientation and the three remaining coordination sites are occupied by a facially bound ida molecule. There is hydrogen bonding between the two molecules through an interaction between an amine hydrogen atom and a coordinating carboxylate oxygen atom. As found in the structure of $[Co(tame)(OH_2)_2Cl]Cl_2$, the tame molecule is twisted. The average Co-NX-CX-C2 torsion angle being 24.921° for molecule A and 12.929° for molecule B. The average NX-CX-C2-C1 torsion angle is 165.580° for molecule A and 172.474° for molecule B. The degree of twisting

in molecule A is consistent with that seen in $[Co(tame)(OH_2)_2Cl]Cl_2$ and the majority of similar structures reported in the literature.[116, 146, 147] The tame in molecule B is less twisted, but this has also been seen in previously reported structures.[146, 147]

The crystallographic characterisation of a complex containing the ligands tame and ida on a cobalt(III) ion is strong evidence that the poorly characterised intermediate complexes do indeed contain a tame ligand, as well as exchangeable ligands, on cobalt(III). However, as discussed in Section 2.2.4.3, this approach was not able to be used for all the triamine complexes synthesised in this work.

2.2.3.2. Use of alternative exchangeable ligands

Another approach that may address the solubility related issues that arise from the use of complexes of the type $[Co(triamine)Cl_3]$ is to use a ligand other than chloride as the exchangeable ligand. The use of an even more easily displaced ligand may lead to complexes that exchange ligands with the aqueous solution more rapidly, and therefore are easier to dissolve. The trifluoromethanesulfonate (triflate) ligand has been demonstrated to be a highly labile ligand in cobalt(III) complexes.[151] The synthesis of the complex $[Co(tame)(OTf)_3]$ (Figure 2.21) was attempted by heating $[Co(tame)(NO_2)_3]$ with triflic acid as described by Dixon *et al*.[152] This reaction produced a brown paste that does not have the correct elemental analysis.

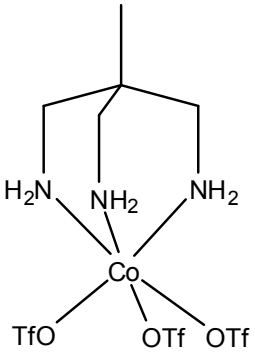

Figure 2.21: $[Co(tame)(OTf)_3]$.

Dissolution in water of the complexes of the type $[Co(triamine)Cl_3]$ likely involves substitution of at least one of the chloride ligands by water. Another way to increase the solubility of these complexes could be to directly synthesise the aqua complex, $[Co(triamine)(OH_2)_3]^{3+}$. This can be achieved by treatment of the nitrite complex with aqueous

triflic acid, and has been reported for $[Co(tacn)(OH_2)_3](CF_3SO_3)_3$.[12] The synthesis of the complex $[Co(tame)(OH_2)_3](CF_3SO_3)$ (Figure 2.22) was attempted using this method.[12]

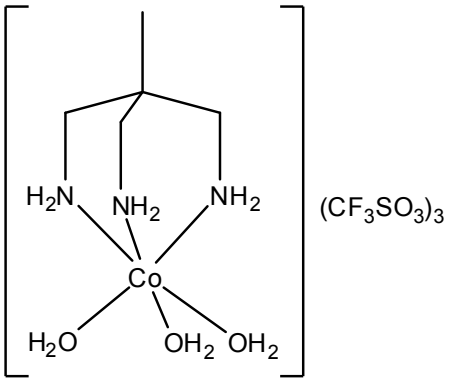

Figure 2.22: $[Co(tame)(OH_2)_3](CF_3SO_3)_3$.

The reaction produced a magenta powder with ^1H and ^{13}C NMR and elemental analysis as expected. This complex dissolves instantly in water, compared to several hours of immersion required for the dissolution of $[Co(tame)Cl_3]$. Complexes of this type may prove more useful for functionalisation of metal surfaces due to their greater solubility in water than the trichlorido complexes that have been used for the studies described in this thesis.

2.2.4. Synthesis of functional tame ligands

The primary aim of this work was to synthesise a family of ligands based on tame. This has been approached in two ways that differ in the point in the synthetic strategy at which the functionality is introduced.

2.2.4.1. Synthesis of triol precursors using Tollens Condensation

In 1891, Tollens reported the synthesis of pentaerythritol from acetaldehyde and formaldehyde in the reaction that now bears his name.[153] In the first step, acetaldehyde reacts with formaldehyde in the presence of calcium hydroxide in sequential aldol reactions to give pentaerythrose. This then reacts with formalin and hydroxide in a Cannizzaro reaction to give pentaerythritol (Figure 2.23).[154]

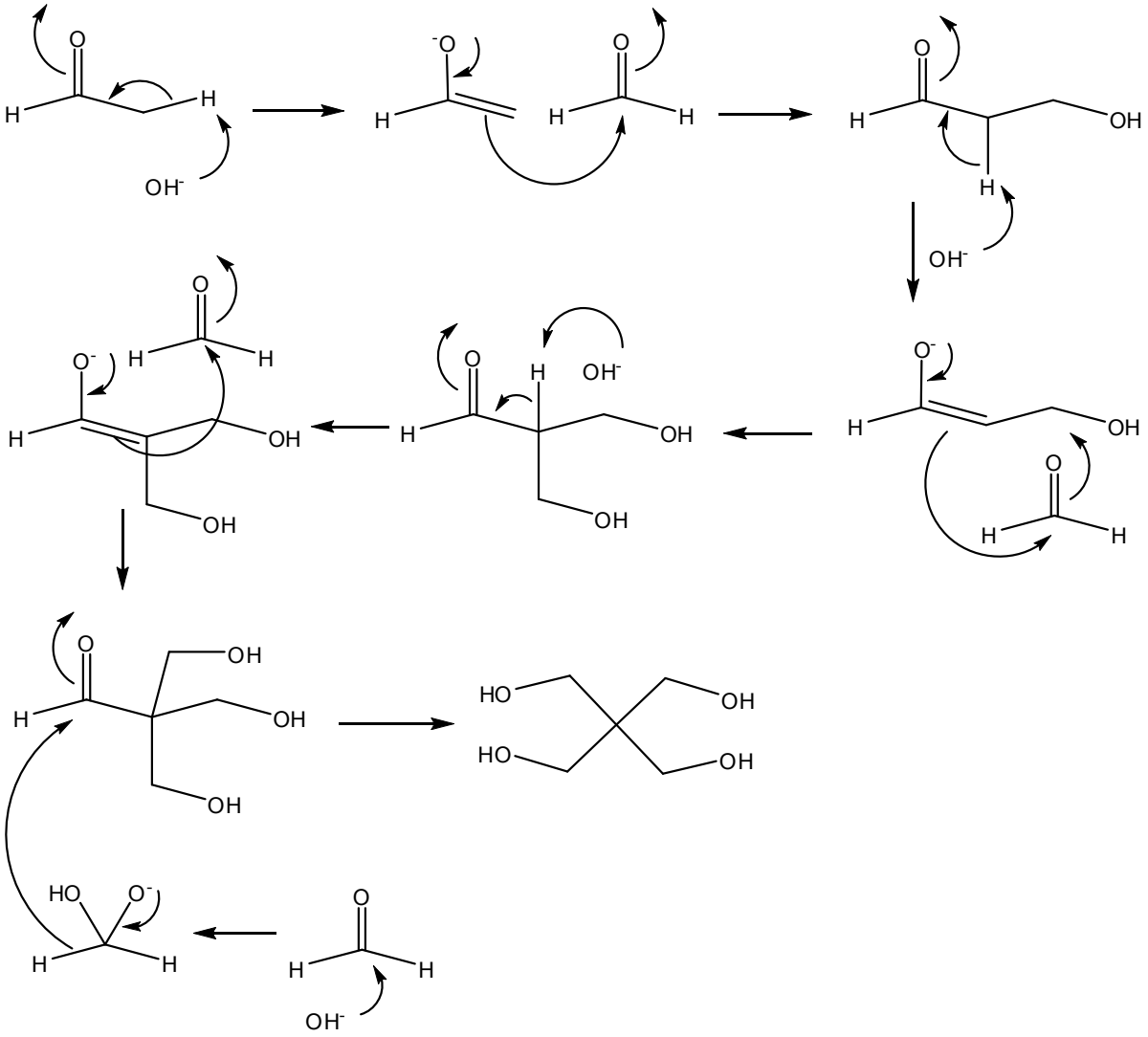

Figure 2.23: Mechanism of the synthesis of pentaerythritol from acetaldehyde and formaldehyde.

Commercially available pentaerythritol is still manufactured today using the same basic method.[155, 156] Since then, the synthesis of various tris(hydroxymethyl)alkanes has been reported using this technique.[142, 157-160] The triamine tame is synthesised from the equivalent triol (Figure 2.10), which is in turn synthesised by the Tollens condensation of propanal and formaldehyde (Figure 2.24).[153, 161]

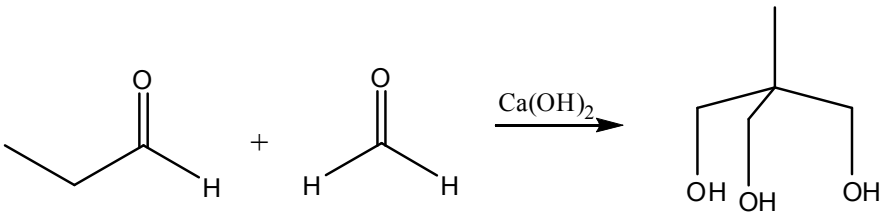

Figure 2.24: Preparation of 1,1,1-tris(hydroxymethyl)ethane by reaction of propanal with formaldehyde.

It therefore follows that tame analogues may be made by first synthesising the appropriate triol from the corresponding acetaldehyde derivative (Figure 2.25). In this manner, a wide variety of tris(hydroxymethyl)alkanes can, at least in principle, be synthesised from the appropriate aldehydes.

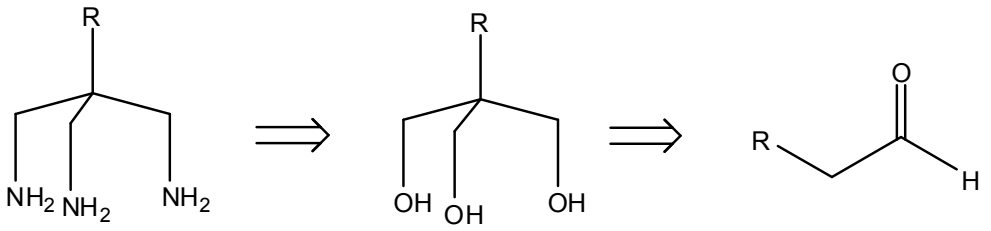

Figure 2.25: Strategy for synthesising tame analogues by using the Tollens condensation.

Using a method based on that of Viguier *et al*,[142] several tris(hydroxymethyl)alkanes have been synthesised. Although this preparation reported the use of paraformaldehyde, and other sources have stated that this provides a better yield,[162] it was found that this reaction only worked when formalin was used in its place. Furthermore, while it was reported that α,α,α-tris(hydroxymethyl)toluene can be recrystallised from ethyl acetate, this was not able to be done, and the product required purification by silica column chromatography. This condensation was carried out with phenylacetaldehyde, octanal and cetyl aldehyde to give the equivalent tris(hydroxymethyl)alkanes (Figure 2.26).

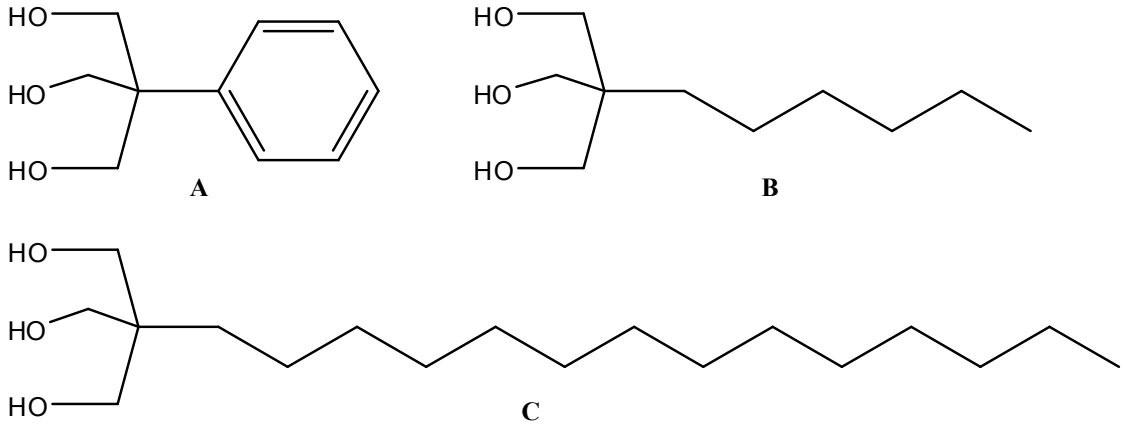

Figure 2.26: Tris(hydroxymethyl)alkane molecules prepared by the Tollens condensation.

Octanal and cetyl aldehyde were prepared by oxidation of n-octanol and cetyl alcohol, respectively, by 2-iodoxybenzoic acid (IBX).[163, 164] The proposed mechanism for this oxidation of primary alcohols into the equivalent aldehyde is shown in Figure 2.27.[165]

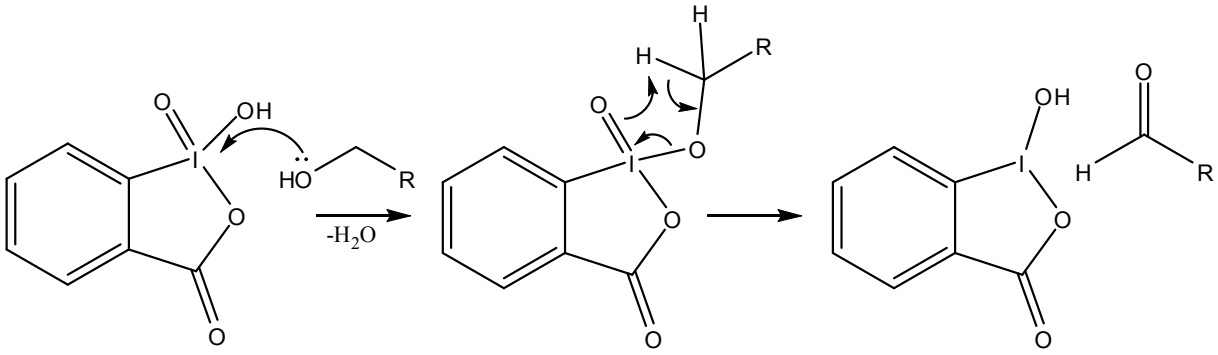

Figure 2.27: Oxidation of a primary alcohol by IBX.

The triamine molecule α,α,α-tris(aminomethyl)toluene (tamt) was prepared by the hydrogenation of the equivalent triazide compound.[142] The trinitro and trichlorido cobalt(III) complexes of tamt were also subsequently prepared. Syntheses of the ligands 1,1,1-tris(aminomethyl)pentadecane and 1,1,1-tris(aminomethyl)heptane were attempted, but unfortunately, no material was able to be isolated from the reaction mixtures.

The synthesis of several tris(hydroxymethyl)alkanes utilising the Tollens condensation was successfully carried out. However, in all cases the reaction yield was very low (5-28%). Such large loss of material is obviously undesirable, and these losses are expected to be even worse for larger, less polar molecules due to the reaction taking place in an aqueous environment. Furthermore, two of the molecules did not react as required at some point in the synthetic scheme. These were not reattempted as this line of work was discontinued due to the low yield of these reactions, and also due to the success achieved with the alternative strategy outlined in Section 2.2.4.2.

2.2.4.2. Methods for functionalisation at later stages

Section 2.2.4.1 outlines the synthesis of functional tame-based ligands by preparation of functional precursors. An alternative would be to add functionality at a later point in the synthetic strategy, which would reduce the number of steps in the synthetic scheme that involve the functional material. This would be advantageous because by exposing the functionality to fewer chemical reactions, there is less opportunity for it to be lost. In addition, the often difficult task of finding appropriate conditions in which to purify and isolate the product at each step is avoided.

It would be particularly attractive to leave the functionalisation until after the low yielding complexation step. This would require a cobalt complex of an easily prepared tame analogue that is able to be functionalised at the appropriate position. The tetraamine tetrakis(aminomethyl)methane (tamm) is relatively easy to prepare, and it might be expected that it would coordinate to a cobalt atom in a tridentate manner. It was proposed that the complex $[Co(tamm)(NO_2)_3]$ may be a suitable target for functionalisation at the uncoordinated aminomethyl arm (Figure 2.28).

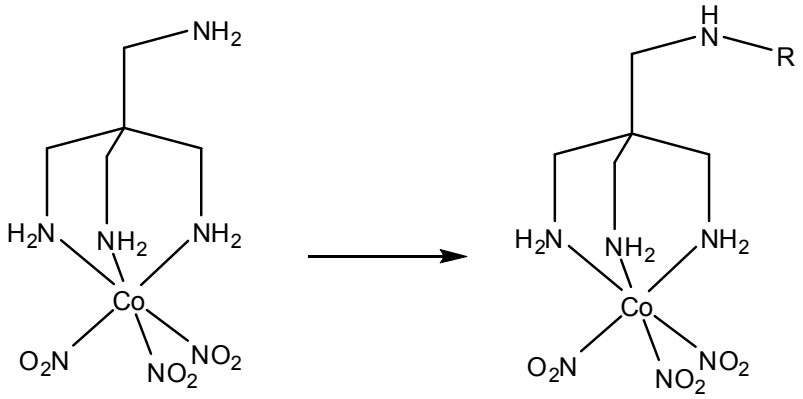

Figure 2.28: Possible method for synthesis of functional complexes by functionalisation of $Co(tamm)(NO_2)_3$.

The ligand tamm was prepared in the same manner as tame (see Section 2.2.1). Starting with tetrakis(toluenesulfonyloxymethyl)methane, the tetraazide tetrakis(azidomethyl)methane was synthesised. This was then catalytically hydrogenated to the corresponding tetraamine, tamm. However, the subsequent reaction of the tetraamine with cobalt produced a material that was not able to be characterised. It is proposed that the extra amine group, which is unable to further chelate to the same metal centre as the other arms of the molecule, may displace a nitrite ligand of a second cobalt complex. This would create bridges between metal centres, possibly resulting in an amorphous polymeric solid (Figure 2.29). For this reason, an alternative method of distinguishing a single aminomethyl arm for functionalisation was sought.

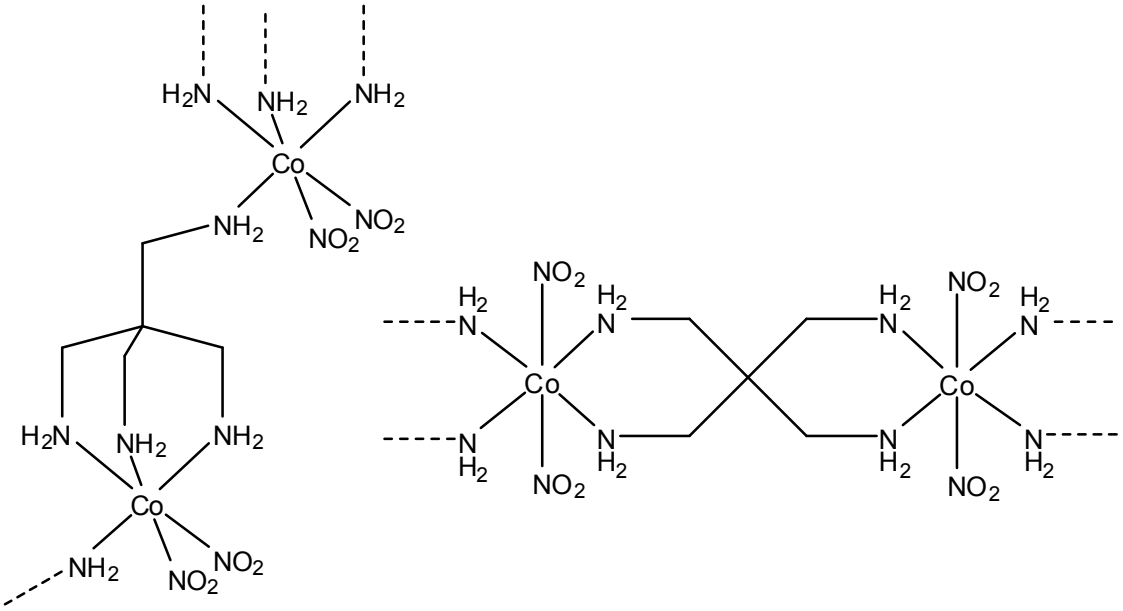

Figure 2.29: Possible polymeric forms of the cobalt complex of tamm.

Dunn *et al* outlined various methods of differentiating a single arm of pentaerythritol in order to produce functionalised tame derivatives.[166] In one method, pentaerythritol is reacted with triethyl orthoacetate, which functions to protect three of the four hydroxyl groups (Figure 2.30). The unprotected fourth hydroxyl group is then reacted with an alkyl halide and the protecting groups cleaved with acid to give a functional triol. This can then be converted into a functional tame derivative by the azide reduction route.

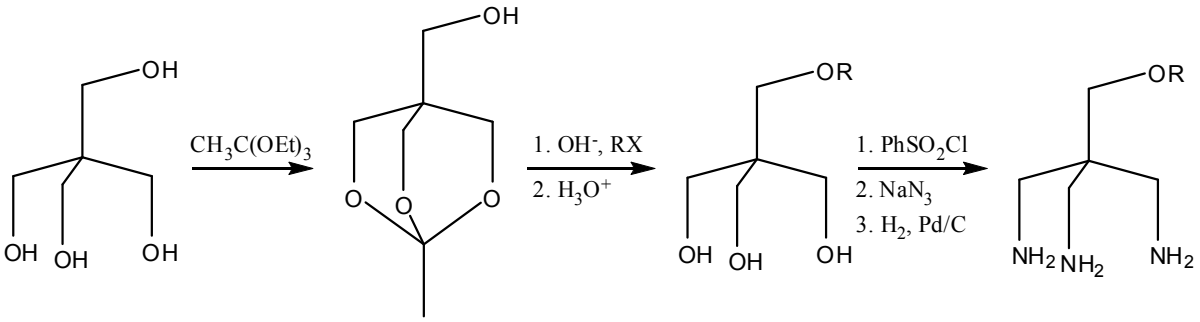

Figure 2.30: Synthesis of a functional tame analogue by the first method of Dunn *et al*: Protection of three of the hydroxyl groups in pentaerythritol followed by functionalisation at the fourth.

However, this method requires the functionality be able to withstand the conditions associated with conversion of the hydroxyl groups to amines. In order to address this problem, a second method was devised, in which the functionality is introduced after this step (Figure 2.31). Using the first method, the derivative where R = benzyl is synthesised, and the benzyl group subsequently removed by hydrogenation. This leaves an analogue of tame bearing a

hydroxyl functionality. In order to prevent reaction at the primary amines, these are protected by reaction with benzaldehyde to form an adamantane-like structure. The hydroxyl group is then able to react with an electrophile, and subsequent acid hydrolysis of the benzaldehyde groups results in the functional tame analogue.

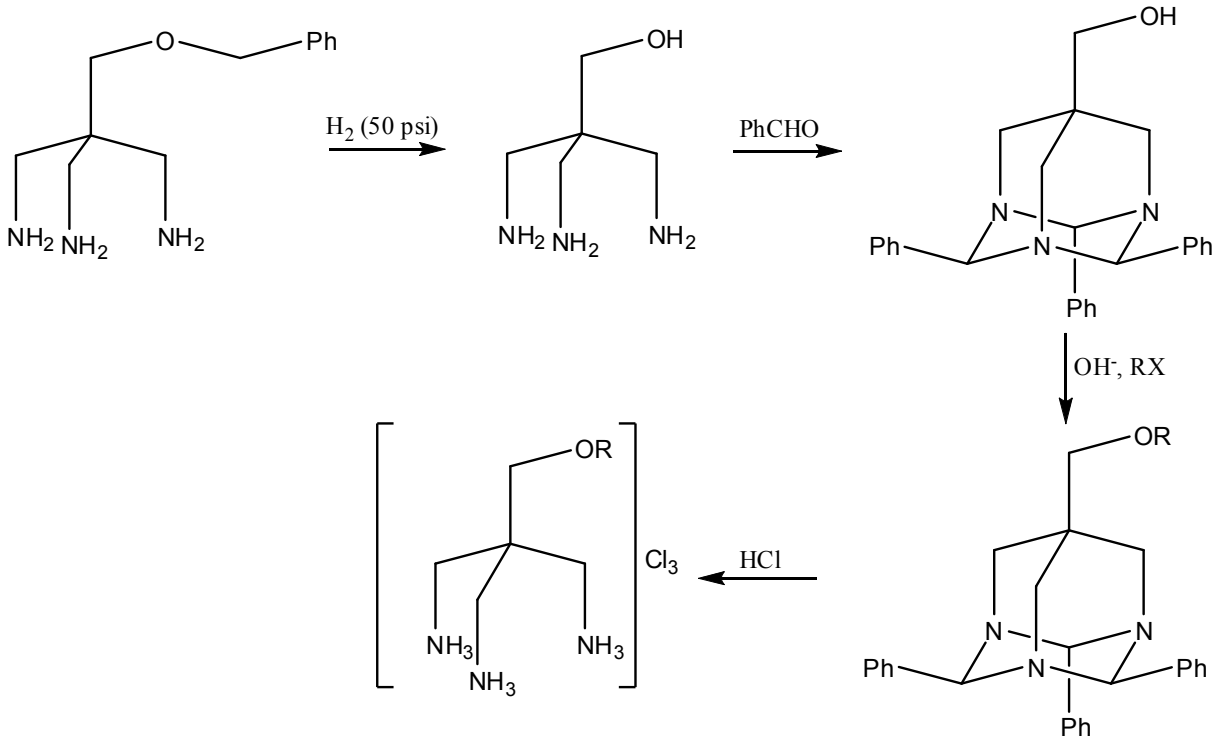

Figure 2.31: Second method of Dunn *et al* for functionalities sensitive to the conditions of amine synthesis.

In a further method, pentaerythritol is first converted to the molecule tamm in the manner already described. This is then reacted with benzaldehyde to protect three of the four amine groups in the same manner as the previous method. In this case, the fourth amino group forms an imine linkage with another molecule of benzaldehyde, and is subsequently reduced with $NaBH_4$ to give a secondary amine (Figure 2.32). This amine is then available to react with an electrophile such as an alkyl halide, acid chloride or sulfonyl chloride. Subsequent hydrolysis with dilute acid removes the benzaldehyde to yield a functionalised triamine.

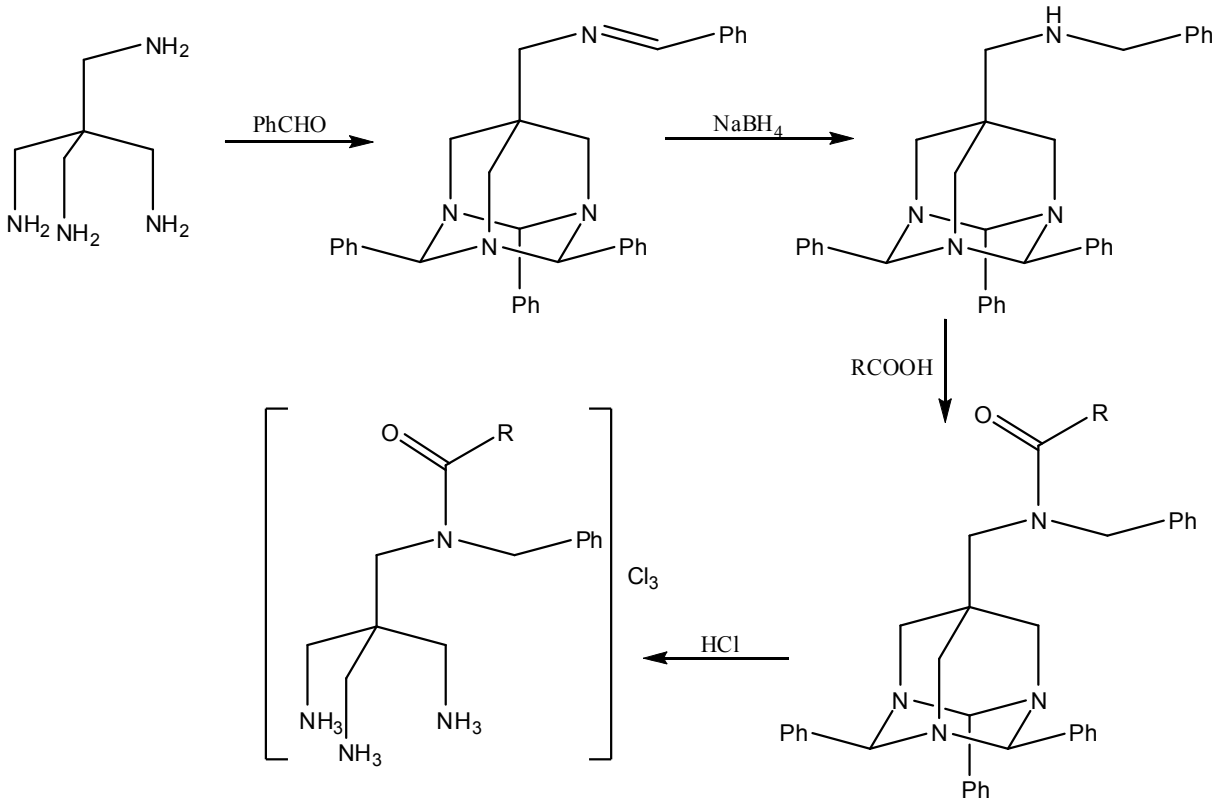

Figure 2.32: A single amine group of tamm is differentiated from the other three by reaction with benzaldehyde in the third method of Dunn *et al*.

It is this route that we chose to pursue as it uses similar chemistry to that we had already employed in the synthesis of tame, and yet offered scope for introducing a wide range of new functional groups. In this work, sulfonyl chlorides rather than carbonyl containing molecules have been used as the electrophile (Figure 2.33).

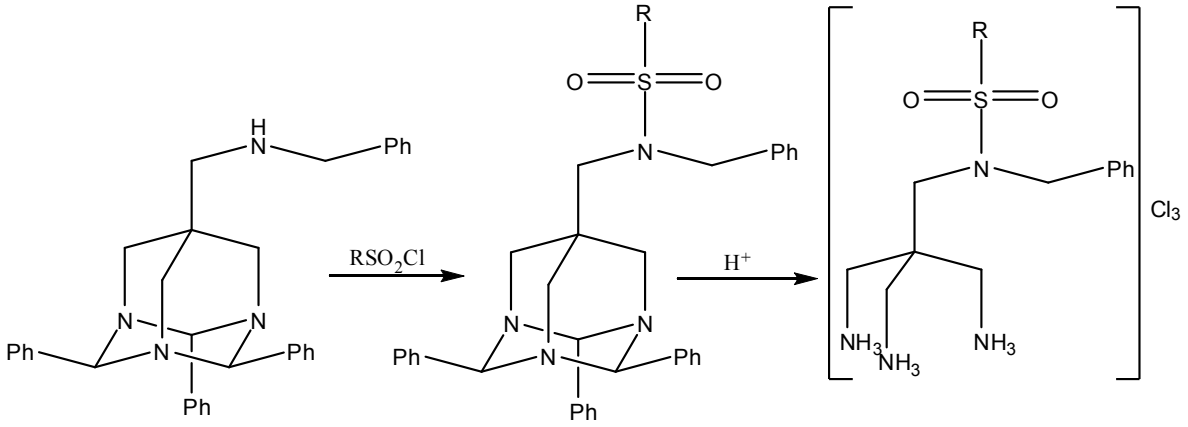

Figure 2.33: Reaction of protected amine with a sulfonyl chloride and subsequent hydrolysis to yield functionalised triamine.

This choice was made primarily due to the stability of sulfonamides toward cleavage.[167]

Additionally, there is a wide range of available sulfonyl chlorides that may be used as sources of functionality. Furthermore, a required sulfonyl chloride can easily be prepared from the appropriate sulfonic acids by reaction with thionyl chloride. This reaction can be catalysed by the use of DMF, the mechanism of which is shown in Figure 2.34.[44]

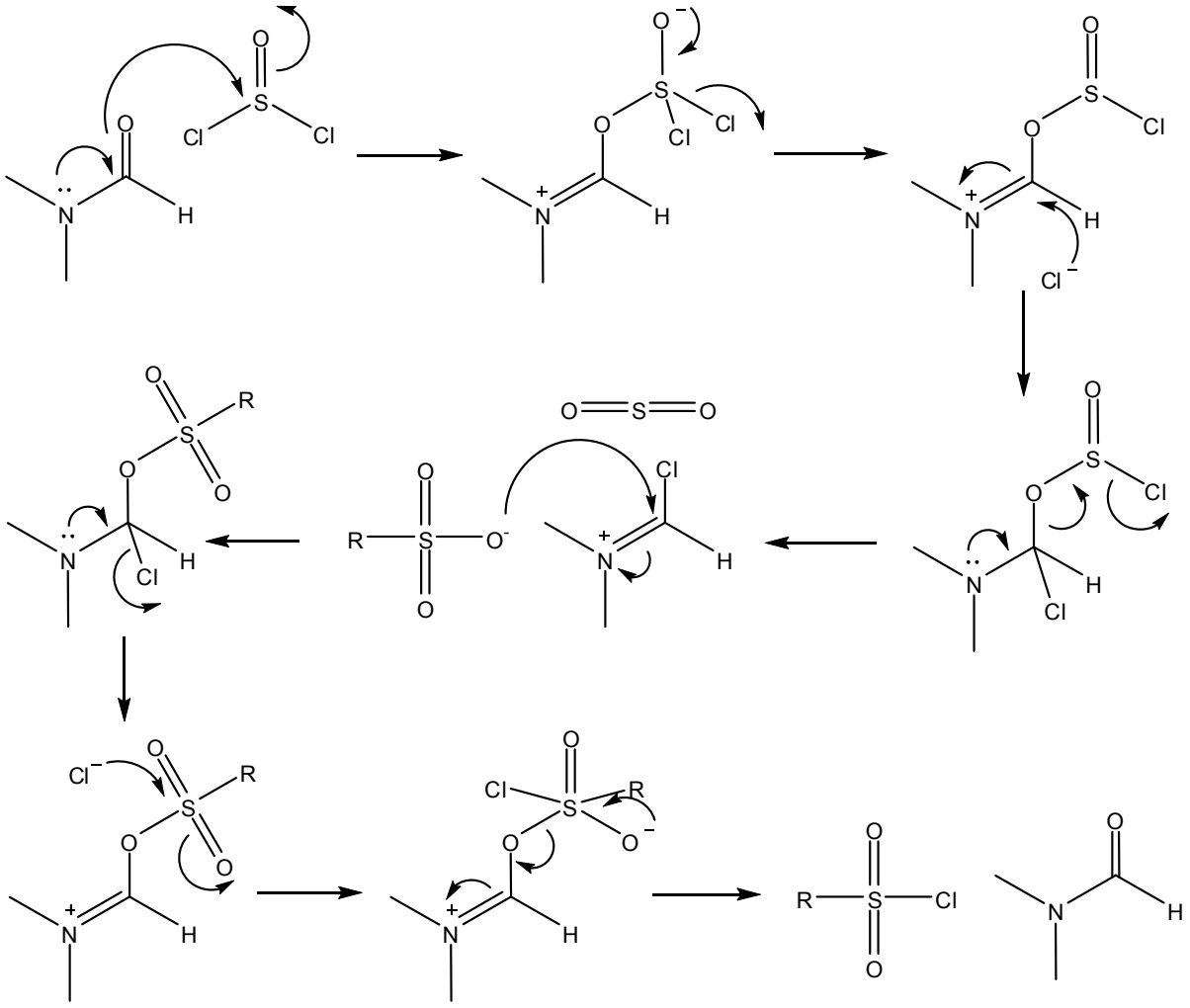

Figure 2.34: Mechanism of conversion of a sulfonate to the corresponding sulfonyl chloride by thionyl chloride catalysed by DMF.

In this work, functionalised analogues of tame have been synthesised where R = tolu-4-yl, naphthalene-2-yl, anthraquinone-2-yl and camphor-10-yl. These ligands have been given non-systematic abbreviations tst, nst, ast and cst respectively where the first letter designates the nature of R, the 's' represents the sulfonamide nature of the ligand, and the 't' stands for tame, reflecting the role of the molecule as a functional derivative of tame. Collectively they will be referred to as xst ligands. These ligands have been thoroughly characterised by NMR techniques and mass spectrometry. However, in some cases the ^{13}C NMR did not show peaks

for one or more of the quaternary carbon atoms. It is not certain which of these are missing, as the quaternary carbon peaks were not able to be distinguished, even with the use of HMBC spectra.

2.2.4.3. Cobalt complexes of xst ligands

Attempts were made to prepare the cobalt complexes $[Co(xst)(NO_2)_3]$ and $[Co(xst)Cl_3]$ for the four well characterised xst ligands. The syntheses were carried out using techniques well established for the preparation of analogous complexes of similar ligands. The resulting materials have similar solubility and characterisation problems to those outlined for the cobalt-tame complexes in Section 2.2.3. As with $[Co(tame)(NO_2)_3]$, the peaks in the ^1H NMR spectra of these materials are too broad to gain any information. In this case, the ^{13}C NMR spectra exhibit low signal to noise ratios due to the poor solubility of the material and are consequently difficult to interpret. The ^{13}C NMR spectrum of the complex $[Co(tst)(NO_2)_3]$, while too noisy to fully assign, does show a peak at 21 ppm that can be assigned to the methyl group of the tosyl moiety. Similarly, the ^{13}C NMR spectrum of $[Co(cst)(NO_2)_3]$ shows peaks at 19.2 and 19.3 ppm that can be assigned to the methyl groups of the camphor moiety. The IR of all the complexes show absorbance bands at approximately 1420, 1330 and 830 cm^{-1} characteristic of an M-NO_2 group. Furthermore, $[Co(ast)(NO_2)_3]$ and $[Co(cst)(NO_2)_3]$ have absorbance bands at 1677 and 1561 cm^{-1} respectively that can be assigned to the C=O group in each ligand. The characterisation of these complexes is poor, and it is for this reason that these materials were not widely used in surface binding studies.

The trichlorido cobalt(III) complexes of xst ligands, $[Co(tst)Cl_3]$, $[Co(nst)Cl_3]$ and $[Co(ast)Cl_3]$ in particular, show very low solubility in water, even after several days in suspension. Whether this is due to slow ligand exchange or low solubility of the aqua complexes has not been explored. Furthermore, the cobalt complexes of the type $[Co(xst)(ida)]Cl_3$, formed on reaction of the complexes $[Co(xst)Cl_3]$ with ida, were not as soluble as hoped, and were therefore neither able to be purified by column chromatography nor able to be characterised by ^{13}C NMR. However, the complex $[Co(tame)(OH_2)_3](CF_3SO_3)_3$ proved to be more soluble and more easily characterised than the complex $[Co(tame)Cl_3]$, which suggests that similarly synthesised complexes may be useful to address these issues in the future.

2.3. Conclusion

The ligand 1,1,1-tris(aminomethyl)ethane (tame) has been selected as the parent compound for the synthesis of C_3 symmetrical triamine ligands. Cobalt complexes of the ligand tame have been prepared, and the crystal structures of three of these complexes have been described.

Functional ligands based on tame have been synthesised using two approaches. In one method, the Tollens condensation has been utilised to synthesise several functional triols for use as triamine precursors. In the other, three amine groups of the tetraamine tetrakis(aminomethyl)methane have been protected with benzaldehyde, allowing the fourth to be functionalised by various sulfonyl chloride molecules. Cobalt complexes of many of these ligands have been prepared and characterised.

Some of the complexes synthesised in this chapter have been used in experiments to probe the interaction of these types of complexes with metal surfaces. In Chapter 3 the binding of cobalt(III) complexes to goethite surfaces is examined, in Chapter 4 the binding to iron and stainless steel surfaces is investigated, and in Chapter 5 the ability of some of these complexes to inhibit the corrosion of iron in HCl solution is studied.

Chapter Three

Binding of cobalt(III) complexes to the surface of goethite (α-FeOOH)

3.1. Introduction

3.1.1. Surface composition of iron

Most metals and alloys react with oxygen. Under atmospheric conditions this results in the surface of the metal being covered in a very thin oxide layer.[168] This formation of a surface layer can also be utilised in the process of passivation, which involves immersion or anodisation of a metal in aqueous medium in order to create a protective layer on its surface. It has been suggested that the composition of the passive layer on iron may be similar to that produced in air.[169] The nature of the passive layer has been studied by various techniques, including Mössbauer spectroscopy[170, 171] and XAS.[65] Mössbauer data suggests a disordered iron oxyhydroxide-like structure, possibly comprising FeO_6 octahedra linked by their edges (see Figure 3.1).[171] The XAS studies give further evidence for this, with the XANES of an iron passive film showing more similarity to the iron oxyhydroxides (FeOOH) than the iron oxides (Fe_2O_3), and the EXAFS indicating the extended structure is most like γ-FeOOH (lepidocrocite) – that is, edge sharing FeO_6 octahedra.[65] This is supported by a study of the composition of layers produced on iron in weakly acidic solution, which found that the surface layer was primarily composed of lepidocrocite (γ-FeOOH), with goethite (α-FeOOH) and feroxyhite (δ-FeOOH) also present.[172]

This chapter is concerned with the measurement of the binding of cobalt(III) complexes onto an iron based surface. The experimental measurement of adsorption from solution involves measuring the change in solution concentration of the adsorbate.[173] In order to effect an observable concentration change, the substrate must have a sufficiently high surface area. For this reason, a high surface area iron oxide similar in composition to the natural layer on the metal is used instead of the metal itself. In this work, goethite (α-FeOOH) has been used as a model for the oxide layer at the iron surface.[174] Goethite has been used in preference to lepidocrocite, despite the latter predominating oxidized iron surfaces, because it is more readily and cheaply available in suitably pure form.

3.1.2. Structure of goethite (α-FeOOH)

The basic structural unit in iron oxides and oxyhydroxides is usually the FeO_6 octahedron.[175] These may be connected by shared corners, edges or faces (Figure 3.1).

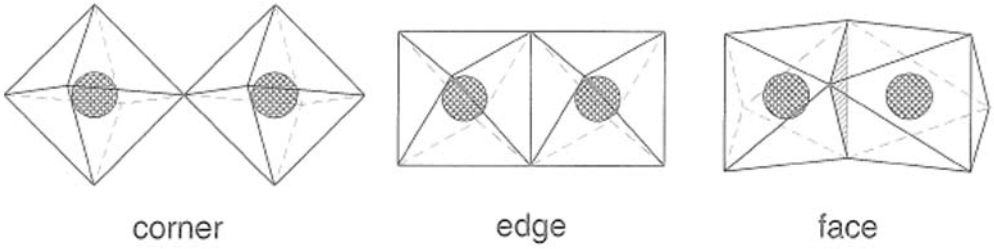

Figure 3.1: Possible bridging modes of FeO_6 octahedra.[175]

The structure of goethite was first described by Goldzstaub[176] and Hoppe[177] using X-ray diffraction photographic techniques. Goethite is isostructural with diaspore (α-AlOOH) and groutite (α-MnOOH).[64] Each Fe ion is surrounded by three O^{2-} and three OH^-, resulting in facial $FeO_3(OH)_3$ octahedra.[64, 175] These octahedra are linked by sharing edges to form double chains which run parallel to the *c* axis. The double chains are then linked via double corner sharing to form the three dimensional structure (Figure 3.2).[64, 175] The unit cell is orthorhombic with $a = 4.5979(2)$ Å, $b = 9.9510(5)$ Å and $c = 3.0178(1)$ Å.[64, 178]

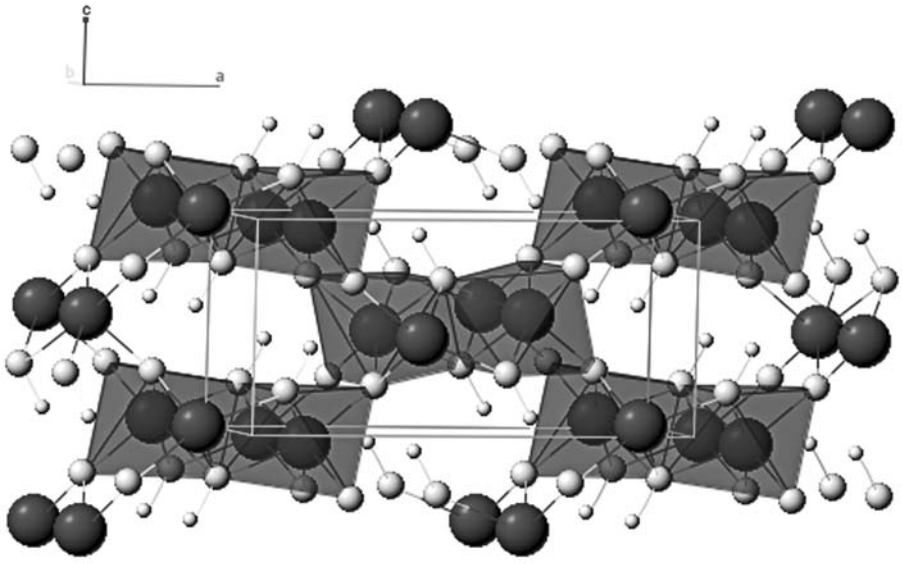

Figure 3.2: Crystal structure of goethite. Unit cell and FeO_6 octahedral outline shown.[179]

3.1.3. Adsorption and isotherms

Adsorption is the process in which molecules bind to a solid surface.[123, 180] One of the earliest observations of adsorption was that of various gases onto charcoal that was made independently by Fontana and Scheele in 1777.[180, 181] In 1881, Kayser measured the adsorption of ammonia onto glass fibres and concluded that the surface area, and not the mass of the fibre was dictating the quantity adsorbed.[180] Langmuir showed that the vacuum inside a light bulb can increase over time, and attributed this to the adsorption of gases onto the tungsten wire.[182]

A solid surface may adsorb molecules from gas, liquid or solid phase. In the case of liquid and solids this is usually from a solution.[183] Molecules can adsorb onto a surface in two ways. In physisorption, a portmanteau word for physical adsorption, a molecule interacts with the substrate through van der Waals forces; chemisorption (chemical adsorption) involves the formation of covalent bonds between substrate and adsorbate.[123] In addition, adsorption may result in the formation of either a monolayer or a multilayer.

Brunauer *et al* classified vapour phase adsorption into five isotherm types.[184] Similarly, a classification system for solid solute adsorption has also been developed by Giles *et al* (Figure 3.3).[185]

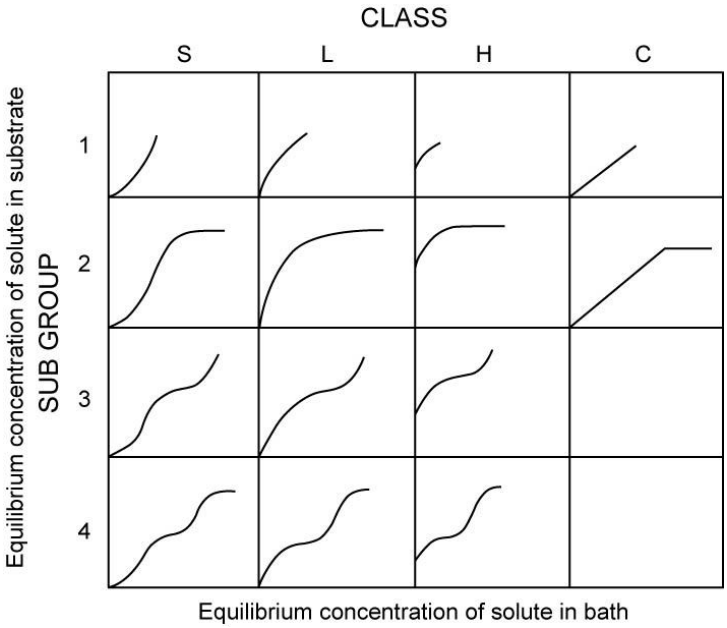

Figure 3.3: Solid solute isotherm classification of Giles *et al*.

The S class of isotherm ('S' shaped), with an initial curve convex to the x axis, results when there is positive interaction between adsorbate molecules causing adsorption to be more stable in proximity to other molecules than in isolation.[173, 186] The L and H class (Langmuir and High affinity) occur when there is negligible interaction between adsorbed molecules.[173] The C class (Constant partition) is seen in situations where the solute penetrates into the substrate. Until the point at which the substrate is saturated, the number of sites appears infinite as adsorption is followed by rapid penetration into the substrate, thus vacating the surface site for adsorption by another solute molecule.[183]

The subgroup refers to the completeness of adsorption. Group 1 represents incomplete adsorption and group 2 is the limit for monolayer adsorption. Groups 3 and 4 are incomplete and complete multilayer adsorption, respectively.[185]

A model of adsorption that is still in use today was proposed by Irving Langmuir in the early twentieth century.[187, 188] This model represents the simplest physically plausible isotherm, and is based on three assumptions:[123, 189]

1. Adsorption results in the formation of a monolayer.

2. All surface sites are equivalent and the surface is uniform.

3. The ability of a molecule to adsorb is independent of surface coverage (that is, adsorbed molecules do not interact with neighbouring molecules).

An adsorbate molecule (A) occupies an adsorption site on the surface of a solid (S):

$$A + S \rightleftharpoons SA \qquad \textbf{(3.1)}$$

The equilibrium constant for the above expression is K_{ad}. It can be expressed as:

$$\frac{[SA]}{[S][A]} = K_{ad} \qquad \textbf{(3.2)}$$

The maximum concentration of surface sites is:

$$[S_{max}] = [S] + [SA] \qquad \textbf{(3.3)}$$

Substituting Equation (3.2) into Equation (3.3) followed by algebraic rearrangement yields:

$$[SA] = [S_{max}] \frac{K_{ad}[A]}{1 + K_{ad}[A]} \quad \textbf{(3.4)}$$

Equation (3.4) is the usual form of the Langmuir equation. It may also be written in the form of Equation (3.5) where θ is the fractional coverage of the surface.

$$K_{ad}[A] = \frac{\theta}{1-\theta} \quad \textbf{(3.5)}$$

In this work, adsorption isotherms have been plotted as amount adsorbed as a function of residual concentration in solution. This data has then been fitted to Equation (3.6) which correlates directly with Equation (3.4), with $y = [SA]$, $x = [A]$, $a = [S_{max}]$ and $b = K_{ad}$.

$$y = \frac{abx}{(1+bx)} \quad \textbf{(3.6)}$$

The parameters of the Langmuir equation can also be estimated through the use of linear regression methods. The most accurate of these was proposed by Langmuir in 1918, and involves a rearrangement of Equation (3.4). [188, 190]

$$\frac{[A]}{[SA]} = \frac{[A]}{[S_{max}]} + \frac{1}{K_{ad}[S_{max}]} \quad \textbf{(3.7)}$$

Plotting $[A]/[SA]$ against $[A]$ will yield a straight line with slope of $1/[S_{max}]$ and intercept $1/K_{ad}[S_{max}]$.[188, 190]

3.1.4. ICP-OES

The cobalt concentrations used for construction of the adsorption isotherms in this work were measured using ICP-OES (inductively coupled plasma optical emission spectrometry), a specific type of atomic spectrometry. In atomic spectrometry, the identity and quantity of an element in a sample is determined by measuring its absorption or emission of light.[89]

The electrons in an atom exist within quantised atomic orbitals that correspond to the electronic energy levels of the atom. The lowest occupied energy level is referred to as the atomic ground state. Absorption of an amount of energy equal to the gap between two energy

bands may result in the promotion of an electron into a higher energy orbital, causing the atom to transition from the atomic ground state to a higher energy atomic excited state.[191] Furthermore, if the amount of energy absorbed is sufficiently high, the electron may dissociate from the atom, resulting in a positively charged ion. Decay from an excited state back to the lower energy ground state is accompanied by the release of energy equal to the difference between the two levels, which may result in the emission of a photon with wavelength equal to that energy. Figure 3.4 shows simplified energy levels and the associated excitation and decay pathways.

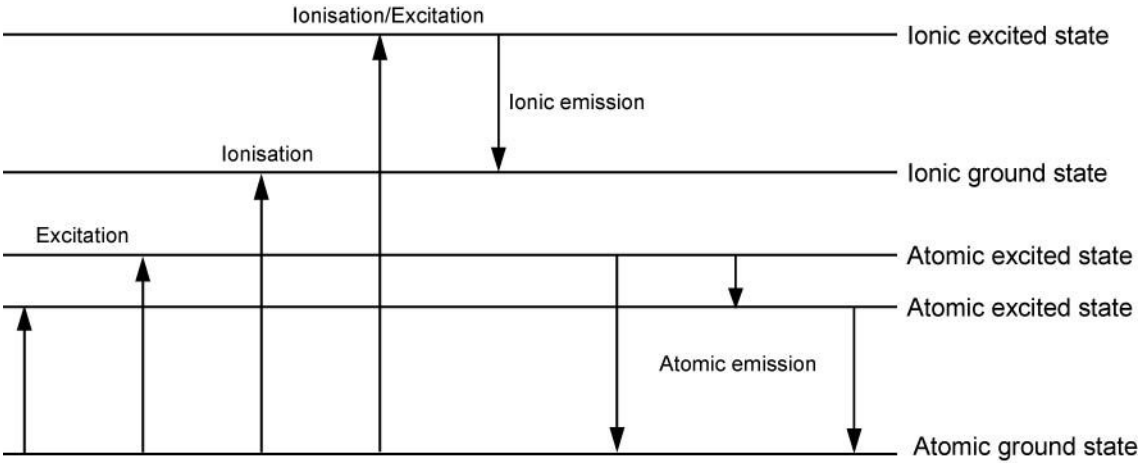

Figure 3.4: Excitation and emission pathways using a simplified energy level diagram.

A commonly used form of atomic spectrometry is atomic absorption spectrometry (AAS). In AAS, sample atomisation is usually achieved utilising either a flame or furnace. The atomised sample is then irradiated with light of appropriate energy to promote an electron to an excited state. The wavelength of light used must be specifically selected to match the energy levels of the species to be analysed. Using a calibration plot, the concentration of the element can be calculated from the amount of light absorbed by the sample.

In another type of atomic spectrometry, optical emission spectrometry (OES), atomisation is achieved using a thermal source that provides enough energy to simultaneously atomise the sample and cause a significant amount of excitation. In most OES this thermal source is an inductively coupled plasma torch (ICP).[89, 191] This is generated by the ionisation of an inert gas, usually argon, and can reach temperatures of 10,000 K. Within the plasma discharge, the sample is desolvated, vaporised, atomised and excited/ionised. Relaxation of these excited species emits photons of light, which are detected by a photosensitive device.

Identification of the elements present is achieved through observation of light of the wavelengths characteristic of the particular elements; their relative amount is determined by comparison of their intensity to a calibration plot.

There are several advantages in the use of ICP-OES. The simultaneous excitation of all elements in the sample by thermal energy allows detection of multiple species in the same run. In contrast, AAS requires the use of a specific hollow cathode lamp for each element of interest. A second advantage in using ICP-OES is that most of the elements can be detected. Some exceptions include short lived radioactive elements, any elements present in the plasma, such as argon, and elements in the solvent or air. ICP-OES also has the advantage of being relatively cheap and easy to use and maintain.

3.1.5. Previous work

A pilot trial to determine the ability of cobalt(III) complexes bearing exchangeable ligands to bind to the surface of goethite was carried out by Cooper as part of her PhD studies at the University of Edinburgh.[27] This was achieved by immersing a sample of goethite in solutions containing various concentrations of the complex and allowing the suspension to equilibrate. The concentration of the complex in solution afterward was then measured by ICP-OES and the isotherm constructed using this data. It was concluded that the cobalt(III) complexes studied were able to bind to the goethite surface provided they had exchangeable ligands. Moreover, a complex bearing three exchangeable ligands showed greater surface coverage than a complex with two. However, no conclusion regarding the relative binding strengths of the complexes was drawn due to the possibility that both complexes may isomerise during binding.

3.2. Results and Discussion

3.2.1. Cobalt(III) complexes used in this work

The complexes examined in this chapter (Figure 3.5) were chosen to complement and expand on the work of Cooper. As with Cooper's work, complexes bearing zero, two and three exchangeable ligands were chosen. However, complexes constrained to the *fac* or *cis* isomers were chosen to eliminate the possibility of isomerisation during binding.

The complexes selected were $[Co(tacn)Cl_3]$ and $[Co(tame)Cl_3]$ with three exchangeable ligands, $[Co(tpa)Cl_2]ClO_4$ and $[Co(tren)Cl_2]Cl$ with two, and $[Co(tame)_2]Cl_3$ with zero (Figure 3.5). Based on the results of Cooper, it was expected that the complexes bearing three exchangeable ligands would give a greater surface coverage than those with two. In extension of that work, it was also expected that in the absence of isomerisation processes, complexes with three exchangeable ligands would have larger adsorption equilibrium constants than complexes bearing two due to the greater number of favourable interactions with the surface.

A series of complexes based on the ligand 1,1,1-tris(aminomethyl)ethane (tame) were also examined in order to determine what effect substitution on a basic framework may have on the binding behaviour of these complexes. The complexes used here are $[Co(tame)Cl_3]$, $[Co(tst)Cl_3]$ and $[Co(nst)Cl_3]$ (Figure 3.5 – see Chapter 2 for discussion on the synthesis of these complexes). Complexes with more bulky substituents (i.e. the ligands tst and nst) may show lower maximum surface coverage due to their occupying a greater area on the substrate surface.

In addition, a chromium(III) complex has been examined in order to compare its behaviour to the analogous cobalt(III) complex. It was expected that this complex will behave similarly to the equivalent cobalt(III) complex.

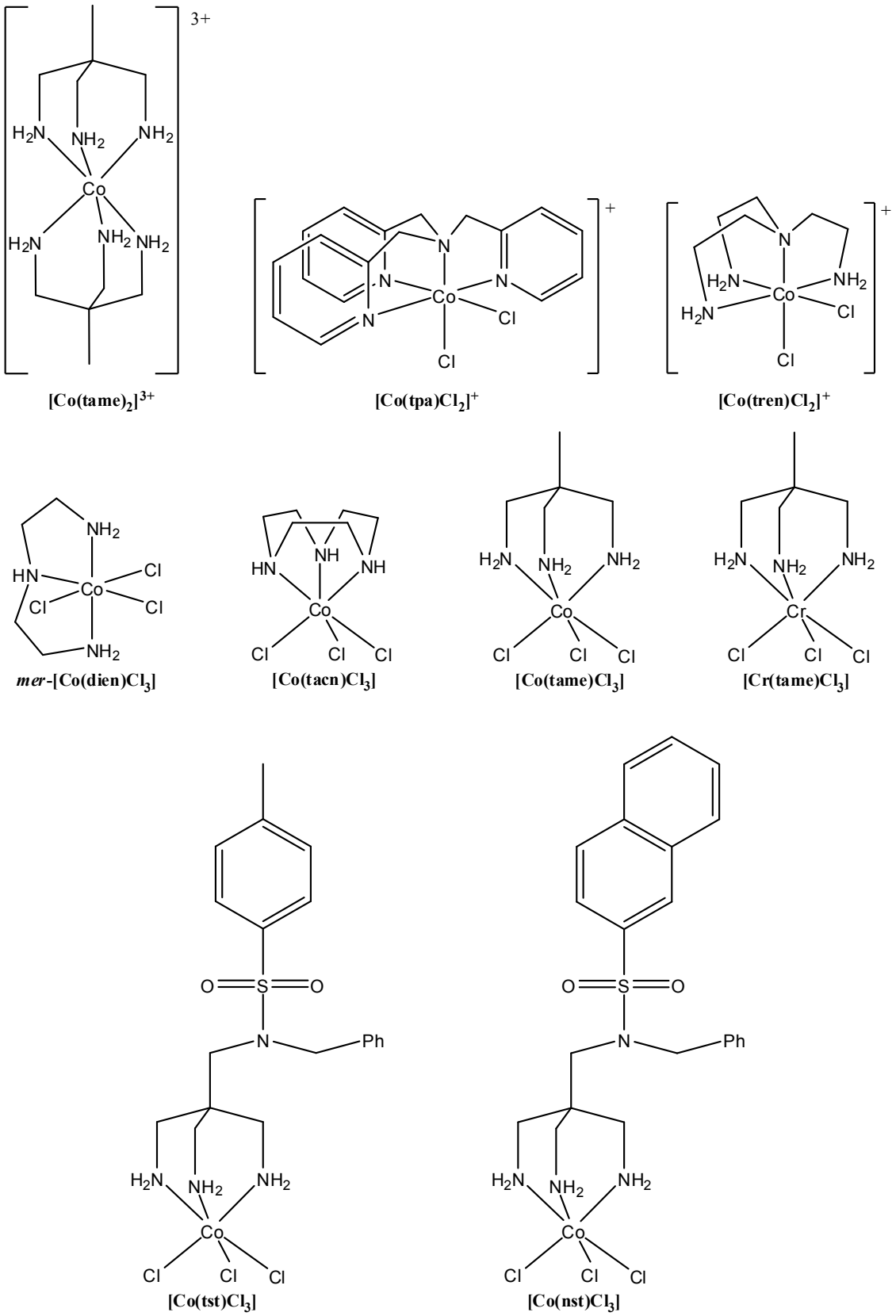

Figure 3.5: Complexes used for adsorption isotherm measurements of goethite.

3.2.2. Isotherm form and interpretation

The plotted data shows the general form of a Langmuir type isotherm (L-2 in Figure 3.3). Using graphical fitting software, the data has been fitted to Equation (3.6). The adsorption isotherm of $[Co(tacn)Cl_3]$ and the resulting fitted curve are shown in Figure 3.6.

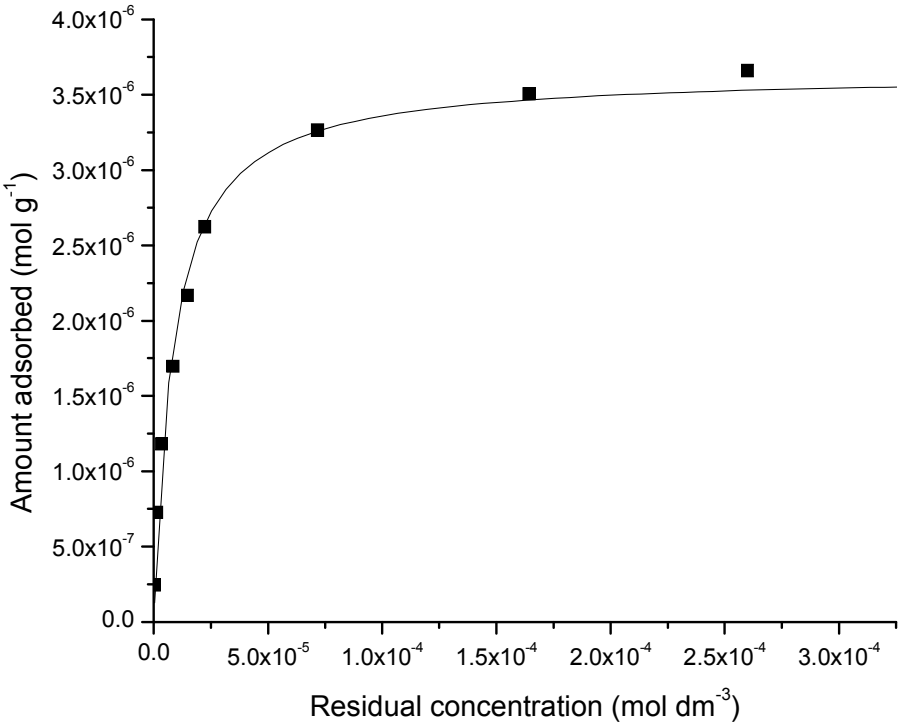

Figure 3.6: Adsorption isotherm of $[Co(tacn)Cl_3]$ on goethite.

The equation fitting has yielded values of a = 3.65 (± 0.08) x 10^{-6} mol g^{-1} and b = 1.2 (± 0.1) x 10^5. As described in Section 3.1.3, the value of a is the maximum surface coverage, [S_{max}], and is observed in Figure 3.6 as the asymptote the curve approaches; b is the adsorption equilibrium constant (K_{ad}) and is observed as the rate at which the curve approaches the asymptote, with a higher value of b resulting in a faster approach.

Alternatively, the isotherm parameters may be estimated using linear regression techniques. The most accurate linear regression technique for the Langmuir isotherm is the one proposed by Langmuir in 1918 (Equation (3.7), p. 64).[188, 190] Using this technique for the above isotherm gives the following (Figure 3.7).

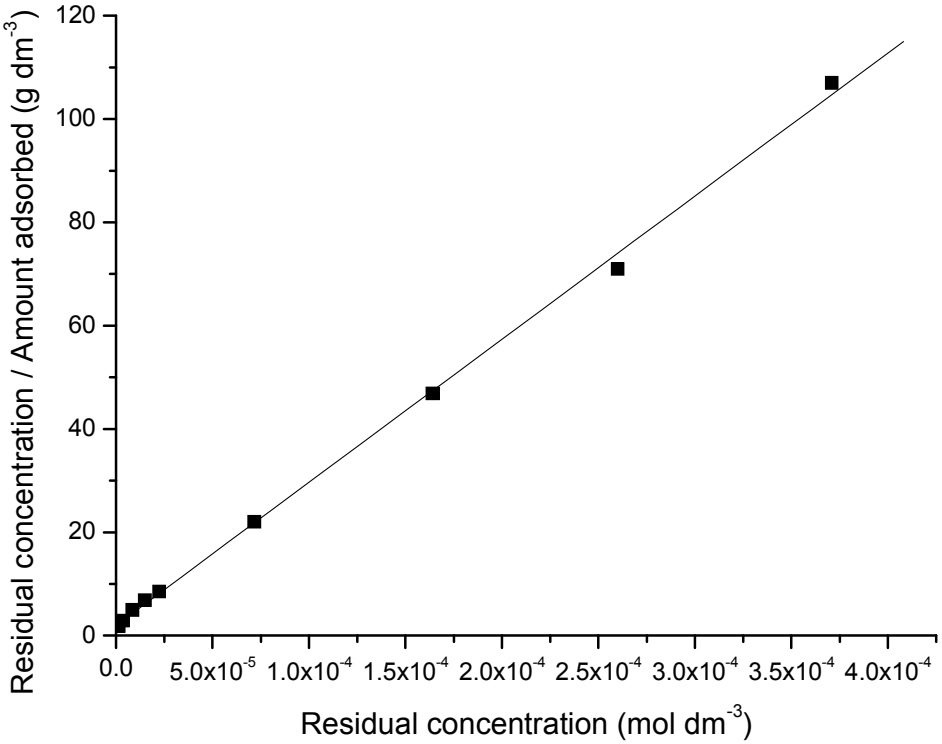

Figure 3.7: Langmuir linear regression plot for the adsorption of [Co(tacn)Cl_3] on goethite.

The graph has a slope of 2.77 (± 0.04) x 10^5 g mol^{-1}, which yields a value for [S_{max}] of 3.61 (± 0.05) x 10^{-6} mol g^{-1}. The intercept is 2.0 (± 0.6) g dm^{-3}, which gives a value for K_{ad} of 1.4 (± 0.4) x 10^5 (note that in a formal sense, activity rather than concentration has been used for this calculation and so the answer is unitless). Both of these values are consistent with those estimated by curve fitting.

3.2.3. Adsorption isotherm parameters for all complexes

All of the complexes that were used for adsorption isotherm measurements are shown in Figure 3.5. Their adsorption isotherm parameters are given in Table 3.1.

One of the complexes used by Cooper ([Co(dien)Cl_3]) was tested again to check the reproducibility of these results between different experimentalists. This was done because the data for these isotherms were collected by several different people, due to the experiments being run at the University of Edinburgh. The data for [Co(tame)Cl_3], [Co(tst)Cl_3] and [Co(nst)Cl_3] were collected by Dr David Henderson, and the data for [Co(tame)$_2$]Cl_3 and [Cr(tame)Cl_3] were collected by Tom Jeffs. The isotherm of [Co(dien)Cl_3] was consistent with the reported data.[27]

Table 3.1: Isotherm parameters for all complexes.

Complex	a ([S_{max}]) (mol g^{-1})	b (K_{ad})	Associated figure(s)
$[Co(tame)_2]Cl_3$	3.4 (± 0.3) x 10^{-7}	-	Figure 3.8
$[Co(tpa)Cl_2]ClO_4$	2.9 (± 1.3) x 10^{-7}	-	
$[Co(tren)Cl_2]Cl$	2.22 (± 0.07) x 10^{-6}	6.9 (± 1.2) x 10^4	Figure 3.8
$[Co(tren)Cl_2]ClO_4$	2.03 (± 0.05) x 10^{-6}	6.9 (± 0.9) x 10^4	
$[Co(dien)Cl_3]$	3.78 (± 0.08) x 10^{-6}	5.2 (± 0.4) x 10^4	
$[Co(tacn)Cl_3]$	3.65 (± 0.08) x 10^{-6}	1.2 (± 0.1) x 10^5	Figure 3.8
$[Co(tame)Cl_3]$	3.2 (± 0.2) x 10^{-6}	1.4 (± 0.7) x 10^5	Figure 3.15, Figure 3.14
$[Cr(tame)Cl_3]$	4.3 (± 0.2) x 10^{-6}	3.0 (± 0.4) x 10^4	Figure 3.15
$[Co(tst)Cl_3]$	2.5 (± 0.1) x 10^{-6}	2.4 (± 0.1) x 10^5	Figure 3.14
$[Co(nst)Cl_3]$	2.1 (± 0.1) x 10^{-6}	9 (± 3) x 10^4	Figure 3.14

3.2.4. Effect of features of the complex on adsorption

The isotherms of complexes that differ in their number of exchangeable ligands, counter ion, metal centre and substitution at the primary ligand have been measured to see what effect these differences may have on their adsorption behaviour.

3.2.4.1. Number of exchangeable ligands

Complexes bearing zero, two, or three exchangeable ligands have had their adsorption isotherm measured. Significant differences in both the adsorption equilibrium and the maximum surface coverage were observed between the complexes with different numbers of exchangeable ligands. These are outlined in the following sections.

3.2.4.1.1. Effect on maximum surface coverage

The observation of Cooper that complexes bearing no exchangeable ligands do not show significant binding to the goethite surface is replicated here. The complex $[Co(tame)_2]Cl_3$, with no readily exchangeable ligands, shows negligible binding to the surface (Figure 3.8). The small amount of binding that is observed (3.4 x 10^{-7} mol g^{-1}) can likely be explained by a low level of physisorption of the complex to the goethite. Furthermore, it was reported by Cooper that the maximum surface coverage of complexes with three exchangeable ligands was

greater than for a complex with two exchangeable ligands.[27] This is also supported by this work, with the complex $[Co(tame)Cl_3]$ showing greater surface coverage (3.2×10^{-6} mol g^{-1}) than $[Co(tren)Cl_2]Cl$ (2.22×10^{-6} mol g^{-1}) (Figure 3.8).

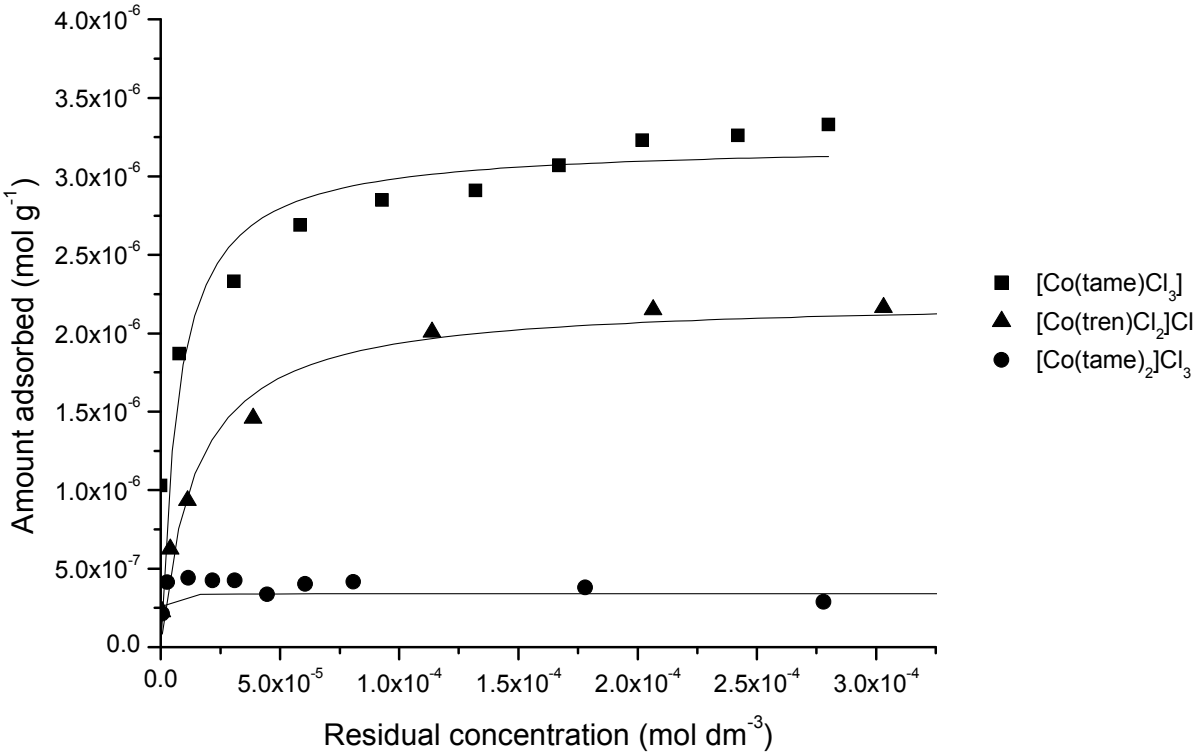

Figure 3.8: Adsorption isotherms of $[Co(tame)_2]Cl_3$, $[Co(tren)Cl_2]Cl$ and $[Co(tame)Cl_3]$.

In order to appreciate the meaning of the measured surface coverage, the surface area of the substrate and the area occupied by a single complex must be considered. The binding of the C_3 symmetric $[Co(tame)Cl_3]$ to the goethite surface can be assumed to utilise oxygen based bridges such as those seen in the structure of $[(tame)Co(\mu\text{-}OH)_3Co(tame)]^{3+}$. The molecular cross section of the cobalt complex, that is, the area it occupies on the surface, can be approximated to that of a circle. Using a fragment of the structure of $[(tame)Co(\mu\text{-}OH)_3Co(tame)]^{3+}$, the radius of this circle can be calculated (Figure 3.9).

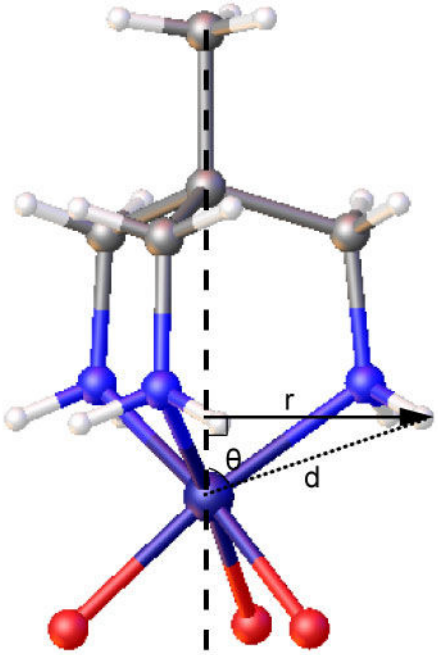

Figure 3.9: [Co(tame)O_3] fragment as proposed to bind to goethite surface. The vertical axis is indicated with the dashed line, the dotted line, d, represents the Co-H distance and r is the radius of the molecular cross section. θ is the angle between the Co-H vector and the vertical axis.

The distance from the vertical axis to the centre of the outermost hydrogen atom is equal to d*sin*θ, where d is the distance from the centre of the cobalt atom to the centre of the hydrogen atom and θ is the angle between this vector and the vertical axis. Calculations in Mercury 2.3[192] give values of d = 2.247 Å and θ = 70.14, yielding a distance of 2.113 Å. Adding the van der Waals radius of hydrogen, 0.320 Å, gives a value of 2.433 Å for r.

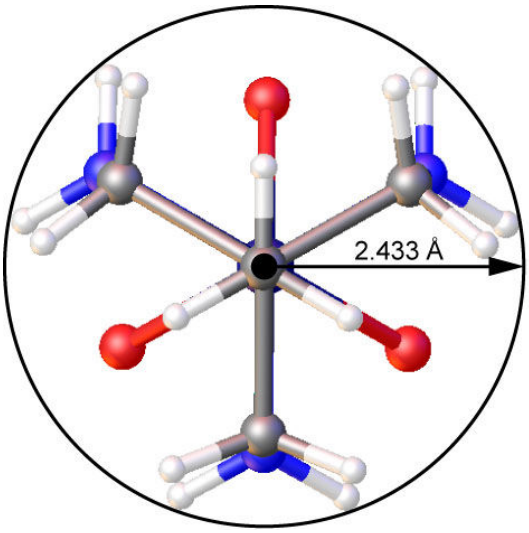

Figure 3.10: Top down view of the [Co(tame)O_3] fragment with the circle that defines its cross sectional area.

Because the complex $[Co(tren)Cl_2]Cl$ is not C_3 symmetrical, it is not possible to fit to a circle in the same way. However, using the crystal structure of $[Co(tren)CO_3]^{+}$[193] as a model for the complex binding to an oxide surface, we can view the complex along the vertical axis of its proposed bidentate binding mode. If we superimpose a circle with radius 2.433 Å (that calculated above for the tame complex), we can see that the complex takes up more space than does the tame complex (Figure 3.11).

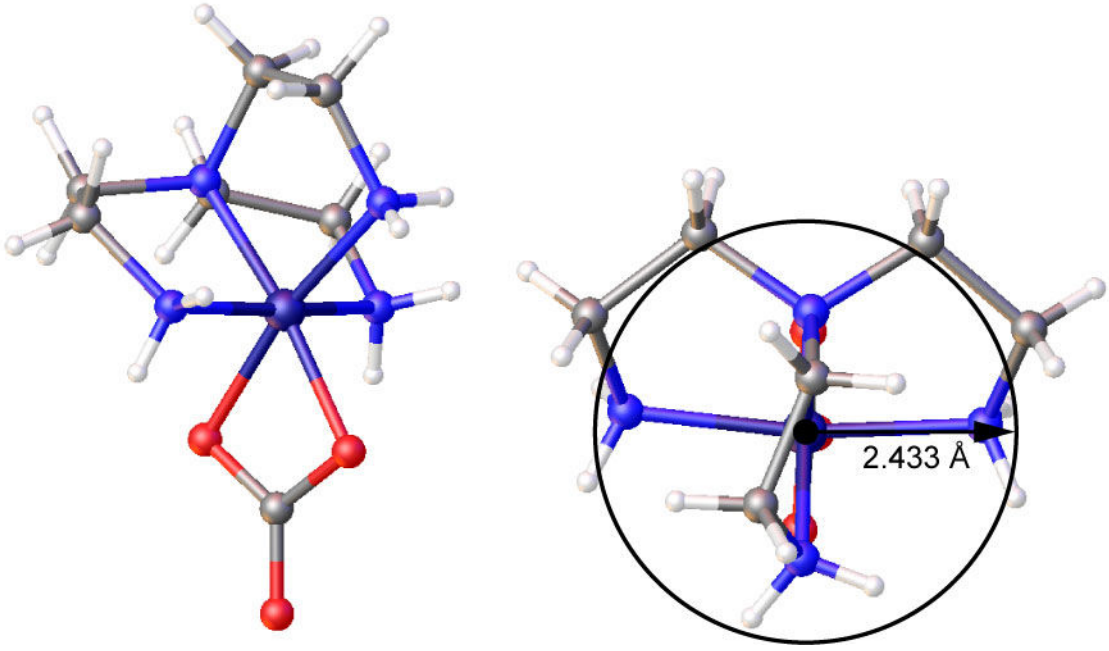

Figure 3.11: $[Co(tren)CO_3]^{+}$. Right: Top down view in proposed mode of binding, with the cross sectional circle of the $[Co(tame)O_3]$ fragment superimposed.

This may explain the lower surface coverage observed for the complexes bearing two exchangeable ligands in comparison to those bearing three. The greater surface area occupied by each unit means fewer can be adsorbed on the same amount of goethite. However, this comparison may not be so straightforward. Similar calculations to determine the cross sectional area of $[Co(tacn)Cl_3]$ and $[Cr(tame)Cl_3]$ surface binding were performed using crystal structures of $[(tacn)Co(\mu\text{-}OH)_3Co(tacn)]^{3+}$[89] and $[Cr(tame)(N_3)_3]$[194] respectively. The value for r calculated in this way is 3.087 Å for the tacn complex and 2.642 Å for the chromium tame complex, both of which are larger than the 2.433 Å calculated for the tame complex. The adsorption isotherm data, however, gives maximum surface coverage values of 3.2 (± 0.2) x 10^{-6} mol g^{-1} for $[Co(tame)Cl_3]$, 3.65 (± 0.08) x 10^{-6} mol g^{-1} for $[Co(tacn)Cl_3]$ and 4.3 (± 0.2) x 10^{-6} mol g^{-1} for $[Cr(tame)Cl_3]$. This does not fit precisely with the analysis above

in which the greater surface coverage of [Co(tame)Cl_3] compared to [Co(tacn)Cl_2]Cl is rationalised as being due to the smaller cross sectional area of the tame complex. Nevertheless, the relationship between molecular cross sectional area and surface coverage may well be real. If the numbers for [Co(tame)Cl_3] are excluded, the complex [Cr(tame)Cl_3] shows the smallest cross sectional area, and greatest surface coverage. [Co(tren)Cl_2]Cl shows the lowest surface coverage, and has the greatest cross sectional area while [Co(tacn)Cl_3] has the middle value for both measurements.

Using the molecular cross sectional area, the area occupied by each molecule can be calculated for a given packing arrangement. This can then be compared to the available surface area on the substrate. If we assume the complex packs in the way shown in Figure 3.12, the area occupied by each unit can be calculated as equal to twice the area of the shown triangle, as the triangle contains three sixths of a circle. Thus, the area is equal to 2 x ($\sqrt{3}/4$) x $(2 \times 2.433)^2 = 20.51$ Å^2.

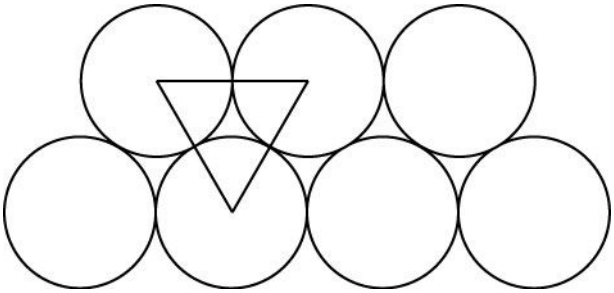

Figure 3.12: Possible packing mode of complexes (circles) on the surface.

The surface area of the goethite has been calculated using BET analysis[195] to be 2.21 x 10^{21} Å^2 g^{-1}. Dividing by the experimentally determined surface coverage for [Co(tame)Cl_3] of 3.2 x 10^{-6} mol g^{-1} gives 6.91 x 10^{25} Å^2 mol^{-1}. This equates to an area of 1147 Å^2 per molecule. Thus, the obtained surface coverage is 1.8% of a monolayer. However, this assessment is based on several assumptions. Firstly, it is assumed that the molecules will pack in the way shown in Figure 3.12, whereas it is possible that the surface packs in a less dense manner. Secondly, the actual cross sectional radius of the surface bound complex may be larger than calculated. Thirdly, the surface of the goethite is not atomically smooth. It will contain irregularities such as steps, kinks and holes, some of which may be too small to accommodate larger molecules. Thus, the calculated surface area available to a complex will be dependent on the size of the probe molecule used to measure it. The relationship between the size of the

probe molecule and the measured surface area that it can access depends on the roughness of the surface. This is known as the fractal dimension. For synthetic goethite samples, the fractal dimension is approximately 2.5, indicating a relatively high dependence of measured surface area on probe molecule size. Because the BET analysis was performed using nitrogen gas, with a much smaller cross sectional area than the cobalt complexes used, this error is likely to be significant.

3.2.4.1.2. Effect on adsorption equilibrium constant

Due to the potential isomerisation of the complexes $[Co(dien)Cl_3]$ and $[Co(en)_2Cl_2]Cl$, no conclusion was drawn by Cooper regarding the relationship between their binding equilibrium constants and the number of exchangeable ligands.[27] In this work, the complexes are constrained to one geometrical isomer due to the rigidity of the ligands. It is observed that the complexes with three exchangeable ligands, in addition to reaching a greater maximum surface coverage, also have larger binding equilibrium constants. The range of equilibrium constants for complexes bearing three exchangeable ligands (excluding the complex *mer*-$[Co(dien)Cl_3]$ due to its potential for isomerisation) is $0.9 \times 10^5 – 3.0 \times 10^5$. The value for $[Co(tacn)Cl_3]$, shown in Figure 3.8, is 1.2×10^5; the equilibrium constant for $[Co(tren)Cl_2]Cl$, with two exchangeable ligands, is 6.9×10^4. This increased binding ability can be attributed to the formation of more bonds to the substrate surface.

It is interesting to note, however, that the complex $[Co(tpa)Cl_2]ClO_4$, shows no significant binding to the surface, despite having two exchangeable ligands. This can be rationalised as being due to the pyridyl ligand needing to be unfavourably close to the metal oxide surface to facilitate binding. The crystal structure of $[Co(tpa)(CO_3)]^+$ is shown in a space filled model (Figure 3.13).[196]

The carbonate ligand occupies the sites which would bind to the iron oxide surface. However, on the surface there would be further oxygen atoms in the same plane as those bound to the cobalt atom. The pyridyl rings can be seen to intrude into this plane, and so binding to the surface is likely obstructed by repulsive interactions between these rings and the surface bound oxygen atoms.

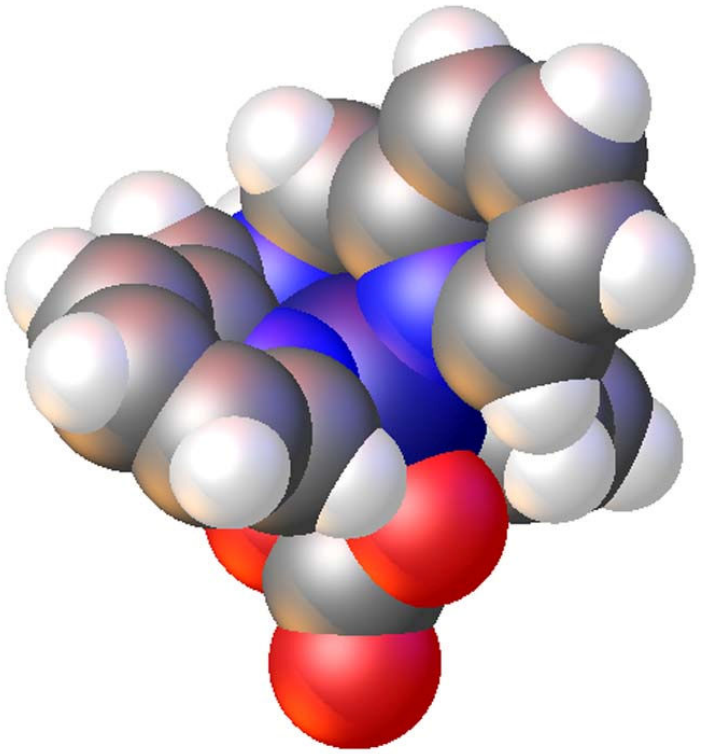

Figure 3.13: Crystal structure of $[Co(tpa)(CO_3)]^+$ shown in space filled model.[196] The coordinating oxygen atoms are shown in red.

3.2.4.2. Identity of the counter ion

Adsorption isotherms were measured for two salts of $[Co(tren)Cl_2]^+$ – the perchlorate and the chloride salts. The two complexes have identical adsorption equilibrium constants of 6.9×10^4, and very similar maximum surface coverage values of 2.22×10^{-6} mol g^{-1} and 2.03×10^{-6} mol g^{-1}. This suggests that the identity of the counter ion has little effect on the binding of the complex to the surface of goethite.

3.2.4.3. Presence of functionality on tame based ligands

The adsorption isotherms of some of the complexes of ligands described in Chapter 2 have been measured (Figure 3.14). The adsorption isotherms show that the complex $[Co(tst)Cl_3]$ has a lower maximum surface coverage than $[Co(tame)Cl_3]$. Furthermore, the isotherm of $[Co(nst)Cl_3]$ has an even lower maximum coverage than $[Co(tst)Cl_3]$ (Figure 3.14). This is likely to be due to the relative size of each complex, as seen in Section 3.2.4.1.1.

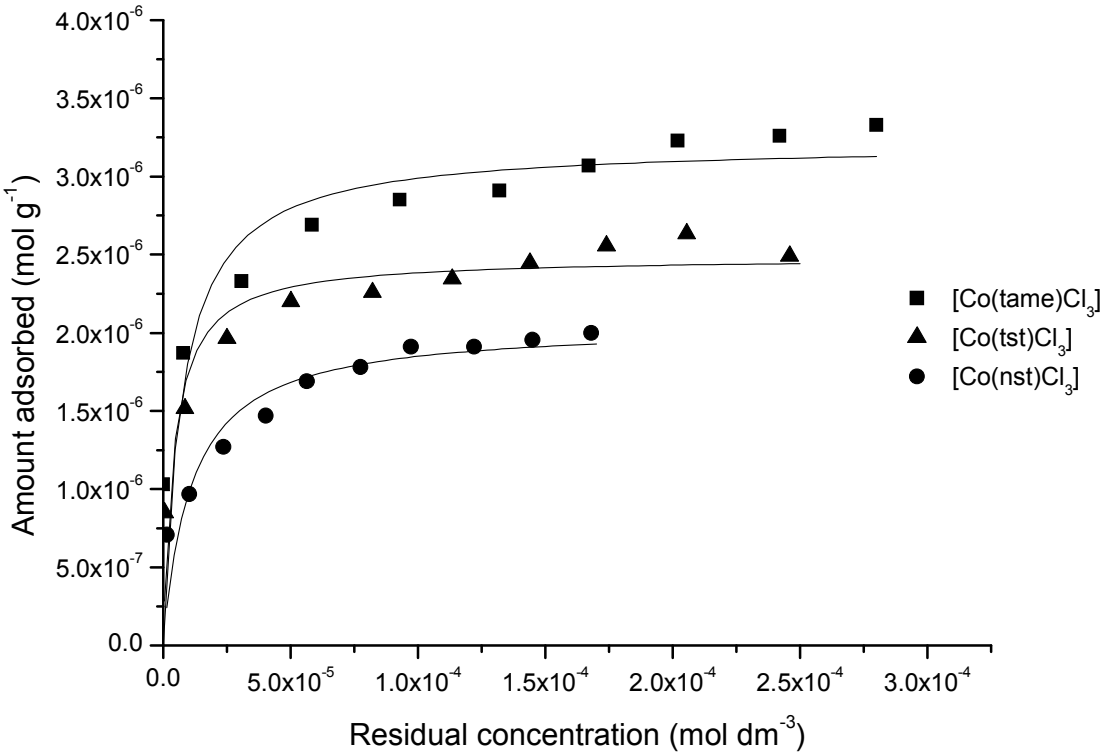

Figure 3.14: Adsorption isotherms of [Co(tame)Cl_3], [Co(tst)Cl_3] and [Co(nst)Cl_3].

3.2.4.4. Identity of the metal (cobalt vs chromium)

The adsorption isotherm of [Cr(tame)Cl_3] has been measured in order to gain a comparison of the relative binding of cobalt and chromium complexes (Figure 3.15). Compared to the cobalt complex, the chromium complex shows slightly higher maximum surface coverage, but lower binding equilibrium constant (Table 3.1). This observation supports the hypothesis that cobalt complexes may bind to iron oxide surfaces in a similar manner to the binding of chromium in various surface treatments.

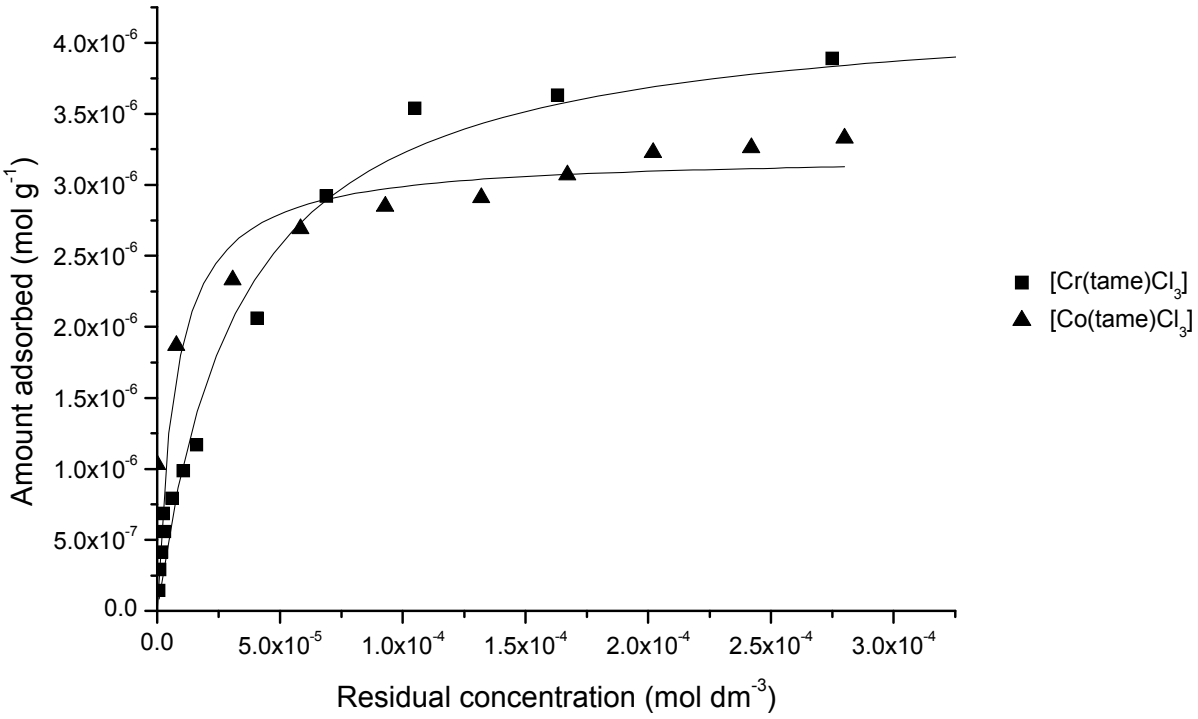

Figure 3.15: Adsorption isotherms of [Cr(tame)Cl_3] and [Co(tame)Cl_3].

3.2.5. Remarks on the binding model

For those complexes of which a significant uptake onto goethite is observed, the data generally fits to the Langmuir model quite well. For the complexes [Co(tame)$_2$]Cl_3 and [Co(tpa)Cl_2]ClO_4 the R^2 value is very low and the error associated with the value of *b* is very high. For the remaining complexes, the R^2 value is between 0.73 ([Co(tame)Cl_3]) and 0.99 ([Co(dien)Cl_3]).

It is worth considering whether the data may indicate a binding mechanism other than the simple Langmuir model utilised herein. The isotherms for [Co(tame)Cl_3] and those for [Co(tst)Cl_3] and [Co(nst)Cl_3] seem to show a pattern in the distribution of data points around the fitted line (Figure 3.14). Rather than being scattered either side of the line, the first half of the isotherm is consistently below the line and the second half consistently above. This may indicate that the true nature of binding in this case is more like an L-4 type in Figure 3.3, a stepped isotherm in which the initial binding is followed by a subsequent process (Figure 3.16).

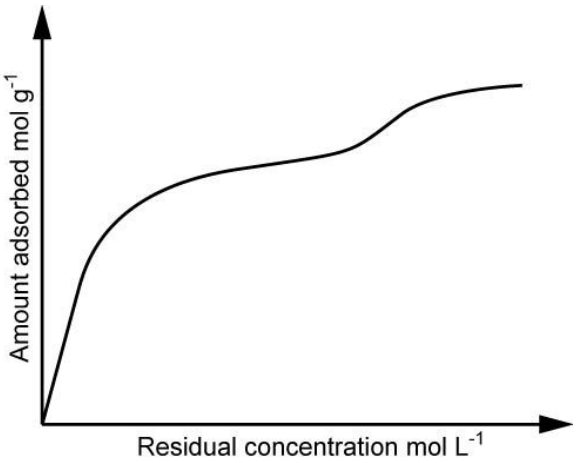

Figure 3.16: A stepped Langmuir isotherm (type L-4 in the classification of Giles *et al*).

There are several possible explanations for such an interpretation. One such possibility is that the initial binding is due to the saturation of the available tridentate domains by facial binding of the complex. The second step could be due to subsequent adsorption of the complex at bidentate or monodentate sites via edge and corner sharing. If the complex has significantly lower affinity for these sites, this would explain the delayed appearance of the second plateau. Another possibility is that the second adsorption process consists of a rearrangement of the complexes at the surface to accommodate greater adsorption. The complex may initially adsorb in a loosely packed manner, and subsequently rearrange to a tighter packing in order to fit in additional molecules. One other possibility is that the second step is due to the displacement of some surface bound entity, such as water.

3.3. Conclusion

The adsorption isotherms of several cobalt complexes and a chromium complex on goethite have been measured. The results show that complexes bearing exchangeable ligands are able to bind to the goethite surface. Complexes with three exchangeable ligands show, in general, greater maximum surface coverage and higher binding equilibrium isotherms than those bearing two. The maximum surface coverage appears to be related to the size of the binding complex, with larger molecules resulting in lower coverage. The binding of chromium seems to be similar in nature to that of cobalt. These results support the hypothesis that cobalt complexes with exchangeable ligands may be able to bind to iron oxide surfaces in a manner similar to that seen for chromium in various metal treatments.

Chapter Four

Additional surface binding studies

4.1. Introduction

In Chapter 3 the binding of cobalt(III) complexes to lightly oxidised iron surfaces was examined. This was achieved by monitoring the decrease in concentration of the cobalt(III) complex in aqueous solution upon exposure to high surface area goethite. However, this method requires that we infer binding to the surface as the mode of removal from solution. It would be desirable to obtain some direct evidence of cobalt(III) complexes binding to the surface of iron or stainless steel.

There are several methods for probing the surface properties of a material. These include scanning electron microscopy, X-ray energy dispersive spectroscopy, contact angle and quartz crystal microbalance. These will be introduced in the following sections.

4.1.1. Scanning electron microscopy

An electron microscope is a type of microscope that illuminates its sample with electrons in place of visible light. Because the wavelength of the electrons used is approximately 10,000 times shorter than that of photons of visible light, a much higher resolution can be obtained than through using light microscopes. The most commonly used electron microscope is the scanning electron microscope (SEM).

An SEM works by focussing an electron beam through electromagnetic lenses to a fine probe. This probe is then scanned along the specimen surface in parallel straight lines to generate a rectangular raster. The interaction between the electron probe and the specimen causes the production of secondary electrons, backscattered electrons and characteristic X-rays. This interaction occurs within a particular volume under the sample surface, which is roughly pear shaped (Figure 4.1).

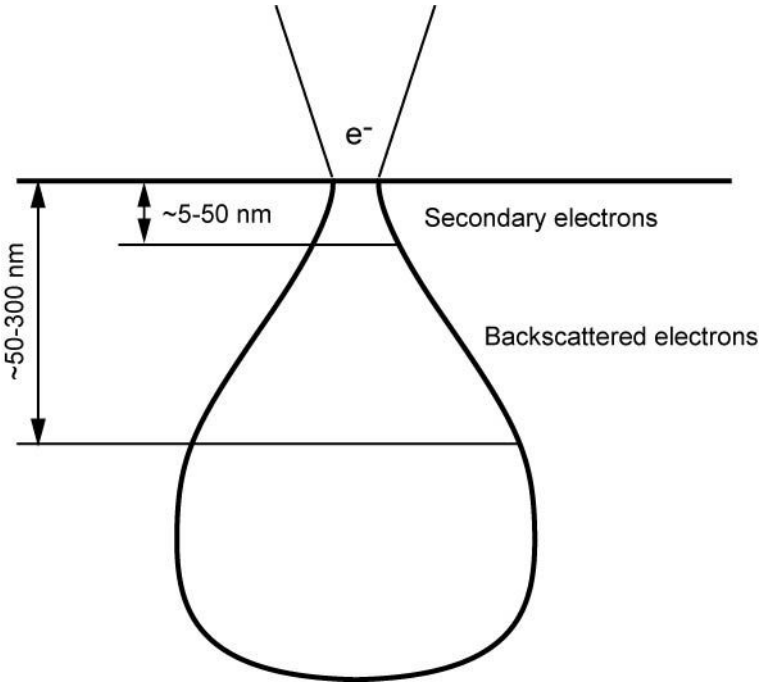

Figure 4.1: Schematic representation of the interaction of the electron probe with the substrate showing the escape depth for each electron type.

Secondary electrons are formed by the transfer of the kinetic energy of an incident electron to an electron of a specimen atom, expelling it from its orbital. These electrons usually have energy of around 3 – 5 eV and so can only escape from a depth of around 5 – 50 nm within the sample. Backscattered electrons result from elastic scattering of the incident electrons from the sample. They have much higher energy than secondary electrons and can therefore escape from greater depths of up to 300 nm. The characteristic X-rays produced can be used for chemical analysis of the surface (see Section 4.1.2).

The signal electrons are collected by the detector, and an image is generated by a one to one correlation between scanned points and picture points – the intensity of detected electrons at any point on the sample determines the brightness for the equivalent pixel in the display. The contrast seen in the image is due in part to the trajectory of the ejected electron. In much the same way as with visible light, surfaces that face the detector will appear lighter, as a larger number of the ejected electrons will reach the detector, while those ejected from surfaces facing away from the detector will not reach it as easily. Thus the brightness is related to shape.

By detecting backscattered electrons, contrast due to the composition of the sample can

also be seen. The ability of a backscattered electron to escape depends on the atomic number of the atoms in the sample, and so surfaces of different elements will appear in different shades.[64] The image in Figure 4.2 comprises two SEM images of the same aluminium-zirconium alloy surface. The upper image was formed using back scattered electron detection, and the composition of the surface is visible, with the lighter areas being zirconium aggregates within the aluminium matrix. The lower image was taken using secondary electrons and allows the topography of the surface to be viewed in greater detail.

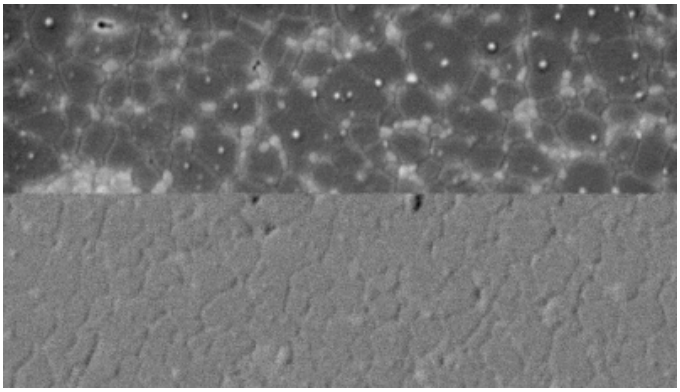

Figure 4.2: SEM images of the same aluminium-zirconium surface using back scattered electron detection (top) and secondary electron detection (bottom).

SEM is able to provide images with excellent three dimensional detail due to its large depth of field. Figure 4.3 shows an SEM image of the pollen of various plants, in which the three dimensional detail is clearly shown.

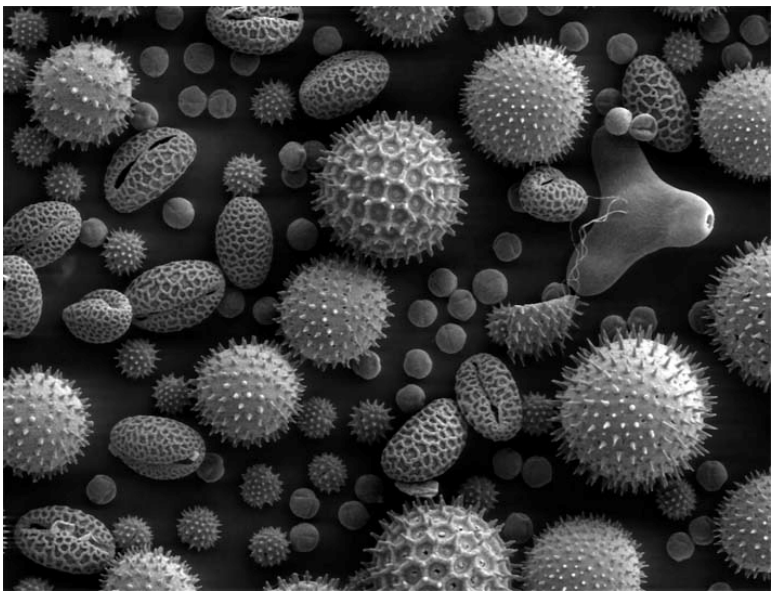

Figure 4.3: SEM image of the pollen of some common plants (Dartmouth Electron Microscope Facility).

4.1.2. Energy-dispersive X-ray spectroscopy

Energy-dispersive X-ray spectroscopy (EDS) is a technique that determines the identity and quantities of chemical elements at a surface. This is achieved by measuring the energy of the characteristic X-rays emitted after bombardment with high energy particles, such as the electrons in the SEM probe. If an incident electron strikes an electron in the inner shell of an atom it may transfer enough energy to cause the electron to be ejected from its orbital within the atom (Figure 4.4). This gap in the orbital will quickly be refilled by an electron from an outer shell, with the generation of an X-ray with energy equal to the difference between the energy of the outer and inner shells.

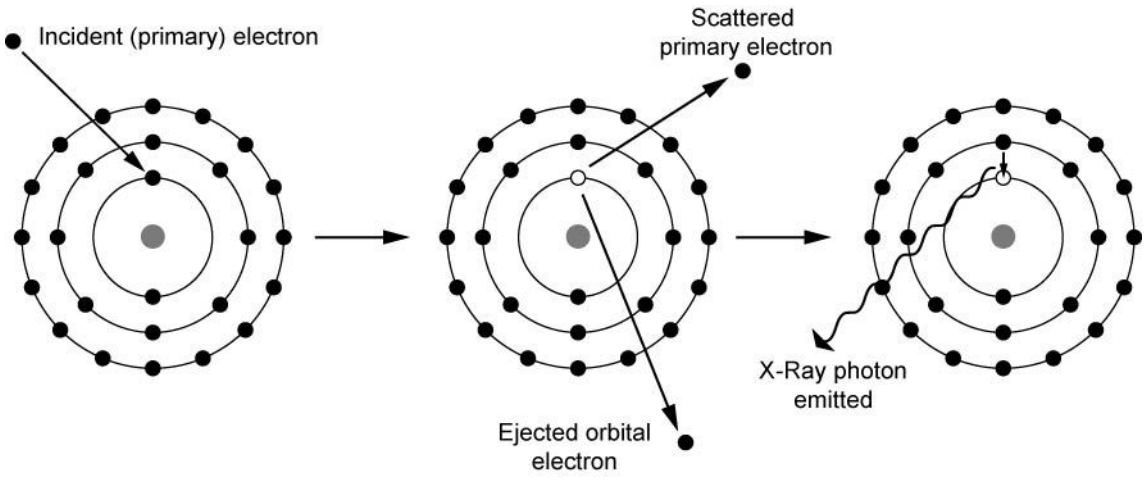

Figure 4.4: Schematic representation of the generation of the $K\alpha_1$ transition in EDS. Other transitions are also possible by electron transfer between different shells. Diagrams showing shells are used for clarity and do not imply a Bohr model of the atom is being employed.

Several different characteristic X-rays can be emitted from any element, depending on shells between which the transfer occurs. These are commonly notated using Siegbahn Notation, comprising a capital letter, a Greek letter and a subscript number. The capital letter refers to the shell into which the electron is transferred, where K is the $n = 1$ shell, L is $n = 2$ and so forth. The Greek letter refers to the intensity of the radiation, with α being the highest; the subscript number is a further indication of the intensity, with 1 the highest.[64] The transition in Figure 4.4 is the $K\alpha_1$ transition.

4.1.3. Contact angle

When a drop of liquid comes into contact with a solid substrate it will form a droplet, the shape of which is dependent on the properties of the liquid and the substrate. For example, water in contact with a hydrophobic surface, such as the panel of a freshly waxed car, forms a bead in order to minimise the interaction between the two phases. This interaction can be quantified by the angle formed between the liquid-vapour interface and the liquid-solid interface, which is defined as the contact angle, θ_e (Figure 4.5).

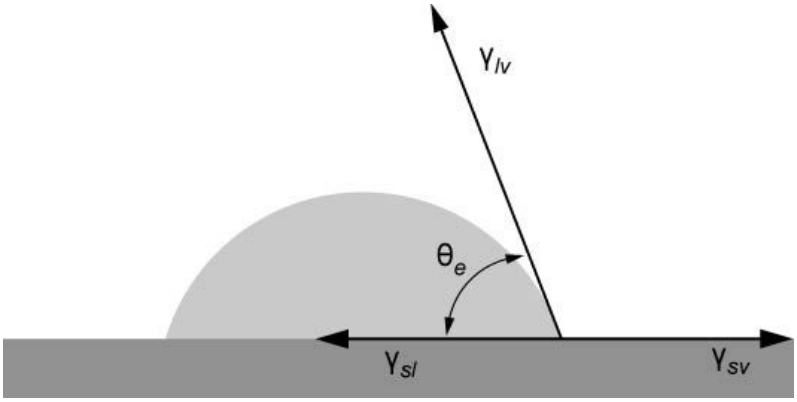

Figure 4.5: The contact angle of a liquid in contact with a solid substrate.

The relationship between the surface, liquid and vapour properties and the contact angle is described by Equation (4.1), Young's equation.

$$\gamma_{lv} \cos \theta_e = \gamma_{sv} - \gamma_{sl} \quad \textbf{(4.1)}$$

Where γ_{sv}, γ_{lv} and γ_{sl} are the solid-vapour, liquid-vapour and solid-liquid interfacial tensions.[197] Because the measured angle is dependent on the properties of the surface, it may be possible to infer formation of a layer on the surface of a substrate through examination of the contact angles of a treated and untreated surface. If the average contact angle on a treated surface is significantly different to that of an untreated surface, this may indicate the surface properties have been modified by deposition of a thin layer.

4.1.4. Quartz crystal microbalance

A quartz crystal microbalance (QCM) measures the mass of a sample per unit area by measuring the change in frequency of an oscillating quartz crystal. This oscillation is due to the piezoelectric effect. This was discovered by Pierre and Jacques Curie, who observed that a

mechanical stress applied to the surface of various crystals generated a potential across the surface of the crystal of magnitude proportional to the applied stress.[198] A simple model for the piezoelectric effect is shown in Figure 4.6. Before the force is applied, the positive and negative charges cancel each other, resulting in a neutral molecule. When a force is applied, the internal structure is deformed which causes the gravity centres of the positive and negative charges to move, generating a small dipole.[199]

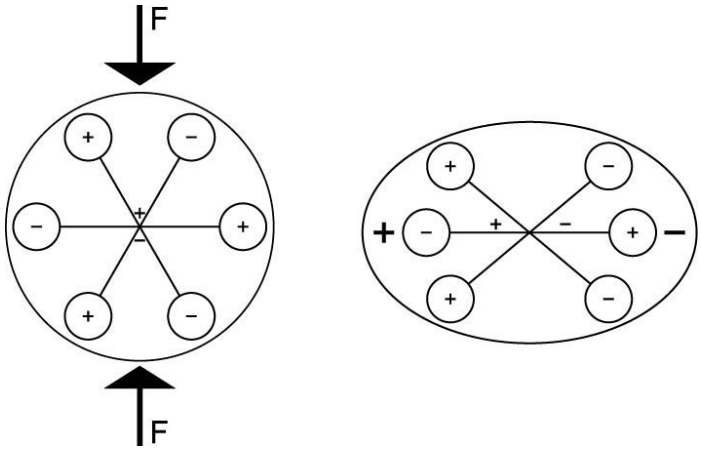

Figure 4.6: Simple model to demonstrate the piezoelectric effect: Force exerted on an unperturbed molecule causes separation of the positive and negative charges.

Shortly after the discovery of the piezoelectric effect, the reverse piezoelectric effect was verified. The application of a voltage across a crystal will result in a mechanical strain. In quartz this is seen as a shear strain (Figure 4.7). The application of a voltage of equal magnitude but of opposite polarity will result in a shear strain of equal magnitude in the opposite direction.

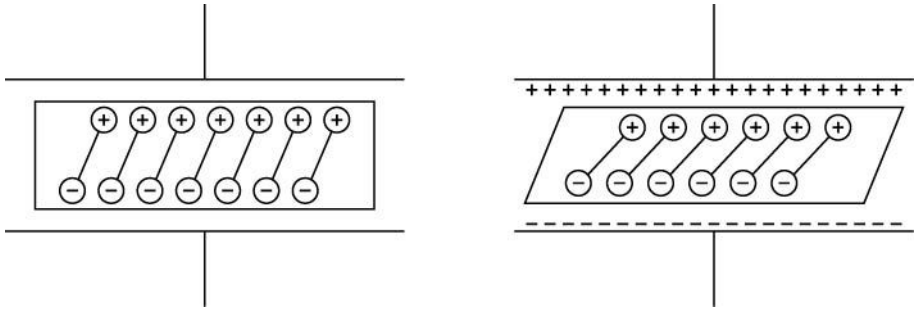

Figure 4.7: Reverse piezoelectric effect.

If an alternating potential is applied across a quartz crystal, this results in the oscillation of the crystal between the two strained forms. This establishes an acoustic wave that propagates the thickness of the crystal, reflecting back into the crystal at its surfaces. The

frequency of this acoustic wave is given by Equation (4.2).

$$f_0 = \frac{\upsilon_{tr}}{2t_q} \quad \textbf{(4.2)}$$

Where v_{tr} is the transverse velocity of sound in AT-cut quartz (3.34 x 10^4 m s^{-1}) and t_q is the thickness of the quartz crystal. A small change in thickness causes a change in the frequency of the acoustic wave, as described by the Sauerbrey equation (Equation (4.3)).[198]

$$\Delta f = -2 f_0^{\,2} \frac{\Delta m}{A(\mu_q \rho_q)^{1/2}} \quad \textbf{(4.3)}$$

In which Δf is the change in frequency, f_0 is the frequency of the quartz crystal before mass change, Δm the mass change, A the piezoelectrically active area, ρ_q the density of quartz and μ_q the shear modulus. The change in thickness has been expressed as a mass change per area unit as governed by the relationship in Equation (4.4).

$$\Delta t = \frac{\Delta m}{\rho_q A} \quad \textbf{(4.4)}$$

This allows the change in mass on the surface of a vibrating quartz crystal to be monitored by measuring the change in frequency that accompanies that deposition of the material.

4.2. Results and Discussion

A polished sample of iron was treated with 5 mM of [Co(nst)Cl_3] solution, and compared to a sample that had not been treated. This was done by analysis with an SEM fitted with an EDS analyser and by observation of the contact angles of water in contact with the surfaces.

4.2.1. SEM/EDS

The SEM images show little difference between the treated and untreated surfaces (Figure 4.8). However, it was not expected that the electron microscope images would show any difference, because a monolayer of cobalt(III) complex would not be visible at the

resolution attainable by this microscope.

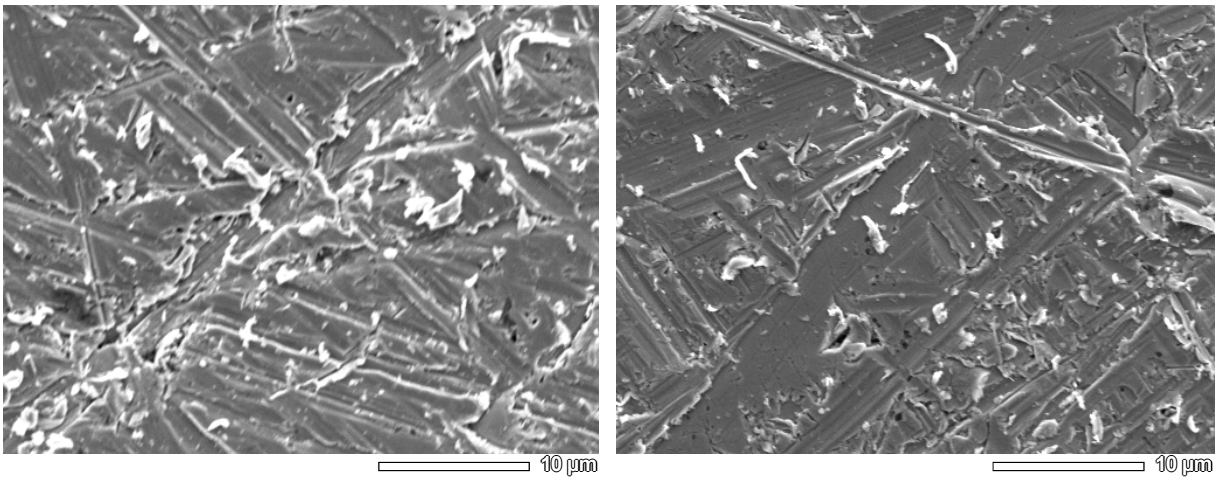

Figure 4.8: SEM of blank surface (left) and treated surface (right).

The areas shown in the SEM images above in Figure 4.8 were analysed by EDS. The two areas showed differences in the percentage of the elements monitored (Table 4.1).

Table 4.1: Percentage of carbon, nitrogen, sulfur, iron and cobalt at the surface of an untreated iron surface and at the surface of an iron surface treated with 5 mM [Co(nst)Cl_3].

Element	Mass % (blank)	Mass % (treated)
C	1.15 (± 0.02)	5.72 (± 0.02)
N	1.01 (± 0.05)	2.23 (± 0.07)
S	0.04 (± 0.06)	0.24 (± 0.07)
Fe	97.80 (± 0.80)	89.34 (± 1.03)
Co	0	2.47 (± 0.68)

The treated sample shows an increase in the amount of cobalt, sulfur, carbon and nitrogen at the surface, and a decrease in the amount of iron relative to the untreated surface. However, the relative amounts do not match those of the complex. For example, the ratio of cobalt to sulfur at the surface is approximately 10:1, whereas in the complex there is one of each atom, which relates to a mass ratio of approximately 1.8:1. Nevertheless, the presence of the appropriate elements in greater amounts than in the untreated sample is encouraging evidence of binding of the complex to the surface. Moreover, the quoted errors are related to the precision of the measurement by the instrument. There may be greater error in the accuracy and the instrument sensitivity may be element dependent, which could mean these

values within error of the ratio of the complex than they are.

4.2.2. Contact angle

The contact angles of the same surfaces used in Section 4.2.1 have been measured (Table 4.2). For each treatment, three different regions on the surface were measured, with nine or ten measurements of the advancing contact angle taken for each region.

Table 4.2: Average contact angle for iron surfaces with and without [Co(nst)Cl_3] treatment.

Treatment	Average contact angle
Blank	115.2°
[Co(nst)Cl_3]	104.5°

The treated surface shows a lower contact angle than that of the untreated complex. This suggests that the surface of the treated sample is different to that of the untreated. However, it is known that the contact angle of a surface can be significantly increased due to the presence of organic contamination on the surface.[200] In order to ensure that the data obtained by these experiments is reproducible, investigations into the optimum conditions for pre-treatment of the surface prior to exposure to the cobalt(III) complex solution are being carried out to provide a foundation for future work in this area. Significant variation has been observed in the contact angle measurement based on surface treatment protocols of steel surfaces.[201]

4.2.3. QCM

The binding of cobalt complexes to stainless steel has been followed using the quartz crystal microbalance (QCM). The stainless steel coated vibrating crystal was exposed to the Milli-Q water medium until a baseline was established, and then exposed to a 5 mM solution of [Co(tacn)Cl_3]. Once the frequency was at a steady level, the Milli-Q water solution was used again to rinse the surface of the crystal.

This measurement was undertaken many times, but unfortunately on most of these occasions the frequency of the crystal was too unsteady to make any valid measurements. However, one measurement was obtained in which the frequency held steady throughout the experiment (Figure 4.9). The sudden changes in frequency at ~1300 seconds and ~3200

seconds relate to the change of the solution being pumped over the crystal to the [Co(tacn)Cl_3] solution and the Milli-Q water, respectively. The dotted lines indicate the steady state frequencies before exposure to the [Co(tacn)Cl_3] solution and after rinsing with Milli-Q water.

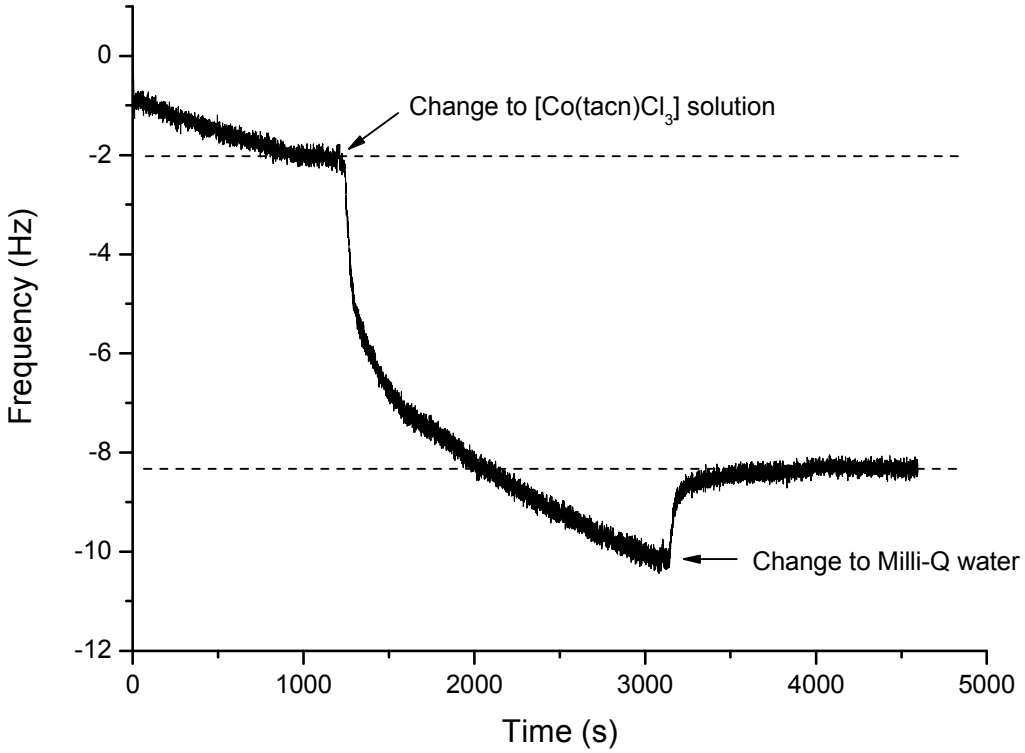

Figure 4.9: Frequency change of a stainless steel coated quartz crystal upon exposure to a 5 mM [Co(tacn)Cl_3] solution and subsequent rinsing.

This experiment showed that the exposure of the [Co(tacn)Cl_3] solution caused the frequency of the crystal's vibration to decrease, suggesting deposition of the complex on the steel surface. Subsequent rinsing of the crystal showed the steady frequency to be approximately 6 Hz lower than that established at the start of the experiment. This suggests that the complex may have been bound to the surface of the steel.

4.3. Conclusion

The binding of cobalt complexes to iron and steel surfaces has been followed using SEM and EDS, contact angle and QCM. Each of these experiments has offered some suggestion that the complexes may be binding to the surface used. Contact angle measurements could be of further interest, but more work on experimental protocol is required to establish that any change in the measured angle is indicative of the formation of a layer on the metallic surface.

The QCM experiments could also be of further use, but are very labour intensive, practically quite difficult, so will require a major investment of time from a future research worker.

Chapter Five

Use of cobalt(III) complexes as inhibitors of corrosion on iron

5.1. Introduction

5.1.1. Corrosion

Corrosion is the result of a destructive reaction between a metal or metal alloy and a substance in physical or electrical contact with the exposed surface.[3, 35, 202] Electrochemical corrosion is caused by the flow of electrons from one metal, or region of metal, to another region or metal. For corrosion to occur, there must be a cathode, an anode, an electrolyte, and some connection between the two electrodes. The electrodes may be two different metals, different components of a metallic alloy or different areas of the same metal surface. The anodic region will corrode.[3]

Consider the reaction of metallic iron with hydrochloric acid:

$$Fe + 2HCl \rightarrow FeCl_2 + H_2$$

$$Fe \rightarrow Fe^{2+} + 2e^- \quad \text{(anodic reaction)} \qquad \textbf{(5.1)}$$

$$2H^+ + 2e^- \rightarrow H_2 \quad \text{(cathodic reaction)}$$

Dissolution by oxidation of the metal at its surface liberates electrons into the bulk metal (the anodic reaction). These then travel to the adjoining cathode, where they react with H^+ from the solution to form H_2.[35]

Many techniques are available to test and monitor corrosion. These include both physical and electrochemical methods, which will be discussed below.

5.1.2. Physical methods for corrosion testing and monitoring

Physical methods utilised in corrosion testing and monitoring involve exposing a sample to corrosive environments and then evaluating the resulting sample. Various techniques are used to analyse the corroded surface and corrosion products. SEM and AFM can be used to visualise the topography of a corroded surface and determine the presence of features such as pits and crevices. Techniques such as AES, EDS and XPS can provide information on the chemical composition of the corroded surface; FTIR and EXAFS, for example, can provide information about the surrounding surface atoms (see p. vii for a list of abbreviations).[203, 204]

Sample exposure can be achieved either through immersion in a corrosive liquid, or by the use of a simulated atmosphere.[34] This can be created in a closed cabinet, using a range of temperatures and humidity. In these cabinets, corrosion may be accelerated by the introduction of corrosive agents such as SO_2, chloride or ammonia. For example, the commonly used 'salt spray' test consists of a fog generated at 35°C by atomising 5% NaCl solution.[34, 205] An example of a physical technique for monitoring the rate of corrosion is measurement of the change in mass of a corroding sample. This can be either a decrease in mass due to the loss of material, or an increase in mass due to the formation of oxide products on the surface. Where this change in mass is small, it can be analysed using techniques such as QCM and TGA.[206]

5.1.3. Electrochemical methods for corrosion testing and monitoring

Electrochemical methods utilised in corrosion testing and monitoring take advantage of the fact that corrosion is an electrochemical process, and that many of the properties of these reactions can be measured.[34] The open circuit potential of a corrosion cell (E_{corr}), which can be measured directly with a high impedance voltmeter, is equivalent to the thermodynamic driving force of the reaction;[34] the current is equivalent to the rate of corrosion. However, because the surface may be acting as both a cathode and an anode (see Section 1.2), this current may not be directly measurable.[207] One approach to determine the corrosion current is to record cathodic and anodic polarisation curves of the corrosion cell and to plot ($E - E_{corr}$) against the logarithm of the current density. The linear region of each curve, known as the Tafel region, can be extrapolated to E_{corr} to give i_{corr} (Figure 5.1).[34, 35, 207, 208]

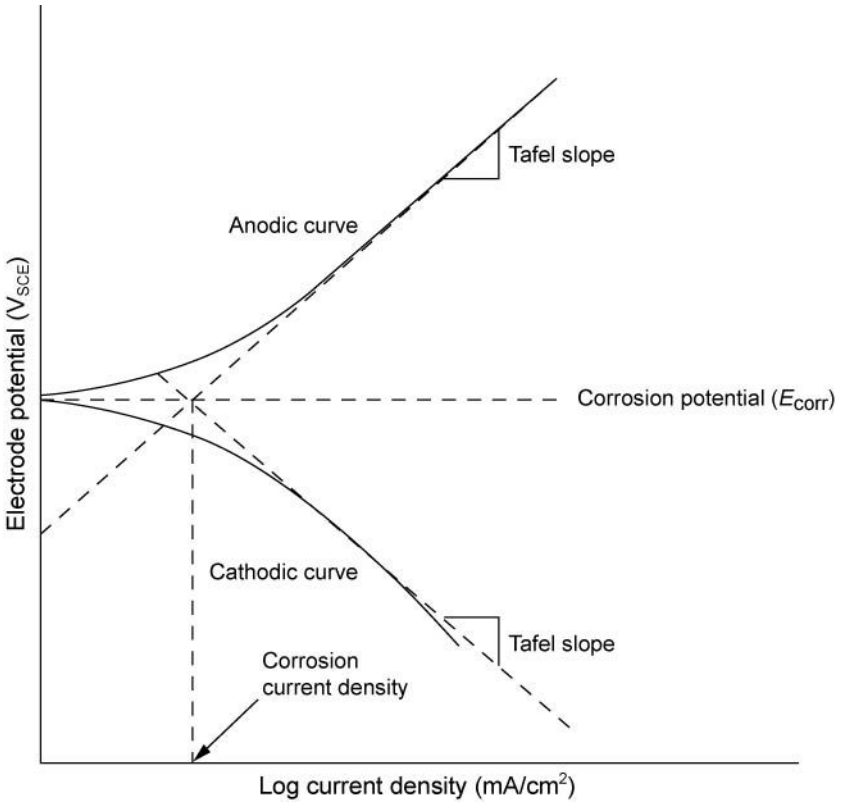

Figure 5.1: Hypothetical cathodic and anodic polarisation curves with Tafel line extrapolation to corrosion current.

The use of a Tafel extrapolation requires the application of a large overpotential, which may be undesirable due to its destructive nature. Another polarisation method that may be preferable is linear polarisation resistance.[207] At the region near the corrosion potential, the relationship between the applied potential and measured current is often linear. The slope of this line is proportional to the corrosion rate in the metal (Figure 5.2).[34, 35, 207, 208] Other electrochemical methods used to monitor corrosion include electrochemical impedance spectroscopy and electrochemical noise resistance.[207]

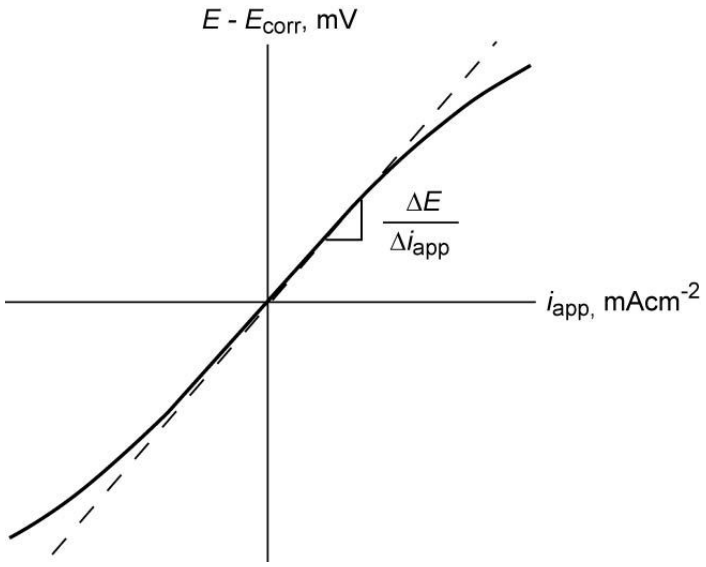

Figure 5.2: Hypothetical Linear Polarisation Resistance plot showing linear region near the corrosion potential.

5.1.4. Summary

Weight loss is the most common method of determining corrosion rate.[209] When this technique has been used in conjunction with electrochemical experiments, there is found to be a good agreement between the data.[210-212] Due to its simplicity, the weight loss of samples immersed in a corrosive solution was chosen as the method for measuring the rate of corrosion of iron in this work.

5.2. Results and Discussion

5.2.1. Inhibition by [Co(tame)Cl_3]

Polished and pre-weighed coupons of iron were suspended in 1 M HCl solutions containing various concentrations of [Co(tame)Cl_3] for four hours (see Section 7.2.2 for experimental detail). Table 5.1 shows the average weight loss recorded (in mg per cm^2 per min) for the different concentrations used. The percentage inhibition efficiency (η) at each concentration has been calculated using Equation (5.2).[210]

$$\eta\,(\%) = \left[\frac{W - W_{\text{inh}}}{W}\right] \times 100 \qquad \textbf{(5.2)}$$

In this equation, W and W_{inh} are the values of the mass loss after immersion in HCl

solutions without and with the inhibitor, respectively.

Table 5.1: Weight loss data for iron samples immersed in 1 M HCl solutions containing various concentrations of [Co(tame)Cl_3] for 4 hours at 53 °C.

Concentration (mM)	W (mgcm^{-2}min^{-1})	Std dev	η (%)
0	0.127	0.009	-
0.1	0.125	0.005	1.6
0.2	0.124	0.007	2.6
0.5	0.117	0.0004	8.2
1	0.107	0.006	16
2	0.097	0.004	24
5	0.089	0.003	30
10	0.078	0.002	39
20	0.065	0.001	49

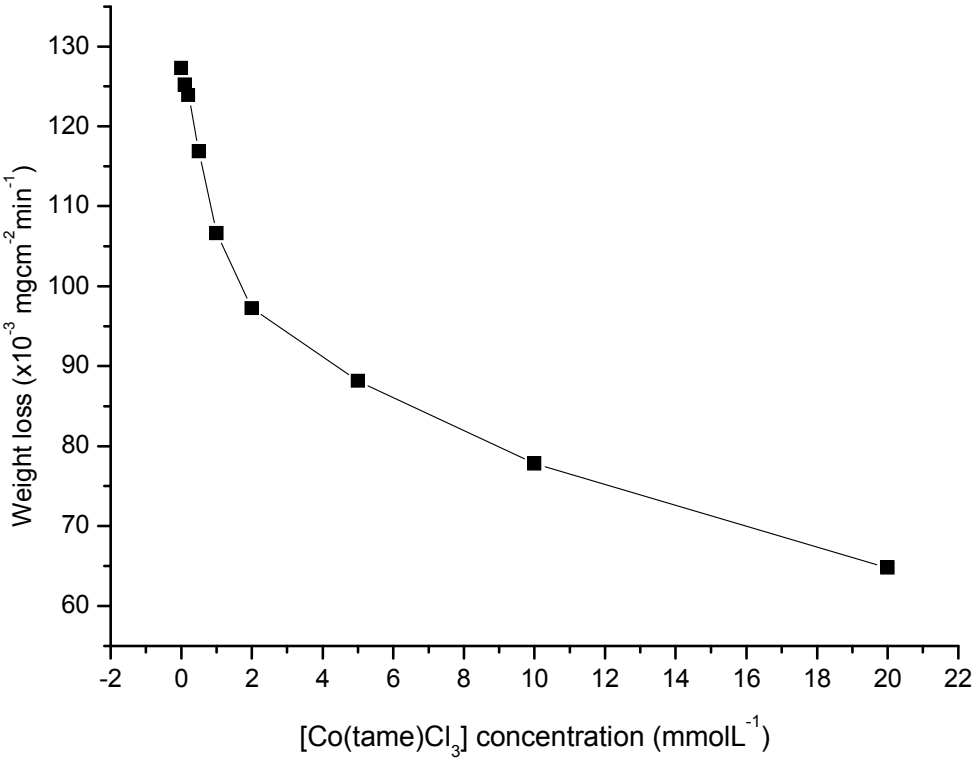

Figure 5.3: Weight loss of iron samples after immersion in 1 M HCl solutions containing various concentrations of [Co(tame)Cl_3] for 4 hours at 53 °C.

Figure 5.3 shows the weight loss of the iron coupons as a function of [Co(tame)Cl_3] concentration. The curve shows that the rate of corrosion decreases with increasing

concentration of [Co(tame)Cl_3]. This can alternatively be plotted as inhibition efficiency as a function of concentration (Figure 5.4). Its form is hyperbolic and has been fitted to Equation (5.3), yielding $a = 53 \pm 3$ %, $b = 2.8 \pm 0.5$ mmolL^{-1} with an R^2 value of 0.983. The value of a can be interpreted as representing the maximum possible inhibition (η_{max}), while b is the concentration required to achieve half of the maximum inhibition.

$$y = \frac{ax}{b+x} \qquad \textbf{(5.3)}$$

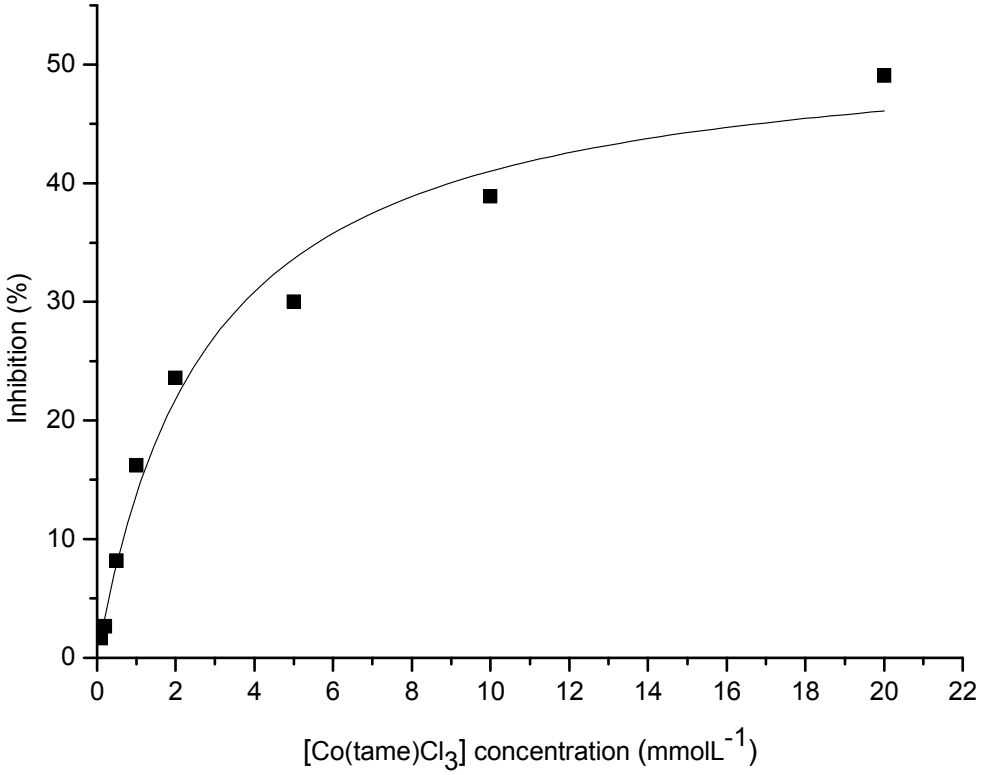

Figure 5.4: The inhibition of corrosion of iron in 1 M HCl solutions by [Co(tame)Cl_3], fitted to a hyperbolic curve yielding $a = 53 \pm 3$ % and $b = 2.8 \pm 0.5$ mmolL^{-1}.

5.2.2. UV-vis monitoring of [Co(tame)Cl_3]

It was observed during the weight loss experiments described above, that in the course of the experiment, the solution would lose its purple colouration, leaving a pale yellow solution. In order to gain further understanding of the corrosion inhibition, the consumption of the complex was examined by monitoring the decrease in the absorbance peak at 540 nm. The UV-vis spectrum of the corrosive solution was collected at various times throughout the experiment. Figure 5.5 shows the spectra collected from a 5 mM [Co(tame)Cl_3] corrosive

solution from the start of the experiment until no further absorbance in the green part of the spectrum is detectable. The decrease in absorbance at 540 nm is accompanied by an increase in absorbance at 400 nm, and the overlaid spectra pass through an isosbestic point at approximately 458 nm. Following the decrease of the absorbance peak at 540 nm to below the detection limit, the absorbance at 400 nm itself starts to decrease.

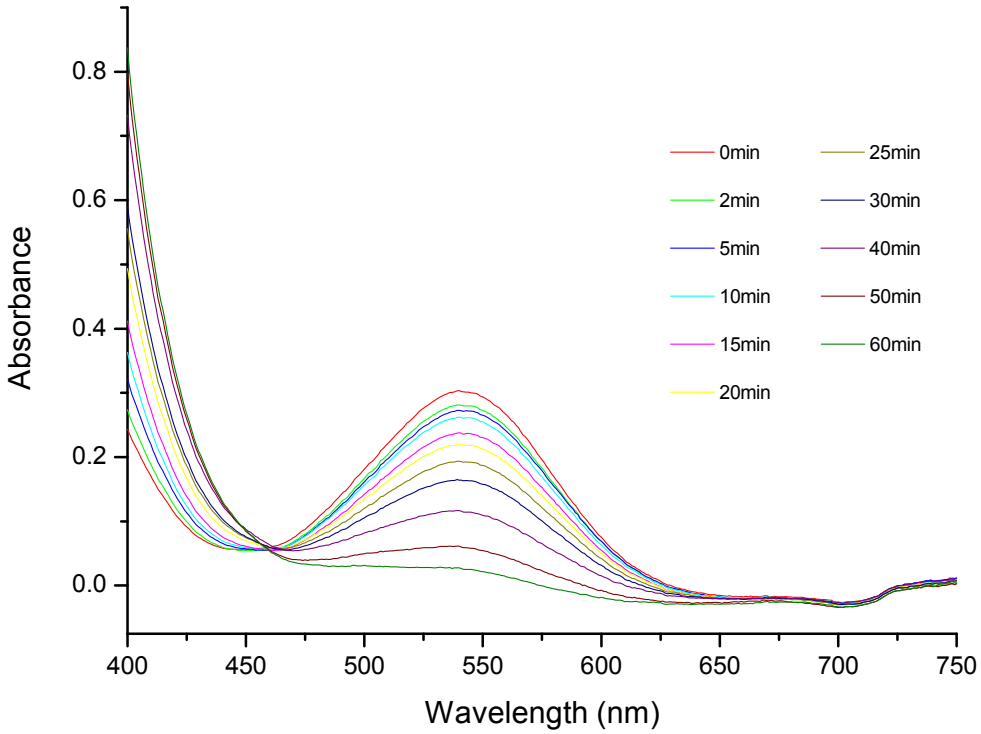

Figure 5.5: UV-vis spectra of the 5 mM [Co(tame)Cl_3] corrosive solution at various times during an immersive corrosion experiment.

The absorbance at 540 nm has been plotted as a function of time (Figure 5.6). The graph appears to be linear over the initial period, suggesting a zero order reaction, but is flat at later stages in the course of the reaction. This flat region has been extrapolated to zero, and this value subtracted from all the values in the data set. This data has been plotted (Figure 5.7) and the linear region has been fitted to yield a slope of -4.6 (± 0.1) x 10^{-3} min^{-1} (Table 5.2).

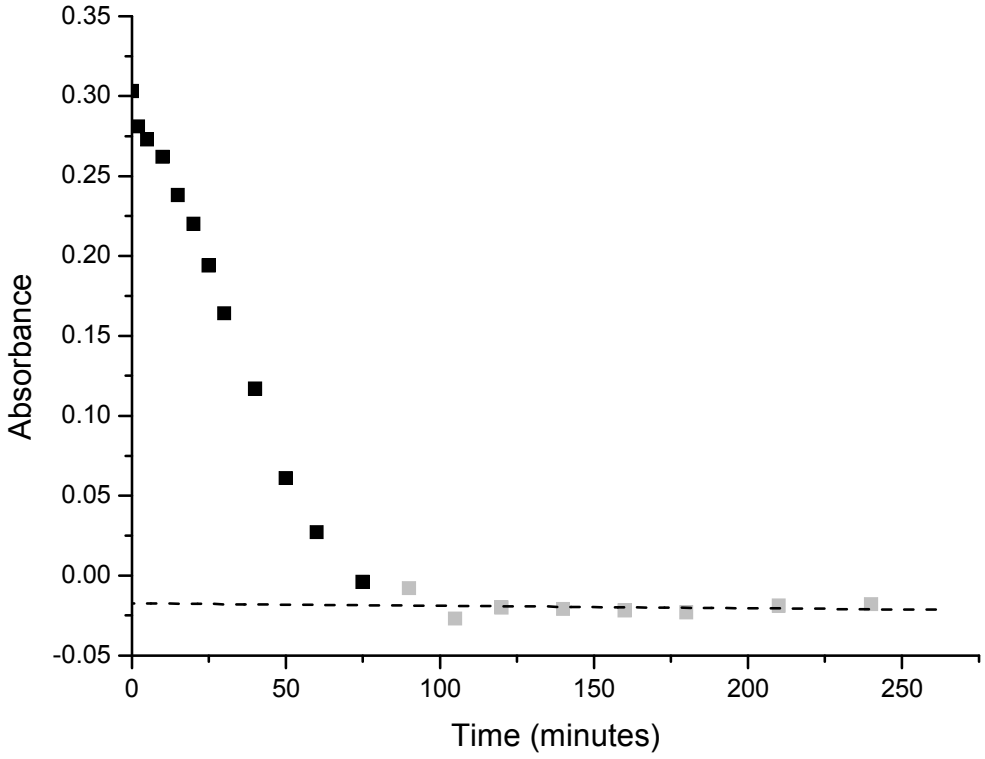

Figure 5.6: Raw data plot of the absorbance at 540 nm of a 5 mM solution of [Co(tame)Cl_3] inhibiting corrosion of iron in 1 M HCl solution. Points in grey were used to extrapolate absorbance to zero.

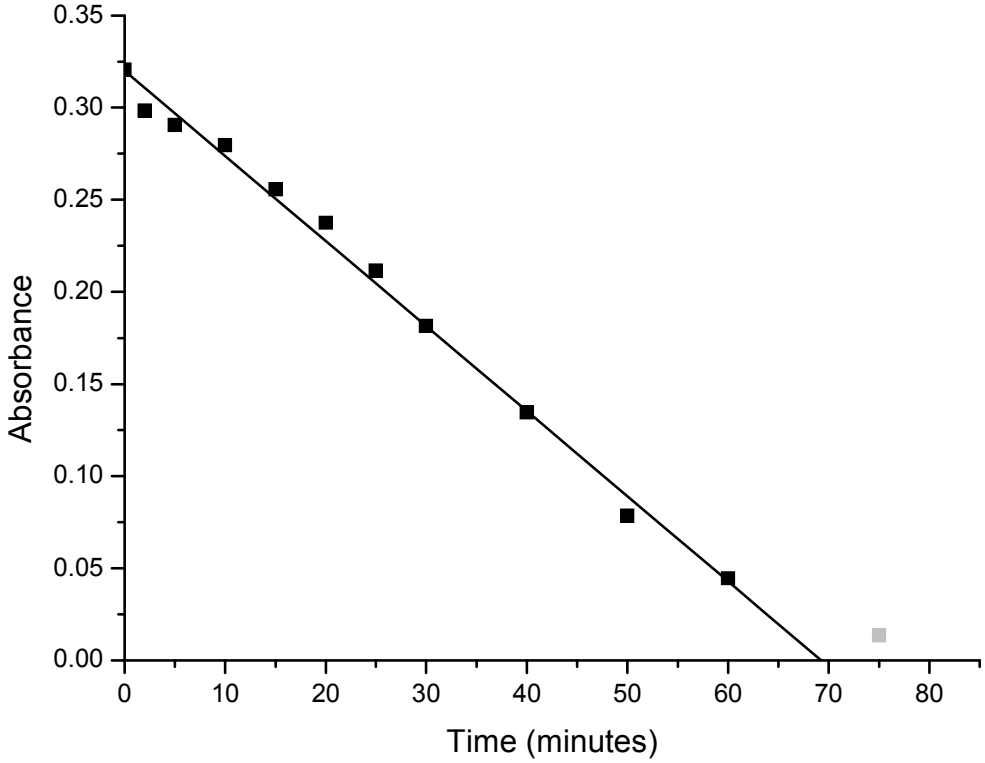

Figure 5.7: Plot of corrected absorbance data against time. Near zero points excluded for clarity. The point in grey was omitted in the fitting of the linear region to yield the line of best fit.

This observation of zero order kinetics can be rationalised if the reactions that contribute to the loss of colour are those of a Langmuir-Hinshelwood mechanism.[213] In this mechanism the species in solution (*A*) adsorbs to the surface (*S*) to form a surface complex (*AS*) which then reacts to give the products in a slow, rate determining step (5.4).

1. $A + S \rightleftharpoons AS$

2. $AS \rightarrow$ products (slow) **(5.4)**

Using a Langmuir isotherm model, sufficiently high concentrations of *A* will result in the saturation of the surface. Because the formation of products is rate limiting, the level of *AS* will remain relatively constant. Any surface sites vacated by the reaction of an *AS* unit will be quickly replaced due to the faster adsorption equilibrium. This means the rate with respect to *A* will be zero order provided its concentration is high enough to maintain surface saturation. Once the concentration drops below the level at which the surface is saturated, the rate may be expected to deviate towards first order kinetics due to the dependence of *AS*, and therefore the rate, on the concentration of *A*. This effect may be visible in Figure 5.6 where the absorbance after 90 minutes appears to deviate from the linear region before flattening out entirely. However, the absorbance readings at this level are very low and right at the limit of detection.

This analysis was also carried out for the corrosion of iron in 1 M HCl solutions containing 10 mM and 20 mM of [Co(tame)Cl_3] and the combined UV-vis spectra and presentation of the absorbance as a function of time are presented in Figure 5.8 – Figure 5.13. As with the 5 mM solutions, both show a linear decrease in absorbance at 540 nm, suggesting a zero order reaction, and have slopes of -9.1 (± 0.2) x 10^{-3} min^{-1} for the 10 mM solution and -12.6 (± 0.2) x 10^{-3} min^{-1} for the 20 mM solution.

Table 5.2: Slopes of Figure 5.7, Figure 5.10 and Figure 5.13.

Concentration	Slope (min^{-1})
5 mM	-4.6 (± 0.1) x 10^{-3}
10 mM	-9.1 (± 0.2) x 10^{-3}
20 mM	-12.6 (± 0.2) x 10^{-3}

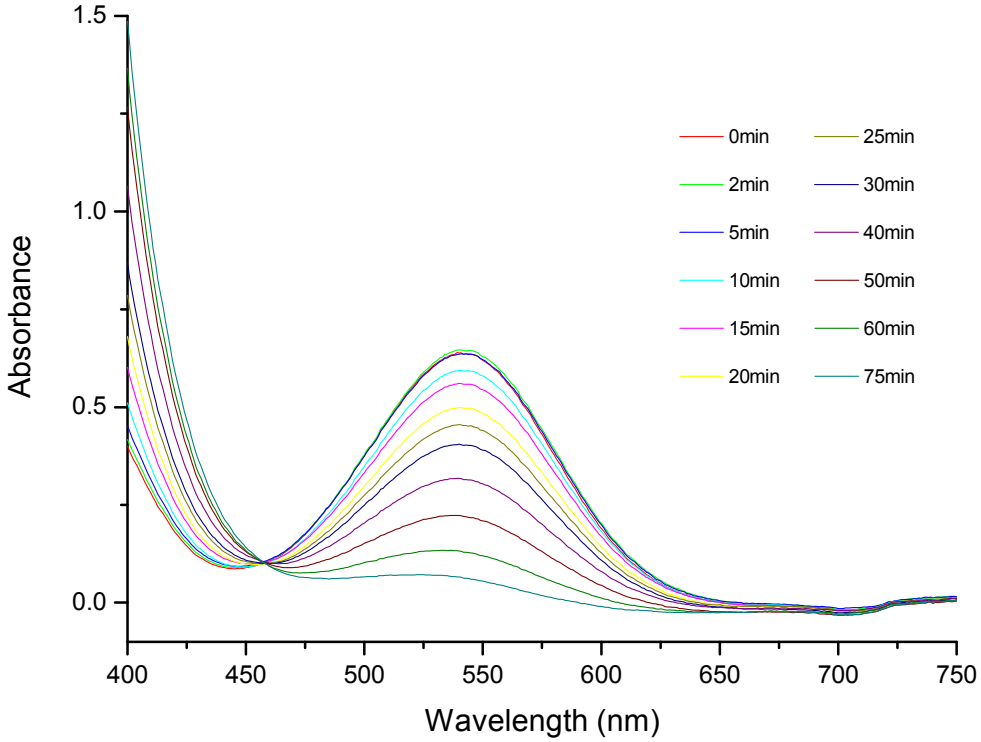

Figure 5.8: UV-vis spectra of the 10 mM [Co(tame)Cl_3] corrosive solution at various times during an immersive corrosion experiment.

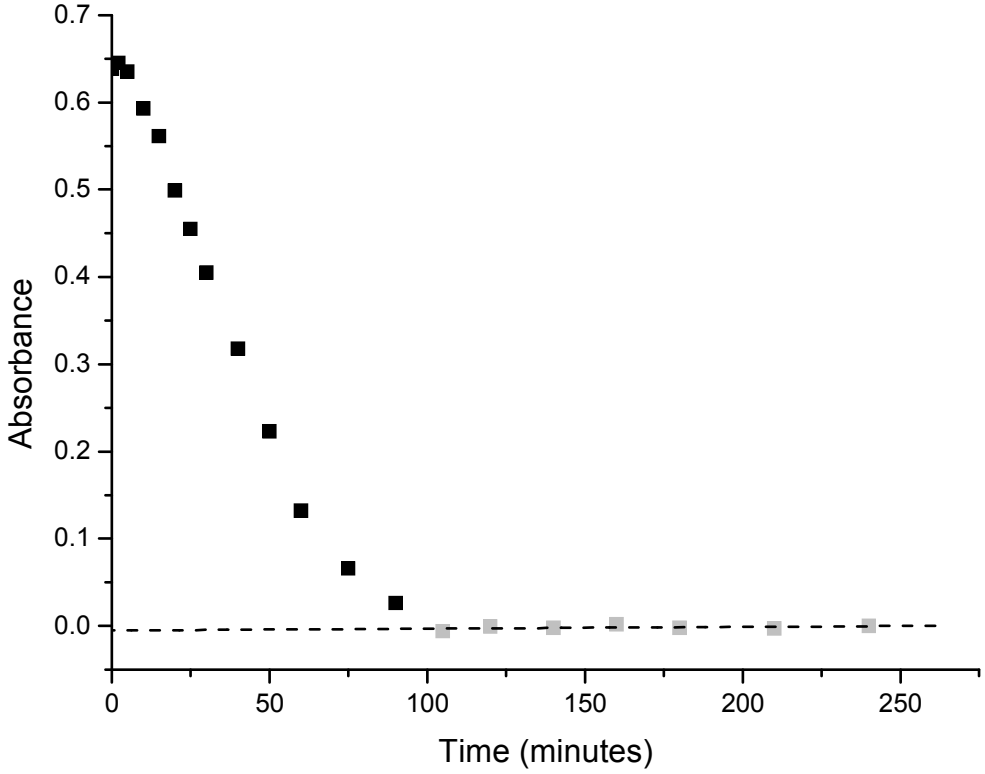

Figure 5.9: Raw data plot of the absorbance at 540 nm of a 10 mM solution of [Co(tame)Cl_3] inhibiting corrosion of iron in 1 M HCl solutions. Points in grey were used to extrapolate absorbance to zero.

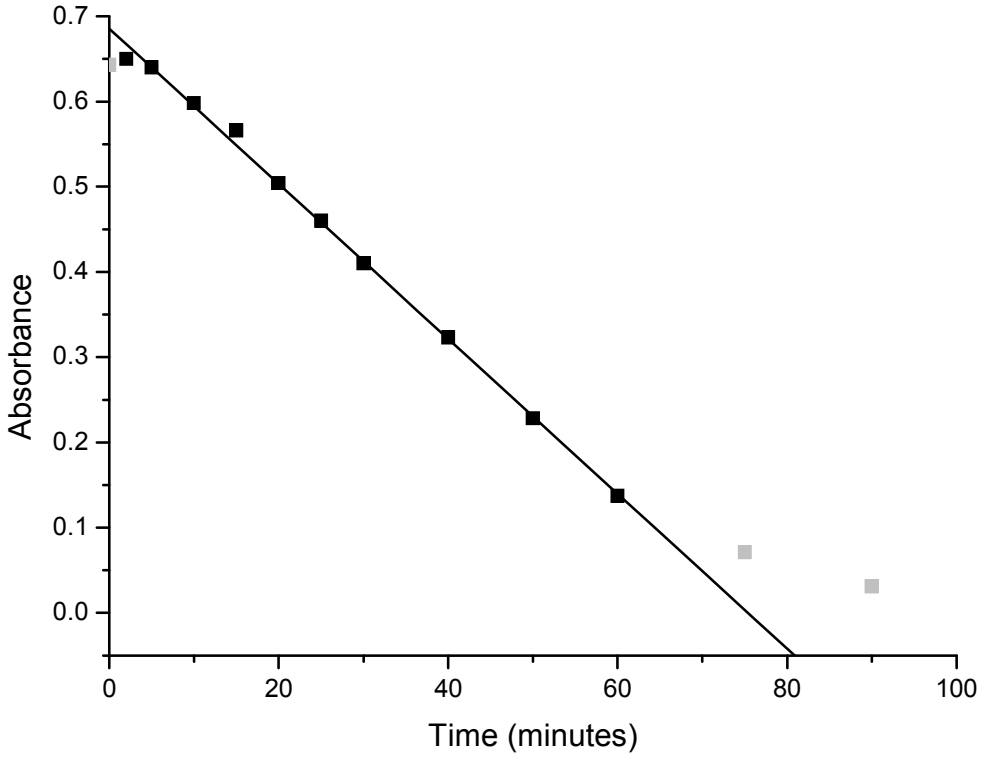

Figure 5.10: Plot of corrected absorbance data against time. Near zero points excluded for clarity. Points in grey were omitted in the fitting of the linear region to yield the line of best fit.

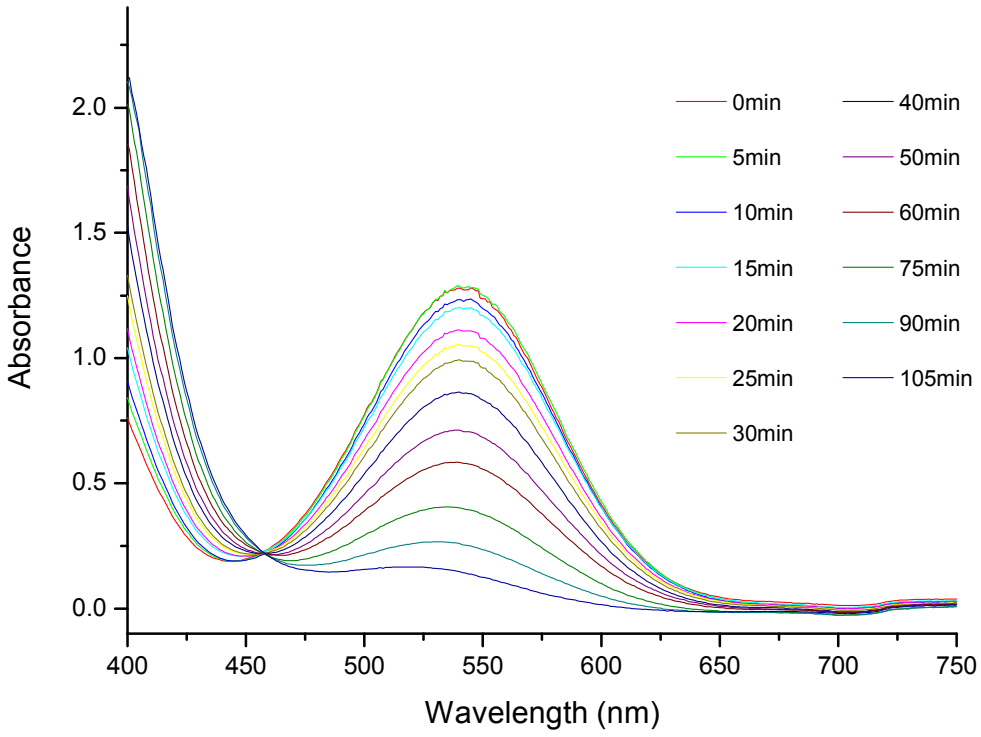

Figure 5.11: UV-vis spectra of the 20 mM [Co(tame)Cl_3] corrosive solution at various times during an immersive corrosion experiment.

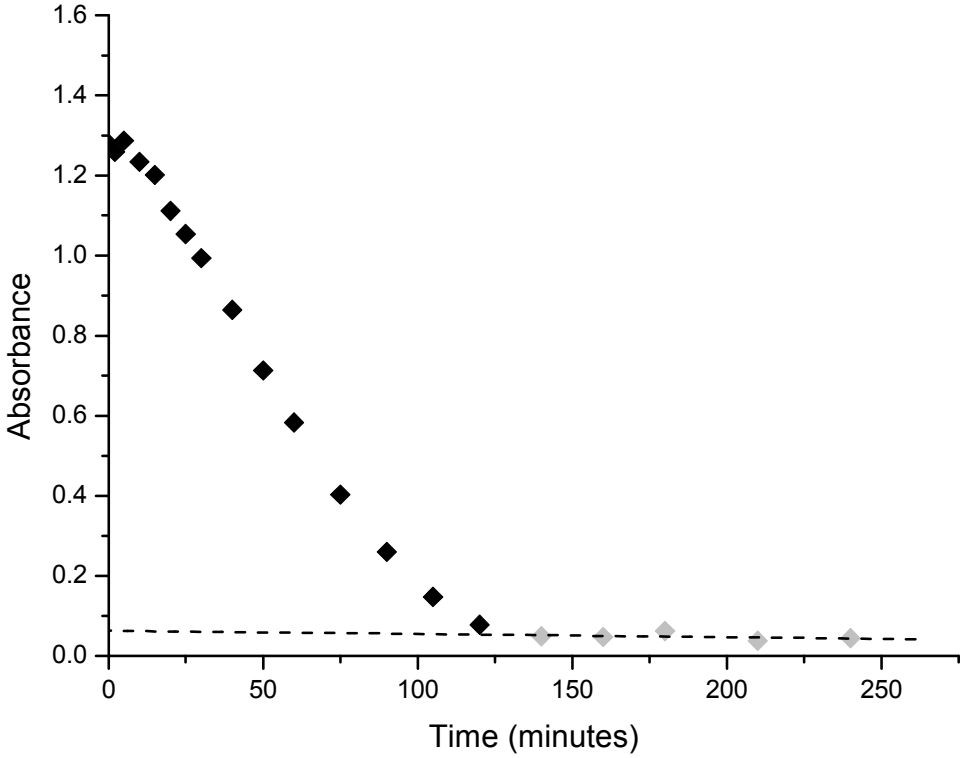

Figure 5.12: Raw data plot of the absorbance at 540 nm of a 20 mM solution of [Co(tame)Cl_3] inhibiting corrosion of iron in 1 M HCl solutions. Points in grey were used to extrapolate absorbance to zero.

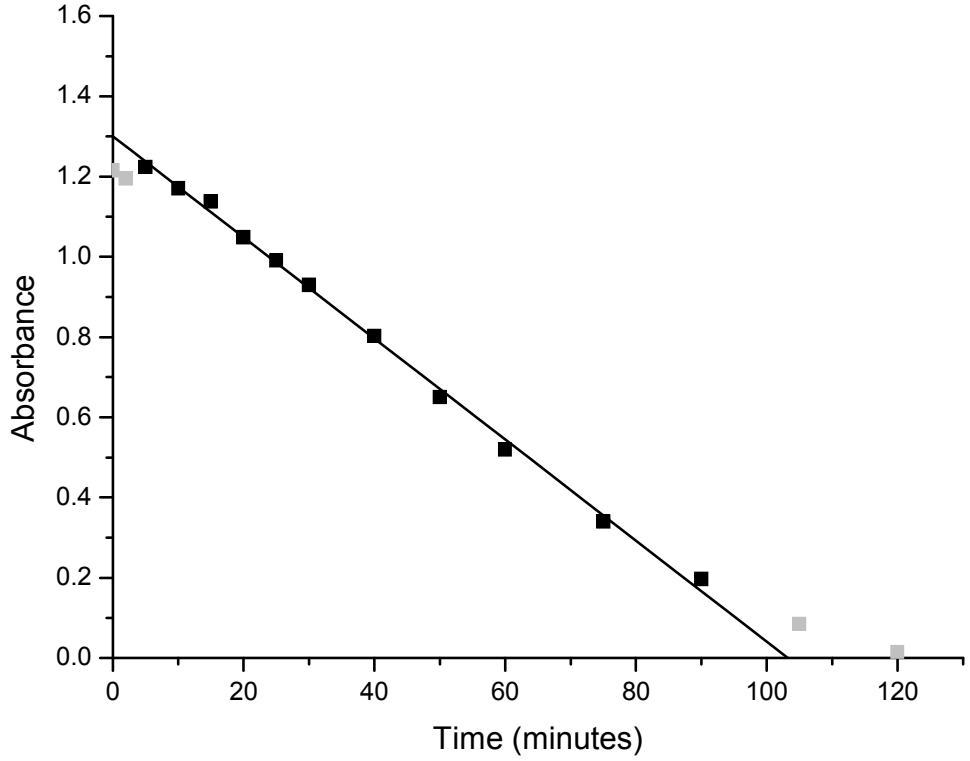

Figure 5.13: Plot of corrected absorbance data against time. Near zero points have been excluded for clarity. Points in grey were omitted in the fitting of the linear region to yield the line of best fit.

5.2.3. Inhibition by other complexes

The ability of other cobalt complexes to inhibit the corrosion of iron in 1 M HCl solution was tested. The complexes chosen were the same as those used for the goethite binding studies described in Chapter 3 (Figure 5.14). All complexes used were the chloride salts.

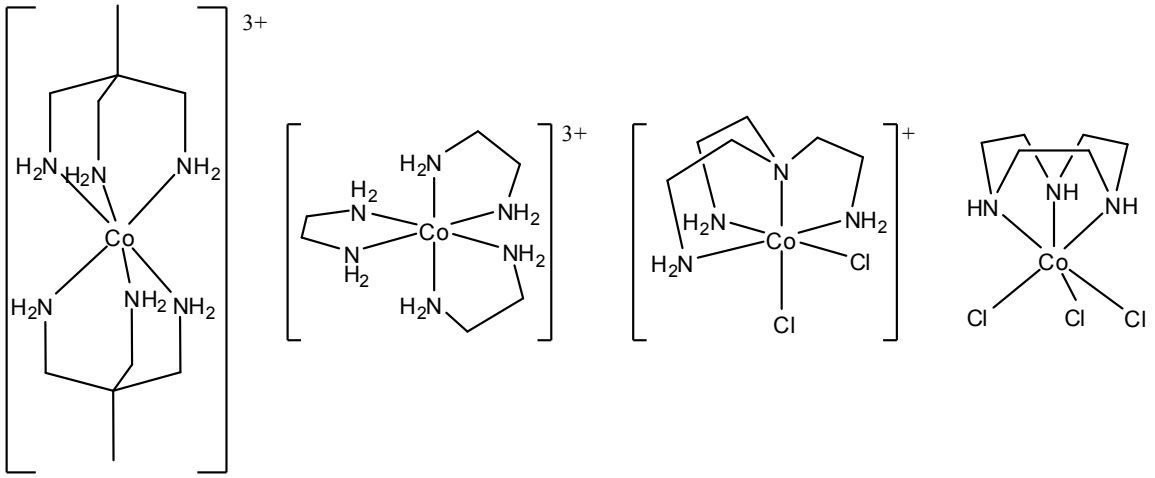

Figure 5.14: Complexes used for corrosion inhibition studies: (left to right) $[Co(tame)_2]Cl_3$, $[Co(en)_3]Cl_3$, $[Co(tren)Cl_2]Cl$ and $[Co(tacn)Cl_3]$. Chloride counter ions have been omitted for clarity.

The complexes were chosen due to the variation in number of exchangeable ligands present. $[Co(tame)_2]Cl_3$ and $[Co(en)_3]Cl_3$ have no exchangeable ligands, $[Co(tren)Cl_2]Cl$ has two, and $[Co(tacn)Cl_3]$, like $[Co(tame)Cl_3]$, has three. Table 5.3 shows the weight loss and inhibition efficiency of the complexes tested.

Table 5.3: Weight loss of iron samples in 1 M HCl solution with 5 mM of various complexes

	W (mgcm^{-2}min^{-1})	Std dev	η %
$[Co(en)_3]Cl_3$	0.0433	0.0009	66
$[Co(tame)_2]Cl_3$	0.034	0.003	73
$[Co(tren)Cl_2]Cl$	0.025	0.002	80
$Co(tacn)Cl_3$	0.0231	0.0008	82
$Co(tame)Cl_3$	0.089	0.003	30

The results of these experiments are inconsistent with what we may expect based on the results of the ability to bind to goethite shown by each complex (see Section 3.2.4). In Figure 5.15 the inhibition efficiency of each complex is represented graphically in a bar graph, with

the bars ordered from left to right in increasing order of their number of exchangeable ligands.

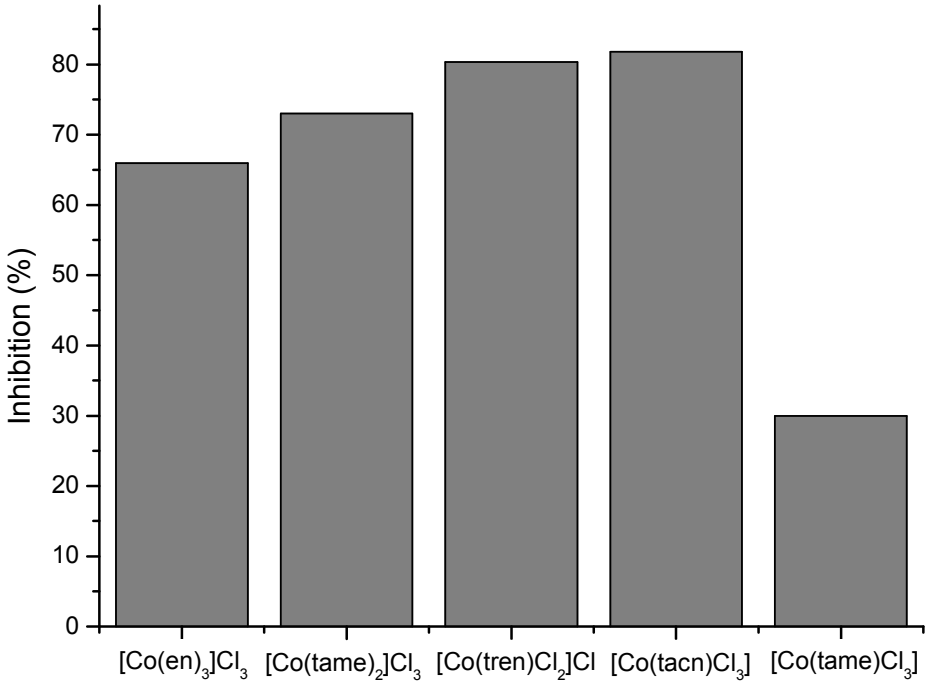

Figure 5.15: Efficiency of different cobalt(III) complexes at inhibition of corrosion of iron in 1 M HCl solution.

This graph is surprising in context of the results from Section 3.2.4 for two reasons. Firstly, whilst the complexes $[Co(en)_3]Cl_3$ and $[Co(tame)_2]Cl_3$ show little to no binding to the goethite surface, their inhibition of the corrosion on iron is far from zero. Additionally, the complex $[Co(tame)Cl_3]$, which shows some of the best binding to goethite, proves to be a comparatively poor inhibitor. This suggests that the inhibition either proceeds by a mechanism other than by binding to the surface in the manner proposed for binding to goethite (see Section 1.6), or that the process is additionally complicated by some means.

The complex $[Co(tren)Cl_2]Cl$ shows far better inhibition of iron in 1 M HCl solution than does $[Co(tame)Cl_3]$. This, and its ease of preparation from a commercially available amine, made it an attractive candidate for further study.

5.2.4. Inhibition by $[Co(tren)Cl_2]Cl$

Table 5.4 shows the average weight loss recorded for the different concentrations of $[Co(tren)Cl_2]Cl$ used. The inhibition efficiency was once again calculated using Equation (5.2).

Table 5.4: Weight loss data $[Co(tren)Cl_2]Cl$.

Concentration (mM)	W ($mgcm^{-2}min^{-1}$)	Std dev	η %
0	0.127	0.009	-
0.1	0.096	0.003	24
0.2	0.065	0.003	49
0.5	0.050	0.003	61
1	0.045	0.003	65
2	0.0341	0.0007	73
5	0.025	0.002	80
10	0.0249	0.0006	80

Figure 5.16 shows the weight loss of 5.4 cm^2 iron samples in 1 M HCl solution as a function of concentration of $[Co(tren)Cl_2]Cl$. The amount of material lost once again decreases with increased concentration of the inhibitor.

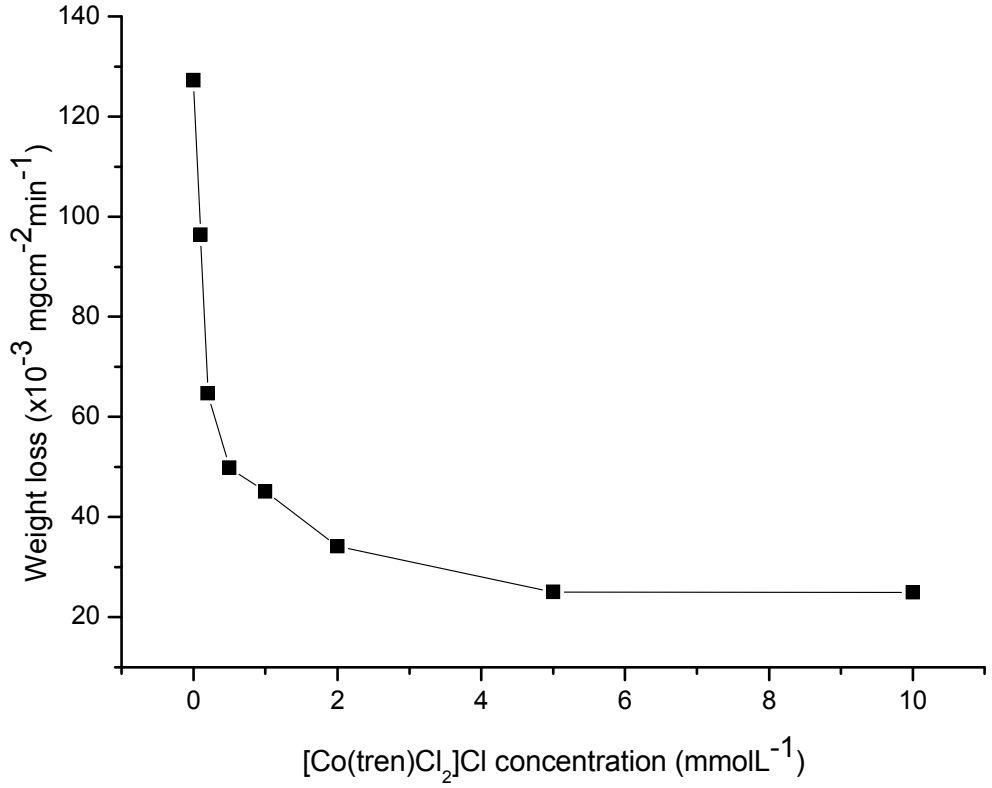

Figure 5.16: Weight loss of iron samples after immersion in 1 M HCl solution containing various concentrations of $[Co(tren)Cl_2]Cl$ for 4 hours at 53°C.

This data has also been plotted as the inhibition efficiency as a function of concentration

(Figure 5.17). Fitting to Equation (5.3) was also performed, yielding values of $a = 81 \pm 3$ %, $b = 0.18 \pm 0.03$ mmolL^{-1} with an R^2 value of 0.963.

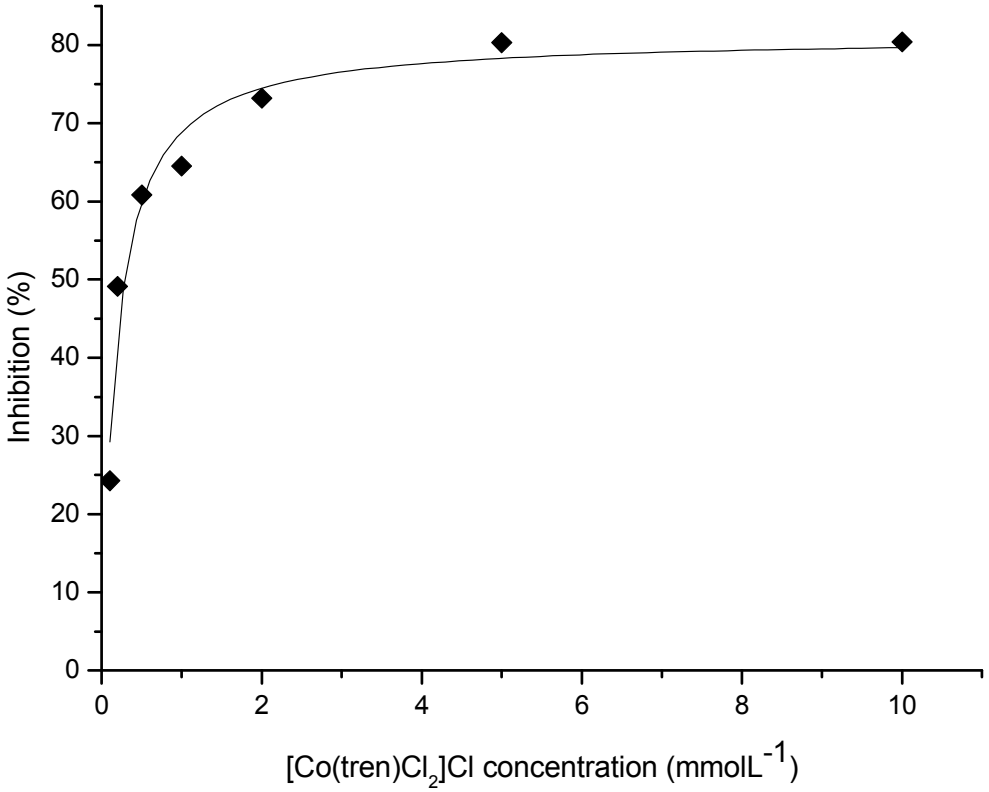

Figure 5.17: Inhibition of corrosion of iron in 1 M HCl solution by [Co(tame)Cl_2]Cl, fitted to a hyperbolic curve yielding $a = 81 \pm 3$ % and $b = 0.18 \pm 0.03$ mmolL^{-1}.

In comparison to [Co(tame)Cl_3], [Co(tren)Cl_2]Cl not only offers greater maximum inhibition (81% compared to 53%), but also reaches this maximum at a much lower concentration (the concentration required for half the maximum inhibition is 0.18 mmoL^{-1} compared to 2.8 mmolL^{-1}). This is in contrast to the effectiveness of each complex at binding to goethite as described in Section 3.2.

5.2.5. UV-vis monitoring of [Co(tren)Cl_2]Cl

In the same manner as for [Co(tame)Cl_3] (see Section 5.2.2), the progress of the inhibition of corrosion of iron in 1 M HCl solutions was monitored by UV-vis spectroscopy. The peak absorbance for the solution is now at 536 nm, compared with 540 nm for the [Co(tame)Cl_3] solutions. This absorbance once again decreases over the duration of the experiment, but in this case there is no accompanying increase of absorbance at 400 nm nor

the accompanying isosbestic point (Figure 5.18).

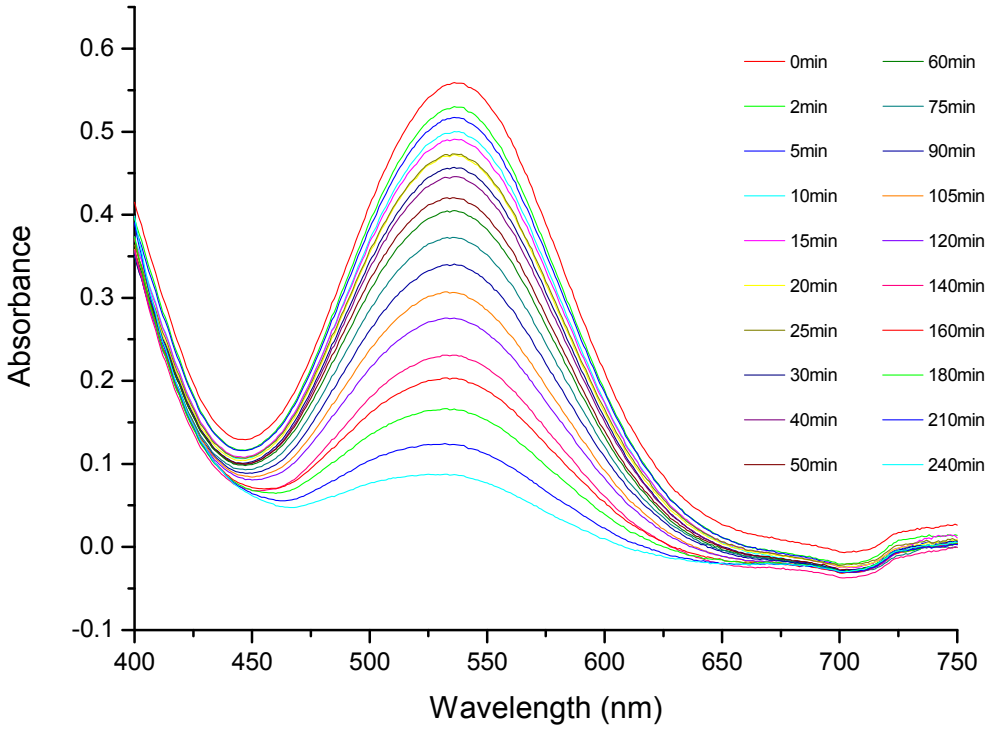

Figure 5.18: UV-vis spectra of the 5 mM [Co(tren)Cl_2]Cl corrosive solution at various times during an immersive corrosion experiment.

As with the [Co(tame)Cl_3] experiments, the peak absorbance has been plotted as a function of time (Figure 5.19). Once again, the rate exhibits zero order kinetics with respect to the cobalt complex (see Section 5.2.2). However, in this case, the absorbance decrease progresses much more slowly (-2.01 (±0.02) × 10^{-3} min^{-1} compared to between -4.6 (± 0.1) x 10^{-3} min^{-1} and -12.6 (± 0.2) x 10^{-3} min^{-1} for the [Co(tame)Cl_3] experiments) and does not reach zero within the course of the experiment (the fitted line would yield zero absorbance at approximately 270 minutes).

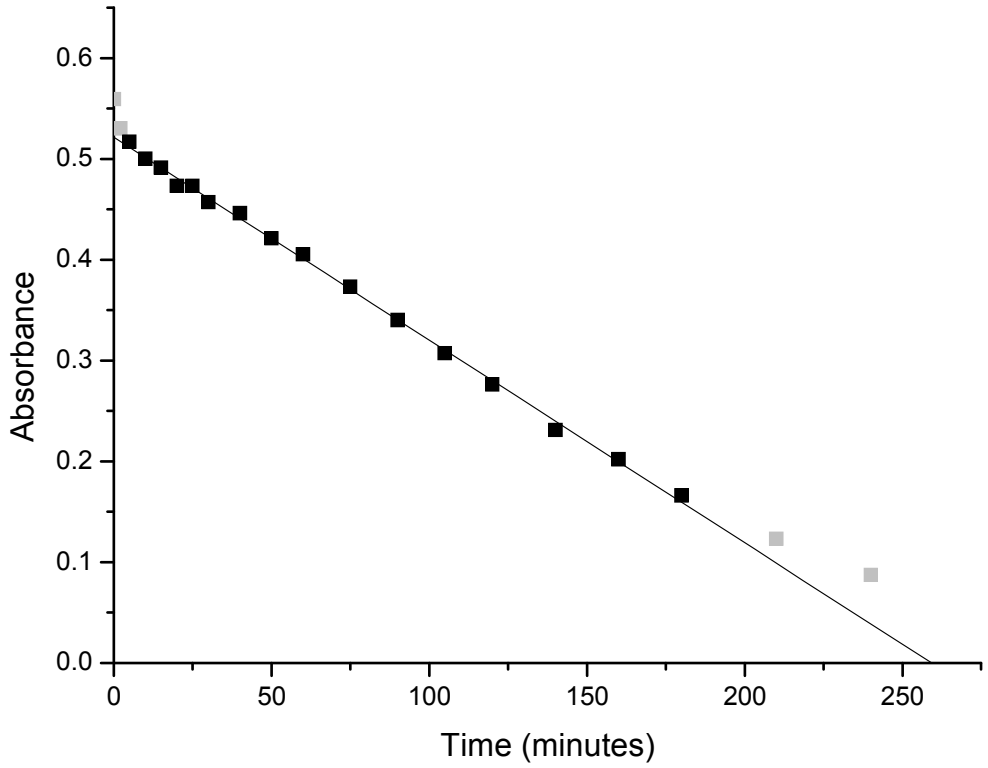

Figure 5.19: Decrease in absorbance at 536 nm of 5 mM [Co(tren)Cl_2]Cl inhibiting corrosion of iron in 1 M HCl solution. Points excluded for the calculation of the linear region are shown in grey.

The results obtained in the UV-vis monitoring of the corrosion of iron as inhibited by various concentrations of [Co(tame)Cl_3] suggested that the amount of the dissolved species in solution decreased over the course of the experiment, with none detectable in solution at 90 – 120 minutes depending on the initial concentration (see Section 5.2.2). The same experiment performed with 5 mM [Co(tren)Cl_2]Cl showed much slower decrease in the concentration of that species, and the amount in solution did not run out in the course of the experiment. Separation by ion exchange chromatography of the components of the yellow solution formed after a corrosion experiment utilising [Co(tame)Cl_3] showed that the solution contained Fe(II) and Co(II) species. This led to the examination of the possibility that the observed disappearance of the complexes may be due to an electrochemical reaction with the iron surface; the more rapid disappearance of [Co(tame)Cl_3] in comparison to the disappearance of [Co(tren)Cl_2]Cl may be related to the ease with which each complex is reduced by the iron surface.

5.2.6. Electrochemical results

In order to test whether the rate of loss of complex from solution is related to its ease of

reduction, the electrochemical behaviour of several complexes was examined by cyclic voltammetry. The cyclic voltammogram of 5 mM $[Co(tame)Cl_3]$, $[Co(tacn)Cl_3]$ and $[Co(tren)Cl_2]Cl$ in 1 M HCl solution were recorded (Figure 5.20). The measurement of the voltammogram of $[Co(tacn)Cl_3]$ was included because it was also observed to change colour over the course of a corrosion experiment. This was not monitored by UV-vis due to technical problems, but the time taken for the colour to disappear was between two and three hours.

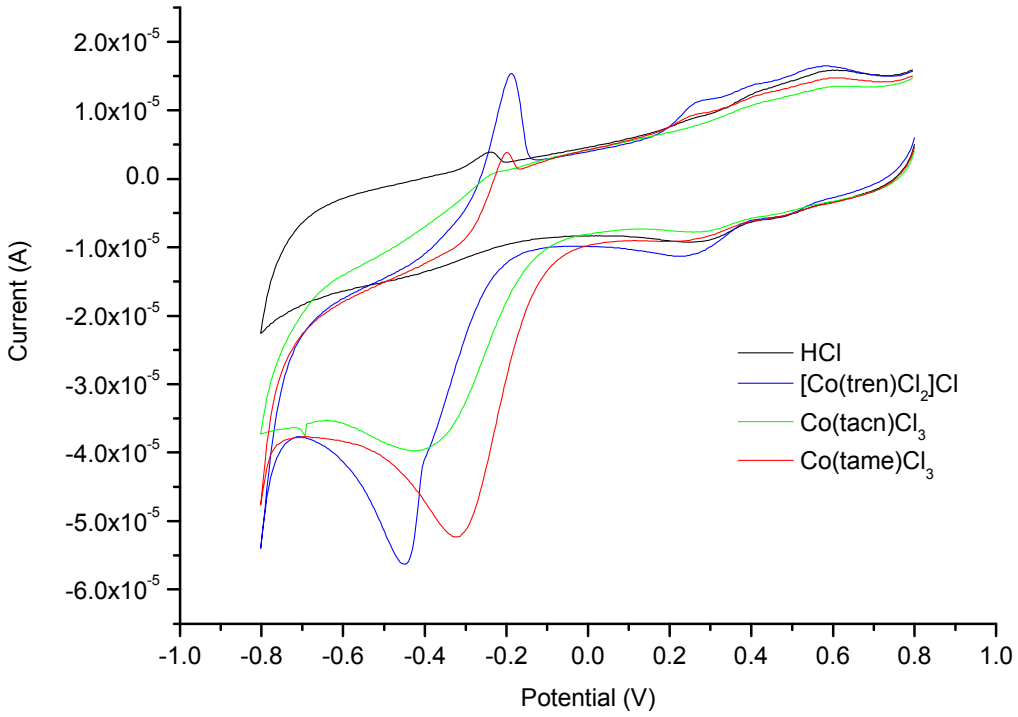

Figure 5.20: Cyclic voltammograms of the complexes $[Co(tren)Cl_2]Cl$, $[Co(tacn)Cl_3]$ and $[Co(tame)Cl_3]$. Also shown is the voltammogram of the HCl medium.

The complex $[Co(tame)Cl_3]$, which is observed to lose its colour the most quickly in corrosion experiments, is the most easily electrochemically reduced of the three complexes. $[Co(tren)Cl_2]Cl$, which retains its colour for the longest, is reduced least easily (Table 5.5).

Table 5.5: Reduction potential of the complexes $[Co(tame)Cl_3]$, $[Co(tacn)Cl_3]$ and $[Co(tren)Cl_2]Cl$.

Complex	Reduction potential (V)
$[Co(tame)Cl_3]$	-0.313
$[Co(tacn)Cl_3]$	-0.430
$[Co(tren)Cl_2]Cl$	-0.450

This can be explained as being due to the increasing stabilisation of the Co(III) oxidation

state by the amine ligands. The ligand tren, with four nitrogen donors, provides more stabilisation than the three nitrogen donors of tacn and tame. Furthermore, the secondary amines of tacn provide greater stabilisation than the primary amines in tame; this complex is observed to lose its colour more slowly than $[Co(tame)Cl_3]$ but more quickly than $[Co(tren)Cl_2]Cl$.

The larger number of donors sites on tren compared to tame and tacn may also explain the difference in reversibility of the voltammograms of their chlorido cobalt complexes. The reduction of the complexes is not reversible in a formal electrochemical sense, but the voltammogram of $[Co(tren)Cl_2]Cl$ shows a small oxidation peak at -0.191 V which may indicate quasi-reversible reduction. In contrast, the complexes $[Co(tacn)Cl_3]$ and $[Co(tame)Cl_3]$ do not display any reversibility. This may be due to the rapid ligand exchange of the labile cobalt(II) species, which may well be faster with the tridentrate ligands tame and tacn than the tetradentate tren.

The electrochemical results are consistent with the proposal of a redox process contributing to the rate at which the solutions of the cobalt(III) complexes change colour. There is a correlation between the reduction potential of the solution, and the time taken for the solution to lose its colour.

5.2.7. Temporal behaviour of inhibition

The complexes $[Co(tren)Cl_2]Cl$ and $[Co(tacn)Cl_3]$ both provide better inhibition against the corrosion of iron in 1 M HCl solution over four hours than the complex $[Co(tame)Cl_3]$. The former two complexes were both also observed to change colour more slowly than the latter. This observation led to the investigation of the rate of inhibition over the course of the experiment. The observed total weight loss may be from a constant rate of inhibition, or from a higher initial level of inhibition up to the point of the colour change, followed by a lower rate of inhibition after this time (Figure 5.21). This two-phase behaviour is what would be expected if redox reactions of the cobalt complex were a significant influence on the observed inhibition. Less inhibition would be observed after the cobalt complex had disappeared.

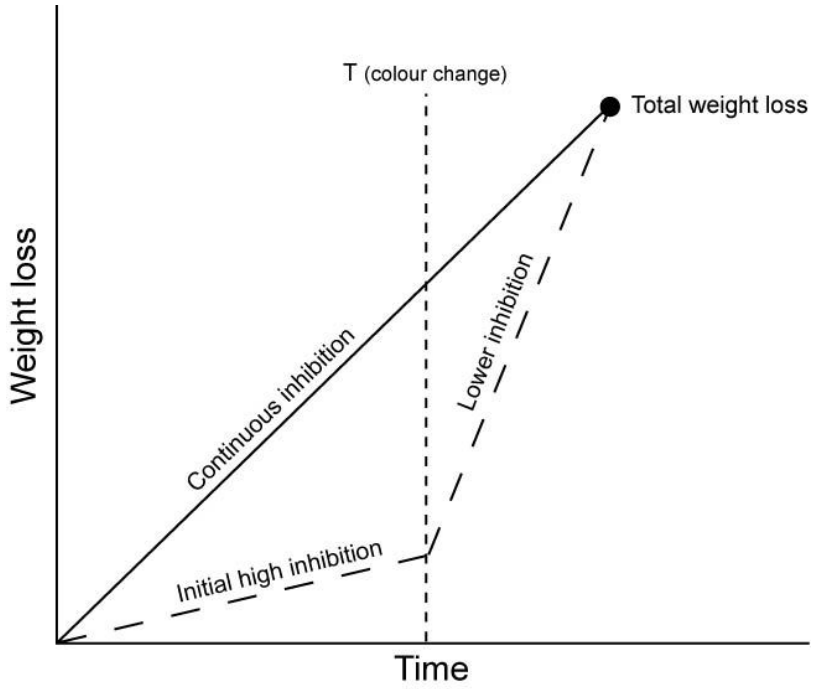

Figure 5.21: Schematic of two possible routes to the observed total weight loss.

To test this hypothesis, data was collected on the corrosion of iron in 1 M HCl solutions with 5 mM [Co(tame)Cl_3] at various time increments. In order to clearly observe the appearance of any increase in corrosion after the disappearance of the species at approximately 60 minutes, data was collected at 15, 30, 45, 60, 120, 180 and 240 minutes. The presence of several points either side of 60 minutes would ensure sufficient data both before and after any change in corrosion rate. The resulting weight loss is plotted as a function of time (Figure 5.22).

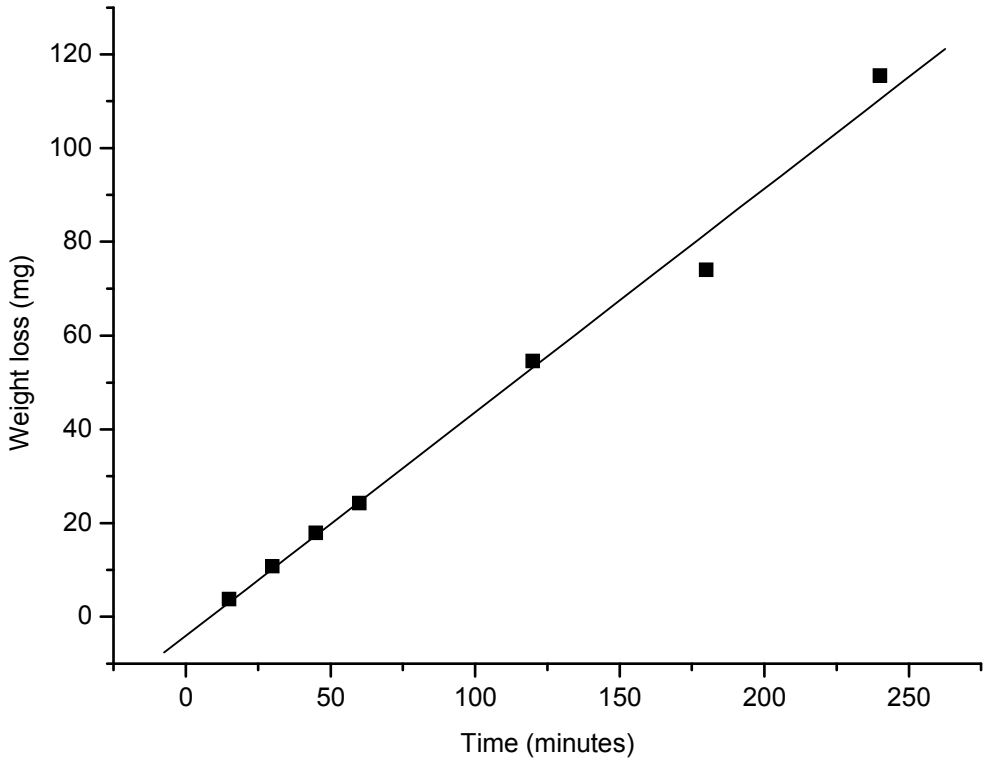

Figure 5.22: Weight loss of iron in 1 M HCl solution with 5 mM [Co(tame)Cl_3] at various times.

The corrosion rate remains constant throughout the experiment; there is no observed increase in the rate of mass loss at around 60 minutes. This suggests that the inhibition of corrosion is dependent on factors other than the concentration of this species in solution, and that the superior performance of [Co(tren)Cl_2]Cl over [Co(tame)Cl_3] is related to factors other than its stability in the corrosive solution. These results are consistent with the zero order kinetics observed in the UV-vis experiments in that the reaction rate is independent of solution concentration of the complex. However, this may be unrelated, as the corrosion rate is unchanged even after all the complex has reacted.

5.2.8. Investigation of inhibition by surface pre-treatment

Several cobalt complexes have been shown to inhibit the corrosion of iron in 1 M HCl solution with varying efficiency. However, one of the aims of the project is to prepare a surface with modified properties. In order to see if it was possible to modify the surface with a cobalt complex to be resistant to corrosion in the absence of any inhibitor, several surface pre-treatment methods were examined. Initially, a surface was simply immersed in a 5 mM solution of [Co(tame)Cl_3] for 2 hours, and then exposed to the corrosion testing. This sample,

however, showed no effect on the surface with the measured weight loss falling within the same range as the uninhibited samples.

It was then investigated whether initial treatment of the iron sample to increase the amount of oxide and hydroxide functionality at the surface may help to bind the complex during pre-treatment. The treatment of iron with nitric acid is known to induce passivity,[35] with formation of a layer that contains iron oxides and hydroxides.[214] Samples of iron were treated with concentrated nitric acid and subsequently immersed in 5 mM [Co(tame)Cl_3] prior to exposure to the corrosive medium. This procedure was also carried out with the use of H_2O_2 solution in place of concentrated nitric acid. However, in both of these experiments the weight loss was also within the same range as the uninhibited samples.

The treatment of mononuclear cobalt(III) ammine complexes bearing chloride or aqua ligands with aqueous base can result in the formation of hydroxo bridged binuclear species.[215] In order to test whether base treatment could also assist in the formation of bridges between the iron surface and a cobalt(III) complex, an iron sample was immersed in a solution of [Co(tame)Cl_3] and the pH adjusted to 7 with dilute sodium hydroxide. Subsequent corrosion testing returned a result consistent with the control samples. These results suggest more work is required to demonstrate whether complexes of this type can be used to modify the corrosion behaviour of iron metal.

5.2.9. Summary

It is not entirely clear exactly how the cobalt(III) complexes are affecting the corrosion rate in these experiments. It is clear from the results described in Section 5.2.3 that the identity of the complex influences the inhibition efficiency. This can be seen in the comparative inhibition level of the five different complexes tested at 5 mM. These range from 30% for [Co(tame)Cl_3] to 82% for [Co(tacn)Cl_3]. Furthermore, the slopes of the zero order reaction at the surface are different for each complex. However, the relative inhibition imparted by each complex does not appear to be related to its ability to bind to the native oxide layer as described in Chapter 3 Moreover, the temporal results described in Section 5.2.7 show that the inhibition of corrosion by [Co(tame)Cl_3] proceeds continuously over the four hour testing period, while the UV-vis monitoring of the corrosive solution as described in Section 5.2.2 suggests that the complex is no longer present in its original form after a period that

depends on the initial concentration. These results in combination suggest that corrosion is inhibited even after the disappearance of the complex. This may suggest some process at the start of the corrosion experiment that alters the surface of the iron sample, protecting it from the corrosive environment. Meanwhile, the redox controlled decomposition of the complex occurs within the solution, but has no effect on the corrosion of the substrate. Experiments in which the surface was exposed to the inhibiting complex and subsequently tested in an uninhibited corrosive solution were undertaken. However, these showed no inhibition of the rate of corrosion. Furthermore, it is not entirely clear why the complexes $[Co(tame)_2]Cl_3$ and $[Co(en)_3]Cl_3$ exhibit such good inhibition while they do not show significant binding to goethite surfaces. It may be that the interaction with the surface that imparts corrosion resistance is different from that with goethite. The interaction may involve an electrostatically controlled physisorption process, with the 3+ charge on these complexes contributing to their inhibiting ability. If this were the case, some difference may be seen when using aqua complexes such as $[Co(tame)(OH_2)_3]^{3+}$ in place of the chlorido complexes used here.

5.3. Conclusion

The ability of several cobalt complexes to inhibit the corrosion of iron in 1 M HCl solution has been studied. At 5 mM concentration, the complexes $[Co(tacn)Cl_3]$ and $[Co(tren)Cl_2]Cl$ show the best inhibition with values of 82% and 80%, respectively. Surprisingly, the complexes $[Co(tame)_2]Cl_3$ and $[Co(en)_3]Cl_3$, which show very low levels of binding to goethite, provide relatively high levels of inhibition, at 73% and 66%, respectively. Also somewhat surprisingly, the complex $[Co(tame)Cl_3]$, which shows good affinity to goethite, shows comparatively low inhibition of only 30% at 5 mM.

The inhibition by $[Co(tame)Cl_3]$ and $[Co(tren)Cl_2]Cl$ were studied more thoroughly. It was determined that the inhibition by $[Co(tren)Cl_2]Cl$ approaches a maximum of 81%, and the half maximum inhibition concentration is 0.18 mM; $[Co(tame)Cl_3]$ approaches 53% and its half maximum inhibition concentration is 2.8 mM. For both of these complexes, its concentration in solution over the course of the experiment was monitored. It was observed that the complex was consumed in a zero order reaction which is attributed to a reaction at the surface following a Langmuir-Hinshelwood mechanism, that is rapid adsorption of the complex at the surface followed by a rate determining reaction. However, the nature of the

reaction that is occurring at the surface is unknown.

The exact mechanism of the inhibition imparted by the cobalt(III) complexes is also unknown. It is clear that the identity of the complex is important, but it does not seem to matter whether it is still in solution or not. The resolution of this problem requires more work, but the exact experiments required are not obvious.

Chapter Six

Conclusions and future work

6.1. Conclusions

This thesis has described the study of the binding of cobalt(III) complexes to lightly oxidised iron surfaces with a view to their use as a method of providing the surface with some functionality.

In Chapter 2 , the synthesis of cobalt(III) complexes with ligands based on 1,1,1-tris(aminomethyl)ethane (tame) and three exchangeable auxiliary ligands was described. The synthesis of these ligands was approached in two ways. Using the Tollens condensation, various triol molecules were synthesised that could be used as precursor molecules to triamine ligands for cobalt(III) complexes. The second method involved functionalisation of tetrakis(aminomethyl)methane (tamm) by protection of three of the amine groups with benzaldehyde, allowing the fourth to be functionalised by reaction with a sulfonyl chloride molecule. Using this method, the ligands tst, nst, cst and ast were synthesised and the chlorido cobalt(III) complexes prepared.

Some difficulty was encountered in the use of trichlorido cobalt(III) complexes of these ligands due to limited solubility in aqueous solutions. As a method of overcoming this problem with regards to characterisation, complexes with the ligands ida (iminodiacetate) were prepared. This approach was successful with the complex of tame, but was not as useful for the xst ligands, due to the complexes with ida themselves being too insoluble to purify or characterise. The use of auxiliary ligands other than chloride was therefore briefly investigated. The trisaqua cobalt(III) complex of tame was successfully prepared, and showed much greater solubility in water than the trichlorido complex. Given the success of this method in its use with the tame complex, it would be useful to extend this to the cobalt(III) complexes of other ligands, particularly the xst series, to obtain complexes with greater solubility and ease of characterisation.

Another area for further work is in the synthesis of further functionalised tame-based complexes using different sulfonyl chloride compounds. It may be of particular interest to investigate the use of molecules that are hydrophilic to complement the work with aromatic molecules that has already been carried out. Another option for introducing novel functionality could be the use of different aldehyde molecules for protection of tamm. One of the groups

used for protection remains on the ligand after substitution, and so could provide the molecule with further functionality.

Chapter 3 describes studies of the binding of cobalt(III) complexes to high surface area goethite. It was demonstrated that cobalt(III) complexes of polyamine ligands with exchangeable ligands are able to bind to the surface of goethite. Moreover, it was shown that complexes with three exchangeable ligands, in general, show greater surface coverage and higher adsorption equilibrium constants than those with two. The higher adsorption equilibrium constants were attributed to the greater stability obtained from three bonds over that from two. The greater surface coverage was rationalised as being, in this case, due to the larger cross sectional area of the complexes with two exchangeable ligands which blocks potential adjacent sites.

It would be desirable to extend this work to include isotherm studies of all the xst complexes synthesised in Chapter 2 However, this first requires the problem of complex solubility is addressed, for example through the use of alternative exchangeable ligands. It would also be interesting to see if the use of alternative exchangeable ligands, such as water, affects the isotherm of a complex. This could be probed by measuring the isotherm parameters of the complex $[Co(tame)(OH_2)_3](OTf)_3$ and comparing to those of the complex $[Co(tame)Cl_3]$. In addition, it may be useful to examine the goethite substrates subsequent to isotherm measurement to obtain more direct evidence of binding of the complex. XPS and FTIR are techniques that could be useful in this regard.

In Chapter 4 some other methods for determining whether cobalt(III) complexes bind to iron and steel surfaces were explored. SEM and EDS, contact angle and QCM measurements all gave some indication of binding of the cobalt complexes to the metallic surfaces. In particular, the work done on the use of the QCM to measure binding of cobalt(III) complexes to stainless steel showed potential. This would be an interesting avenue for a future researcher to pursue full time. The use of the contact angle measurements is also promising, but requires further work on the preparation of samples to ensure the measured angles are representative of the surface and not of contamination.

The ability of cobalt(III) complexes to inhibit the corrosion of iron in HCl solutions was investigated in Chapter 5 . It was found that the ability of the complexes to inhibit corrosion

does not strictly correlate with the observed binding to iron oxide surfaces as observed in Chapter 3 The complexes $[Co(tame)_2]Cl_3$ and $[Co(en)_3]Cl_3$, which do not bind to goethite, show inhibition at 5 mM of 73% and 66% respectively. Moreover, the complex $[Co(tren)Cl_2]Cl$ inhibits with a maximum inhibition efficiency of 81%, and a half maximum inhibition concentration of 0.18 mM. In contrast, the complex $[Co(tame)Cl_3]$, with much better binding to goethite, has a maximum inhibition efficiency of only 53% and a half maximum efficiency concentration of 2.8 mM. It is thought that inhibition may be imparted by some initial reaction with the surface which is dependent on the complex and its concentration. This is based on the observations that the complex decreases in concentration over the duration of the experiment, while the rate of corrosion is unaffected by this loss of complex. However, attempts to reproduce this effect by pre-treatment of the iron surface with cobalt(III) complexes has not resulted in any reduction in corrosion rate, which may indicate this is not the correct mechanism.

The direction in which to take is work is not obvious. More work could be done on measuring the inhibition of other cobalt(III) complexes, which may unearth some pattern that has not yet been seen due to the size of the series examined. It would be of interest to measure the inhibition of complexes such as $[Co(tame)(OH_2)_3]OTf_3$, to see if it gives markedly different inhibition to that of $[Co(tame)Cl_3]$. The inhibition of the complexes of the xst series would also be interesting, to see if they also show lower inhibition in the same manner as the chlorido cobalt(III) complex of their parent, tame. More work could also be done on the pre-treatment of samples. It could be useful to initiate corrosion in a solution containing an inhibitor, and then transfer the sample to a corrosive solution with a different or no inhibitor. This may shed light on the role of the inhibiting species at the beginning and during the bulk of the experiment.

6.2. Additional future work

In the course of this work we initially only considered the well known ligands tacn and tame. Another C_3 symmetrical tripodal amine ligand with potential for functionalisation that could be used as a parent molecule is *cis*,*cis*-cyclohexane-1,3,5-triamine (tach) (Figure 6.1).[144]

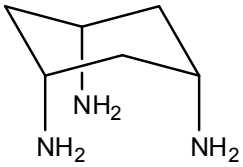

Figure 6.1: *cis*,*cis*-cyclohexane-1,3,5-triamine (tach).

The 2,4,6-trihydroxy analogue of this molecule is known, and could provide a route for synthesis of a series of functionalised ligands for use in this work.

The unexpectedly high corrosion inhibition shown by the complex $[Co(tren)Cl_2]Cl$ suggests that complexes of this type may be more useful for this work than previously thought. It would be interesting to prepare a series of cobalt complexes of ligands based on tren to study their interaction with iron oxide surfaces as a parallel to the work with tame based systems.

A possible synthetic scheme for the synthesis of functional tren based molecules starting from amino acids is shown in Figure 6.2 and Figure 6.3. The amino acid can be reduced using lithium aluminium hydride to the corresponding amino alcohol.[216] This can then be N-protected as the phthalimide by reaction with phthalic anhydride,[217] and conversion of the alcohol to a suitable leaving group can be achieved by reaction with phosphorous tribromide[217] or tosyl chloride.[218] This could then be reacted with a phthalimide protected dien molecule[219] to give the functional tren derivative.

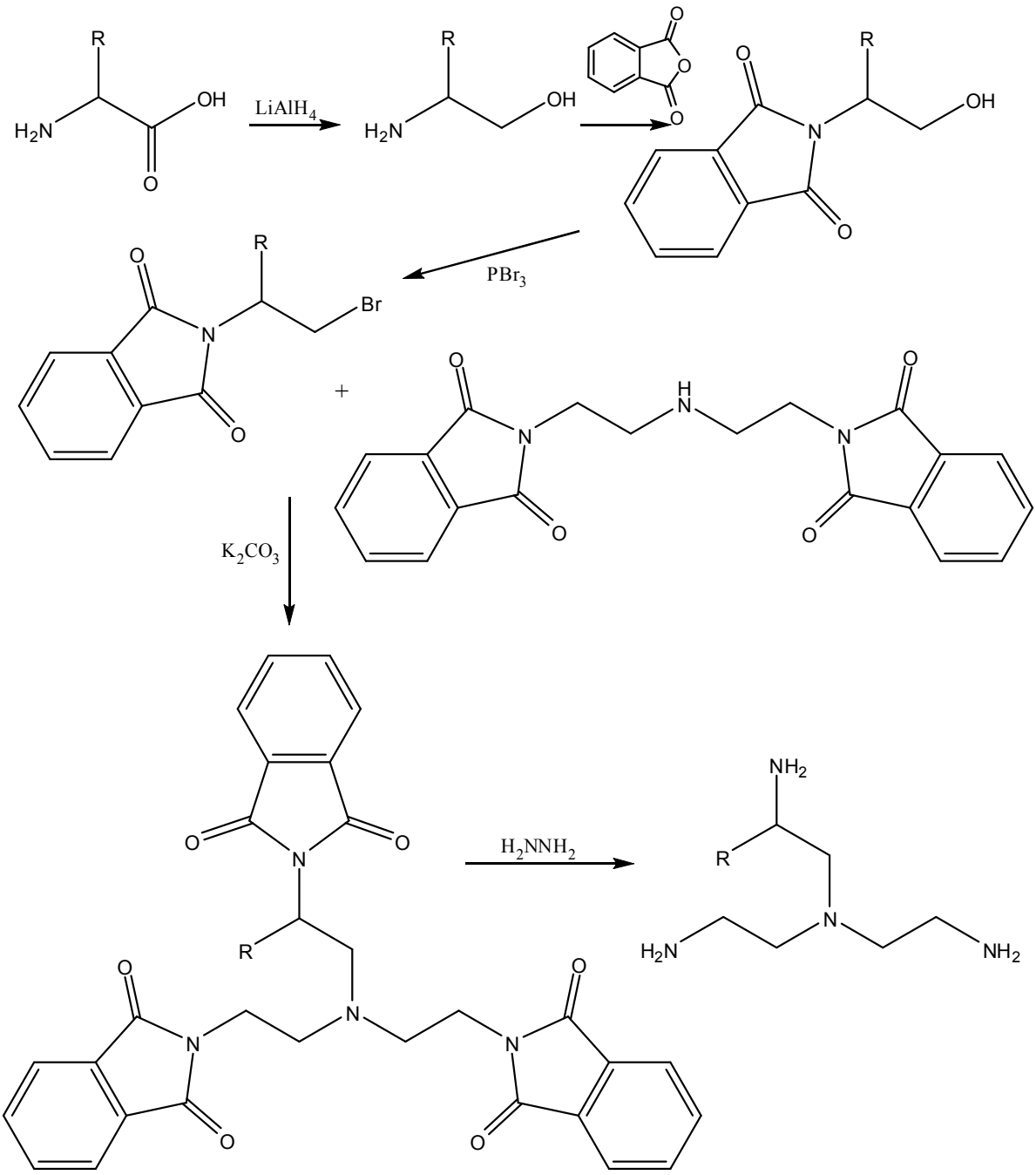

Figure 6.2: Proposed synthetic scheme for synthesis of functionalised tren derivatives.

Alternatively, reaction of two equivalents with the singly protected en[20] would produce a doubly functionalised tren derivative. The phthalimide protecting groups can subsequently be cleaved using standard procedures.[220] The use of amino acids as the source of functionality provides easy access to several functional possibilities.

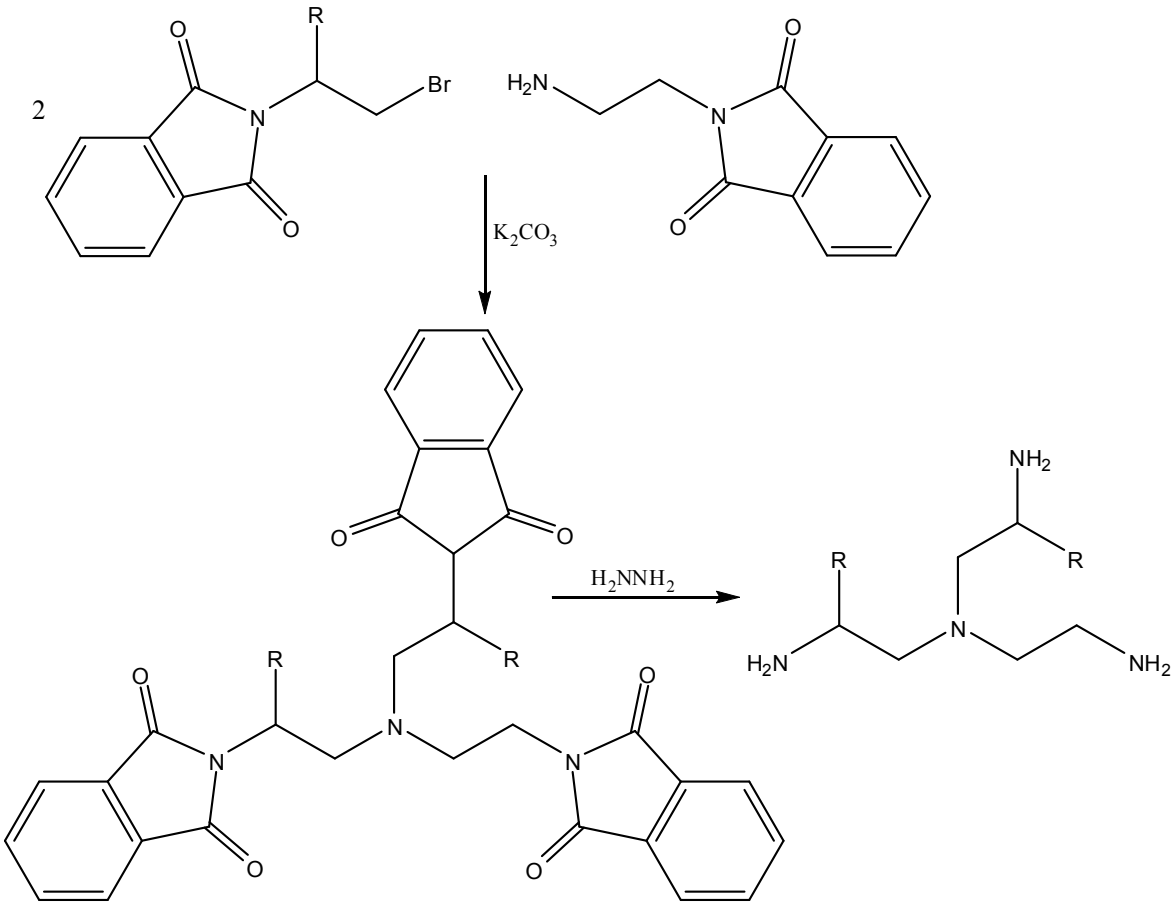

Figure 6.3: Proposed synthetic scheme for bifunctionalised tren complexes.

Chapter Seven

Experimental

7.1. Materials

Reagents and solvents were obtained commercially, were of reagent grade or better, and were used without purification unless explicitly stated. High surface area goethite was supplied by Bayer (Bayferrox 415). Iron (99.5%) was sourced from Goodfellow.

THF, DMF and diethyl ether were dried over 4 Å molecular sieves, and ethanol and methanol were dried over 3 Å molecular sieves. Pyridine was dried by distillation over calcium hydride, and thionyl chloride was purified by distillation over triphenyl phosphite.

Dowex 50WX2-200 and Dowex 50WX2-400 were obtained from Sigma Aldrich. The resins were cleaned between uses by thorough washing with 6 M HCl solution, followed by water until the washings were neutral. Strongly discoloured resin was cleaned by stirring in a solution comprising equal parts 6 M HCl and 50% H_2O_2 solution, followed by rinsing with water until the washings were neutral.

$[Co(tren)Cl_2]Cl$,[220] $[Cr(thf)Cl_3]$[221] and IBX[163] were prepared by literature methods with no changes. $[Co(tpa)Cl_2]ClO_4$,[222] *mer*-$[Co(dien)Cl_3]$,[223] $[Co(tacn)Cl_3]$[98, 124] and $[Co(en)_3]Cl_3$[58] were made by former members of the Hartshorn group by literature procedures. $[Co(tame)_2]Cl_3$ was a generous gift from Professor Alan Sargeson.

7.2. Instrumentation and measurements

^{1}H NMR spectra were recorded on either a Varian INOVA 500 spectrometer at 23°C, operating at 500 MHz or a Varian UNITY 300 NMR spectrometer at 23°C operating at 300 MHz. gCOSY, HSQCAD and gHMBC experiments were all performed on a Varian INOVA 500 spectrometer at 23°C, operating at 500 MHz. ^{13}C NMR spectra were recorded on either a Varian INOVA 500 spectrometer at 23°C operating at 125 MHz or a Varian UNITY 300 NMR spectrometer at 23°C operating at 75 MHz. The INOVA was equipped with a variable temperature and inverse-detection 5 mm probe or a triple-resonance indirect detection PFG probe. The UNITY was equipped with a variable temperature direct broadband 5 mm probe. Chemical shifts are expressed in parts per million (ppm) on the δ scale and were referenced to the appropriate solvent peaks, TMS or TMPS. DMSO-d_6 referenced to $CD_3(C\mathbf{H}D_2)SO$ at δ_H 2.50 (^{1}H) and $(\mathbf{C}D_3)_2SO$ at δ_C 39.6 (^{13}C). TMS and TMPS were both referenced to δ_H 0 (^{1}H)

and δ_C 0 (^{13}C).

Infrared spectra were obtained using a Shimadzu 8201PC Series FTIR using diffuse reflectance method in solid KBr.

High Resolution Electrospray Ionisation Mass Spectra were recorded on a Micromass LCT spectrometer using a probe voltage of 3200 V, an operating temperature of 150°C and a source temperature of 80°C. The carrier solvent was 1:1 CH_3CN/H_2O at 20 μL min^{-1}. Typically, 10 μL of a 10 μL mL^{-1} solution was injected. Leucine enkephalin was used as the lock mass internal standard.

UV-visible spectra were recorded on a Varian CARY Probe 50 UV-vis spectrophotometer or a Varian CARY 100 UV-vis spectrophotomer.

X-Ray crystal data was collected by Dr Chris Fitchett or Dr Jeni Burgess on a Bruker-Nonius APEX II system using graphite monochromatised Mo K*a* (λ = 0.71073 Å) radiation at the temperature indicated in the tables that may be found in Appendix 1. The data collection, cell determination and data reduction were all performed with the APEX software.[224] All structures had intensities corrected for Lorentz and polarisation effects and for absorption using SAINT. All structures were solved by direct methods using SHELXS and refined on F^2 using all data by full-matrix least squares procedures using SHELXL-97. Unless otherwise stated, all non-hydrogen atoms were refined with anisotropic displacement parameters 1.2 and 1.5 times the isotropic equivalent of their carrier carbon atoms. Some of the refinements reported may change a little upon preparation for final publication. The crystal structure pictures were generated using $Olex^2$.[225]

Elemental analyses were performed by the Campbell Microanalytical Laboratory at the University of Otago.

All electrochemical measurements were performed using computer-controlled Ecochemie Autolab PGSTAT 302 potentiostat. The working electrode was a glassy carbon rod with exposed area of 0.071 cm^2. Prior to use, the electrode was polished in a slurry of 1 mm alumina on a Leco polishing cloth and rinsed with Milli-Q water and acetone ultrasonication for 10 minutes. In all experiments, the secondary electrode was a Pt wire and the reference was an SCE (saturated calomel electrode). ΔE_p for 1 mM $K(FeCN_6)$ in 0.1 M phosphate buffer

was 87 mV. Solutions for electrochemistry were degassed with N_2 and kept under an N_2 atmosphere during measurement. All voltammetric measurements were obtained with scan rate of 100 mV s^{-1}.

7.2.1. Adsorption isotherms

Aqueous stock solutions of the complexes of concentration ~5 mM were made up. Approximately 0.4 g of high surface area goethite was accurately weighed in polycarbonate centrifuge tubes. Various amounts of stock solution and water of total volume 10 mL (Table 7.1) were added to the centrifuge tubes and the suspension was stirred for 2 hours at 25°C.

Table 7.1: Solution preparation for isotherm determination with the relative amounts of the ligand stock solution (5 mM) and distilled water.

Sample #	Stock volume	Water volume	Total volume
1	0.1	9.9	10
2	0.2	9.8	10
3	0.4	9.6	10
4	0.6	9.4	10
5	0.8	9.2	10
6	1	9	10
7	2	8	10
8	3	7	10
9	4	6	10
10	5	5	10
11	6	4	10
12	7	3	10
13	8	2	10
14	9	1	10
15	10	0	10

The mixtures were centrifuged, filtered under pressure (N_2) through glass micro fibre filter paper and the resulting supernatant solutions were analysed for their elemental content (Co and Fe) by ICP-OES using a Perkin Elmer Optima 5300 DV. Calibration standards were

prepared by weight and the instrument was calibrated using 1, 10, 50, 100 and 170 ppm cobalt solutions and 1 and 5 ppm iron solutions. The spectral lines Co_228.616 and Fe_238.204 were selected for use. Data was processed using the software programme, WinLab32 for ICP-OES, version 3.0.0.0103, 2004. The measured cobalt content defined the amount of the complex remaining in solution and hence the amount adsorbed onto goethite could be calculated. The iron content was measured as a precaution to eliminate possible interferences; no significant levels (< 1 ppm) were detected in the aqueous phase after equilibration with goethite. The amount of cobalt adsorbed (mol g^{-1}) was plotted against the residual concentration in solution (mol dm^{-3}) using Origin 7.5 and plots were subject to a non-linear curve fit (rectangular hyperbola) from which the surface coverage and adsorption equilibrium constant were calculated.

All isotherms were run at the University of Edinburgh. The isotherms for $[Co(tame)_2]Cl_3$ and $[Cr(tame)Cl_3]$ were run by Thomas Jeffs of the University of Edinburgh, and the isotherms for $[Co(tame)Cl_3]$, $[Co(tst)Cl_3]$ and $[Co(nst)Cl_3]$ were run by Dr David Henderson also of the University of Edinburgh.

7.2.2. Corrosion mass loss experiments

150 mm x 150 mm sheets of 99.5% iron of 1.5 mm thickness (Goodfellow) were cut into 15 mm x 15 mm coupons and a 2 mm diameter hole was drilled at one edge. The coupons were polished with 600 grade emery paper with ethanol, rinsed in water and acetone, dried under a stream of N_2 and weighed. 100 mL solutions of 0 – 20 mM of cobalt(III) complexes in 1 M HCl were made and preheated in a water bath to 53°C for 30 minutes. The iron samples were suspended in the corrosive solution for four hours, after which they were rinsed in water and acetone, dried under a stream of N_2 and reweighed. Weight loss was recorded in mg per cm^2 per min and inhibition efficiency calculated using Equation (5.2). The total geometrical surface area of the samples was ~5.4 cm^2.

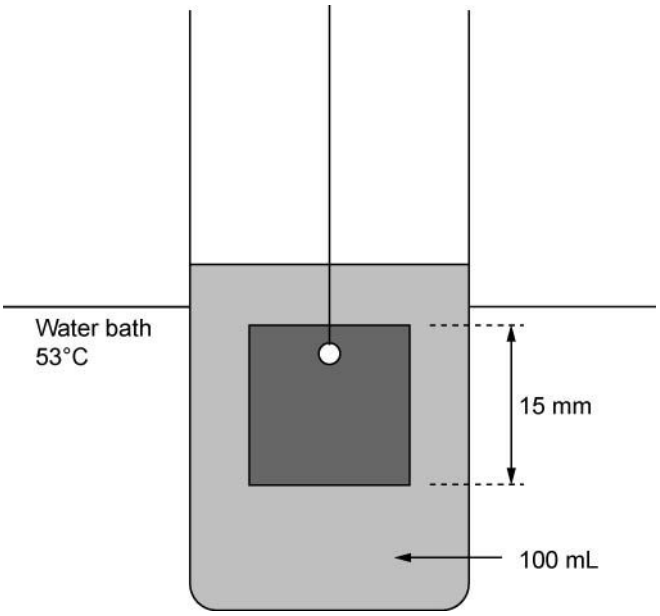

Figure 7.1: Experimental set up for corrosion experiments.

UV-vis monitoring of the corrosion experiments was carried out by removing ~5 mL samples at 0, 2, 5, 10, 15, 20, 25, 30, 40, 50, 60, 75, 90, 105, 120, 140, 160, 180, 210 and 240 minutes, recording the UV-vis spectrum and replacing the sample into the corrosive experiment.

7.2.3. SEM and EDS

SEM and EDS measurements were performed by Deborah Clearwater on a JEOL JSM 7000F field emission, high resolution scanning electron microscope and a JEOL energy dispersive x-ray detector with Moran analyser.

7.2.4. QCM

A Q-4 model QCM (Q-Sense, Goteborg, Sweden) with frequency and dissipation monitoring (QCM-D) and AT-cut quartz crystals with a fundamental resonant frequency of 5 MHz and a diameter of 14 mm were used. One side of each diaphragm crystal was coated by the manufacturer with 100 nm of gold and then 50 nm of stainless steel (SS2343). The composition of the stainless steel was carbon (0.03%), chromium (16.5-18.5%), nickel (11-14.5%), molybdenum (2.5-3%) and iron (64-70%). The crystals were cleaned prior to runs by immersion in a 5:1:1 mixture of Milli-Q water, ammonia (25% v/v) and hydrogen peroxide (30% v/v) for 5 minutes at 75°C, followed by thorough rinsing with Milli-Q water and drying

with a moisture-free nitrogen gas stream. To finish the cleaning, the crystals were treated with UV light and ozone for 5-10 minutes to remove organic contamination. The quartz crystal was mounted in a flow cell with the stainless steel surface exposed to the solution. Modification of the surface was achieved in situ. Milli-Q water was pumped through the flow cell by a peristaltic pump at a flow rate of 100 μL min^{-1}, followed by the 5 mM $[Co(tacn)Cl_3]$ solution and finally Milli-Q water again to rinse the surface. The measurement was done with the system temperature stabilised at 25 ± 0.5°C.[226]

7.2.5. Contact angle

Contact angles were measured on a CAM 200 (KSV Instruments, FL). The samples were the same as those used for SEM and EDS measurements. To make a measurement, the sample was mounted on the instrument analysis platform. The camera was switched on and the focus adjusted to give a clear image of the sample and the dispenser needle. The needle height was adjusted, and a small drop of water dispensed onto the surface. As the drop was slowly enlarged, the software recorded an image every two seconds. Using the CAM software, the contact angle of the advancing drop was calculated.

7.3. Preparations

7.3.1. 1,1,1-Tris(toluenesulfonyloxymethyl)ethane

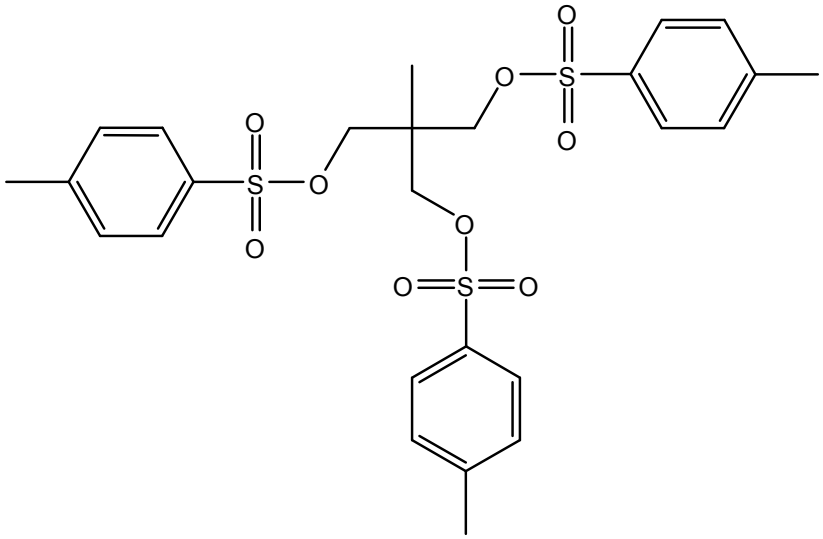

1,1,1-Tris(toluenesulfonyloxymethyl)ethane was synthesised using a modified method

of Hein and Burkhardt.[227] 40 g 1,1,1-Tris(hydroxymethyl)ethane was dissolved in 100 mL of pyridine and slowly added from a dropping funnel to a stirred suspension of 181 g of *p*-toluenesulfonyl chloride in 215 mL of pyridine in an ice bath. After stirring overnight, the solvent was removed on a rotary evaporator and the residue precipitated in 400 mL water, collected by suction on a sintered glass crucible and washed thoroughly with water. The product was used as synthesised with no further purification.

Yield 182 g (93.8%); ^{1}H NMR ($CDCl_3$) δ 7.71 (d, Ar**H**, 6 H), 7.36 (d, Ar**H**, 6 H), 3.76 (s, C**H**$_2$, 6 H), 2.47 (s, ArC**H**$_3$, 9 H), 0.89 (s, CC**H**$_3$, 3 H)

7.3.2. 1,1,1-Tris(azidomethyl)ethane

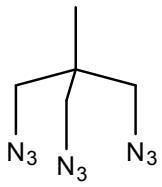

WARNING organic polyazides are potentially explosive compounds and should be handled with care. Handling of the isolated product was kept to a minimum and no attempt at purification was made.

1,1,1-Tris(azidomethyl)ethane was synthesised using a modified method of Fleischer *et al*.[128] 15.20 g (26.1 mmol) of 1,1,1-Tris(toluenesulfonyloxymethyl)ethane and 9.10 g of sodium azide were suspended in 50 mL of diethylene glycol and this mixture was stirred under N_2 at 135 °C overnight. The resulting orange brown solution was cooled and added to 100 mL water. This was then extracted with 3x 100 mL diethyl ether, the solution dried with $MgSO_4$, stirred at room temperature with activated charcoal, filtered, and the solvent evaporated to give a yellow oil.

^{1}H NMR ($CDCl_3$) δ 3.26 (s, C**H**$_2$, 6 H), 0.97 (s, C**H**$_3$, 3 H)

7.3.3. 1,1,1-Tris(aminomethyl)ethane (tame)

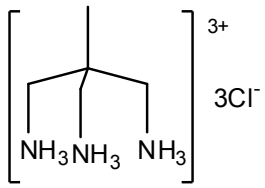

7.3.3.1. Reduction by lithium aluminium hydride

Using the method of Fleischer *et al*,[128] 2 g of 1,1,1-tris(azidomethyl)ethane was dissolved in 8 mL of dry THF and added dropwise to a stirred suspension of 2.3 g of lithium aluminium hydride in 40 mL of dry THF. This was then heated at reflux overnight, and then carefully neutalised with 2 mL of water, followed by 2 mL of 15% NaOH solution, and finally 18 mL of water. The white precipitate was collected and extracted with THF using a Soxhlet apparatus for 72 hours. The resulting oil was dissolved in methanol and the hydrochloride salt precipitated with hydrochloric acid.

Yield 0.92g (39.6%) (See below for spectral properties)

7.3.3.2. Reduction by catalytic hydrogenation

The polyazide product was catalytically hydrogenated using a modified method of Viguier *et al*.[142] 26.1 mmol 1,1,1-Tris(azidomethyl)ethane was dissolved in 100 mL of anhydrous ethanol and degassed for 30 minutes. 2.5 g of 10% Palladium on charcoal was added and the mixture stirred under an atmosphere of H_2 (balloon) overnight. The suspension was then filtered through celite, and the product precipitated as the hydrochloride salt by addition of concentrated hydrochloric acid.

Yield (5.3 g, 91%); ^{1}H NMR: HCl salt – (D_2O) δ 3.14 (s, C**H**$_2$, 6 H), 1.20 (s, C**H**$_3$, 3 H) free amine – ($CDCl_3$) δ 2.60 (s, C**H**$_2$, 6 H), 1.46 (br s, N**H**$_2$, 6 H), 0.81 (s, C**H**$_3$, 3 H)

7.3.4. [Co(tame)(NO_2)$_3$]

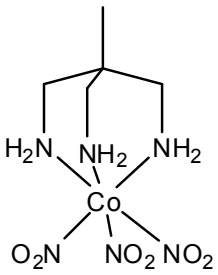

[Co(tame)(NO_2)$_3$] was made by a modified method of Okamoto *et al*.[98] 3.21 g of cobaltous nitrate and 3.50 g of sodium nitrite were dissolved in a buffer solution comprising 0.9 g of sodium hydroxide and 2.6 mL of glacial acetic acid in 22 mL of water. The solution was placed in a gas bottle and aeration commenced. 1.83 g of Tame.3HCl was dissolved in 22

mL of water with 1.0 g of sodium hydroxide, and this was added to the former solution. After 3 hours of aeration, the orange brown crystals were collected by suction and washed with water.

Yield 1.15 g (45.3%); ^{13}C NMR (DMSO-d_6) δ 45.57 (**C**H_2), 21.46 (**C**H_3); IR (KBr) ν/cm^{-1} 3635, 3510, 3244, 3153, 1598, 1412, 1312, 1186, 1128, 1017, 824, 739.

7.3.5. [Co(tame)Cl_3]

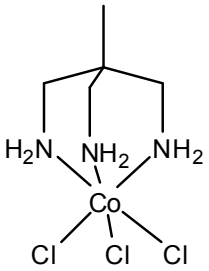

1.15 g of [Co(tame)$(NO_2)_3$] was covered with 3 molL^{-1} hydrochloric acid and heated on a steam bath. The resulting purple solution was left to heat to dryness. The purple solid was then heated in anhydrous ethanol to remove cobalt(II) impurities, and collected by suction.

Yield 0.98 g (94%); IR (KBr) ν/cm^{-1} 3544, 3250, 3152, 1586, 1470, 1283, 1189, 1120, 1017. Calculated for $C_5H_{17}N_3OCl_3Co$ (Co(tame)Cl_3.H_2O): C: 19.98, H: 5.70, N: 13.98. Found: C: 20.13, H: 5.75, N: 13.67

7.3.6. [Co_2(tame)$_2$(μ-OH)$_3$]$(NO_3)_3$

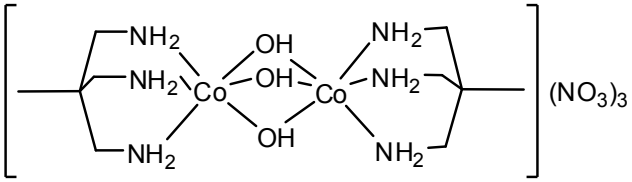

Using a modified method of Williams *et al*,[150] 0.47 g [Co(tame)Cl_3] was dissolved in 5 mL of water. The pH was adjusted to 7 using 0.1 M NaOH. The solvent was then removed and the residue recrystallised from 0.1 M $NaNO_3$ to give a small number of red hexagonal crystals suitable for X-ray analysis.

7.3.7. [Co(tame)(ida)]Cl

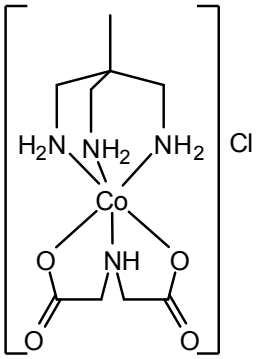

0.52 g of [Co(tame)Cl_3] was dissolved in 25 mL water. 1 g Sodium iminodiacetate was added and the mixture heated on a steam bath for four hours. The resulting red solution was loaded onto a DOWEX column and washed with copious amounts of water to remove iminodiacetate. The product was then eluted with 1 M HCl, and the red solution evaporated to give a red powder. Crystals suitable for X-ray analysis were grown by diffusion of methanol into a concentrated aqueous solution of the complex.

^{13}C NMR (D_2O, TMPS) δ 188.74 (**C**O_2), 58.49 (CO**C**H_2NH), 45.43 (C**C**H_2NH_2), 41.37 (CH_3**C**CH_2), 20.29 (**C**H_3); ESI-MS: *m*/*z* 307.24; IR (KBr) *v*/cm^{-1} 3073, 1681, 1420, 1216, 917, 763; Calculated for $C_9H_{23}N_4O_5Cl_2Co$ ([Co(tame)(ida)]Cl.H_2O.HCl): C: 27.22, H: 5.84, N: 14.11. Found: C: 27.36, H: 5.77, N: 13.86.

7.3.8. [Co(tame)$(OH_2)_3$]$(OTf)_3$

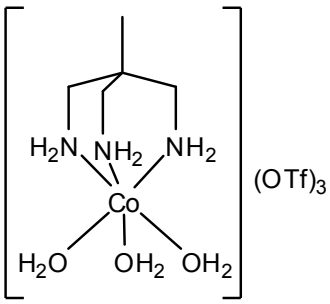

0.32 g [Co(tame)$(NO_2)_3$] was covered with 2 mL of 7 M aqueous trifluoromethanesulfonic acid and heated in a boiling water bath for one hour. The resulting magenta precipitate was filtered and washed with ether. The product is hygroscopic and was stored in a desiccator.

^{1}H NMR (D_2O, TMPS) δ 2.22 (br s, C**H**$_2$, 6 H), 0.96 (s, C**H**$_3$, 3 H); ^{13}C NMR (D_2O, TMPS) δ 47.2 (**C**H_2), 22.4 (**C**H_3). Calculated for $C_8H_{21}N_3O_{12}F_9S_3Co$: C: 14.18, H: 3.12, N: 6.20. Found: C: 14.81, H: 2.85, N: 6.24.

7.3.9. α,α,α-Tris(hydroxymethyl)toluene

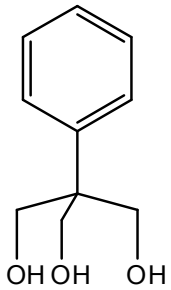

Using a modified method of Viguier *et al*,[142] 8.04 g of phenylacetaldehyde, 3.89 g of $Ca(OH)_2$ and 34.66 g of 37% formalin were suspended in 45 mL THF and stirred at 65 °C for four days. The resulting brown solution was filtered through celite, then evaporated to dryness. The residue was loaded onto a silica column and eluted with 3:1 EtOAc/pet ether (R_f = 0.167). The combined fractions were evaporated to give 2.63 g of an off white solid.

Yield 2.63 g (21%) ^{1}H NMR ($CDCl_3$) δ 7.27 – 7.40 (m, Ar**H**, 5 H), 4.10 (s, C**H**$_2$, 6 H)

7.3.10. α,α,α-Tris(toluenesulfonyloxymethyl)toluene

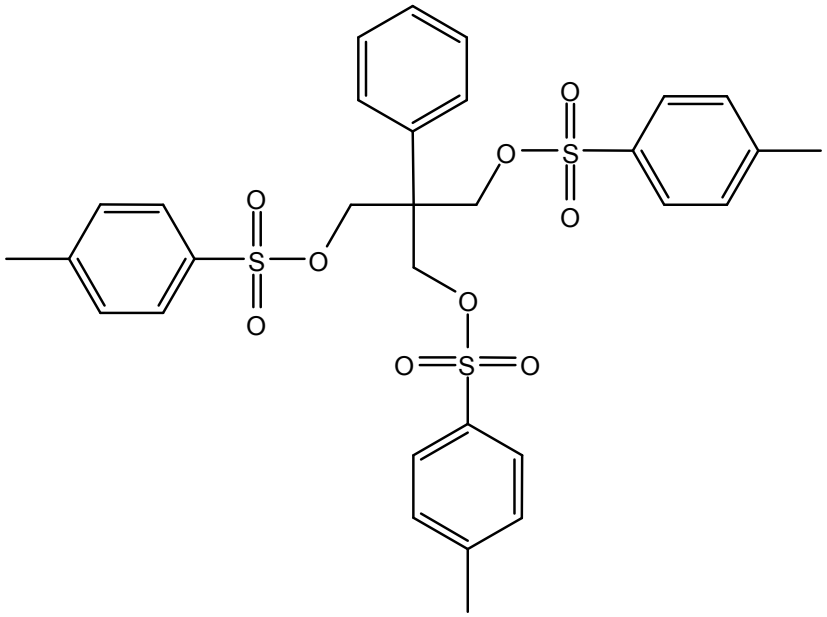

Using a modified method of Viguier *et al*,[142] 2.89 g of α,α,α-

tris(hydroxymethyl)toluene was dissolved in 40 mL of pyridine and cooled in an ice bath. 15 g of *p*-toluenesulfonyl chloride was added and stirred overnight. The resulting solution was poured into 100 mL of water and the white precipitate collected. A portion of this was recrystallised by dissolving in the minimum amount of chloroform, which was dried with magnesium sulfate and filtered, and adding ethanol to induce crystallisation.

Yield 9.2 g (90%); ^{1}H NMR ($CDCl_3$) δ 7.62 (d, Ts Ar**H**, 6 H), 7.31 (d, Ts Ar**H**, 6 H), 7.18 (m, Ph Ar**H**, 3 H), 6.94 (d, Ph Ar**H**, 2 H), 4.19 (s, C**H**$_2$, 6 H), 2.46 (s, C**H**$_3$, 9 H).

7.3.11. α,α,α-Tris(azidomethyl)toluene

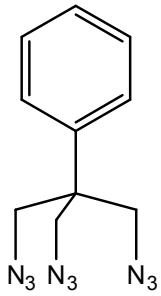

WARNING organic polyazides are potentially explosive compounds and should be handled with care. Handling of the isolated product was kept to a minimum and no attempt at purification was made.

Using a modified method of Viguier *et al*,[142] 3.22 g of α,α,α-tris(toluenesulfonyloxymethyl)toluene and 2.95 g of sodium azide were dissolved in 50 mL of DMSO and stirred at 90 C for 3.5 hours. The cooled solution was added to 250 mL of water and extracted with 3 x 100 mL of ether. The solution was dried with magnesium sulfate and the solvent removed to give the title product as a light yellow oil.

Yield 1.39 g (quantitative); ^{1}H NMR ($CDCl_3$) δ 7.33 – 7.47 (m, Ar**H**, 5 H), 3.78 (s, C**H**$_2$, 6 H)

7.3.12. α,α,α-Tris(aminomethyl)toluene (tamt)

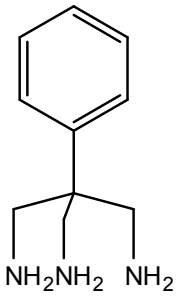

Using the method of Viguier *et al*,[142] 1.39 g of α,α,α-tris(azidomethyl)toluene was dissolved in 25 mL anhydrous ethanol and degassed for 30 minutes. 0.5 g of 10% palladium on charcoal was added and the suspension stirred under an atmosphere of H_2 (balloon) overnight. The catalyst was removed by filtering through celite and the solvent evaporated to give a light yellow oil of the triamine.

Yield 0.89 g (99%) ^{1}H NMR ($CDCl_3$) δ 7.30 – 7.39 (m, Ar**H**, 5 H), 3.06 (s, C**H**$_2$, 6 H)

7.3.13. [Co(tamt)(NO$_2$)$_3$]

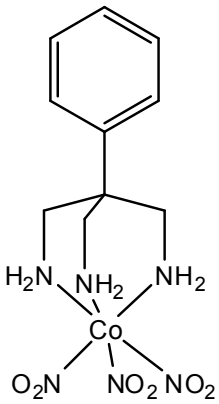

Using a modified method of Okamoto *et al*,[98] 9.65 g of cobaltous nitrate and 10.50 g of sodium nitrite were dissolved in a buffer solution comprising 7.8 mL of glacial acetic acid and 2.70 g of sodium hydroxide in 60 mL of water. Aeration was commenced and several drops of octanol were added to reduce foaming. 4.37 g of tamt in 60 mL of water was added and aeration continued for several hours. The brown precipitate was collected by suction and washed with small volumes of ethanol and ether.

Yield: 2.82 g (31.0%); ^{13}C NMR (DMSO-d_6) δ 129.52, 128.97, 127.92, 126.47, 45.63,

44.97; IR (KBr) ν/cm^{-1} 3222, 1581, 1416, 1268, 1181, 1020, 953, 820, 705.

7.3.14. [Co(tamt)Cl$_3$]

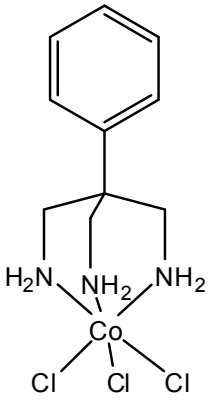

2.82 g of [Co(tamt)(NO$_2$)$_3$] was covered with 3 M hydrochloric acid and heated on a steam bath. The resulting purple solution was left to heat to dryness. The purple solid was then heated in anhydrous ethanol to remove cobalt(II) impurities, and collected by suction. This was then used directly in the following step.

7.3.15. [Co(tamt)(ida)]Cl

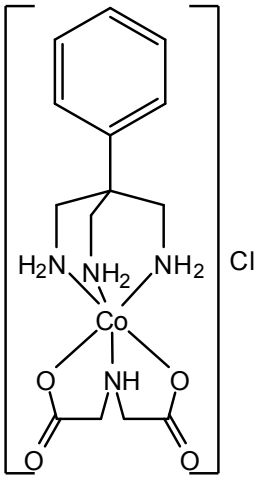

0.1 g of [Co(tamt)Cl$_3$] was dissolved in 25 mL water. 0.1 g sodium iminodiacetate was added and the mixture heated on a steam bath for four hours. The resulting red solution was loaded onto a DOWEX column and washed with water to remove iminodiacetate. The product was then eluted with 6 M HCl, and the red solution evaporated to give a very small amount of red powder.

^{13}C NMR (D_2O, TMPS) δ 183.76 (**C**OO), 133.88, 129.23, 127.61, 125.96 (Ph), 58.55 (**C**H_2N, ida), 44.9 (**C**H_2N, tamt), 42.69 (Ph**C**CH_2).

7.3.16. 1,1,1-Tris(hydroxymethyl)pentadecane

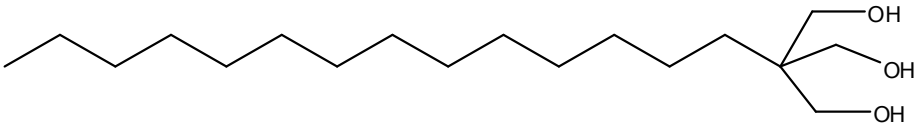

8.2 g Cetyl alcohol was suspended in ~200 mL ethyl acetate. 10.31 g IBX[163] added and the solution heated at reflux overnight. ~200 mL Diethyl ether was added and the suspension filtered. The filtrate was evaporated to dryness to give 4.14 g of cetyl acetaldehyde. This residue, 2.02 g of $Ca(OH)_2$ and 18.18 g formalin were suspended in 100 mL THF and stirred at 65°C for four days. The resulting brown solution was filtered through celite, then evaporated to dryness. The residue was loaded onto a silica column and eluted with 3:1 EtOAc/pet ether. The combined fractions were evaporated to give 2.35 g of an off white solid.

Yield 2.35 g (23%) ^{1}H NMR ($CDCl_3$) δ 3.75 (s, C**H**$_2$OH, 6 H), 1.26 (br s, C**H**$_2$, 26 H), 0.88 (t, C**H**$_3$, 3 H).

7.3.17. 1,1,1-Tris(hydroxymethyl)heptane

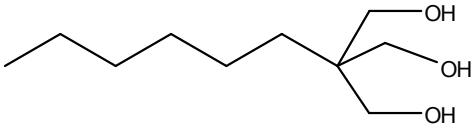

1.55 Octanol was dissolved in 25 mL ethyl acetate. 3.02 g IBX[163] added and the solution heated at reflux overnight. 25 mL diethyl ether was added and the suspension filtered. The filtrate was evaporated to dryness to give octanal. This residue, 0.75 g of $Ca(OH)_2$ and 6 g formalin were suspended in 20 mL THF and stirred at 65°C for four days. The resulting brown solution was filtered through celite, then evaporated to dryness. The residue was loaded onto a silica column and eluted with 3:1 EtOAc/pet ether (R_f = 0.160). The combined fractions were evaporated to give 0.55 g of an off white solid.

Yield 0.55 g (24%) ^{1}H NMR ($CDCl_3$) δ 3.76 (s, C**H**$_2$OH, 6 H), 1.26 (m, C**H**$_2$, 10 H), 0.88 (t, C**H**$_3$, 3 H).

7.3.18. Tetrakis(toluenesulfonyloxymethyl)methane

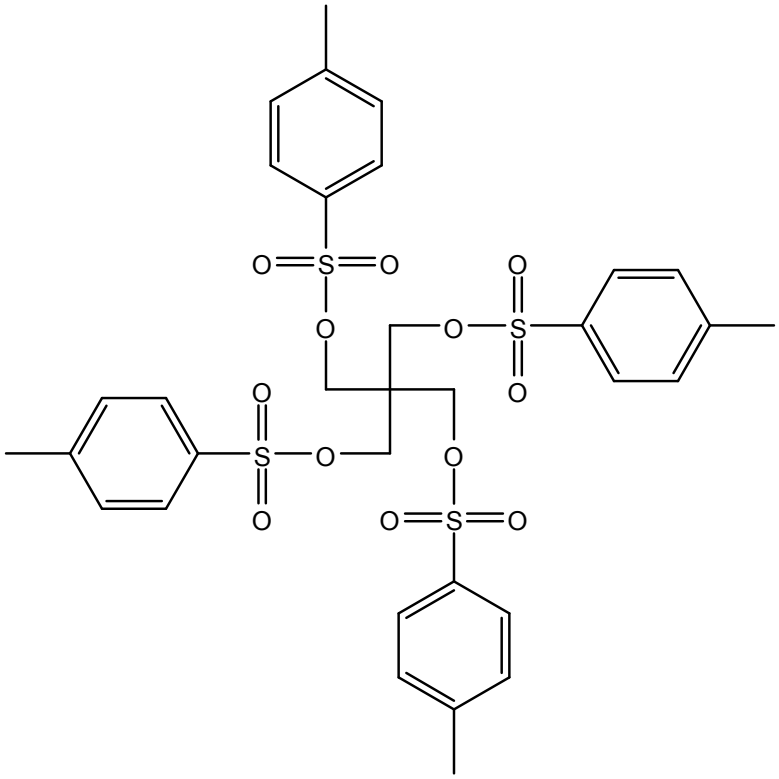

Tetrakis(toluenesulfonyloxymethyl)methane was synthesised using a modified method of Hein and Burkhardt.[227] 40 g pentaerythritol was dissolved in 100 mL pyridine and cooled in an ice bath. 270 g of *p*-toluenesulfonyl chloride in 200 mL pyridine was slowly added dropwise from a dropping funnel overnight with stirring. The pyridine was removed on a rotary evaporator and the residue precipitated in water. The product was used as synthesised with no further purification.

Yield 98% ; ^{1}H NMR ($CDCl_3$) δ 7.69 (d, Ar**H**, 2 H), 7.36 (d, Ar**H**, 2 H), 3.82 (s, CC**H**$_2$, 2 H), 2.47 (s, PhC**H**$_3$, 3 H)

7.3.19. Tetrakis(azidomethyl)methane

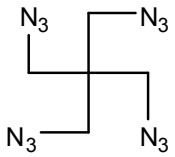

WARNING organic polyazides are potentially explosive compounds and should be handled with care. Handling of the isolated product was kept to a minimum and no

attempt at purification was made.

Tetrakis(azidomethyl)methane was synthesised using a modified method of Fleisher *et al*.[128] 15.20 g (20.2 mmol) of tetrakis(toluenesulfonyloxymethyl)methane and 8.70 g of sodium azide were suspended in 50 mL of diethylene glycol and this mixture was stirred under N_2 at 135 °C overnight. The resulting orange brown solution was cooled and added to 100 mL water. This was then extracted with 3x 100 mL diethyl ether, the solution dried with $MgSO_4$, treated with activated charcoal and the solvent evaporated to give a yellow oil of the title product.

^{1}H NMR ($CDCl_3$) δ 3.33 (s, C**H**$_2$, 6 H)

7.3.20. Tetrakis(aminomethyl)methane

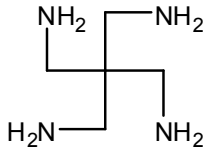

The polyazide product was catalytically hydrogenated using a modified method of Viguier *et al*.[142] 20.2 mmol of tetrakis(azidomethyl)methane was dissolved in 100 mL of anhydrous ethanol and degassed for 30 minutes. 2.0 g of 10% palladium on charcoal was added and the mixture stirred under an atmosphere of H_2 (balloon) overnight. The suspension was then filtered through celite. For the following step, the solvent was removed without addition of hydrochloric acid to yield the crude amine. However, in order to obtain a pure sample for analysis, the amine was precipitated as the hydrochloride salt by the addition of concentrated hydrochloric acid to the ethanolic solution.

Yield 64.6% ^{1}H NMR ($CDCl_3$) δ 3.36 (C*H*$_2$, 6 H) (D_2O, HCl salt) δ 3.14 (C**H**$_2$, 6 H)

7.3.21. 7-[(Benzylideneamino)methyl]-1,3,5-triaza-2,4,9-triphenyladamantane

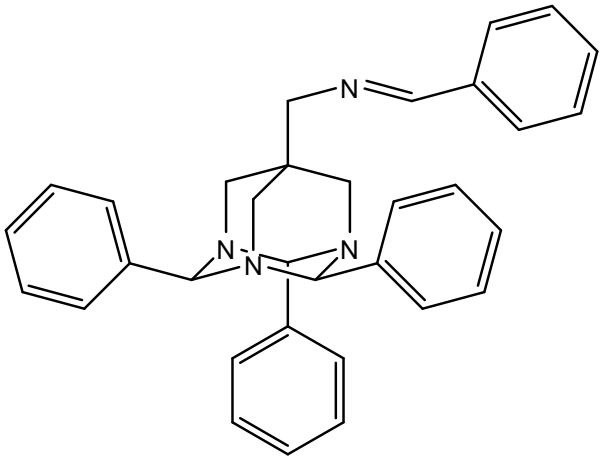

7-[(Benzylideneamino)methyl]-1,3,5-triaza-2,4,9-triphenyladamantane was synthesised using a modified method of Dunn *et al*.[166] 20.2 mmol of tamm was dissolved in 60 mL methanol and 10 mL benzaldehyde added. The solution was heated at reflux for 10 minutes, and upon cooling a white precipitate formed. This was collected by suction and the crude product used in subsequent steps.

Yield (over three steps) 60% ; ^{1}H NMR ($CDCl_3$) δ 8 04 (s, N=C**H**, 1 H), 7.23 – 7.99 (m, Ar**H**, 20 H), 5.67 (s, NC$\mathbf{H}_{eq}$(Ph)N, 1 H), 5.47 (s, NC$\mathbf{H}_{ax}$(Ph)N, 2 H), 3.45 (AB q, J = 12.8 Hz, C$\mathbf{H}_2$N, 4 H), 2.99 (s, C$\mathbf{H}_2$N, 2 H), 2.93 (s, C$\mathbf{H}_2$N, 2 H)

7.3.22. 7-[(Benzylamino)methyl]- 1,3,5-triaza-2,4,9-triphenyladamantane

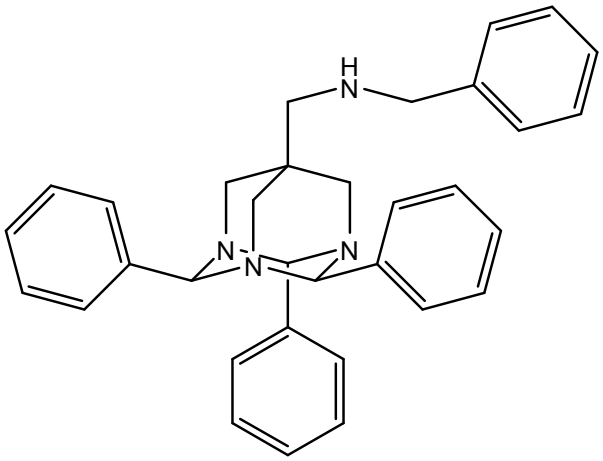

Using the method of Dunn *et al*,[166] 1.95 g benzylideneamine (7.3.21) dissolved in 10 mL 1:1 $CHCl_3/CH_3OH$ and cooled in an ice bath. 200 mg finely ground sodium borohydride

was added and the mixture stirred for 2 hours. The resulting slurry was added to 50 mL H_2O and the organic layer collected. The aqueous layer was extracted with ether (3x 50 mL), and the combined organic fractions were dried with $MgSO_4$ and the solvent removed to give a tacky white residue.

Yield 1.89 g (96.9%) ; ^{1}H NMR ($CDCl_3$) δ 7.22 – 7.82 (m, Ar**H**, 20 H), 5.68 (s, NC**H**$_{eq}$(Ph)N, 1 H), 5.42 (s, NC**H**$_{ax}$(Ph)N, 2H), 3.50 (m, C**H**$_2$N, 4 H), 2.97 (s, ArC**H**$_2$NH, 2 H), 2.90 (s, CC**H**$_2$NH, 2 H)

7.3.23. *N*-[(1,3,5-Triaza-2,4,9-triphenyladamant-7-yl)methyl]-*N*-benzyl-toluene-4-sulfonamide

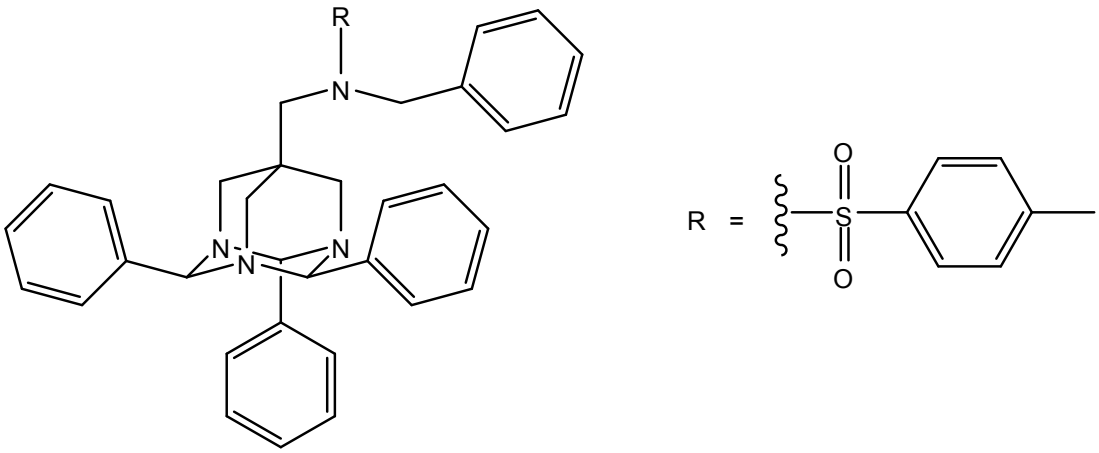

3.67 g Benzylamine (7.3.22) dissolved in 70 mL dry pyridine and cooled in an ice bath. 1.80 g Tosyl chloride added and the yellow solution stirred overnight. The solution was added to 100 mL saturated sodium bicarbonate solution and extracted with ether (3 x 50 mL). This was dried ($MgSO_4$), filtered and the solvent removed to near dryness. Upon addition of methanol, the product precipitated as a yellow solid.

Yield 3.2 g (67%) ^{1}H NMR ($CDCl_3$) δ 6.92 – 7.85 (m, Ar**H**, 24 H), 5.55 (s, NC**H**$_{eq}$(Ph)N, 1 H), 5.38 (s, NC**H**$_{ax}$(Ph)N, 2H), 4.05 (s, ArC**H**$_2$NH, 2 H), 3.45 (AB q, C**H**$_2$N, 4 H), 2.81 (s, C**H**$_2$N, 2 H), 2.56 (s, C**H**$_2$N, 2 H), 2.45 (s, TsC**H**$_3$, 3 H)

7.3.24. *N*-(3-Amino-2,2-bis(aminomethyl)propyl)-*N*-benzyl-toluene-4-sulfonamide trihydrochloride (tst)

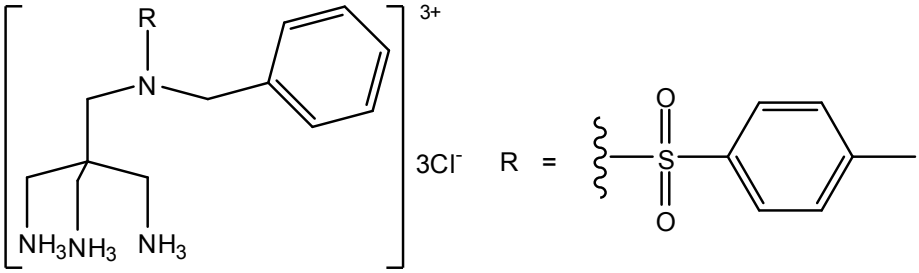

3.2 g of *N*-[(1,3,5-Triaza-2,4,9-triphenyladamant-7-yl)methyl]-*N*-benzyl-toluene-4-sulfonamide (7.3.23) dissolved in 60 mL THF and 60 mL 3 M HCl added. The solution was stirred at room temperature for 10 minutes. The THF was removed, and the aqueous solution washed with DCM (3 x 50 mL) to remove benzaldehyde. The aqueous solution was then evaporated to dryness to give the product as the hydrochloride salt.

Yield 2.23 g (92%) ^{1}H NMR (D_2O, TMPS) δ 7.86 (d, Ts**H**, 2 H), 7.50 (d, Ts**H**, 2 H), 7.41 (m, Ph**H**, 3 H), 7.27 (m, Ph**H**, 2 H), 3.48 (s, C**H**$_2$, 2 H), 3.18 (s, C**H**$_2$NH$_2$, 6 H), 2.47 (s, C**H**$_3$, 3 H); ^{13}C NMR (D_2O, TMPS) δ 149.1, 137.6, 135.1, 133.1, 132.1, 131.5, 131.1, 130.6, 59.0, 54.4, 42.4, 23.5; IR (KBr) ν/cm^{-1} 3009, 2920, 1595, 1513, 1340, 1201, 1161; ESI-MS: *m/z* 377.08.

7.3.25. [Co(tst)(NO$_2$)$_3$]

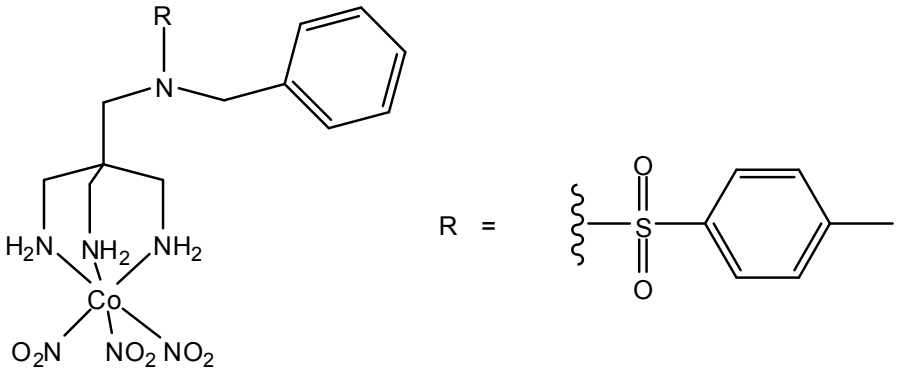

A buffer solution was made comprising 0.77 g NaOH and 2.25 mL glacial acetic acid in 20 mL water. In this, 2.81 g $Co(NO_3)_2$ and 3.08 g $NaNO_2$ were dissolved and aeration was begun. 3.36 g Tst was dissolved in 20 mL water with 0.55 g NaOH and added dropwise to the

aerating solution. After 2 hours, the solution was filtered to give a brown powder.

Yield 1.32 g (33%); ^{13}C NMR (DMSO-d_6) δ 143.7, 135.8, 135.5, 130.0, 128.6, 128.4, 128.2, 128.0, 127.5, 127.4, 53.4, 52.0, 42.9, 42.5, 21.0; IR (KBr) ν/cm^{-1} 3258, 1598, 1421, 1318, 1160, 1089, 820, 738.

7.3.26. [Co(tst)Cl$_3$]

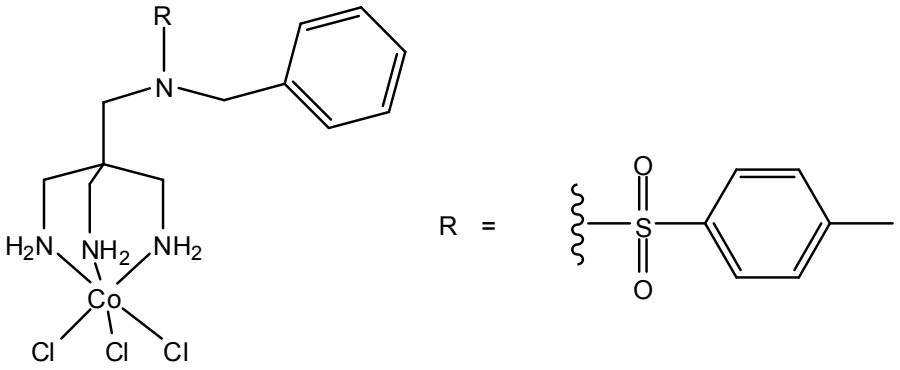

1.32 g [Co(tst)(NO$_2$)$_3$] was covered with ~20 mL of 3 M HCl and heated on a steam bath to dryness. The blue powder was ground in dry ethanol and filtered.

Yield 1.01 g (77%); IR (KBr) ν/cm^{-1} 3517, 3207, 1651, 1591, 1454, 1340, 1158, 1088, 1037.

7.3.27. *N*-[(1,3,5-Triaza-2,4,9-triphenyladamant-7-yl)methyl]-*N*-benzyl-naphthalene-2-sulfonamide

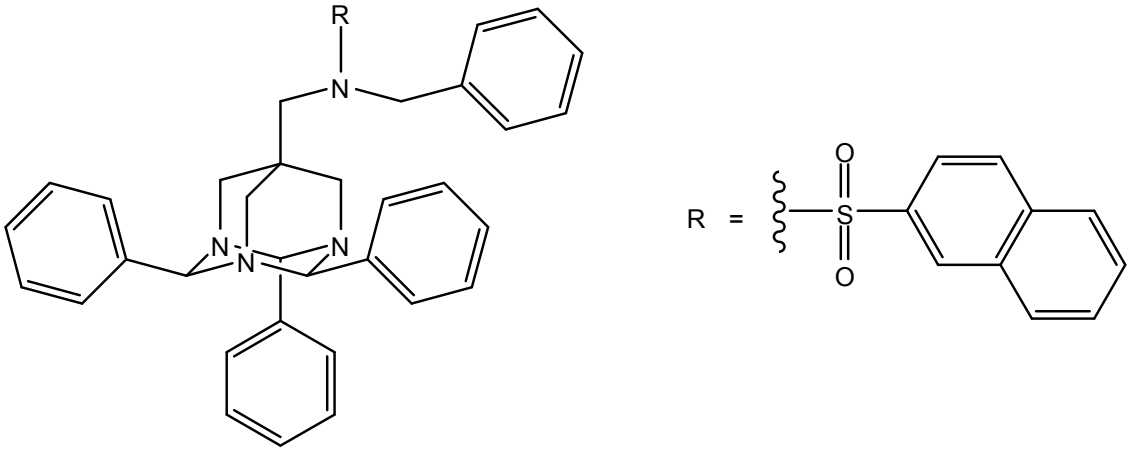

2.7 g Benzylamine (7.3.22) was dissolved in 70 mL dry pyridine and cooled in an ice bath. 1.4 g 2-Naphthalene sulfonyl chloride was added and the yellow solution stirred

overnight. The solution was added to 100 mL saturated sodium bicarbonate solution and extracted with ether (3 x 100 mL). This was dried ($MgSO_4$), filtered and the solvent removed to near dryness. Upon addition of methanol, the product precipitated as a yellow solid.

Yield 2.1 g (56%) ^{1}H NMR ($CDCl_3$) δ 6.98 – 7.94 (m, Ar**H**, 27 H), 5.58 (s, NC**H**$_{eq}$(Ph)N, 1 H), 5.39 (s, NC**H**$_{ax}$(Ph)N, 2H), 4.11 (s, ArC**H**$_2$NH, 2 H), 3.26 (AB q, C**H**$_2$N, 4 H), 2.68 (s, C**H**$_2$N, 2 H), 1.99 (s, C**H**$_2$N, 2 H); ESI-MS: *m/z* 677.08

7.3.28. *N*-(3-Amino-2,2-bis(aminomethyl)propyl)-*N*-benzyl-naphthalene-2-sulfonamide trihydrochloride (nst)

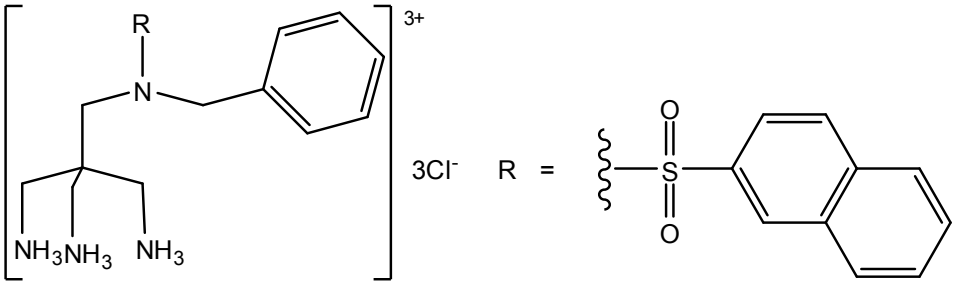

2.1 g of *N*-[(1,3,5-Triaza-2,4,9-triphenyladamant-7-yl)methyl]-*N*-benzyl-naphthalene-2-sulfonamide (7.3.27) dissolved in 80 mL THF and 80 mL 3 M HCl added. The solution was stirred at room temperature for 10 minutes. The THF was removed, and the aqueous solution washed with DCM (3 x 50 mL) to remove benzaldehyde. The aqueous solution was then evaporated to dryness to give the product as the hydrochloride salt.

Yield 1.30 g (80%); ^{1}H NMR (D_2O, TMPS) δ 8.56 (s, Np**H**, 1 H), 8.16 (d, Np**H**, 1 H), 8.08 (dd, Np**H**, 2 H), 7.90 (d, Np**H**, 1 H), 7.81 (t, Np**H**, 1 H), 7.74 (t, Np**H**, 1 H), **7**.31 (m, Ph**H**, 3 H), 7.23 (m, Ph**H**, 2 H), 4.49 (br s, C**H**$_2$, 2 H), 3.39 (s, C**H**$_2$N, 2 H), 3.26 (s, C**H**$_2$NH$_2$, 6 H); ^{13}C NMR (D_2O, TMPS) δ 137.9, 137.3, 135.5, 134.6, 132.9, 132.6, 132.1, 131.9, 131.4, 131.0, 130.9, 130.7, 124.7, 58.9, 54.4, 43.4, 42.4; IR (KBr) ν/cm^{-1} 3036, 2920, 2094, 1602, 1514, 1335, 1226, 1164, 1074; ESI-MS: *m/z* 413.37

7.3.29. [Co(nst)$(NO_2)_3$]

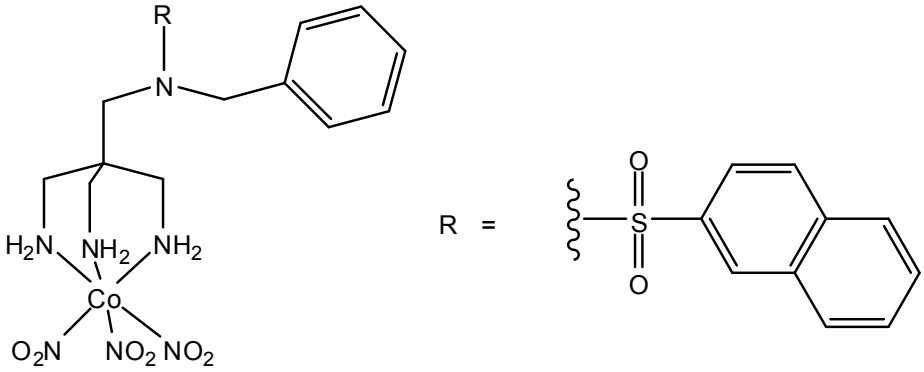

A buffer solution was made comprising 0.28 g NaOH and 0.80 mL glacial acetic acid in 10 mL water. In this, 1.01 g $Co(NO_3)_2$ and 1.12 g $NaNO_2$ were dissolved and aeration begun. 1.30 g Nst was dissolved in 10 mL water with 0.21 g NaOH and added dropwise to the aerating solution. After 2 hours, the solution was filtered to give a brown powder.

Yield 0.65 g (43%).

7.3.30. [Co(nst)Cl_3]

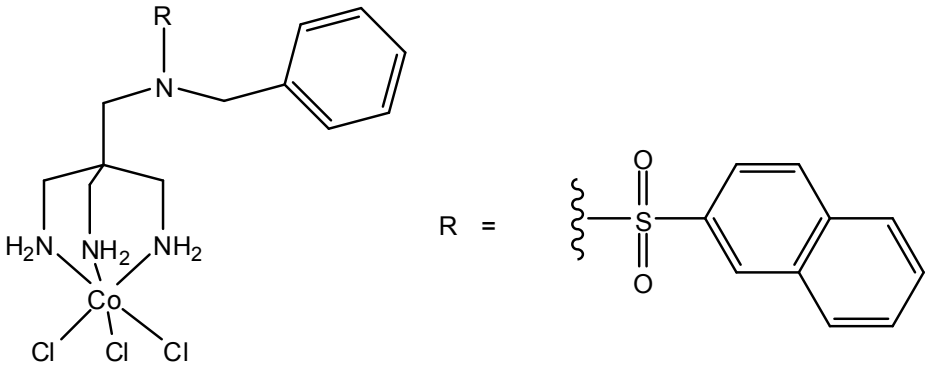

0.65 g [Co(nst)$(NO_2)_3$] was covered with ~10 mL of 3 M HCl and heated on a steam bath to dryness. The blue powder was ground in dry ethanol and filtered.

Yield 0.55 g (91%) IR (KBr) ν/cm^{-1} 3235, 1585, 1458, 1330, 1156, 711.

7.3.31. Anthraquinone-2-sulfonyl chloride

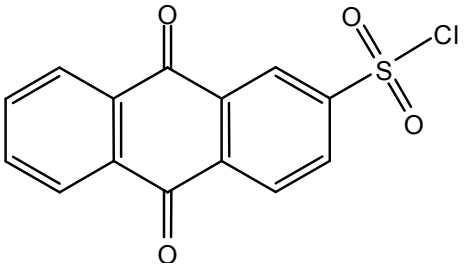

Anthraquinone-2-sulfonyl chloride was synthesised using a modified method of Aquino *et al*.[228] 5.2 g of Sodium anthraquinone-2-sulfonate monohydrate was covered with thionyl chloride in a round bottom flask fitted to a condenser with a drying tube of $CaCl_2$. After the bubbling ceased, the mixture was heated to reflux. After 30 min 1 mL of DMF was added carefully, and the solution allowed to reflux for a further 2 hours. After cooling, the yellow solution was poured onto ice, and the resulting precipitate was collected by suction.

mp 192 °C (lit 195 °C); ^{1}H NMR ($CDCl_3$) δ 8.97 (d, 1 H), 8.57 (d, 1 H), 8.42 (dd, 1 H), 8.37 (m, 2 H), 7.90 (m, 2 H); ^{13}C NMR ($CDCl_3$) δ 181.3, 180.8, 146.5, 137.2, 135.1, 135.0, 134.5, 133.0, 131.3, 129.2, 127.8, 127.7, 126.3.

7.3.32. *N*-[(1,3,5-Triaza-2,4,9-triphenyladamant-7-yl)methyl]-*N*-benzyl-anthraquinone-2-sulfonamide

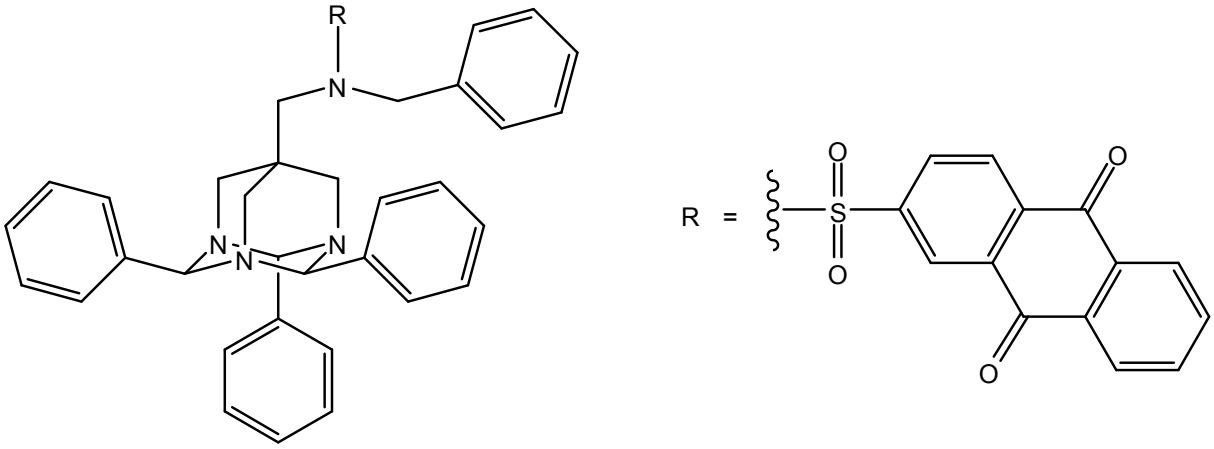

2.07 g 7-[(Benzylamino)methyl]-1,3,5-triaza-2,4,9-triphenyladamantane was dissolved in 50 mL of pyridine and cooled in an ice bath. 2.0 g Anthraquinone-2-sulfonyl chloride was added and the mixture stirred for 1 hour. The brown mixture was then added to 100 mL of

saturated sodium bicarbonate solution, and extracted with ~300 mL of ether. The solvent was the dried with magnesium sulfate, filtered, and removed on a rotary evaporator to near dryness. Addition of methanol precipitated the product as a yellow solid.

Yield 0.45 g (14%) ^{1}H NMR δ 6.83 – 7.81 (m, Ar**H**, 27 H), 5.51 (s, NC**H**$_{eq}$(Ph)N, 1 H), 5.30 (s, NC**H**$_{ax}$(Ph)N, 2H), 4.12 (s, ArC**H**$_2$NH, 2 H), 3.30 (AB q, C**H**$_2$N, 4 H), 2.81 (s, C**H**$_2$N, 2 H), 2.65 (s, C**H**$_2$N, 2 H); ESI-MS: *m/z* 757.55

7.3.33. *N*-(3-Amino-2,2-bis(aminomethyl)propyl)-*N*-benzyl-anthraquinone-2-sulfonamide trihydrochloride (ast)

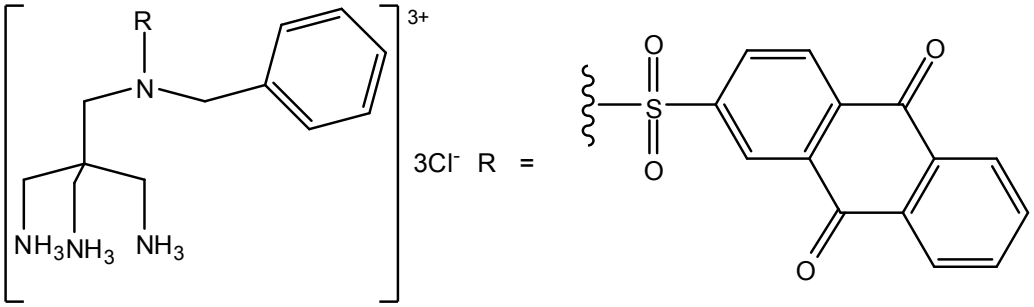

0.45 g of *N*-[(1,3,5-Triaza-2,4,9-triphenyladamant-7-yl)methyl]-*N*-benzyl-anthraquinone-2-sulfonamide (7.3.32) dissolved in 20 mL THF and 20 mL 3 M HCl added. The solution was stirred at room temperature for 10 minutes. The THF was removed, and the aqueous solution washed with DCM (3 x 20 mL) to remove benzaldehyde. The aqueous solution was then evaporated to dryness to give the product as the hydrochloride salt.

Yield 0.28 g (91%); ^{1}H NMR (D_2O, TMPS) δ 8.64 (d, Ar**H**, 1 H), 7.95 (m, Ar**H**, 5 H), 8.08 (dd, Np**H**, 2 H), 7.73 (br s, Ar**H**, 1 H), 7.81 (t, Np**H**, 1 H), 7.43 (m, Ar**H**, 2 H), **7**.36 (m, Ar**H**, 3 H), 4.27 (s, C**H**$_2$, 2 H), 3.42 (s, C**H**$_2$N, 2 H), 3.31 (s, C**H**$_2$NH$_2$, 6 H); ^{13}C NMR (D_2O, TMPS) δ 150.0, 143.8, 133.1, 132.8, 132.5, 131.9, 131.7, 131.1, 130.2, 56.4, 49.6, 41.7, 41.6; IR (KBr) *ν*/cm^{-1} 3007, 2927, 2094, 1676, 1588, 1514, 1346, 1288, 1176, 1151; ESI-MS: *m/z* 493.50; Calculated for $C_{26}H_{34}N_4O_4S.3.5HCl$: C: 50.35, H: 5.12, N: 9.03. Found: C: 49.57, H: 5.13, N: 8.87.

7.3.34. [Co(ast)$(NO_2)_3$]

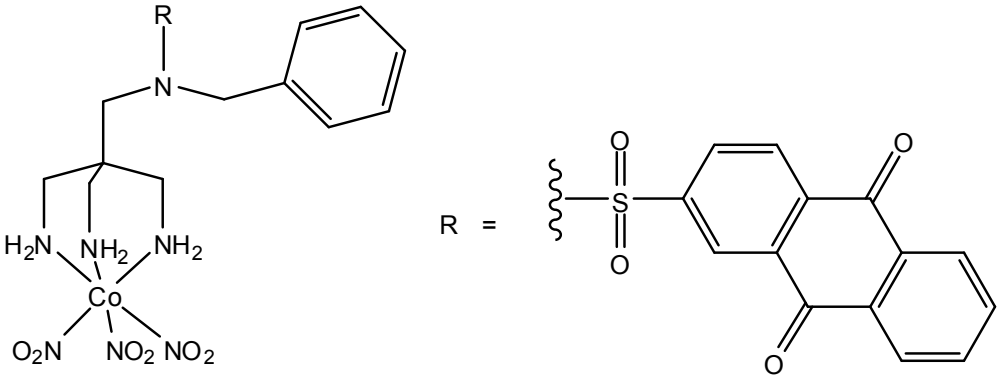

A buffer solution was prepared using 0.9 g NaOH and 2.6 mL glacial acetic acid in 22 mL of water, To this, 3.21 g of $Co(NO_3)_2$ and 3.50 g of $NaNO_2$ were added and the solution aerated. 0.28 g Ast dissolved in 22 mL water with 1 g NaOH was added slowly, and aeration continued for 3 hours. The solution was filtered to give a brown powder.

Yield 0.20 g (62%); IR (KBr) ν/cm^{-1} 3515, 1677, 1589, 1418, 1324, 1288, 1176, 1150, 1071, 961, 930, 826.

7.3.35. [Co(ast)Cl_3]

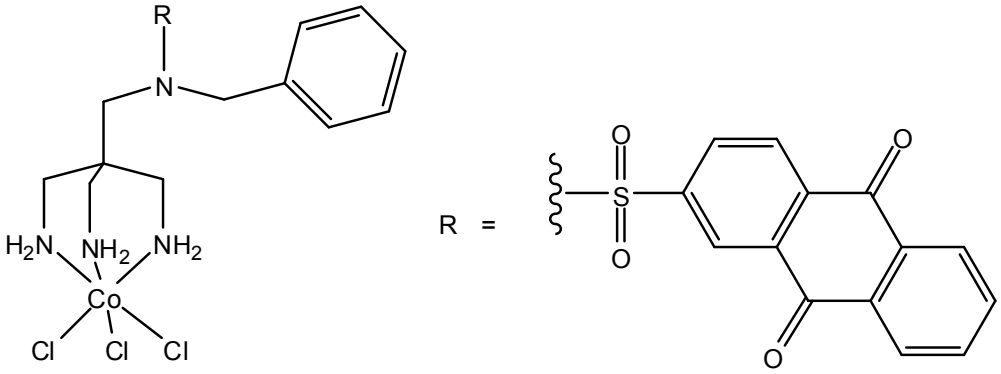

0.20 g [Co(ast)$(NO_2)_3$] was covered with ~10 mL of 3 M HCl and heated on a steam bath to dryness. The green powder was heated in anhydrous ethanol and filtered to give 0.12 g of a green product.

Yield 0.12 g (63%); IR (KBr) ν/cm^{-1} 3347, 1677, 1590, 1496, 1455, 1325, 1290, 1177, 1149, 1073.

7.3.36. d-Camphor-10-sulfonyl chloride

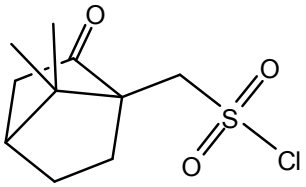

5 g of d-Camphor-10-sulfonic acid was covered with thionyl chloride in a round bottom flask fitted to a condenser with a drying tube of $CaCl_2$. After the bubbling ceased, the mixture was heated to reflux for 2 hours. After cooling, the solvent was removed and the resulting oil was recrystallised from pet ether to give the title compound.

Yield 2.90 g (51.7%); mp 68 °C (lit 67 °C)[229]; ^{1}H NMR[230] ($CDCl_3$) δ 4.30 (d, 1 H), 3.72 (d, 1 H), 2.40 – 2.49 (m, 2 H), 2.16 (t, 1 H), 2.04 – 2.13 (m, 1 H), 1.98 (d, 1 H), 1.78 (m, 1 H), 1.48 (m, 1 H), 1.13 (s, 1 H), 0.92 (s, 3 H)

7.3.37. *N*-[(1,3,5-Triaza-2,4,9-triphenyladamant-7-yl)methyl]-*N*-benzyl-d-camphor-10-sulfonamide

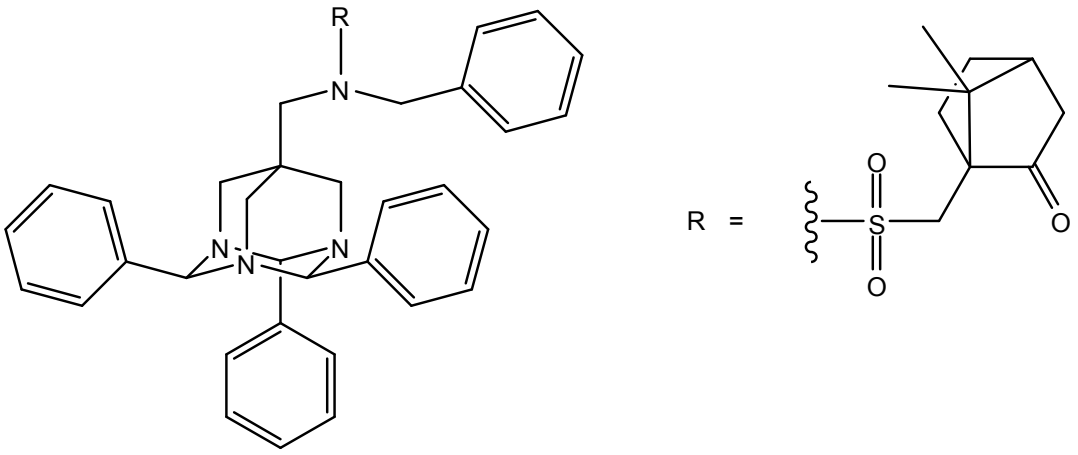

1.95 g 7-[(Benzylamino)methyl]-1,3,5-triaza-2,4,9-triphenyladamantane was dissolved in 10 mL of pyridine and cooled in an ice bath. 0.98 g d-Camphor-10-sulfonyl chloride was added and the mixture stirred overnight. The yellow mixture was then added to saturated sodium bicarbonate solution, and extracted with ether. The solvent was the dried with magnesium sulfate, filtered, and removed on a rotary evaporator to dryness. The product was used without analysis in the subsequent step.

7.3.38. *N*-(3-Amino-2,2-bis(aminomethyl)propyl)-*N*-benzyl-d-camphor-10-sulfonamide trihydrochloride (cst)

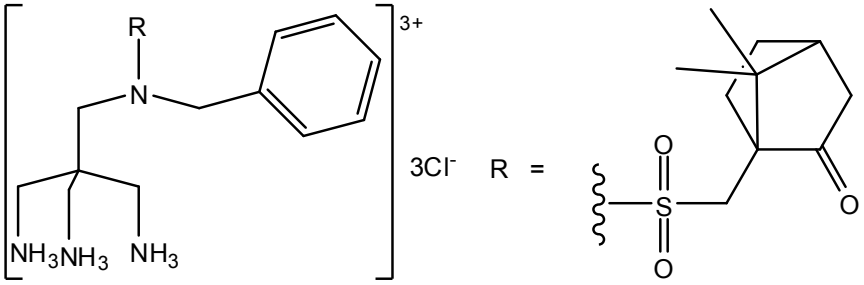

N-[(1,3,5-Triaza-2,4,9-triphenyladamant-7-yl)methyl]-*N*-benzyl-d-camphor-10-sulfonamide (7.3.37) dissolved in 20 mL THF and 20 mL 3 M HCl added. The solution was stirred at room temperature for 10 minutes. The THF was removed, and the aqueous solution washed with chloroform (3 x 40 mL) to remove benzaldehyde. The aqueous solution was then evaporated to dryness to give the product as the hydrochloride salt.

Yield 2.48 g (88% over two steps) ^{1}H NMR δ 7.53 (m, Ar**H**, 5 H), 4.60 (br s, PhC**H**$_2$, 2 H), 4.46 (s, C**H**$_2$, 2 H), 3.62 (s, C**H**$_2$, 2 H), 3.22 (s, C**H**$_2$, 6 H), 2.48 (m, 1 H), 2.25 (m, 1 H), 2.19 (t, 1 H), 2.05 (m, 2 H), 1.74 (m, 1 H), 1.49 (m, 1 H); IR (KBr) ν/cm^{-1} 2985, 2869, 1745, 1606, 1537, 1483, 1342, 1197, 1154, 1054; ESI-MS: *m/z* 493.50; ESI-MS: *m/z* 437.5.

7.3.39. [Co(cst)(NO$_2$)$_3$]

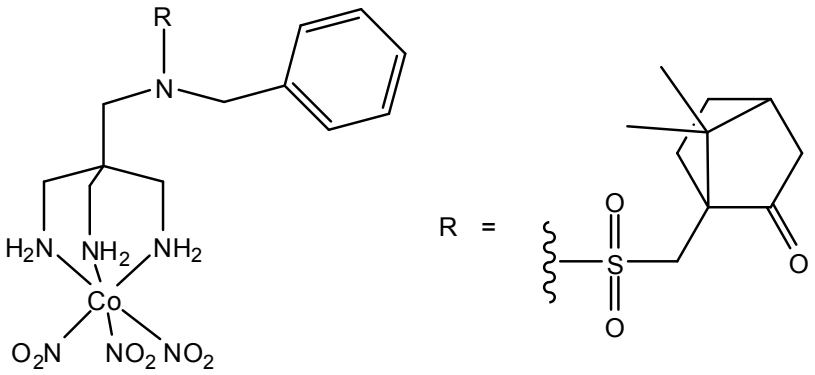

A buffer solution was prepared using 0.9 g NaOH and 2.6 mL glacial acetic acid in 22 mL of water, To this, 3.21 g of Co(NO$_3$)$_2$ and 3.50 g of NaNO$_2$ were added and the solution aerated. 1.75 g Cst dissolved in 22 mL water with 1 g NaOH was added slowly, and aeration continued for 3 hours. The solution was filtered to give a brown powder.

Yield 0.95 g (46.6%); ^{13}C NMR (DMSO-d_6) δ 128.5, 58.0, 54.5, 47.6, 42.8, 42.4, 42.1,

42.0, 26.2, 25.5, 19.2, 19.3 ; IR (KBr) ν/cm^{-1} 3443, 1742, 1651, 1561, 1414, 1335, 1270, 1149, 1046, 1022, 926, 827.

7.3.40. [Co(cst)Cl$_3$]

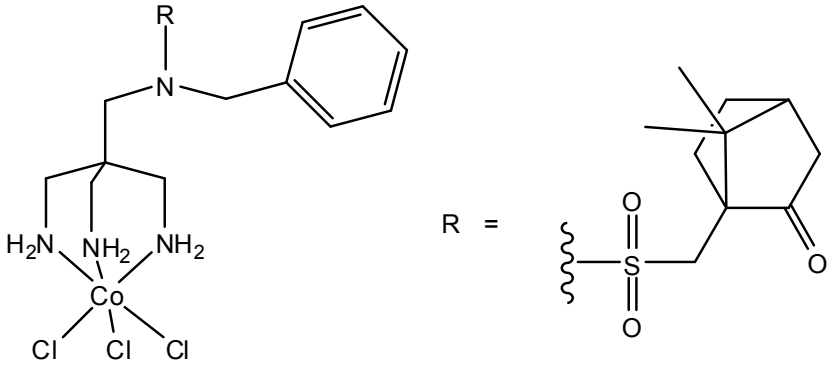

0.95 g of the yellow [Co(cst)(NO$_2$)$_3$] was covered in 3 M HCl and heated on a steam bath for several hours to dryness. The resultant green-blue solid was heated in anhydrous ethanol and filtered.

Yield 0.77 g (85.3%); IR (KBr) ν/cm^{-1} 3202, 2958, 1744, 1626, 1598, 1454, 1335, 1208, 1148, 1045.

7.3.41. [Cr(tame)Cl$_3$]

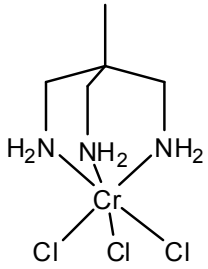

Following the method of Glerup *et al*,[221] 6.3 g of [Cr(thf)$_3$Cl$_3$][231] was dissolved in boiling THF and 2.1 g of tame in THF was added. The green precipitate was collected and washed with boiling THF.

Calculated for C$_7$H$_{20}$N$_3$OCl$_3$Cr (Cr(tame)Cl$_3$.0.5THF.0.5H$_2$O): C: 26.22, H: 6.29, N: 13.11; Found: C: 26.27, H: 6.23, N: 13.19.

Appendices

Appendix 1: X-Ray crystal data

$[Co(tame)(OH_2)_2Cl]Cl_2$

Identification code	$[Co(tame)(OH_2)_2Cl]Cl_2$	
Empirical formula	C5 H19 Cl3 Co N3 O2	
Formula weight	318.51	
Temperature	296(2) K	
Wavelength	0.71073 Å	
Crystal system	Monoclinic	
Space group	P 2(1)/n	
Unit cell dimensions	a = 12.3732(4) Å	α= 90°.
	b = 7.4602(2) Å	β= 91.263(2)°.
	c = 13.4224(4) Å	γ = 90°.
Volume	1238.67(6) $Å^3$	
Z	4	
Density (calculated)	1.708 Mg/m^3	
Absorption coefficient	2.014 mm^{-1}	
F(000)	656	
Crystal size	0.41 x 0.16 x 0.06 mm^3	
Theta range for data collection	2.26 to 30.00°.	
Index ranges	-17<=h<=17, -10<=k<=10, -18<=l<=18	
Reflections collected	32302	
Independent reflections	3616 [R(int) = 0.0446]	
Completeness to theta = 30.00°	99.9 %	
Absorption correction	Semi-empirical from equivalents	
Max. and min. transmission	0.7469 and 0.6186	
Refinement method	Full-matrix least-squares on F^2	
Data / restraints / parameters	3616 / 8 / 162	
Goodness-of-fit on F^2	1.057	
Final R indices [I>2sigma(I)]	R1 = 0.0224, wR2 = 0.0520	
R indices (all data)	R1 = 0.0293, wR2 = 0.0548	
Largest diff. peak and hole	0.414 and -0.387 $e.Å^{-3}$	

[(tame)Co(μ-OH)$_3$Co(tame)](NO$_3$)$_3$.H$_2$O

Identification code	[(tame)Co(μ-OH)$_3$Co(tame)](NO$_3$)$_3$.H$_2$O	
Empirical formula	C10 H32 Co2 N9 O13	
Formula weight	604.31	
Temperature	124(2) K	
Wavelength	0.71073 Å	
Crystal system	Hexagonal	
Space group	P 63/m m c	
Unit cell dimensions	a = 7.47120(10) Å	α= 90°.
	b = 7.47120(10) Å	β= 90°.
	c = 24.5720(10) Å	γ = 120°.
Volume	1187.82(5) Å^3	
Z	2	
Density (calculated)	1.690 Mg/m^3	
Absorption coefficient	1.474 mm^{-1}	
F(000)	668	
Crystal size	0.45 x 0.28 x 0.05 mm^3	
Theta range for data collection	3.26 to 25.15°.	
Index ranges	-8<=h<=8, -8<=k<=8, -29<=l<=29	
Reflections collected	21046	
Independent reflections	457 [R(int) = 0.0538]	
Completeness to theta = 25.15°	99.3 %	
Absorption correction	Semi-empirical from equivalents	
Max. and min. transmission	1 and 0.832	
Refinement method	Full-matrix least-squares on F^2	
Data / restraints / parameters	457 / 10 / 57	
Goodness-of-fit on F^2	1.111	
Final R indices [I>2sigma(I)]	R1 = 0.0683, wR2 = 0.2160	
R indices (all data)	R1 = 0.0707, wR2 = 0.2216	
Largest diff. peak and hole	1.108 and -0.997 e.Å^{-3}	

[Co(tame)(ida)]Cl.2H_2O.2CH_3OH

Identification code	[Co(tame)(ida)]Cl.2H_2O.2CH_3OH	
Empirical formula	C10.25 H25 Cl Co N4 O6.25	
Formula weight	398.72	
Temperature	296(2) K	
Wavelength	0.71073 Å	
Crystal system	Monoclinic	
Space group	P 2(1)/n	
Unit cell dimensions	a = 16.5988(9) Å	α= 90°.
	b = 9.3802(4) Å	β= 109.350(3)°.
	c = 24.3576(13) Å	γ = 90°.
Volume	3578.2(3) $Å^3$	
Z	8	
Density (calculated)	1.480 Mg/m^3	
Absorption coefficient	1.141 mm^{-1}	
F(000)	1668	
Crystal size	0.48 x 0.06 x 0.02 mm^3	
Theta range for data collection	2.53 to 25.05°.	
Index ranges	-19<=h<=19, -11<=k<=11, -29<=l<=29	
Reflections collected	62589	
Independent reflections	6327 [R(int) = 0.1378]	
Completeness to theta = 25.05°	99.9 %	
Absorption correction	Semi-empirical from equivalents	
Max. and min. transmission	0.7452 and 0.6487	
Refinement method	Full-matrix least-squares on F^2	
Data / restraints / parameters	6327 / 6 / 425	
Goodness-of-fit on F^2	1.062	
Final R indices [I>2sigma(I)]	R1 = 0.0683, wR2 = 0.1801	
R indices (all data)	R1 = 0.1127, wR2 = 0.2036	
Largest diff. peak and hole	3.310 and -0.736 $e.Å^{-3}$	

Appendix 2: Adsorption isotherm data

Adsorption isotherm data for $[Co(tame)_2]Cl_3$:

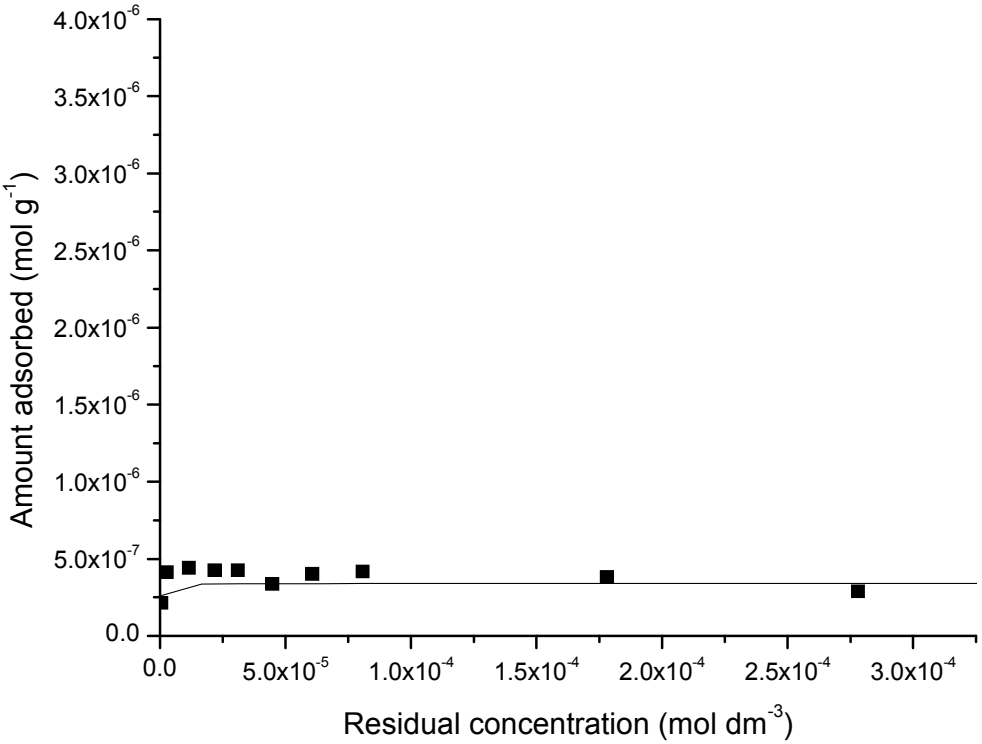

Residual concentration (x 10^{-5} mol dm^{-3})	Amount adsorbed (x 10^{-7} mol g^{-1})
0.059	2.14
0.268	4.13
1.15	4.41
2.18	4.26
3.1	4.26
4.47	3.36
6.06	4.02
8.07	4.17
17.8	3.8
27.8	2.88

Adsorption isotherm data for $[Co(tpa)Cl_2]ClO_4$

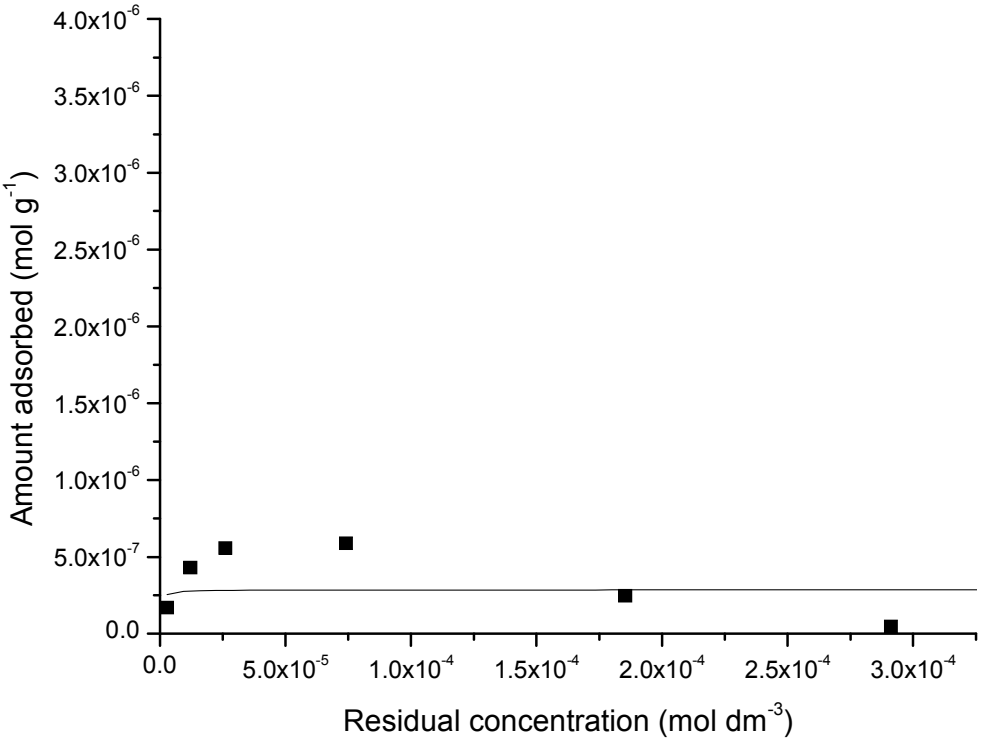

Residual concentration (x 10^{-5} mol dm^{-3})	Amount adsorbed (x 10^{-7} mol g^{-1})
0.2869	1.697
1.205	4.298
2.608	5.582
7.407	5.864
18.53	2.463
29.11	0.4565
39.4	-0.8415

Adsorption isotherm data for $[Co(tren)Cl_2]Cl$

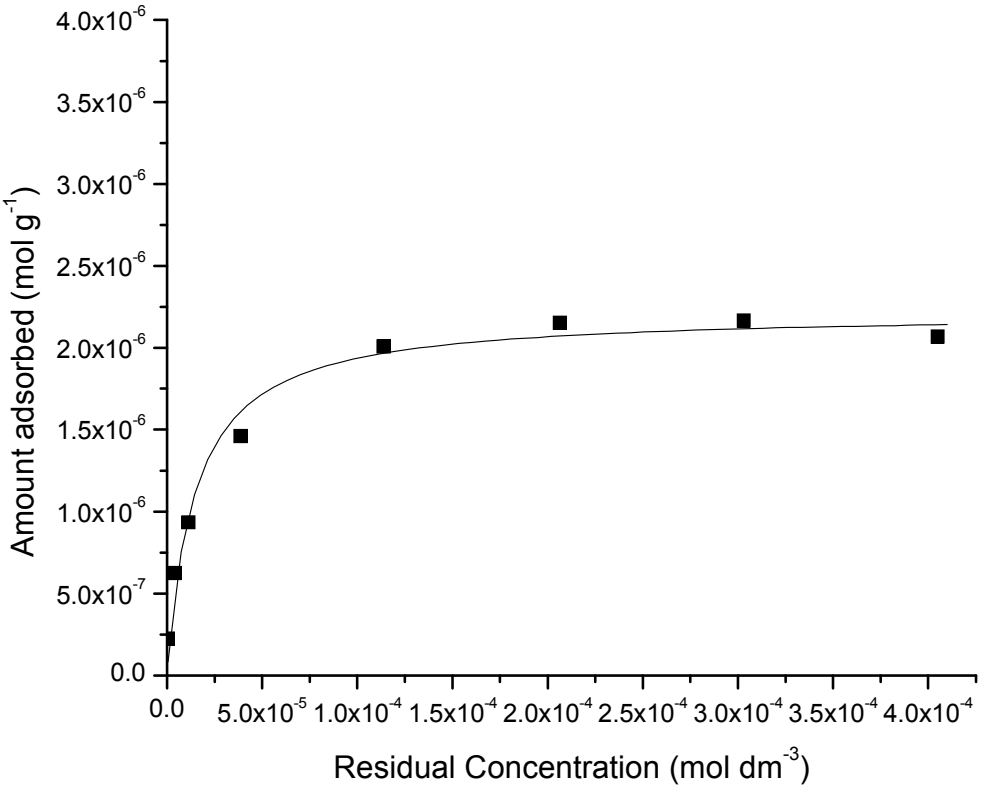

Residual concentration (x 10^{-5} mol dm^{-3})	Amount adsorbed (x 10^{-7} mol g^{-1})
0.05772	2.252
0.4.041	6.259
1.129	9.351
3.878	14.6
11.38	20.08
20.65	21.51
30.31	21.66
40.51	20.68

Adsorption isotherm data for $[Co(tren)Cl_2]ClO_4$

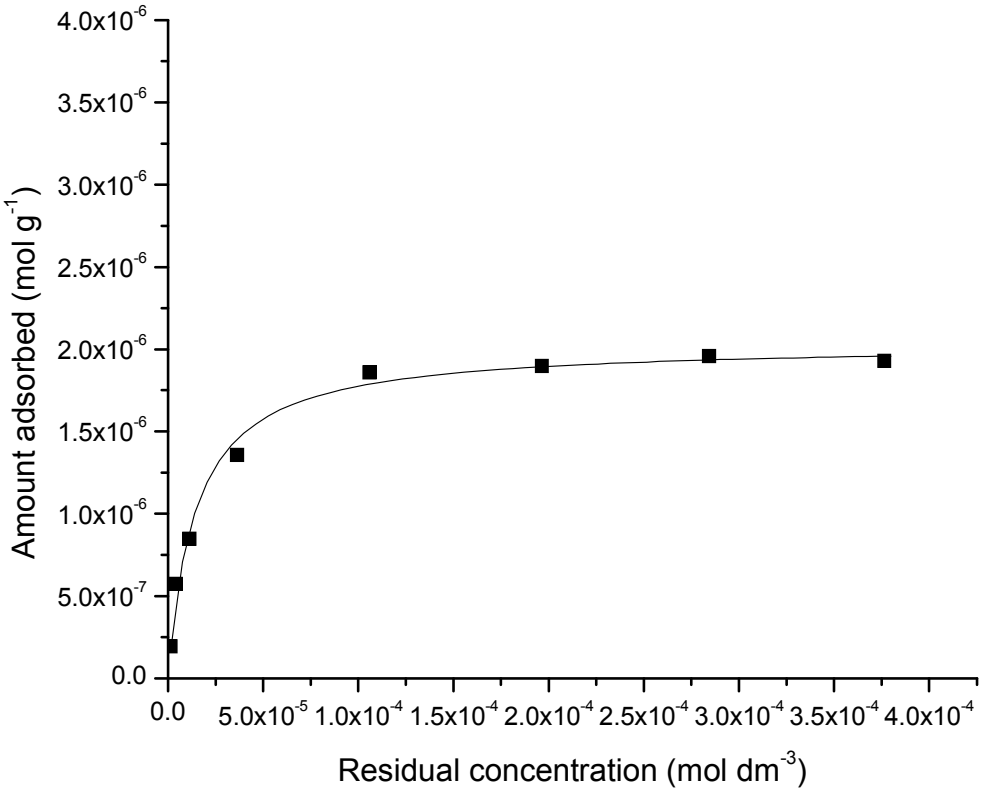

Residual concentration (x 10^{-5} mol dm^{-3})	Amount adsorbed (x 10^{-7} mol g^{-1})
0.1307	1.927
0.4075	5.73
1.143	8.485
3.643	13.57
10.6	18.58
19.65	18.97
28.44	19.59
37.64	19.29

Adsorption isotherm data for *mer*-[Co(dien)Cl_3]

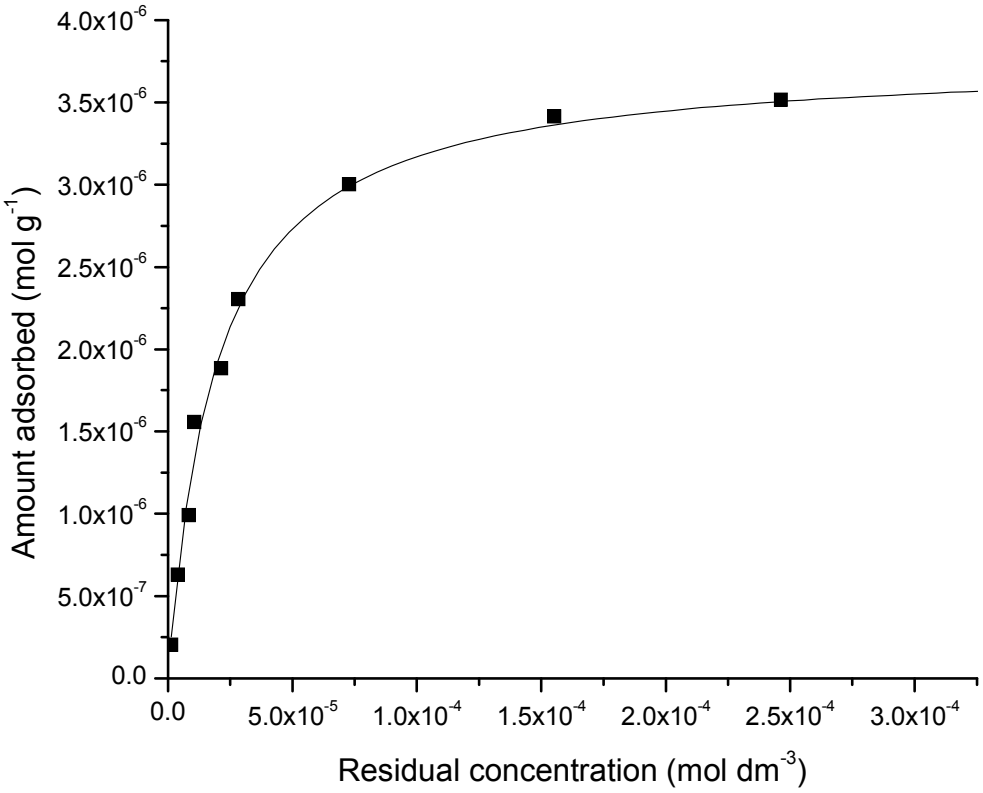

Residual concentration (x 10^{-5} mol dm^{-3})	Amount adsorbed (x 10^{-7} mol g^{-1})
0.1375	2.051
0.3973	6.301
0.837	9.921
1.059	15.58
2.139	18.84
2.83	23.03
7.277	30.01
15.52	34.13
24.64	35.15
34.57	35.17

Adsorption isotherm data for [Co(tacn)Cl_3]

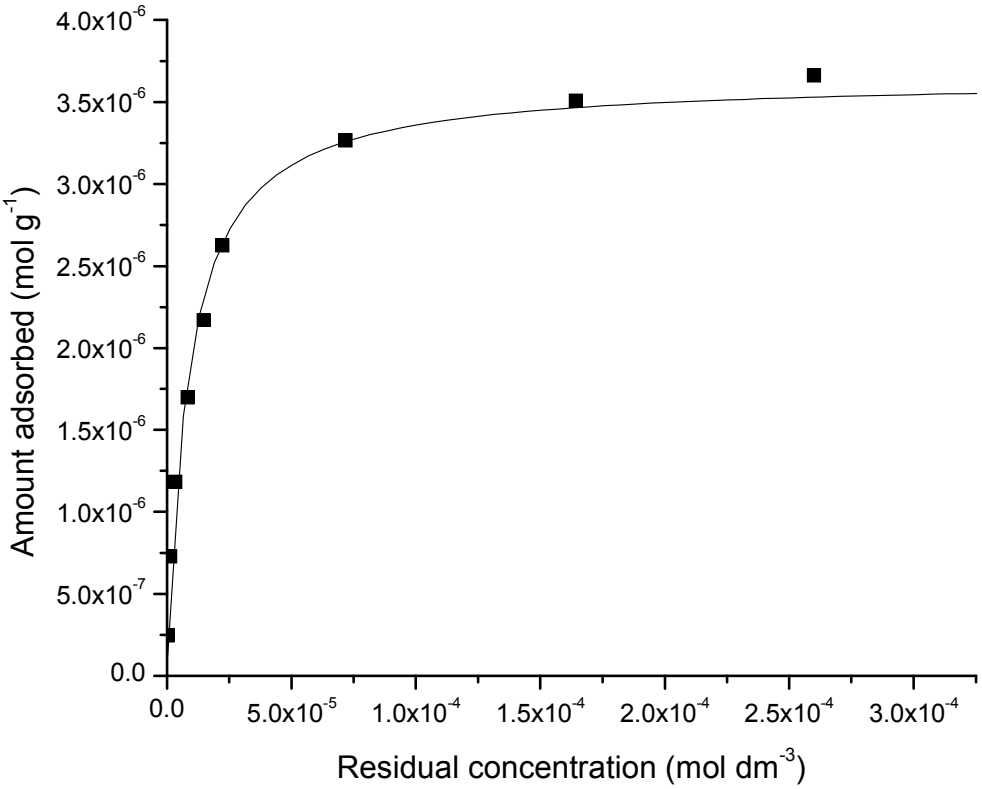

Residual concentration (x 10^{-5} mol dm^{-3})	Amount adsorbed (x 10^{-7} mol g^{-1})
0.03056	2.447
0.1324	7.272
0.3396	11.82
0.8404	16.98
1.486	21.69
2.236	26.24
7.17	32.65
16.44	35.06
26	36.62
37.05	34.72

Adsorption isotherm data for [Co(tame)Cl_3]

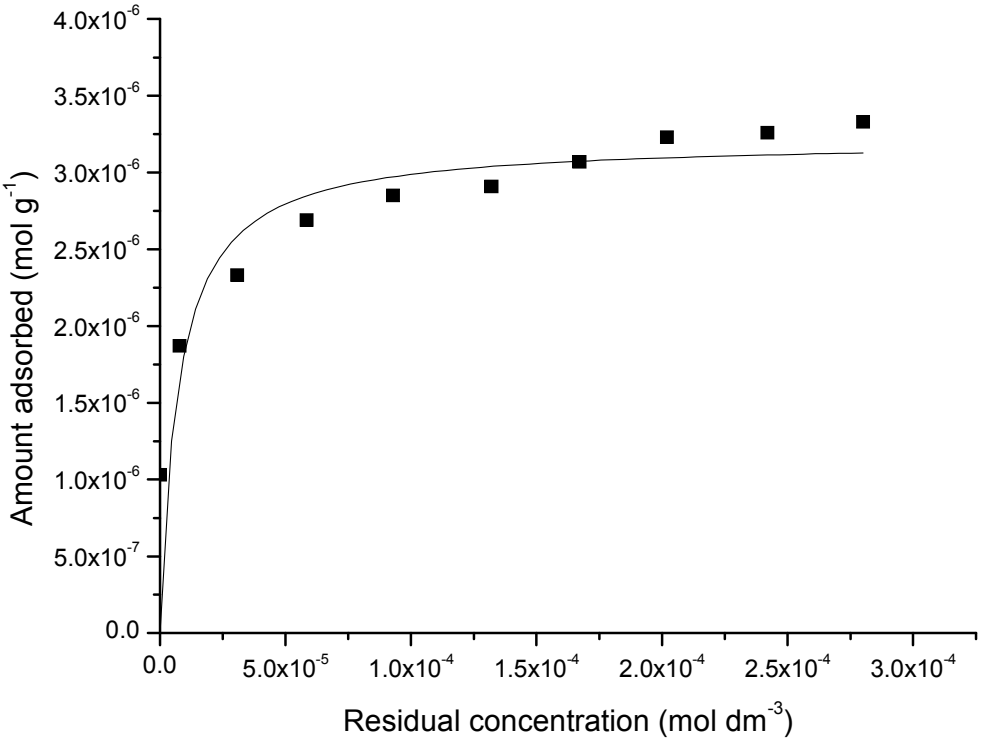

Residual concentration (x 10^{-5} mol dm^{-3})	Amount adsorbed (x 10^{-7} mol g^{-1})
0	10.3
0.778	18.7
3.07	23.3
5.84	26.9
9.29	28.5
13.2	29.1
16.7	30.7
20.2	32.3
24.2	32.6
28	33.3

Adsorption isotherm data for [Cr(tame)Cl_3]

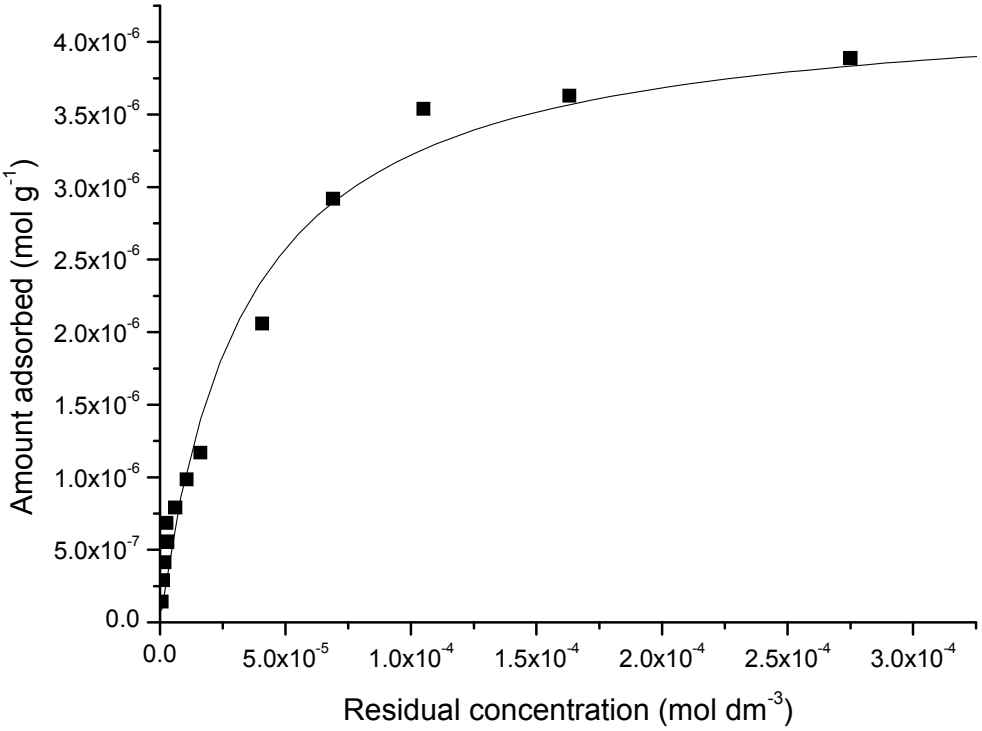

Residual concentration (x 10^{-5} mol dm^{-3})	Amount adsorbed (x 10^{-7} mol g^{-1})
0.0662	1.44
0.108	2.91
0.188	4.14
0.294	5.57
0.258	6.86
0.606	7.93
1.07	9.86
1.61	11.7
4.07	20.6
6.89	29.2
10.5	35.4
16.3	36.3
27.5	38.9

Adsorption isotherm data for $[Co(tst)Cl_3]$

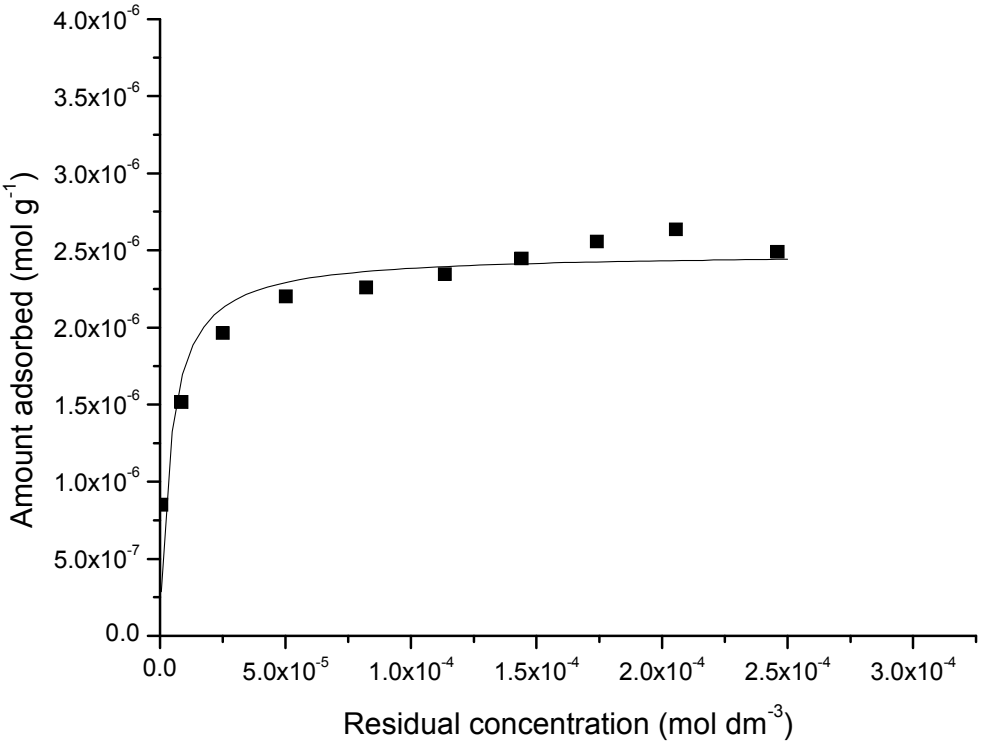

Residual concentration (x 10^{-5} mol dm^{-3})	Amount adsorbed (x 10^{-7} mol g^{-1})
0.0543	8.5
0.85	15.15
2.51	19.64
5.01	22
8.218	22.6
11.35	23.45
14.4	24.46
17.41	25.57
20.55	26.36
24.59	24.9

Adsorption isotherm data for $[Co(nst)Cl_3]$

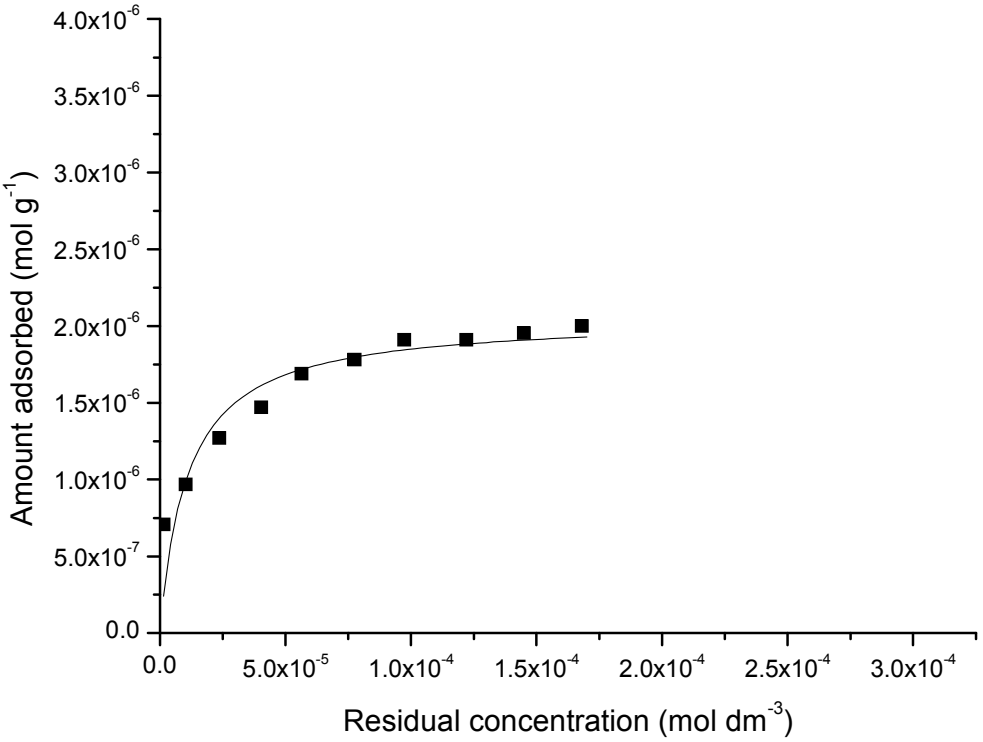

Residual concentration (x 10^{-5} mol dm^{-3})	Amount adsorbed (x 10^{-7} mol g^{-1})
0.1476	7.08
0.103	9.675
2.36	12.7
4.035	14.7
5.639	16.9
7.75	17.8
9.725	19.1
12.2	19.1
14.5	19.55
16.8	20

Appendix 3: Corrosion mass loss experimental data

Control: 240 minutes, 1 M HCl

Initial mass (g)	Final mass (g)	Δm (mg)	Δm (mg cm^{-2} min^{-1})
2.7735	2.5938	179.7	0.138657
2.6994	2.5217	177.7	0.137114
2.7137	2.5608	152.9	0.117978
2.6904	2.5378	152.6	0.117747
2.7186	2.5548	163.8	0.126389
2.7206	2.5576	163	0.125772
		Mean	0.127276
		Standard deviation	0.009018

[Co(tame)Cl_3] variable concentration, 1 M HCl, 240 minutes

Concentration (mM)	Initial mass (g)	Final mass (g)	Δm (mg)	Δm (mg cm^{-2} min^{-1})
0.1	2.7627	2.5918	170.9	0.131867
	2.6938	2.5344	159.4	0.122994
	2.6329	2.4769	156	0.12037
	2.7828	2.62	162.8	0.125617
			Mean	**0.125212**
			Standard deviation	0.004927
0.2	2.7635	2.6083	155.2	0.119753
	2.761	2.6098	151.2	0.116667
	2.6959	2.5312	164.7	0.127083
	2.842	2.6707	171.3	0.132176
			Mean	**0.12392**
			Standard deviation	0.007027

Concentration (mM)	Initial mass (g)	Final mass (g)	Δm (mg)	Δm (mg cm^{-2} min^{-1})
0.5	2.7402	2.589	151.2	0.116667
	2.7286	2.5768	151.8	0.11713
	2.7986	2.6466	152	0.117284
	2.7293	2.5784	150.9	0.116435
			Mean	**0.116879**
			Standard deviation	0.000395
1	2.8045	2.658	146.5	0.11304
	2.7913	2.65	141.3	0.109028
	2.653	2.5234	129.6	0.1
	2.7424	2.607	135.4	0.104475
			Mean	**0.106636**
			Standard deviation	0.00564
2	2.6251	2.5056	119.5	0.092207
	2.7771	2.6534	123.7	0.095448
	2.7322	2.6016	130.6	0.100772
	2.6355	2.5052	130.3	0.10054
			Mean	**0.097242**
			Standard deviation	0.00416
5	2.8435	2.7263	117.2	0.090432
	2.7776	2.6618	115.8	0.089352
	2.8787	2.764	114.7	0.088503
	2.7028	2.5935	109.3	0.084336
	2.8276	2.7101	117.5	0.090664
	2.7847	2.6665	118.2	0.091204
			Mean	**0.089082**
			Standard deviation	0.00252
10	2.8059	2.7031	102.8	0.079321
	2.6682	2.5691	99.1	0.076466
	2.6383	2.5408	97.5	0.075231
	2.7368	2.633	103.8	0.080093
			Mean	**0.077778**
			Standard deviation	0.002305

Concentration (mM)	Initial mass (g)	Final mass (g)	Δm (mg)	Δm (mg cm^{-2} min^{-1})
20	2.6572	2.5741	83.1	0.06412
	2.8459	2.761	84.9	0.065509
			Mean	**0.064815**
			Standard deviation	0.000982

Various complexes, 5 mM, 1 M HCl, 240 minutes

Complex	Initial mass (g)	Final mass (g)	Δm (mg)	Δm (mg cm^{-2} min^{-1})
$[Co(tacn)Cl_3]$	2.799	2.7679	31.1	0.023997
	2.867	2.8368	30.2	0.023302
	2.5739	2.5453	28.6	0.022068
	2.6309	2.6008	30.1	0.023225
			Mean	**0.023148**
			Standard deviation	0.000799
$[Co(en)_3]Cl_3$	2.8597	2.8029	56.8	0.043827
	2.8326	2.7776	55	0.042438
	2.8161	2.7586	57.5	0.044367
	2.5857	2.5303	55.4	0.042747
			Mean	**0.043345**
			Standard deviation	0.000905
$[Co(tame)_2]Cl_3$	2.6829	2.6385	44.4	0.034259
	2.7355	2.6851	50.4	0.038889
	2.661	2.6204	40.6	0.031327
	2.8244	2.7818	42.6	0.03287
			Mean	**0.034336**
			Standard deviation	0.003263

$[Co(tren)Cl_2]Cl$ variable concentration, 1 M HCl, 240 minutes

Concentration (mM)	Initial mass (g)	Final mass (g)	Δm (mg)	Δm (mg cm^{-2} min^{-1})
0.1	2.7233	2.6008	122.5	0.094522
	2.7949	2.6739	121	0.093364
	2.7376	2.6098	127.8	0.098611
	2.811	2.6828	128.2	0.09892
			Mean	**0.096354**
			Standard deviation	0.002827
0.2	2.6906	2.6052	85.4	0.065895
	2.7414	2.6529	88.5	0.068287
	2.7682	2.6886	79.6	0.06142
	2.8079	2.7258	82.1	0.063349
			Mean	**0.064738**
			Standard deviation	0.002993
0.5	2.6569	2.5975	59.4	0.045833
	2.7792	2.7157	63.5	0.048997
	2.7817	2.7129	68.8	0.053086
	2.6402	2.5735	66.7	0.051466
			Mean	**0.049846**
			Standard deviation	0.00316
1	2.7082	2.6551	53.1	0.040972
	2.765	2.7015	63.5	0.048997
	2.7893	2.7295	59.8	0.046142
	2.7747	2.7172	57.5	0.044367
			Mean	**0.04512**
			Standard deviation	0.003359
2	2.7161	2.6709	45.2	0.034877
	2.6442	2.5995	44.7	0.034491
	2.7713	2.7283	43	0.033179
	2.7196	2.6756	44	0.033951
			Mean	**0.034124**
			Standard deviation	0.000736

Concentration (mM)	Initial mass (g)	Final mass (g)	Δm (mg)	Δm (mg cm^{-2} min^{-1})
5	2.6819	2.6495	32.4	0.025
	2.8116	2.7786	33	0.025463
	2.7387	2.7072	31.5	0.024306
	2.9119	2.8738	38.1	0.029398
	2.7275	2.6982	29.3	0.022608
	2.6656	2.6353	30.3	0.02338
			Mean	**0.025026**
			Standard deviation	0.002383
10	2.7243	2.6912	33.1	0.02554
	2.7346	2.7033	31.3	0.024151
	2.6632	2.6312	32	0.024691
	2.6913	2.6585	32.8	0.025309
			Mean	**0.024923**
			Standard deviation	0.000627

5 mM [Co(tame)Cl_3], 1 M HCl, variable time

Time (minutes)	Initial mass (g)	Final mass (g)	Δm (mg)	Δm (mg cm^{-2} min^{-1})
15	2.7504	2.7467	3.7	0.045679
	2.8254	2.8216	3.8	0.046914
			Mean	0.046296
			Standard deviation	0.000873
30	2.7142	2.703	11.2	0.138272
	2.6518	2.6416	10.2	0.125926
			Mean	0.132099
			Standard deviation	0.00873
45	2.6499	2.632	17.9	0.220988
	2.777	2.7591	17.9	0.220988
			Mean	0.220988
			Standard deviation	0

Time (minutes)	Initial mass (g)	Final mass (g)	Δm (mg)	Δm (mg cm^{-2} min^{-1})
60	2.7577	2.7331	24.6	0.303704
	2.6886	2.6648	23.8	0.293827
			Mean	0.298765
			Standard deviation	0.006984
120	2.586	2.5318	54.2	0.669136
	2.7362	2.6813	54.9	0.677778
			Mean	0.673457
			Standard deviation	0.006111
180	2.6282	2.5588	69.4	0.85679
	2.7018	2.6232	78.6	0.97037
			Mean	0.91358
			Standard deviation	0.080313

5 mM [Co(tame)Cl_3], 120 minutes – 1 M HCl, 240 minutes

Initial mass (g)	Final mass (g)	Δm (mg)	Δm (mg cm^{-2} min^{-1})
2.7452	2.6196	125.6	0.096914
2.6664	2.5425	123.9	0.095602
		Mean	**0.096258**
		Standard deviation	0.000928

Concentrated HNO_3, 10 minutes – 1 M HCl, 240 minutes

Initial mass (g)	Final mass (g)	Δm (mg)	Δm (mg cm^{-2} min^{-1})
2.7196	2.5872	132.4	0.10216
2.6037	2.4756	128.1	0.098843
		Mean	**0.100502**
		Standard deviation	0.002346

10% H_2O_2, 10 minutes – 1 M HCl, 240 minutes

Initial mass (g)	Final mass (g)	Δm (mg)	Δm (mg cm^{-2} min^{-1})
2.8732	2.7307	142.5	0.109954
2.7231	2.5896	133.5	0.103009
		Mean	**0.106481**
		Standard deviation	0.00491

Conc. HNO_3, 10 min. – 5 mM [Co(tame)Cl_3], 120 min. – 1 M HCl, 240 min.

Initial mass (g)	Final mass g)	Δm (mg)	Δm (mg cm^{-2} min^{-1})
2.6288	2.4634	165.4	0.127623
2.7215	2.5527	168.8	0.130247
		Mean	**0.128935**
		Standard deviation	0.001855

10% H_2O_2, 10 min. – 5 mM [Co(tame)Cl_3], 120 min. – 1 M HCl, 240 min.

Initial mass (g)	Final mass (g)	Δm (mg)	Δm (mg cm^{-2} min^{-1})
2.7291	2.579	150.1	0.115818
2.8533	2.6958	157.5	0.121528
		Mean	**0.118673**
		Standard deviation	0.004037

Concentrated HNO_3, 10 minutes – 5 mM [Co(tame)Cl_3], 1 M HCl, 240 minutes

Initial mass (g)	Final mass (g)	Δm (mg)	Δm (mg cm^{-2} min^{-1})
2.7503	2.6405	109.8	0.084722
2.6505	2.5436	106.9	0.082485
		Mean	**0.083603**
		Standard deviation	0.001582

10% H_2O_2, 10 minutes – 5 mM [Co(tame)Cl_3], 1 M HCl, 240 minutes

Initial mass (g)	Final mass (g)	Δm (mg)	Δm (mg cm^{-2} min^{-1})
2.6694	2.5851	84.3	0.065046
2.8028	2.7117	91.1	0.070293
		Mean	**0.06767**
		Standard deviation	0.00371

References

[1] T. Burakowski and T. Wierzchon, *Surface Engineering of Metals: Principles, Equipment, Technologies*, CRC Press, 1999.

[2] *ASM Handbook, Volume 5: Surface Engineering*, ASM International, 1994.

[3] J. R. Davis, *Surface Engineering for Corrosion and Wear Resistance*, ASM International : Institute of Materials, 2001.

[4] E. P. DeGarmo, J. T. Black, and R. A. Kohser, *Materials and Processes in Manufacturing*, John Wiley & Sons, 1999.

[5] H. K. D. H. Bhadeshia and R. W. K. Honeycombe, *Steels: Microstructure and Properties*, Butterworth-Heinemann, 2006.

[6] G. S. Frankel and R. L. McCreery, *Electrochem. Soc. Interface*, **2001**, *10*, 34.

[7] R. L. Twite and G. P. Bierwagen, *Prog. Org. Coat.*, **1998**, *33*, 91.

[8] J. D. Venables, D. K. McNamara, J. M. Chen, T. S. Sun, and R. L. Hopping, *Appl. Surf. Sci.*, **1979**, *3*, 88.

[9] P. G. Miney, P. E. Colavita, M. V. Schiza, R. J. Priore, F. G. Haibach, and M. L. Myrick, *Electrochem. Solid-State Lett.*, **2003**, *6*, B42.

[10] S. W. M. Chung, J. Robinson, G. E. Thompson, G. C. Wood, and H. S. Isaacs, *Philos. Mag. B*, **1991**, *63*, 557.

[11] F. Schreiber, *Prog. Surf. Sci.*, **2000**, *65*, 151.

[12] F. Galsbol, C. H. Peterson, and K. Simonsen, *Acta Chem. Scand.*, **1996**, *50*, 567.

[13] J. C. Love, L. A. Estroff, J. K. Kriebel, R. G. Nuzzo, and G. M. Whitesides, *Chemical Reviews*, **2005**, *105*, 1103.

[14] M. A. Neouze and U. Schubert, *Monatsh. Chem.*, **2008**, *139*, 183.

[15] A. Ulman, *Chemical Reviews*, **1996**, *96*, 1533.

[16] R. G. Nuzzo and D. L. Allara, *J. Am. Chem. Soc.*, **1983**, *105*, 4481.

[17] G. M. Whitesides, J. K. Kriebel, and J. C. Love, *Sci. Prog.*, **2005**, *88*, 17.

[18] P. E. Laibinis, G. M. Whitesides, D. L. Allara, Y. T. Tao, A. N. Parikh, and R. G. Nuzzo, *J. Am. Chem. Soc.*, **1991**, *113*, 7152.

[19] A. J. Dickie, D. C. R. Hockless, A. C. Willis, J. A. McKeon, and W. G. Jackson, *Inorg. Chem.*, **2003**, *42*, 3822.

[20] J. C. Love, D. B. Wolfe, R. Haasch, M. L. Chabinyc, K. E. Paul, G. M. Whitesides, and R. G. Nuzzo, *J. Am. Chem. Soc.*, **2003**, *125*, 2597.

[21] C. M. Ruan, T. Bayer, S. Meth, and C. N. Sukenik, *Thin Solid Films*, **2002**, *419*, 95.

[22] Y. X. Weng, L. Li, Y. Liu, L. Wang, and G. Z. Yang, *J. Phys. Chem. B*, **2003**, *107*, 4356.

[23] M. Gratzel, *Nature*, **2001**, *414*, 338.

[24] B. O'Regan and M. Gratzel, *Nature*, **1991**, *353*, 737.

[25] N. Robertson, *Angewandte Chemie-International Edition*, **2006**, *45*, 2338.

[26] S. S. De Silva, P. J. Camp, D. K. Henderson, D. C. R. Henry, H. McNab, P. A. Tasker, and P. Wight, *Chemical Communications*, **2003**, 1702.

[27] R. J. Cooper, Surface Engineering of Metal Oxides Using Polynucleating Ligands, PhD Thesis, University of Edinburgh, 2006.

[28] S. Pawsey, K. Yach, and L. Reven, *Langmuir*, **2002**, *18*, 5205.

[29] A. Paszternak, S. Stichleutner, I. Felhosi, Z. Keresztes, F. Nagy, E. Kuzmann, A. Vertes, Z. Homonnay, G. Peto, and E. Kalman, *Electrochim. Acta*, **2007**, *53*, 337.

[30] J. G. Van Alsten, *Langmuir*, **1999**, *15*, 7605.

[31] E. S. Gawalt, M. J. Avaltroni, N. Koch, and J. Schwartz, *Langmuir*, **2001**, *17*, 5736.
[32] R. Luschtinetz, G. Seifert, E. Jaehne, and H. J. P. Adler, *Macromol. Symp.*, **2007**, *254*, 248.
[33] G. H. Koch, M. P. H. Brongers, N. G. Thompson, Y. P. Virmani, and J. H. Payer, *Corrosion Cost and Preventive Strategies in the United States*, FHWA-RD-01-156, Office of Infrastructure Research and Development, McLean, VA, September 2001.
[34] J. R. Davis, *Corrosion: Understanding the Basics*, ASM International, 2000.
[35] D. A. Jones, *Principles and prevention of corrosion*, Macmillan Publishing Company, 1991.
[36] Galvanic Corrosion of Cadmium Plated Steel Washer, http://www.corrosionsource.com/technicallibrary/corrdoctors/Modules/Aircraft/galv-exam1.htm, (last accessed November 2009)
[37] Conserving Outdoor Metal Sculpture, http://www.buildingconservation.com/articles/conservingsculp/conservingsculp.htm, (last accessed November 2009)
[38] Civil Structures: Corrosion, http://www.hsc.csu.edu.au/engineering_studies/civil_structures/3211/index.html, (last accessed November 2009)
[39] Erosion Corrosion, http://corrosion.ksc.nasa.gov/eroscor.htm, (last accessed November 2009)
[40] Dealloying, http://corrosion.ksc.nasa.gov/dealloying.htm, (last accessed November 2009)
[41] N. N. Greenwood and A. Earnshaw, *Chemistry of the Elements*, Pergamon Press, 1984.
[42] J. A. Jacobs and S. M. Testa, in *Chromium (VI) Handbook*, ed. J. A. Jacobs, J. Guertin, and C. Avakian, CRC Press, 2005.
[43] K. M. MacKay, R. A. MacKay, and W. Henderson, *Introduction to Modern Inorganic Chemistry*, Nelson Thornes, 2002.
[44] J. Clayden, N. Greeves, S. Warren, and P. Wothers, *Organic Chemistry*, Oxford University Press, 2001.
[45] W. E. Motzer, in *Chromium (VI) Handbook*, ed. J. A. Jacobs, J. Guertin, and C. Avakian, CRC Press, 2005.
[46] R. Codd and P. A. Lay, *Chem. Res. Toxicol.*, **2003**, *16*, 881.
[47] J. Guertin, in *Chromium (VI) Handbook*, ed. J. A. Jacobs, J. Guertin, and C. Avakian, CRC Press, 2005.
[48] D. Rai, L. E. Eary, and J. M. Zachara, *Sci. Total Environ.*, **1989**, *86*, 15.
[49] F. Y. Saleh, T. F. Parkerton, R. V. Lewis, J. H. Huang, and K. L. Dickson, *Sci. Total Environ.*, **1989**, *86*, 25.
[50] L. F. Larkworthy and K. B. Nolan, in *Comprehensive Coordination Chemistry*, ed. G. Wilkinson, R. D. Gillard, and J. A. McCleverty, Pergamon Press, 1987.
[51] J. E. Earley and R. D. Cannon, *Transition Metal Chem.*, **1965**, *1*, 33.
[52] J. P. Hunt and H. Taube, *J. Chem. Phys.*, **1951**, *19*, 602.
[53] T. W. Swaddle, J. P. Hunt, and L. F. Coleman, *Inorg. Chem.*, **1963**, *2*, 950.
[54] H. Stunzi and W. Marty, *Inorg. Chem.*, **1983**, *22*, 2145.
[55] H. Stunzi, F. P. Rotzinger, and W. Marty, *Inorg. Chem.*, **1984**, *23*, 2160.
[56] F. P. Rotzinger, H. Stunzi, and W. Marty, *Inorg. Chem.*, **1986**, *25*, 489.
[57] H. Stunzi, L. Spiccia, F. P. Rotzinger, and W. Marty, *Inorg. Chem.*, **1989**, *28*, 66.
[58] J. Springborg, *Adv. Inorg. Chem.*, **1988**, *32*, 55.

[59] A. D. Covington, *Chem. Soc. Rev.*, **1997**, *26*, 111.
[60] S. Imer and T. Varnali, *Appl. Organomet. Chem.*, **2000**, *14*, 660.
[61] S. Mischler, A. Vogel, H. J. Mathieu, and D. Landolt, *Corros. Sci.*, **1991**, *32*, 925.
[62] L. J. Oblonsky, M. P. Ryan, and H. S. Isaacs, *J. Electrochem. Soc.*, **1998**, *145*, 1922.
[63] V. Maurice, W. P. Yang, and P. Marcus, *J. Electrochem. Soc.*, **1996**, *143*, 1182.
[64] Y. Leng, *Materials Characterization: Introduction to Microscopic and Spectroscopic Methods*, John Wiley & Sons, 2008.
[65] M. Kerkar, J. Robinson, and A. J. Forty, *Faraday Discuss.*, **1990**, 31.
[66] P. Schmuki, S. Virtanen, A. J. Davenport, and C. M. Vitus, *J. Electrochem. Soc.*, **1996**, *143*, 3997.
[67] J. K. Dennis and T. E. Such, *Nickel and Chromium Plating*, Woodhead Publishing, 1993.
[68] E. McCafferty, M. K. Bernett, and J. S. Murday, *Corros. Sci.*, **1988**, *28*, 559.
[69] E. J. Calvo, C. D. Pallotta, S. Hild, and E. Garcia, *J. Electrochem. Soc.*, **1988**, *135*, 314.
[70] Z. Szklarska-Smialoska and R. W. Staehle, *J. Electrochem. Soc.*, **1974**, *121*, 1146.
[71] S. Virtanen and M. Buchler, *Corros. Sci.*, **2003**, *45*, 1405.
[72] P. Schmuki, S. Virtanen, H. S. Isaacs, M. P. Ryan, A. J. Davenport, H. Bohni, and T. Stenberg, *J. Electrochem. Soc.*, **1998**, *145*, 791.
[73] V. P. Parkhutik, V. T. Belov, and M. A. Chernyckh, *Electrochim. Acta*, **1990**, *35*, 961.
[74] F. W. Eppensteiner and M. R. Jenkins, *Met. Finish.*, **1975**, *73*, 29.
[75] H. A. Katzman, G. M. Malouf, R. Bauer, and G. W. Stupian, *Applications of Surface Science*, **1979**, *2*, 416.
[76] G. M. Brown, K. Shimizu, K. Kobayashi, G. E. Thompson, and G. C. Wood, *Corros. Sci.*, **1993**, *34*, 1045.
[77] M. W. Kendig, A. J. Davenport, and H. S. Isaacs, *Corros. Sci.*, **1993**, *34*, 41.
[78] J. Zhao, G. Frankel, and R. L. McCreery, *J. Electrochem. Soc.*, **1998**, *145*, 2258.
[79] W. R. McGovern, P. Schmutz, R. G. Buchheit, and R. L. McCreery, *J. Electrochem. Soc.*, **2000**, *147*, 4494.
[80] L. Xia and R. L. McCreery, *J. Electrochem. Soc.*, **1999**, *146*, 3696.
[81] F. W. Lytle, R. B. Greegor, G. L. Bibbins, K. Y. Blohowiak, R. E. Smith, and G. D. Tuss, *Corros. Sci.*, **1995**, *37*, 349.
[82] L. Xia and R. L. McCreery, *J. Electrochem. Soc.*, **1998**, *145*, 3083.
[83] L. Xia, E. Akiyama, G. Frankel, and R. McCreery, *J. Electrochem. Soc.*, **2000**, *147*, 2556.
[84] G. O. Ilevbare and J. R. Scully, *Corrosion*, **2001**, *57*, 134.
[85] G. O. Ilevbare and J. R. Scully, *J. Electrochem. Soc.*, **2001**, *148*, B196.
[86] A. Sehgal, G. S. Frankel, B. Zoofan, and S. Rokhlin, *J. Electrochem. Soc.*, **2000**, *147*, 140.
[87] W. J. Clark, J. D. Ramsey, R. L. McCreery, and G. S. Frankel, *J. Electrochem. Soc.*, **2002**, *149*, B179.
[88] M. Kendig and S. Jeanjaquet, *J. Electrochem. Soc.*, **2002**, *149*, B47.
[89] E. Larsen, S. Larsen, G. B. Paulsen, J. Springborg, and D. N. Wang, *Acta Chem. Scand.*, **1994**, *48*, 107.
[90] G. A. Lawrence, *Adv. Inorg. Chem.*, **1989**, *34*, 145.
[91] G. B. Kauffman, *Werner Centennial: A Symposium*, American Chemical Society, 1967.

[92] S. E. Dolan, L. R. Carlson, and J. R. Pierce, Aqueous redox bath with cobalt cations for adherent protective coating on metal surfaces, WO 96/21,753, 1996
[93] M. P. Schriever, Conversion bath for chromate-free coating with cobalt oxide on aluminum alloy substrates, US 5,873,953, 1999
[94] J. A. Sturgill, A. W. Phelps, and J. T. Swartzbaugh, Non-toxic conversion bath with stabilized cobalt ions for corrosion-resistant coating on metals and alloys, WO 2003/060,191, 2003
[95] M. E. Baldwin, S. C. Chan, and M. L. Tobe, *Journal of the Chemical Society*, **1961**, 4637.
[96] S. H. Caldwell and D. A. House, *J. Inorg. Nucl. Chem.*, **1969**, *31*, 811.
[97] H. Koyama and T. Yoshino, *Bull. Chem. Soc. Jpn.*, **1972**, *45*, 481.
[98] M. S. Okamoto and E. K. Barefield, *Inorg. Chim. Acta*, **1976**, *17*, 91.
[99] P. Andersen, J. Glerup, A. Gumm, S. K. Hansen, and M. Magnussen, *Dalton Trans.*, **2004**, 2929.
[100] M. Nonoyama and K. Sakai, *Inorg. Chim. Acta*, **1983**, *72*, 57.
[101] S. Fujinami, T. Hosokawa, and M. Shibata, *Bull. Chem. Soc. Jpn.*, **1983**, *56*, 113.
[102] S. Shimba, S. Fujinami, and M. Shibata, *Chem. Lett.*, **1979**, 783.
[103] K. Wieghardt, P. Chaudhuri, B. Nuber, and J. Weiss, *Inorg. Chem.*, **1982**, *21*, 3086.
[104] J. H. Koek, S. W. Russell, L. van der Wolf, R. Hage, J. B. Warnaar, A. L. Spek, J. Kerschner, and L. Del Pizzo, *J. Chem. Soc., Dalton Trans.*, **1996**, 353.
[105] T. Beissel, B. Dellavedova, K. Wieghardt, and R. Boese, *Inorg. Chem.*, **1990**, *29*, 1736.
[106] L. R. Gahan, G. A. Lawrence, and A. M. Sargeson, *Aust. J. Chem.*, **1982**, *35*, 1119.
[107] K. Wieghardt, U. Bossek, P. Chaudhuri, W. Herrmann, B. C. Menke, and J. Weiss, *Inorg. Chem.*, **1982**, *21*, 4308.
[108] A. Hammershoi and A. M. Sargeson, *Inorg. Chem.*, **1983**, *22*, 3554.
[109] K. Wieghardt, I. Tolksdorf, and W. Herrmann, *Inorg. Chem.*, **1985**, *24*, 1230.
[110] S. F. Mason and R. D. Peacock, *Inorg. Chim. Acta*, **1976**, *19*, 75.
[111] P. G. Graham and D. C. Weatherburn, *Aust. J. Chem.*, **1983**, *36*, 2349.
[112] M. H. Ansari, M. Ahmad, and K. A. Dicke, *Bioorg. Med. Chem. Lett.*, **1993**, *3*, 1067.
[113] M. Studer and C. F. Meares, *Bioconjugate Chem.*, **1992**, *3*, 337.
[114] G. Argouarch, G. Stones, C. L. Gibson, A. R. Kennedy, and D. C. Sherrington, *Org. Biomol. Chem.*, **2003**, *1*, 4408.
[115] B. M. Kim, S. M. So, and H. J. Choi, *Org. Lett.*, **2002**, *4*, 949.
[116] R. J. Geue and M. R. Snow, *Inorg. Chem.*, **1977**, *16*, 231.
[117] P. Kofod, E. Larsen, J. Springborg, S. Larsen, T. A. Larsen, R. J. Geue, and G. H. Searle, *Aust. J. Chem.*, **1994**, *47*, 111.
[118] K. Yamanari, J. Hidaka, and Y. Shimura, *Bull. Chem. Soc. Jpn.*, **1975**, *48*, 1653.
[119] L. H. Gade and N. Mahr, *J. Chem. Soc., Dalton Trans.*, **1993**, 489.
[120] A. H. R. Al-Obaidi, K. B. Jensen, J. J. McGarvey, H. Toftlund, B. Jensen, S. E. J. Bell, and J. G. Carroll, *Inorg. Chem.*, **1996**, *35*, 5055.
[121] R. J. Geue and G. H. Searle, *Aust. J. Chem.*, **1983**, *36*, 927.
[122] A. Hohn, R. J. Geue, and A. M. Sargeson, *J. Chem. Soc., Chem. Commun.*, **1990**, 1473.
[123] J. E. Richman and T. J. Atkins, *J. Am. Chem. Soc.*, **1974**, *96*, 2268.
[124] G. H. Searle and R. J. Geue, *Aust. J. Chem.*, **1984**, *37*, 959.
[125] S. Gabriel, *Ber. Dtsch. Chem. Ges.*, **1887**, *20*, 2224.
[126] M. S. Gibson and R. W. Bradshaw, *Angew. Chem., Int. Ed.*, **1968**, *7*, 919.

[127] H. Stetter and W. Bockmann, *Chem. Ber. Recl.*, **1951**, *84*, 834.
[128] E. B. Fleischer, A. E. Gebala, A. Levey, and P. A. Tasker, *J. Org. Chem.*, **1971**, *36*, 3042.
[129] L. J. Zompa and J. P. Anselme, *Org. Prep. Proced. Int.*, **1974**, *6*, 103.
[130] F. C. Whitmore and G. H. Fleming, *J. Am. Chem. Soc.*, **1933**, *55*, 4161.
[131] F. C. Whitmore and H. S. Rothrock, *J. Am. Chem. Soc.*, **1932**, *54*, 3431.
[132] I. Dostrovsky and E. D. Hughes, *J. Chem. Soc.*, **1946**, 157.
[133] I. Dostrovsky and E. D. Hughes, *J. Chem. Soc.*, **1946**, 161.
[134] I. Dostrovsky and E. D. Hughes, *J. Chem. Soc.*, **1946**, 164.
[135] I. Dostrovsky and E. D. Hughes, *J. Chem. Soc.*, **1946**, 169.
[136] I. Dostrovsky and E. D. Hughes, *J. Chem. Soc.*, **1946**, 171.
[137] P. D. Bartlett and L. J. Rosen, *J. Am. Chem. Soc.*, **1942**, *64*, 543.
[138] I. Dostrovsky, E. D. Hughes, and C. K. Ingold, *J. Chem. Soc.*, **1946**, 173.
[139] H. R. Ing and R. H. F. Manske, *J. Chem. Soc.*, **1926**, 2348.
[140] M. N. Khan, *J. Org. Chem.*, **1995**, *60*, 4536.
[141] H. C. Kolb, M. G. Finn, and K. B. Sharpless, *Angew. Chem., Int. Ed.*, **2001**, *40*, 2004.
[142] R. Viguier, G. Serratrice, A. Dupraz, and C. Dupuy, *Eur. J. Inorg. Chem.*, **2001**, 1789.
[143] D. A. Buckingham, in *Encyclopedia of Inorganic Chemistry*, ed. R. B. King, Wiley, 1994.
[144] P. V. Bernhardt and G. A. Lawrence, in *Comprehensive Coordination Chemistry*, ed. J. A. McCleverty and T. J. Meyer, Elsevier Ltd, 2004.
[145] K. Nakamoto, *Infrared and Raman Spectra of Inorganic and Coordination Compounds*, Wiley, 1997.
[146] S. A. Dalrymple and G. K. H. Shimizu, *J. Mol. Struct.*, **2006**, *796*, 95.
[147] J. R. Fluckiger, C. W. Schlapfer, and C. Couldwell, *Inorg. Chem.*, **1980**, *19*, 2493.
[148] G. H. Searle and T. W. Hambley, *Aust. J. Chem.*, **1982**, *35*, 1297.
[149] K. Wieghardt, W. Schmidt, B. Nuber, and J. Weiss, *Chem. Ber. Recl.*, **1979**, *112*, 2220.
[150] N. H. Williams and P. Wyman, *J. Chem. Soc., Perkin Trans. 2*, **2001**, 2068.
[151] N. E. Dixon, W. G. Jackson, M. J. Lancaster, G. A. Lawrance, and A. M. Sargeson, *Inorg. Chem.*, **1981**, *20*, 470.
[152] N. E. Dixon, W. G. Jackson, G. A. Lawrance, and A. M. Sargeson, *Inorg. Synth.*, **1983**, *22*, 103.
[153] B. Tollens and P. Wigand, *Liebigs Ann. Chem.*, **1891**, *265*, 316.
[154] M. S. Peters and J. A. Quinn, *Ind. Eng. Chem. Prod. Res. Dev.*, **1955**, *47*, 1710.
[155] R. D. Ashford, *Ashford's Dictionary of Industrial Chemicals: Properties, Production, Uses*, Wavelength, 1994.
[156] S. Budavari and Merck Research Laboratories, *The Merck Index: An Encyclopedia of Chemicals, Drugs, and Biologicals*, Merck & Co., 2001.
[157] J. Haldar, P. Kondaiah, and S. Bhattacharya, *J. Med. Chem.*, **2005**, *48*, 3823.
[158] D. J. Moore and E. H. Pryde, *J. Am. Oil Chem. Soc.*, **1968**, *45*, 517.
[159] N. Rockendorf, O. Sperling, and T. K. Lindhorst, *Aust. J. Chem.*, **2002**, *55*, 87.
[160] B. Weibull and M. Matell, *Acta Chem. Scand.*, **1962**, *16*, 1062.
[161] H. Hosaus, P. Rave, P. Wigand, and B. Tollens, *J. Am. Chem. Soc.*, **1893**, *15*, 704.
[162] H. B. J. Schurink, *Org. Synth.*, **1925**, *4*, 53.
[163] M. Frigerio, M. Santagostino, and S. Sputore, *J. Org. Chem.*, **1999**, *64*, 4537.
[164] J. D. More and N. S. Finney, *Org. Lett.*, **2002**, *4*, 3001.
[165] J. T. Su and W. A. Goddard, *J. Am. Chem. Soc.*, **2005**, *127*, 14146.

[166] T. J. Dunn, W. L. Neumann, M. M. Rogic, and S. R. Woulfe, *J. Org. Chem.*, **1990**, *55*, 6368.
[167] S. Searles and S. Nukina, *Chem. Rev.*, **1959**, *59*, 1077.
[168] I. Iliuc, *Tribology of thin layers*, Elsevier, 1980.
[169] M. Nagayama and M. Cohen, *J. Electrochem. Soc.*, **1963**, *110*, 670.
[170] M. E. Brett, K. M. Parkin, and M. J. Graham, *J. Electrochem. Soc.*, **1986**, *133*, 2031.
[171] W. E. O'Grady, *J. Electrochem. Soc.*, **1980**, *127*, 555.
[172] G. M. Atenas, E. Mielczarski, and J. A. Mielczarski, *J. Colloid Interface Sci.*, **2005**, *289*, 157.
[173] G. D. Parfitt and C. H. Rochester, *Adsorption from Solution at the Solid/Liquid Interface*, Academic Press, 1983.
[174] M. Frey, S. G. Harris, J. M. Holmes, D. A. Nation, S. Parsons, P. A. Tasker, S. J. Teat, and R. E. P. Winpenny, *Angew. Chem., Int. Ed.*, **1998**, *37*, 3246.
[175] R. M. Cornell and U. Schwertmann, *The Iron Oxides: Structure, Properties, Reactions, Occurrence and Uses*, VCH, 1996.
[176] S. Goldsztaub, *Bull. Soc. Fr. Mineral.*, **1935**, *58*, 6.
[177] W. Hoppe, *Z. Kristallogr. Kristallgeom. Kristallphys. Kristallchem.*, **1940**, *103*, 73.
[178] C. F. Sampson, *Acta Crystallogr., Sect. B: Struct. Sci.*, **1969**, *B 25*, 1683.
[179] A. F. Gualtieri and P. Venturelli, *Am. Mineral.*, **1999**, *84*, 895.
[180] R. I. Masel, *Principles of Adsorption and Reaction on Solid Surfaces*, Wiley, 1996.
[181] S. J. Gregg and K. S. W. Sing, *Adsorption, Surface Area and Porosity*, Academic Press, 1982.
[182] I. Langmuir, *J. Am. Chem. Soc.*, **1912**, *34*, 1310.
[183] C. H. Giles, D. Smith, and A. Huitson, *J. Colloid Interface Sci.*, **1974**, *47*, 755.
[184] S. Brunauer, L. S. Deming, W. E. Deming, and E. Teller, *J. Am. Chem. Soc.*, **1940**, *62*, 1723.
[185] C. H. Giles, T. H. Macewan, S. N. Nakhwa, and D. Smith, *J. Chem. Soc.*, **1960**, 3973.
[186] C. H. Giles, A. P. Dsilva, and I. A. Easton, *J. Colloid Interface Sci.*, **1974**, *47*, 766.
[187] I. Langmuir, *J. Am. Chem. Soc.*, **1916**, *38*, 2221.
[188] I. Langmuir, *J. Am. Chem. Soc.*, **1918**, *40*, 1361.
[189] W. Stumm, L. Sigg, and B. Sulzberger, *Chemistry of the Solid-Water Interface: Processes at the Mineral-Water and Particle-Water Interface in Natural Systems*, Wiley, 1992.
[190] K. V. Kumar and S. Sivanesan, *J. Hazard. Mater.*, **2005**, *123*, 288.
[191] F. Rouessac and A. Rouessac, *Chemical Analysis: Modern Instrumentation Methods and Techniques*, John Wiley and Sons, 2007.
[192] I. J. Bruno, J. C. Cole, P. R. Edgington, M. Kessler, C. F. Macrae, P. McCabe, J. Pearson, and R. Taylor, *Acta Crystallographica Section B-Structural Science*, **2002**, *58*, 389.
[193] E. O. Schlemper, P. K. Sengupta, and T. P. Dasgupta, *Acta Crystallographica Section C-Crystal Structure Communications*, **1983**, *39*, 1012.
[194] A. Kadziola and A. Dossing, *J. Coord. Chem.*, **2008**, *61*, 1671.
[195] S. Brunauer, P. H. Emmett, and E. Teller, *J. Am. Chem. Soc.*, **1938**, *60*, 309.
[196] S. E. Cheyne, L. F. McClintock, and A. G. Blackman, *Inorg. Chem.*, **2006**, *45*, 2610.
[197] J. Gaydos and A. W. Neumann, in *Applied Surface Thermodynamics*, ed. A. W. Neumann and J. K. Spelt, Marcel Dekker Inc., 1996.
[198] D. A. Buttry and M. D. Ward, *Chem. Rev.*, **1992**, *92*, 1355.

[199] A. Arnau and D. Soares, in *Piezoelectric Transducers and Applications*, ed. A. Arnau, Springer, 2008.
[200] J. K. Spelt and E. I. Vargha-Butler, in *Applied Surface Thermodynamics*, ed. A. W. Neumann and J. K. Spelt, Marcel Dekker Inc., 1996.
[201] N. Ayling, R. Hartshorn, and K. Morison, Unpublished results, 2009
[202] R. G. Kelly, *Electrochemical Techniques in Corrosion Science and Engineering*, CRC Press, 2003.
[203] G. A. Cragnolino, in *Techniques for Corrosion Monitoring*, ed. L. Yang, Woodhead Publishing, 2008.
[204] P. Marcus and F. Mansfeld, *Analytical Methods in Corrosion Science and Engineering*, CRC Press, 2006.
[205] C. L. Meade, in *Corrosion Tests and Standards: Application and Interpretation*, ed. R. Baboian, ASTM International, 2005.
[206] K. Chiang and T. Mintz, in *Techniques for Corrosion Monitoring*, ed. L. Yang, Woodhead Publishing, 2008.
[207] J. R. Scully, in *Corrosion Tests and Standards: Application and Interpretation*, ed. R. Baboian, ASTM International, 2005.
[208] S. Papavinasam, in *Techniques for Corrosion Monitoring*, ed. L. Yang, Woodhead Publishing, 2008.
[209] D. C. Silverman, in *Corrosion Tests and Standards: Application and Interpretation*, ed. R. Baboian, ASTM International, 2005.
[210] F. Bentiss, M. Lagrenee, M. Traisnel, and J. C. Hornez, *Corros. Sci.*, **1999**, *41*, 789.
[211] A. A. El-Shafei, M. N. H. Moussa, and A. A. El-Far, *Mater. Chem. Phys.*, **2001**, *70*, 175.
[212] S. Kertit and B. Hammouti, *Appl. Surf. Sci.*, **1996**, *93*, 59.
[213] C. N. Hinshelwood, *The Kinetics of Chemical Change*, The Clarendon Press, 1940.
[214] P. Mutombo and N. Hackerman, *J. Solid State Electrochem.*, **1997**, *1*, 194.
[215] A. G. Sykes and J. A. Weil, *Prog. Inorg. Chem.*, **1970**, *13*, 1.
[216] D. Z. Feng, Y. L. Song, X. H. Jiang, L. Chen, and Y. Q. Long, *Org. Biomol. Chem.*, **2007**, *5*, 2690.
[217] T. O. Soine and M. R. Buchdahl, *Org. Synth.*, **1952**, *32*, 18.
[218] P. Casara, C. Danzin, B. Metcalf, and M. Jung, *J. Chem. Soc., Perkin Trans. 1*, **1985**, 2201.
[219] S. Teramae, T. Osako, S. Nagatomo, T. Kitagawa, S. Fukuzumi, and S. Itoh, *J. Inorg. Biochem.*, **2004**, *98*, 746.
[220] E. Kimura, S. Young, and J. P. Collman, *Inorg. Chem.*, **1970**, *9*, 1183.
[221] J. Glerup, S. Larsen, and H. Weihe, *Acta Chem. Scand.*, **1993**, *47*, 1154.
[222] C. A. Otter and R. M. Hartshorn, *Dalton Trans.*, **2004**, 150.
[223] P. H. Crayton, *Inorg. Synth.*, **1963**, *7*, 207.
[224] Bruker (2007), APEX2 (Version 2.1-4), SAINT (Version 7.34A), SADABS (Version 2004/1), Bruker AXS Inc., Madison, WI, USA
[225] O. V. Dolomanov, L. J. Bourhis, R. J. Gildea, J. A. K. Howard, and H. Puschmann, *J. Appl. Crystallogr.*, **2009**, *42*, 339.
[226] N. Ngadi, J. Abrahamson, C. Fee, and K. Morison, *Int. J. Chem. Biomol. Eng.*, **2008**, *1*, 126.
[227] F. Hein and R. Burkhardt, *Chem. Ber. Recl.*, **1957**, *90*, 928.
[228] A. M. Aquino, C. J. Abelt, K. L. Berger, C. M. Darragh, S. E. Kelley, and M. V.

Cossette, *J. Am. Chem. Soc.*, **1990**, *112*, 5819.
[229] J. R. Beckwith and L. P. Hager, *J. Org. Chem.*, **1961**, *26*, 5206.
[230] V. K. Aggarwal, G. Fang, C. G. Kokotos, J. Richardson, and M. G. Unthank, *Tetrahedron*, **2006**, *62*, 11297.
[231] J. Shamir, *Inorg. Chim. Acta*, **1989**, *156*, 163.